Cyclophanes II

Editor: F. Vögtle

With Contributions by
F. Gerson, E. Heilbronner, Y. Murakami,
F. Vögtle, Z. Yang

With 71 Figures and 39 Tables

This series presents critical reviews of the present position and future trends in modern chemical research. It is addressed to all research and industrial chemists who wish to keep abreast of advances in their subject.

As a rule, contributions are specially commissioned. The editors and publishers will, however, always be pleased to receive suggestions and supplementary information. Papers are accepted for "Topics in Current Chemistry" in English.

Managing Editor:

Dr. *Friedrich L. Boschke*
Springer-Verlag, Postfach 105280, D-6900 Heidelberg 1

Editorial Board:

Table of Contents

Table of Contents of Volume 113

Cyclophanes I

The Electronic Structure of Cyclophanes as Suggested by their Photoelectron Spectra

"Dedicated to Prof. J. D. Dunitz on the occasion of his 60th birthday"

Edgar Heilbronner and Zhong-zhi Yang[1]

Physikalisch-Chemisches Institut der Universität Basel, Klingelbergstraße 80, CH-4056 Basel, Switzerland

Table of Contents

---

[1] Permanent address: Theoretical Chemistry Institute. Jilin University, Chang Chun, People's Republic of China.

1 Introduction

The most intriguing question relating to cyclophanes is how the forced proximity of two π-systems influences their chemical and physical properties, in particular their photophysical behaviour. In this review we discuss the ionization energies (I_j) of cyclophanes, as determined by He(Iα) photoelectron (PE) spectroscopy.

The X-ray analysis of the cyclophane prototype [2.2](1,4)cyclophane (*1*) (= para-cyclophane) [1)] reveals that the two benzene moieties are separated by a mean interdeck distance $D = 299$ pm, much smaller than the usual π-system van der Waals contact distance of ~ 340 pm between parallel aromatic hydrocarbons in crystals [2)], or even the graphite layer distance of 335 pm. As shown, the bridged centres are only 278 pm apart, the others 309 pm, which means that the two rings are bent out of plane by a fold angle of 12.6°.

How are these rather unique structural features of *1* going to affect its ionization energies I_j^m, in particular the first one I_1^m, relative to that of the parent compound benzene? Rather naively one might have expected that the π^{-1} ionization energy I_1^m of *1* differs from the corresponding $e_{1g}(\pi)^{-1}$ ionization energy of benzene ($I_1^m = 9.25$ eV) for at least three reasons:

1) *Inductive and/or hyperconjugative effect of the bridging groups.* It is known that the π^{-1} ionization energies I_1^m and I_2^m of 1,4-dialkylbenzenes are significantly smaller than $I_1^m = I_2^m = 9.25$ eV of benzene, e.g.

$$
\begin{array}{lll}
\text{1,4-dimethylbenzene,} & I_1^m = 8.6_0 \text{ eV,} & I_2^m = 9.1_5 \text{ eV } [3)]; \\
\text{1,4-diethylbenzene,} & I_1^m = 8.4_5 \text{ eV,} & I_2^m = 9.1_0 \text{ eV}; \\
\text{1,4-dipropylbenzene,} & I_1^m = 8.3_0 \text{ eV,} & I_2^m = 9.0_0 \text{ eV } [4)].
\end{array}
$$

This trend is the one expected, if we assume that the ionization energy reduction due to an alkylsubstituent R is measured by its σ_R^* value [5)] ($\sigma_H^* = 0.49$, $\sigma_{Me}^* = 0.00$, $\sigma_{Et}^* = -0.10$, $\sigma_{Pr}^* = -0.12$) or, more precisely by the alkyl group parameters μ_R^H deduced from the mean $5p^{-1}$ ionization energies of alkyliodides RI [6)] ($\mu_M^H = 0.00$,

3
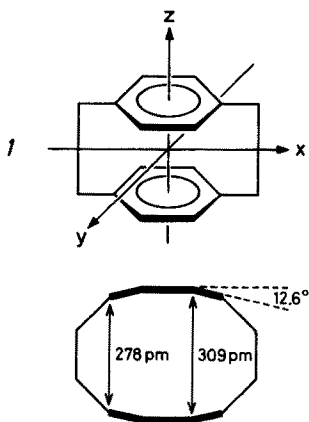
$\mu_{Me}^H = -0.89$, $\mu_{Et}^H = -1.08$, $\mu_{Pr}^H = -1.18$). Other things being equal, one would therefore expect that the two bridging CH_2CH_2 groups shift I_1^m of 1 to ~ 8.5 eV by virtue of their inductive and/or hyperconjugative effect.

2) *Steric interference of the π clouds.* Obviously the two π clouds of the upper and lower benzene rings in 1 seem to be pressed hard against each other as indicated by the small mean distance $D = 299$ pm and the bent structure of the two rings. This should lead to additional repulsion between the π-electrons crowded into the space between the two rings. Intuitively one would predict that this destabilizing interaction can be relieved by lowering the number of interacting π-electrons i.e. by ionization. If this were true, we would be in the presence of a "toothpaste tube effect" i.e. the harder you press the electrons the easier they pop out. Needless to say that this effect would tend to further reduce the ionization energy of 1 relative to that of benzene. However, it is not obvious how big such an effect would be, except that it should increase with decreasing distance D.

3) *Bending of the π-systems.* Curiously, but perhaps not unexpectedly, qualitative reasoning along "resonance energy" lines is rather inadequate for dealing with the question whether bending will increase or decrease the π^{-1} ionization energies. Indeed, lack of planarity of the benzene system could be construed to decrease its "aromaticity" and hence its stability with the consequence that ionization should be facilitated. On the other hand, bending a π-system will tend to localize its bonds i.e. push it towards a more polyenic type of structure which should then be more difficult to ionize.

As we shall see none of these explanations holds. In contrast to the usual conjugative interaction of an alkyl group with a π-system, hyperconjugation in 1 is severely limited by symmetry, so that a comparison e.g. with alkylsubstituted benzenes is quite misleading. Furthermore, the postulated "toothpaste tube effect" is probably very small if not negligible, and finally it is known that bending of tightly bound π-systems such as double bonds [7], triple bonds [7,8] or benzene rings [4] has no significant influecne on their π^{-1} ionization energies, as long as the deformations do not exceed a critical limit [9].

In view of the failure of seemingly "obvious" explanations it is gratifying that the body of experimental data accumulated to date can be rationalized in a straightforward manner by using well-established model concepts borrowed from simple molecular orbital theory, such as Hoffmann's "through-space" and "through-bond" orbital interaction scheme [10].

2 Nomenclature and Experimental Details

2.1 Designation of Structure

With few exceptions, the systems we are going to discuss consist of an upper and a lower deck, M_u and M_l shifted along the z-axis by a mean distance D with respect to each other. They are linked by $(CH_2)_n$ bridges (mainly n = 2) which connect e.g. centres a, b of M_u to c, d of M_l as shown in the following diagram.

4

$$(1)$$

For simplicity we number the π-centres of the upper and lower deck of 1 as indicated in the left-hand formula, rather than according to the rules used normally shown on the right. This has the advantage of assigning the same index to 2p atomic orbitals facing each other.

$$(2)$$
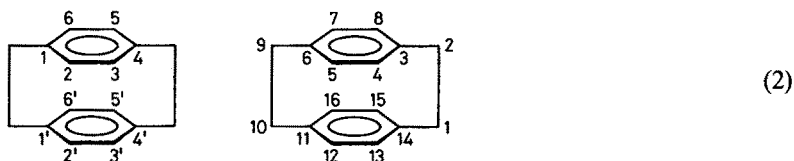
Consequently, the linked centres in e.g. $[2_4](1,2,4,5)$cyclophane are given as $1-1'$, $2-2'$, $4-4'$, $5-5'$ rather than $3-12$, $5-14$, $6-15$, $8-11$, as required by the usual convention depicted in the following formula.
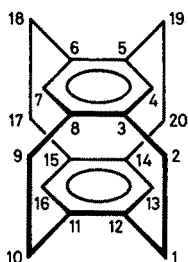
To avoid any ambiguity in the symmetry designations of orbitals, configurations and states of cyclophanes belonging to the point groups C_{2v} and D_{2h}, the orientation of the respective coordinate systems has been included in the structure formulae.

2.2 Characterization of the Radical Cation States and Numbering of the PE-Bands

As is customary in PE spectroscopy the observed radical cation states $^2\Psi_j$ of M^+ are labeled $\tilde{X}$, $\tilde{A}$, $\tilde{B}$, $\tilde{C}$, etc. in ascending order of energy. If possible, they are specified by including in parenthesis either the symmetry designation of the state $^2\Psi_j$ or, implying Koopmans' theorem, the vacated canonical molecular orbital φ_j. Thus the first four states of the paracyclophane radical cation 1^+ would be given as $\tilde{X}(^2B_{2g})$, $\tilde{A}(^2B_{3g})$, $\tilde{B}(^2B_{3u})$, $\tilde{C}(^2B_{2u})$ or $\tilde{X}(b_{2g}^{-1})$, $\tilde{A}(b_{3g}^{-1})$, $\tilde{B}(b_{3u}^{-1})$, $\tilde{C}(b_{2u}^{-1})$.

5

The bands in the PE spectra are numbered ①, ②, ... , ①, in order of increasing ionization energy I_j. Whenever possible each individual band carries its own number. However, in some cases where deconvolution of close lying bands is impossible, a given number may refer to two (or even more) overlapping bands. Consequently the band number sequence will not always match the sequence of states.

The band positions are characterized by I_j^m, the position of the band maximum, j being the number of band ①. The theoretically relevant ionization energies are I_j^v, the vertical and I_j^a the adiabatic ionization energies. The former corresponds to an ionization process

$$M(^1\Psi_0) + h\nu \rightarrow M^+(^2\Psi_j) + e^- \tag{3}$$

in which the closed-shell molecule M and the radical cation M^+ have the identical set of internal coordinates (i.e. that of M) whereas in the latter, adiabatic process, M^+ in the state $^2\Psi_j$ has relaxed to its own minimal energy structure. Therefore $I_j^a < I_j^v$. The choice of I_j^m is dictated by practical considerations as in traditional electronic spectroscopy, I_j^m being easier to determine and with greater precision than either I_j^a or I_j^v. Furthermore, for all practical purposes we may safely assume that $I_j^m \approx I_j^v$, especially for such large systems as the ones under consideration.

The precision with which I_j^m can be assessed depends on the shape of the band and its overlapping with other, close lying bands. In the following the limits of error are ± 0.02 eV if two decimals are given, ± 0.05 eV if the second decimal figures as a subscript and ± 0.1 eV to ± 0.2 eV if only one decimal is given.

2.3 Recording of the He(Iα) PE Spectra

The He(Iα) PE spectra stemming from the Basel group have been recorded on spectrometers built according to the specifications given by Turner[11]. They incorporate a $\pi/\sqrt{2}$ cylindrical condenser analyser of 10 cm radius and a He(Iα) source of excitation. The spectra of the cyclophanes have to be recorded at elevated temperatures ($\sim 100°$ to 200 °C). Under these conditions, the effective working resolution is of the order $E/\Delta \approx 250$. The ionization energies were determined by an internal calibration procedure using a rare gas mixture. For the experimental details concerning the spectra taken from work of other authors, the reader is referred to the original literature.

The relatively high sample and inlet temperatures raise the question whether the cyclophanes are stable under these conditions. This has been tested, and it is safe to assume that none of the PE spectra are contaminated by decomposition products. Indeed, Koenig et al.[12] had to flash-photolyse 1 at 600 °C to obtain the PE-spectrum of p-quinodimethane, according to

6
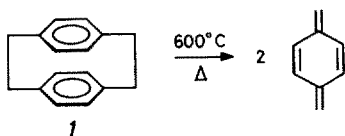
The only example we have encountered so far, where such a dissociation occurs at low enough temperatures to prevent the recording of the PE-spectrum of a cyclophane was that of [2.2](9,10)anthracenophane, which yields at ~200 °C exclusively the PE-spectrum of dibenzoquinodimethane [13]:
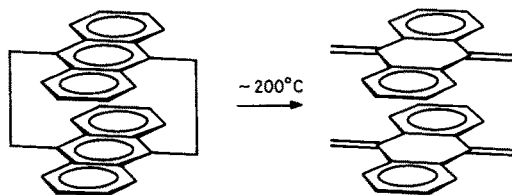
3 PE-Spectra

3.1 [2.2]Paracyclophane and Derivatives

The PE-spectrum of the parent compound [2.2]paracyclophane *1* was first recorded by Pignataro et al. [14] who attributed the broad feature at 8 eV (cf. Fig. 1) to two π^{-1} ionization processes. Boschi and Schmidt [15] have shown that in agreement with a theoretical prediction by Gleiter [16] this feature should be assigned to three close-lying π^{-1} ionizations. This interpretation is supported by later work [17,18,19], as will be discussed in chapter 5.1. However, it should be mentioned that a different

π,π	π	π	---- 14)
π,π,π	π	σ	---- 15), 16)
π,π,π,π	σ	σ	---- 20)
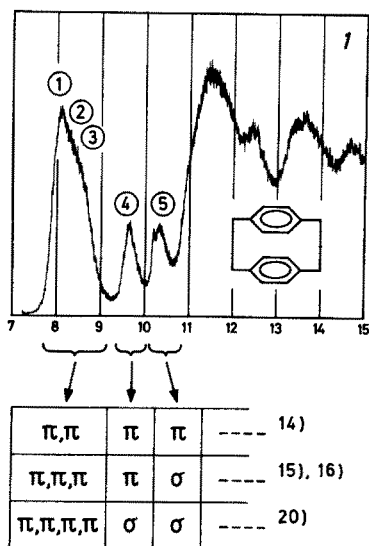
Fig. 1. PE-Spectrum of [2.2] Paracyclophane and Various Suggested Assignments

7

assignment, assuming four π^{-1} ionization processes has also been proposed on the basis of some semiempirical calculations [20].

In Fig. 2 are presented the PE-spectra of some typical examples of methyl-substituted [2.2]paracyclophanes [19,21,22] the ionization energies I_j^m of which are given, among others, in Table 1. They are correlated in the diagram of Fig. 3.

The PE-spectra of the [2.2]paracyclophanes *16, 17* in which the two decks are linked by two double bonds [23] or two cyclopropane units [24] are shown in Fig. 4. Their ionization energies I_j^m, together with those of the [2.2]paracyclophanes *15* and *18* to *22* are collected in Table 2.
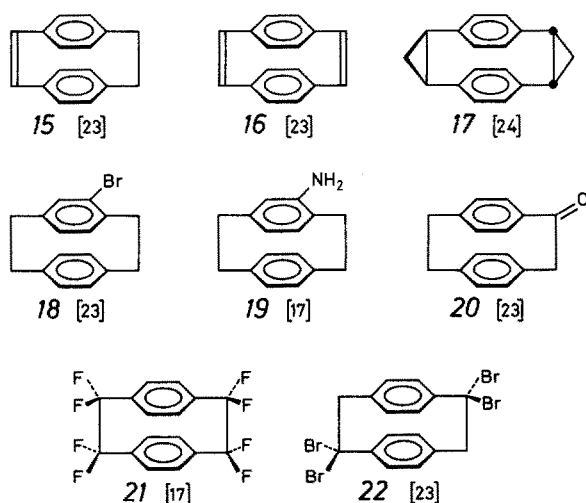
Table 1. Ionization Energies I_j^m in eV of [2.2]Paracyclophane *1* and of Methyl-substituted [2.2]Paracyclophanes *2* to *14*. (See formulae in Fig. 3) [19,21,22]

Compound No.	Number n and positions of Me-groups[a]	Bands				
		① ②	③	④	⑤	
1	0	8.1_0	8.4	9.6_5	10.3	
2	1	7.9_0	8.2	9.3_5	10.0_5	
3	2 (2,5)	7.7_5	8.3	9.1_5	9.9_0	
4	2 (2; 5')	7.8_5	8.2	9.2_0	9.9_5	
5	2 (2; 6')	7.8_5	8.1	9.1_5	10.0_0	
6	3 (2,3; 2')	7.7_0	8.1	8.9_5	9.8_0	
7	4 (2,3; 5', 6')	7.6_0	8.1	8.7_0	9.8_0	
8	4 (2,5; 2', 5')	7.7_5	8.1	8.8_0	9.6_0	
9	4 (2,5; 3', 6')	7.5_5	8.2	8.8_0	9.8_0	
10	4 (2,3,5,6)	7.5_0	8.2	8.9_5	9.6_5	
11	5 (2,3,6; 5'6')	7.5_5	8.1	8.5_5	9.6_5	
12	6 (2,3,6; 3'5'6')	7.4_5	7.9	8.4_0	9.4_5	
13	7	7.4_0	7.8	8.3_5	9.4_0	
14	8	7.1_5	7.7	8.1_0	9.2_0	

[a] Following the number of methyl groups, their position (if necessary) is given with reference to the convention explained in 2.1, formula (2), left.
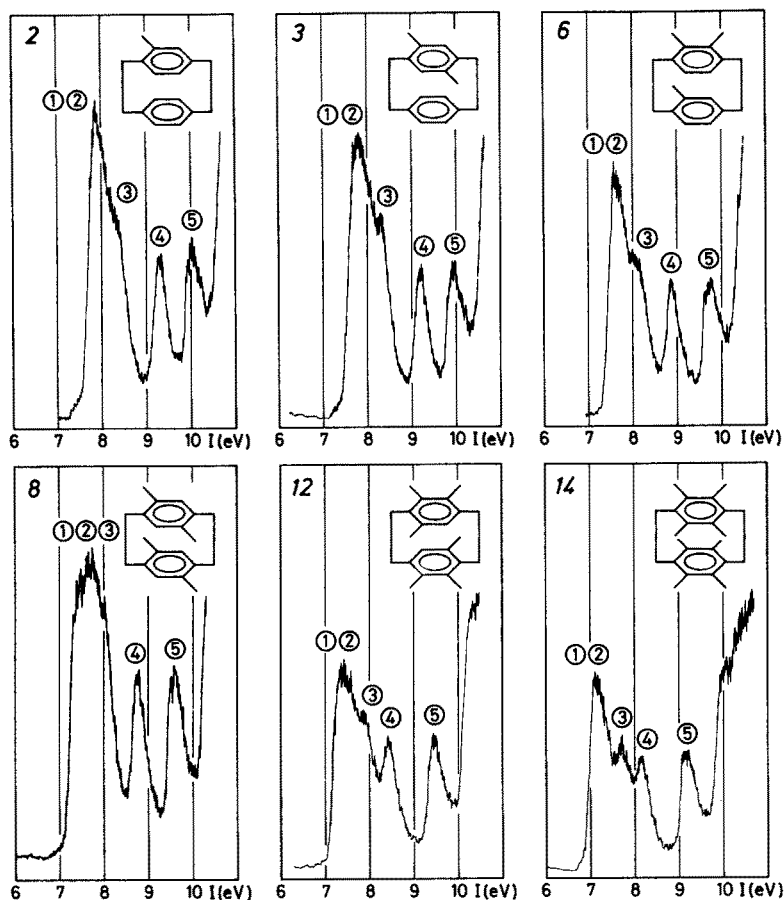
Fig. 2. PE-Spectra of Selected Examples of Methyl-substituted [2.2]Paracyclophanes

Table 2. Ionization Energies I_j^m in eV of [2.2]Paracyclophane Derivatives *15* to *22*

Compound No.	Bands						Ref.
	①	②	③	④	⑤	⑥	
15	8.1_0	8.1_0	8.6_5	9.3_0	9.7_0	10.2	[23]
16	8.1_0	8.1_0	8.9_5	9.4_0	9.8_5	10.3	[23]
17	7.9	8.1	8.1	9.5			[24]
18	8.1_0	8.1_0	8.5_0	9.3_5	10.1_0	10.5_5	[23]
19	7.5_0	7.9_0	8.2_0	9.0_0	10.0_0	10.7	[17]
20	8.2_5	8.5_0	9.0_5	9.4_5	9.8_5	10.7	[23]
21	9.3_0	9.3_0	10.5_0	10.7_5	11.7_5	12.7	[17]
22	8.5	8.5	9.2	10.0			[23]
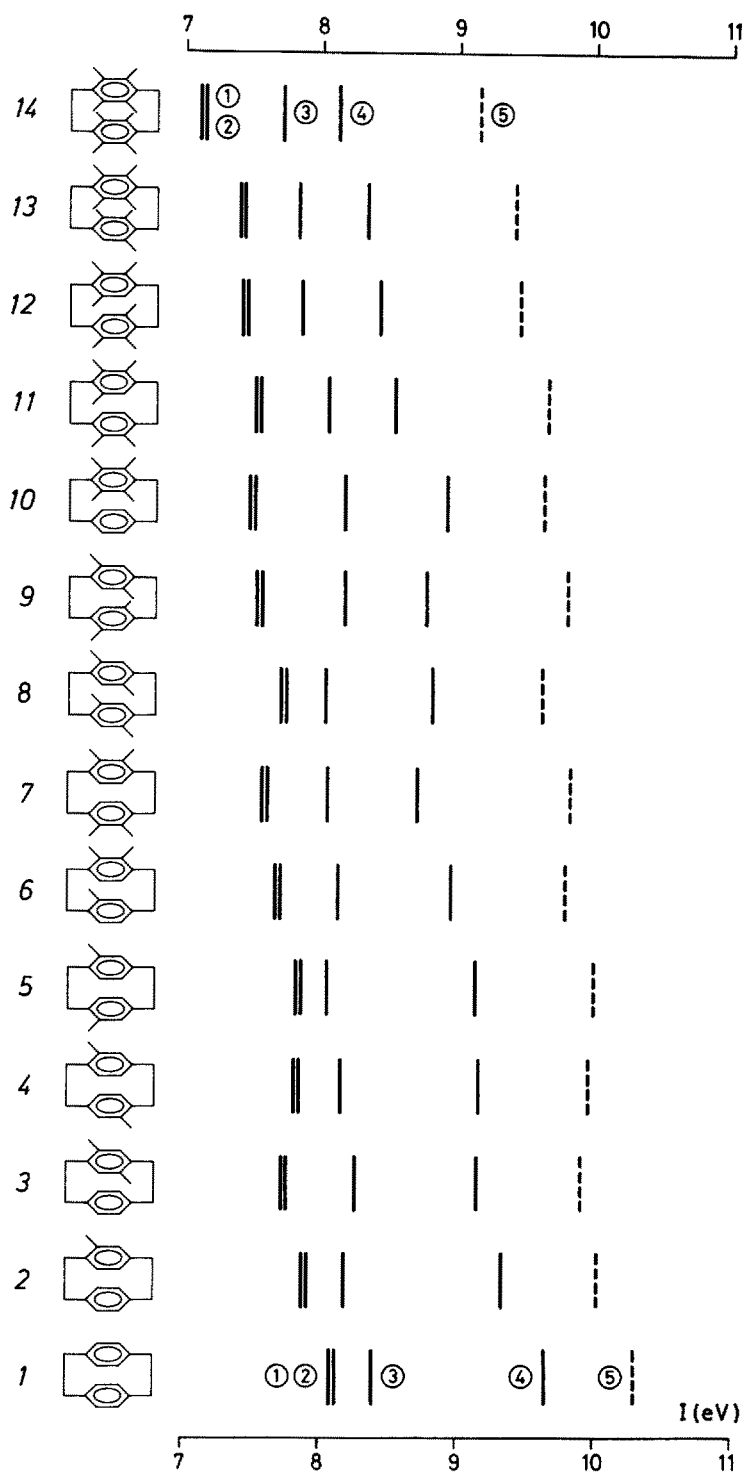
Fig. 3. Correlation of the Ionization Energies I_j^m of Methyl-substituted [2.2]Paracyclophanes (cf. Table 1)

10
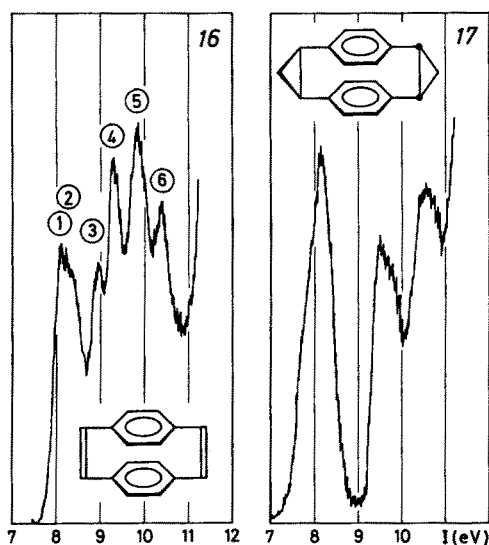
Fig. 4. PE-Spectra of the Paracyclophanes *16*[23] and *17*[24] (Spectrum of *17* redrawn from ref. [24])

3.2 [2$_n$]Cyclophanes

In Fig. 5 are presented the PE-spectra of the complete set of the [2$_n$]cyclophanes *1*, *23* to *30* (n = 2 to 6)[19] with the exception of [2.2]ortho- and [2.2]metacyclophane,
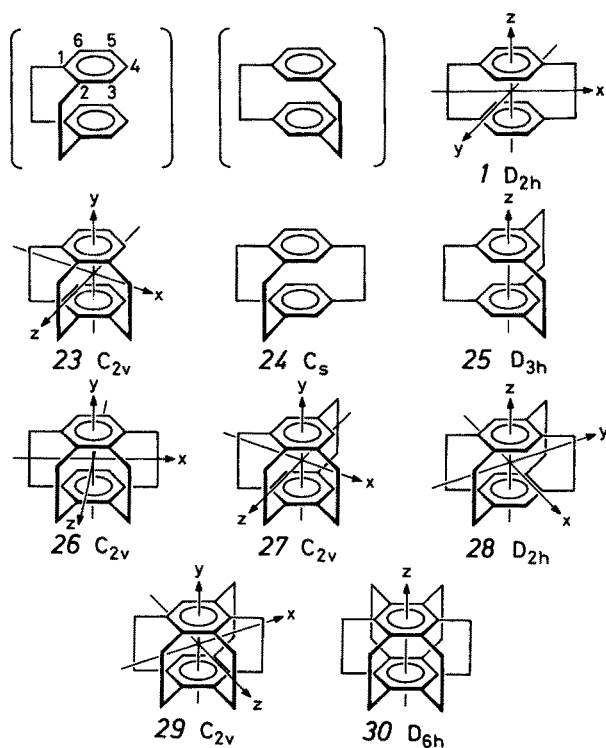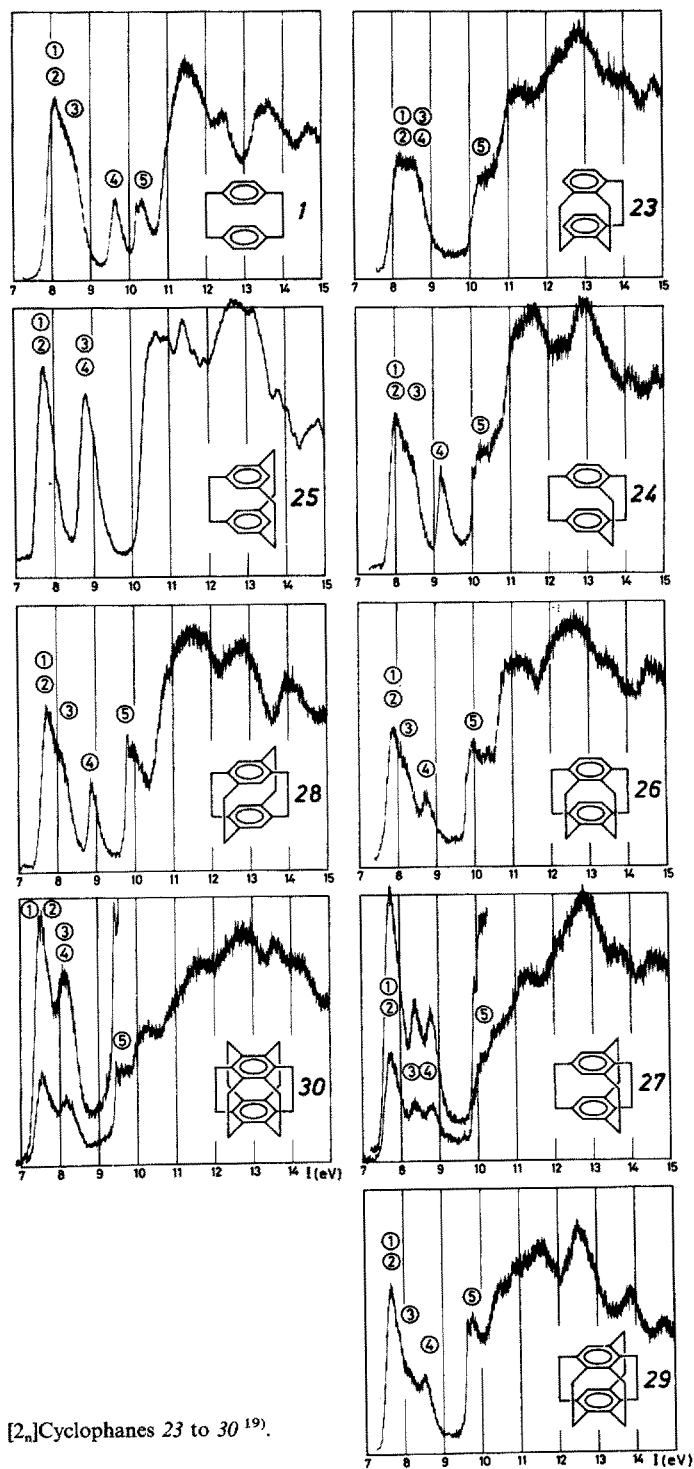
Fig. 5. PE-Spectra of the [2$_n$]Cyclophanes *23* to *30* [19].
(cf. Table 3)

Table 3. Ionization Energies I_j^m in eV of $[2_n]$Cyclophanes *23* to *32*. (See formulae in Fig. 5.)

Compound No.	Bridged centres	Bands					Ref.
		①	②	③	④	⑤	
1	(1,4)	8.1_0	(8.1_0)	8.4	9.6_5	10.3	[19]
23	(1,2,3)	8.2_0	—————————		(8.7)	10.3	[19]
24	(1,2,4)	8.0	(8.0)	8.3	9.2	10.2	[19]
25	(1,3,5)	7.70	7.70	8.75	8.75		[19, 25, 26]
26	(1,2,3,4)	7.9	(7.9)	8.1	8.7		[19]
27	(1,2,3,5)	7.75	(7.75)	8.37	8.77	~10.0	[19]
28	(1,2,4,5)	7.67	(7.67)	~8.1	8.82	9.79	[19]
29	(1,2,3,4,5)	7.67	(7.67)	~8.2	8.56	9.67	[19]
30	all	7.55	7.55	8.17	8.17	~ 9.6	[19]
31	(1,3,5)	8.06	8.06	9.24	9.24	9.4	[19, 25]
32	(1,2,4)	7.98	(7.98)	8.4	9.12	9.61	[23]
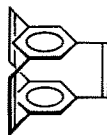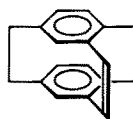
31 [25]   *32* [23]

both of which have "open" structures. The coordinate systems to which the symmetry labels will be referred to are shown in the formulae *1* and *23* to *30*. In Fig. 5, the first column of spectra contains the highly symmetric systems, (D_{2h}, D_{3h}, D_{6h}), the second those of low symmetry (C_{2v} or C_s). Their ionization energies I_j^m, as well as those of *31* [25] and *32* [23] containing unsaturated bridges are given in Table 3.

3.3 [2.2]Phanes Involving Higher Aromatic Systems

The PE-spectra of the [2.2]phanes *33* to *42* [22, 27] are shown in Fig. 6 and 7 and their ionization energies I_j^m are collected in Table 4. (Note that *34* and *37* to *40* are chiral molecules.) In all these cases the two decks are held in a more or less rigid arrangement

13
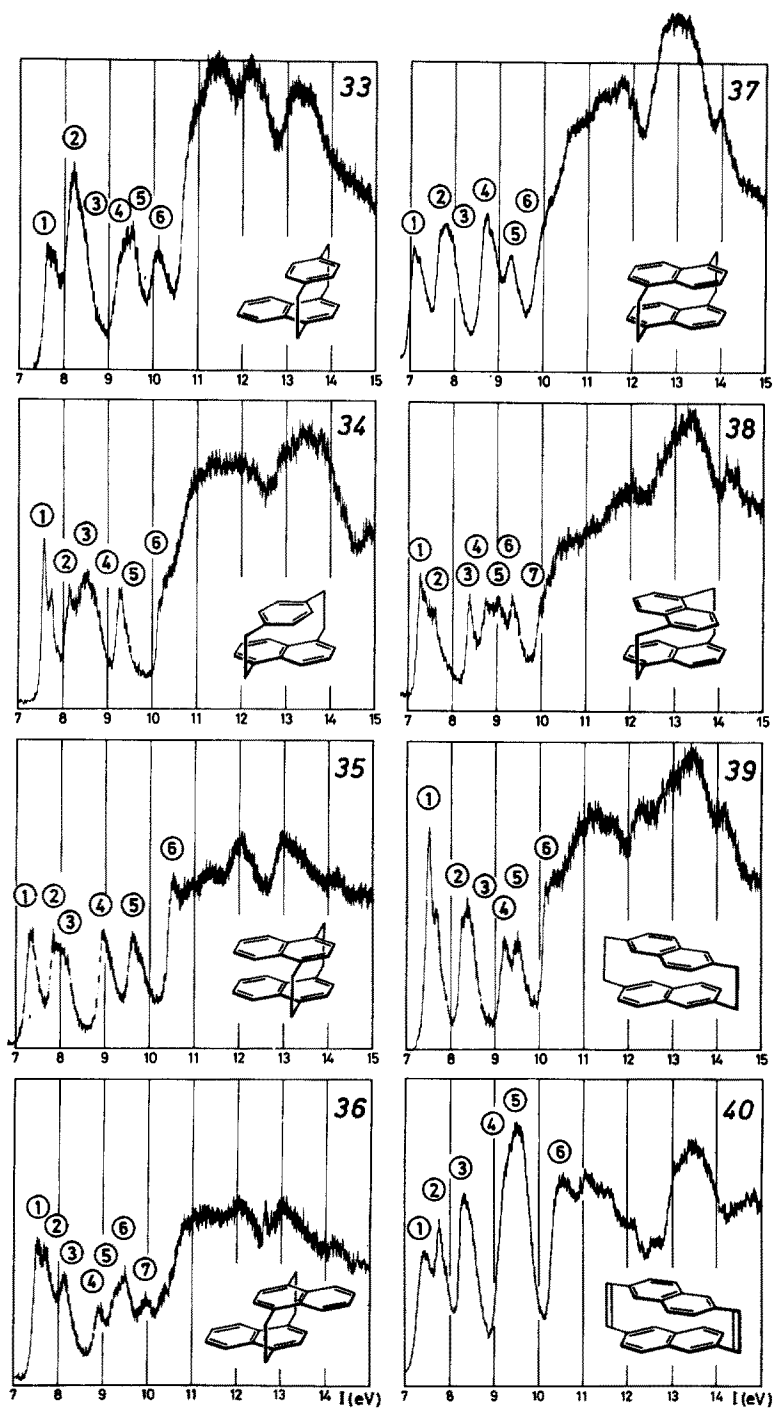
Fig. 6. PE-Spectra of the [2.2]Phanes *33* to *40* Containing Naphthalene Rings [22] (cf. Table 4)
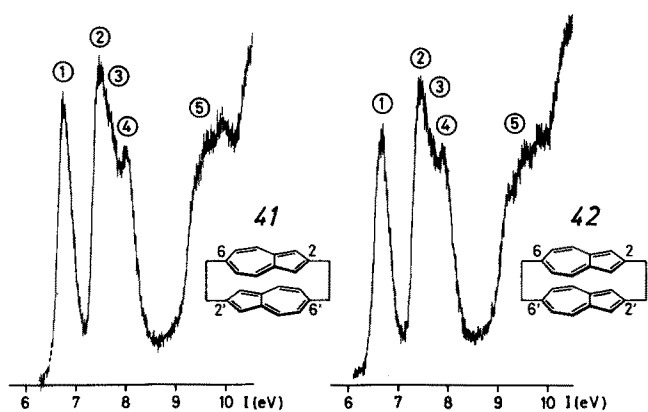
Fig. 7. PE-Spectra of *anti-* and *syn-*[2.2](2,6)Azulenophanes *41* and *42* [27)] (cf. Table 4)
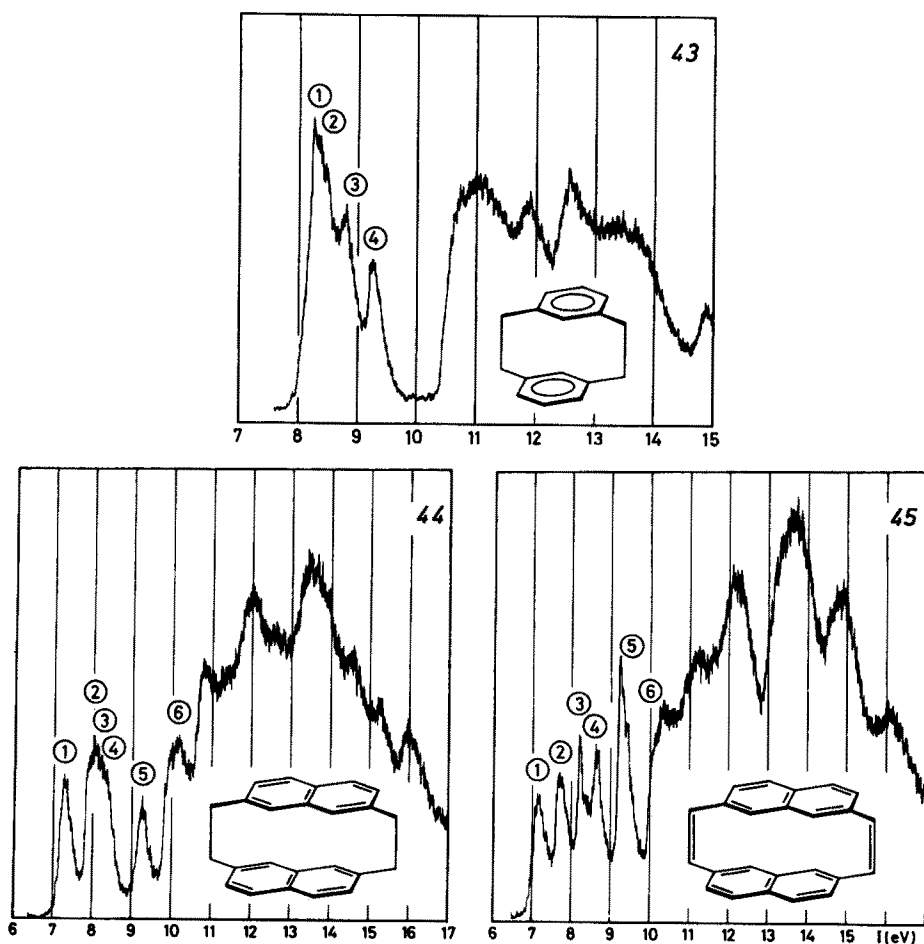
Fig. 8. PE-Spectra of [2.2]Metacyclophane *43*, [2.2](2,7)Naphthalenophane *44* and [2.2](2,7)Naphthalenophane-1,11-diene [22)]. (cf. Table 5)

Table 4. Ionization Energies I_j^m in eV of [2.2]Phanes *33* to *42*. (See formulae in Figs. 6 and 7)

Compound No.	Compound	Bands ①	②	③	④	⑤	⑥	⑦	Ref.
33	[2]Paracyclo[2](1,4)naphthalenophane	7.6_0	8.1_5		9.2_0	9.5_0	10.0_5		22)
34	[2]Paracyclo[2](1,5)naphthalenophane	7.5_6	8.1_5	8.5_0	8.7_0	9.2_5	10.2		22)
35	*syn*-[2.2](1,4)Naphthalenophane	7.2_5	7.7_5	8.0_5	8.9_0	9.5_5	10.6		22)
36	*anti*-[2.2](1,4)Naphthalenophane	7.5_0	7.7_0	8.1_0	8.9_0	9.2_5	9.5_0	9.9_5	22)
37	[2.2](1,5)Naphthalenophane (achiral)	7.0_5	7.7_0		8.7_0	9.2_5	10.0		22)
38	[2.2](1,5)Naphthalenophane (chiral)	7.2_5	7.5_0	8.3_0	8.7_0	8.9_0	9.3_0	10.0	22)
39	[2.2](2,6)Naphthalenophane (chiral)	7.52	8.30	8.4_0	9.2_5	9.6_5	10.3		22)
40	[2.2](2,6)Naphthalenophane-1,11-diene (chiral)	7.4_0	7.7_0	8.3_0		9.2	9.6	10.5	22)
41	*anti*-[2.2](2,6)Azulenophane	6.75	7.50	(7.7)	8.0_0	9.4			27)
42	*syn*-[2.2](2,6)-Azulenophane	6.65	7.45	(7.7)	7.9_0	8.2			27)

Table 5. Ionization Energies I_j^m in eV of [2.2]Metacyclophane *43*, [2.2](2,7)Naphthalenophane *44* and [2.2](2,7)Naphthalenophane-1,11-diene *45*. (See formulae in Fig. 8.)

Compound No.	Bands						Ref.
	①	②	③	④	⑤	⑥	
43[a]	8.2_0	8.4	8.7_5	9.2_0	10.7		[15,22]
44	7.3_5	——	8.0	——	9.2_5	10.1	[22]
45	7.2_0	7.7_5	8.2_0	8.6_5	9.2_5	10.1	[22]

[a] In the 6,13-dimethyl derivative of *43* the first four bands are shifted to: ① 8.0_0, ② 8.2_0, ③ ④ ~8.8 eV respectively [26].

corresponding to the situation depicted in (1), i.e. with the two parallel π-systems aligned for efficient overlap.

This is no longer the case for [2.2](2,7)naphthalenophane *44* and [2.2](2,7)naphthalenophane-1,11-diene *45* [22] which are related to [2.2]meta-cyclophane (= [2.2]-(1,3)cyclophane) *43* [15,22], the PE-spectra of which are shown in Fig. 8 (cf. Table 5) for the sake of completeness.

3.4 Heterocyclic Phanes

In Fig. 9 and 10 are shown the PE-spectra of the heterocyclic phanes *46* to *54* (with the exception of *52* [22]), the ionization energies I_j^m of which are collected in Table 6. The relative orientation of the heterocyclic moiety in *49*, *50* and *51* with respect to the naphthalene ring corresponds to that shown in the formula for *50* given below.

50   *52*
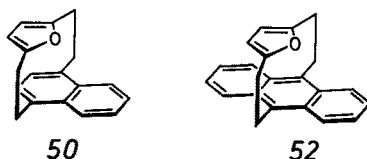
In Table 7 are presented the ionization energies I_j^m of the following cyclic phanes related to [2.2]meta-cyclophane *43*:

55   *56*   *57*

58   *59*   *60*
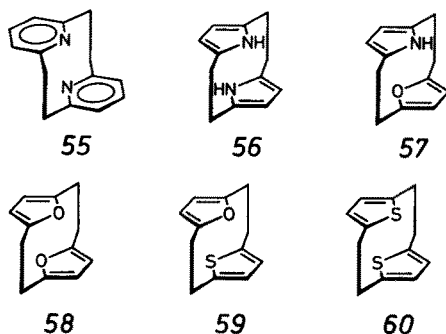
Table 6. Ionization Energies I_j^m in eV of Heterocyclic Phanes. (See formulae in Fig. 9 and 10)

Compound No.	Bands							Ref.
	①	②	③	④	⑤	⑥	⑦	
46 [2](2,5)Pyrrolo[2]paracyclophane	7.42	8.3_5		9.2_0	10.6_5	11.3		22)
47 [2](2,5)Furano[2]paracyclophane	7.78	8.00	8.7_5	9.7_5	10.5_0	11.3		22)
48 4-Aza[2.2]paracyclophane	8.2_0	8.5_0	8.8_5	9.2_0	10.0_5	10.6		22)
49 anti-[2](2,5)Pyrrolo[2](1,4)naphthalenophane	7.3_5	7.7_5	8.3_0	9.00	9.5_5	10.1_5	11.0	22)
50 anti-[2](2,5)Furano[2](1,4)naphthalenophane	7.46	7.95	8.4_5	9.3_0	9.7_0	10.0_5	10.8_5	22)
51 anti-[2](2,5)Thiopheno[2](1,4)naphthalenophane	7.5_0	7.9_5		9.2_5	10.1_5	10.9		22)
52 [2](2,5)Furano[2](9,10)anthracenophane	6.87	7.7_5	8.2_0	8.86	9.3_5	9.7_5	10.5_0	22)
53 4,13-Diaza[2$_4$](1,2,4,5)cyclophane		~8.2		8.9		9.7	10.5	28)
54 4,16-Diaza[2$_4$](1,2,4,5)cyclophane	8.1		8.6		9.3	9.8	10.5	28)

Table 7. Ionization Energies I_j^m in eV of the Heterocyclic Phanes related to meta-Cyclophane 43

Compound No.	Bands					Ref.
	①	②	③	④	⑤	
55 anti-[2.2](2,6)Pyridinophane	8.3_5	8.9_5	9.8_0	10.03		29)
56 anti-[2.2](2,5)Pyrrolophane	7.4_5	7.8_0		8.9_0	11.3	22,30)
57 anti-[2.2](2,5)Furano(2,5)pyrrolophane	7.35	8.3_0	8.6_5	10.0_0	11.4	22)
58 anti-[2.2](2,5)Furanophane	7.67	8.19		9.7_0	11.6	22,30)
59 anti-[2.2](2,5)Thiopheno(2,5)furanophane	7.8_5	8.0_5	8.6_5	9.7_0		30)
60 anti-[2.2](2,5)Thiophenophane	7.9_5		8.2_5	9.1_5	10.7_0	22,30)
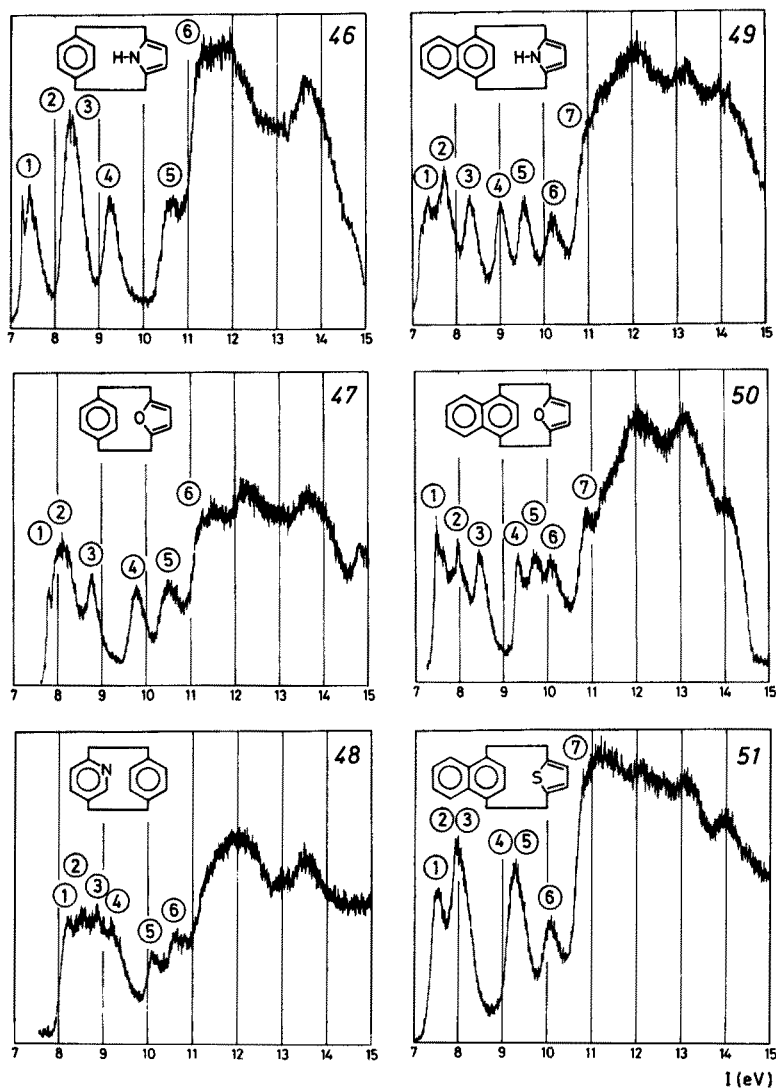
Fig. 9. PE-Spectra of the Heterocyclic Phanes *46* to *51* [22]. (cf. Table 6)

3.5 Miscellaneous Systems

Although there are many molecules in which two π-systems are held in close contact, and which are therefore relevant to the cyclophane problem, we limit ourselves to only a few systems, to which we shall have occasion to refer in the subsequent chapters.
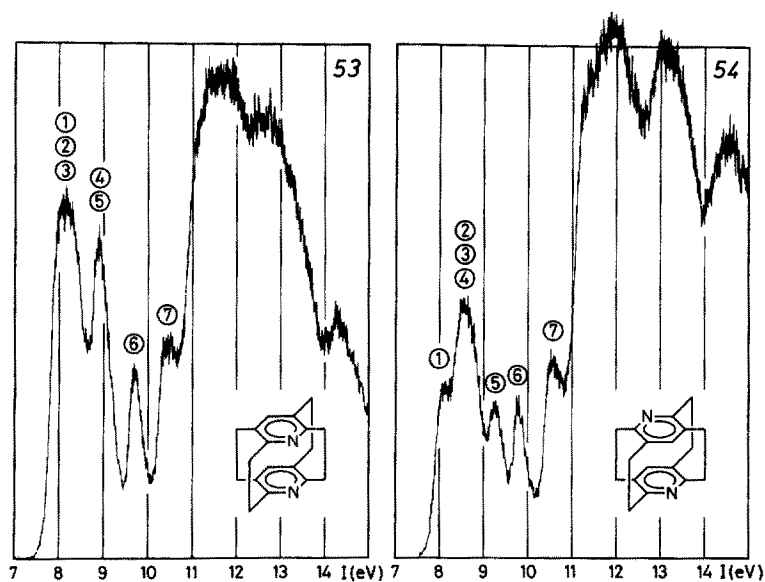
Fig. 10. PE-Spectra of 4,13-Diaza- and 4,16-Diaza-[2₄](1,2,4,5)cyclophanes *53* and *54*. (cf. Table 6)

In Fig. 11 are shown the PE-spectra of the [m.n](1,4)cyclophanes (= [n.m]para-cyclophanes) [23)] with [m.n] = [2.3], [3.3], [3.4] and [4.4]. Their ionization energies I_j^m are listed in Table 8, together with those of the compounds *65* to *71*.
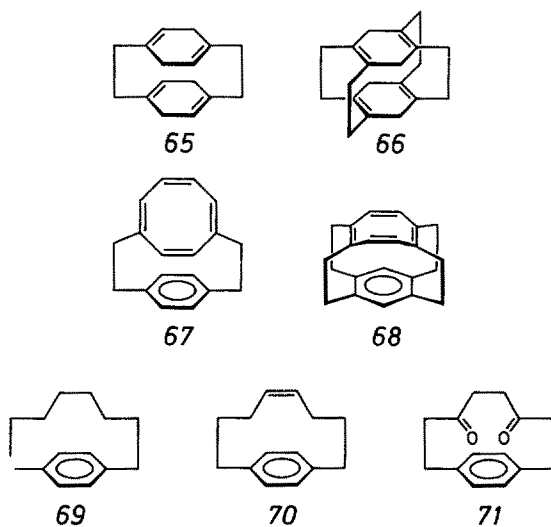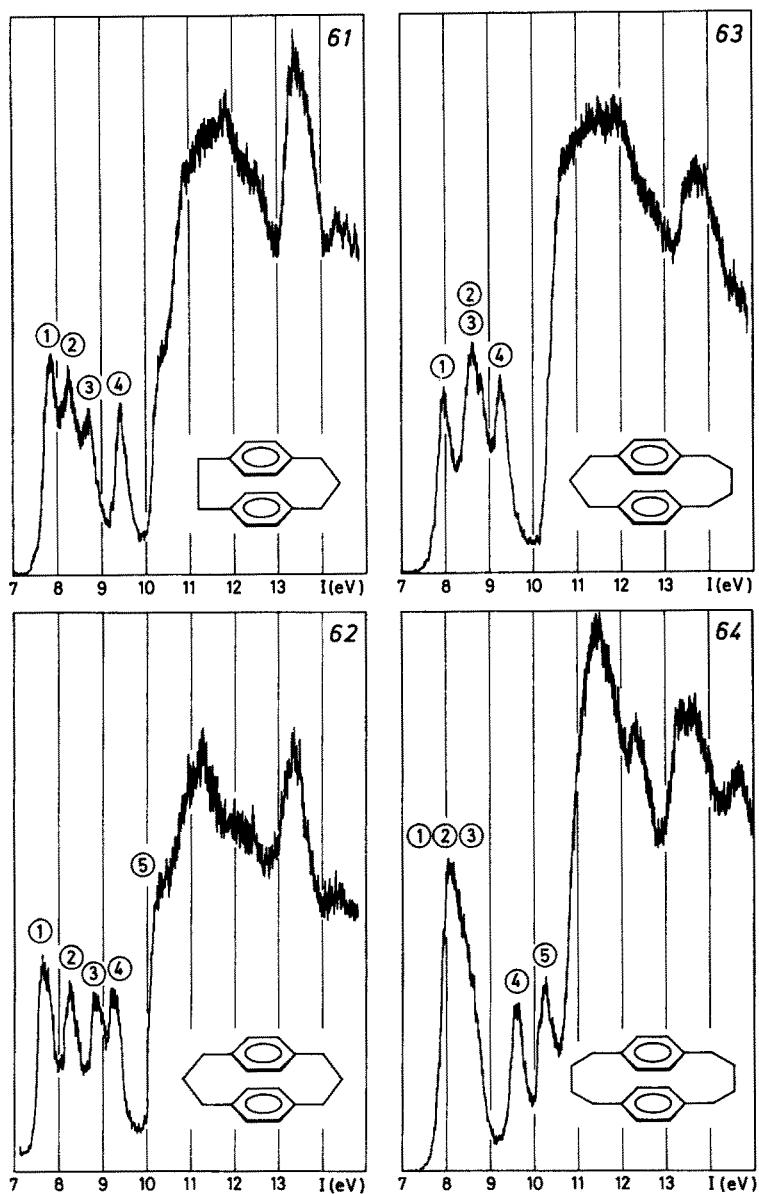
Fig. 11. PE-Spectra of [m.n]Paracyclophanes with [m.n.] = [2.3], [3.3], [3.4] and [4.4]

Table 8. Ionization Energies I_j^m in eV of Miscellaneous Cyclophanes

Com-pound No.		Bands					Ref.
		①	②	③	④	⑤	
61	[2.3]Paracyclophane	7.8_5	8.2_5	8.7_0	9.4_5		[23]
62	[3.3]Paracyclophane						[23]
63	[3.4]Paracyclophane	7.9_5	——— 8.6 ———		9.2_5		[23]
64	[4.4]Paracyclophane	——— 8.0_5 ———			9.5_5	10.2_0	[23]
65		——— 8.3_0 ———		——— 8.8_0 ———		10.5	[31]
66		——— $7.8\text{--}8.5$ ———				9.5_5	[19]
67		7.6_5	8.1_0	8.9_5	9.2_5	9.5_0	[32]
68		7.8_5	8.3_5	8.7_0	9.2_0	9.9_0	[32]
69	[8]Paracyclophane	8.17	8.81				[4,31]
70	[8]Paracyclophane-4-ene	8.37	9.02				[4,31]
71	[8]Paracyclophane-3,6-dione	8.9_5	9.6_0				[23]

4 Theoretical Model

4.1 Basis π-Orbitals

In view of the abundant experimental material, the discussion and rationalization of the electronic structure of the cyclophanes, and thus of their PE-spectra, can be couched in a simple Hückel-type molecular orbital (HMO) language. This implies that the HMO energies ε_j calculated according to such a calibrated scheme satisfy the Koopmans' relationship

$$I_j^m = -\varepsilon_j \tag{3}$$

and that the corresponding vacated HMO ψ_j determines the symmetry behaviour of the radical cation state ψ_j^{-1}.
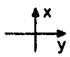
As a start we use *standard* HMO°s (superscript "o") [33]

$$\Phi_{r, J}^o = \sum_\mu c_{\mu J}^o \phi_\mu \tag{4}$$

for the π-orbitals of the lower (r = l) and upper (r = u) moieties M_r of the cyclophanes as defined in (1). The $1a_{2u}$ π-HMO° of a benzene ring is abbreviated as O_r^o and the two $1e_{1g}$ π-HMO°s, in real representation, as A_r^o and S_r^o, the former being anti-symmetric, the latter symmetric with respect to the symmetry plane passing through centres 1 and 4. For the naphthalene systems, the five bonding π-HMO°s are $N_{r,1}^o$, $N_{r,2}^o$, $N_{r,3}^o$, $N_{r,4}^o$ and $N_{r,5}^o$ in ascending order of energy [33] (cf. Table 9). In a simple, but adequate approximation, the two moieties M_l and M_u in (1) are restricted to two hypothetical, parallel planes separated by a mean inter-deck distance D. It will prove necessary to compute overlap integrals

$$S_{I, J} = \langle \Phi_{l, I} \mid \Phi_{u, J} \rangle \tag{5}$$

Table 9. Basis π-HMOs. The Index r Refers to the Lower (r = l) or Upper (r = u) Moieties M_r of (1)

Orbital	$\begin{array}{c} \uparrow x \\ \overline{}\!\!\rightarrow y \end{array}$	Local Symm.[a]	Renorm. Factor N_J	Basis energy $A(\Phi_{r,J})/eV$
S_r		B_{2g}	0.9147	— 9.0
		(E_{1g})		
A_r		B_{3g}	0.9147	— 9.0
O_r		(A_{2u}) B_{1u}	0.7977	—12.2
$N_{r,5}$		A_u	0.9599	— 7.90
$N_{r,4}$		B_{1u}	0.9209	— 8.63
$N_{r,3}$		B_{2g}	0.8830	— 9.73
$N_{r,2}$		B_{3g}	0.8399	—10.59
$N_{r,1}$		B_{1u}	0.7714	—12.25

[a] Local symmetries are given with respect to the group D_{2h}. Values in brackets refer to D_{6h} local symmetry.

between pairs of π-HMOs $\Phi_{l,I}$ and $\Phi_{u,J}$ as a function of the inter-deck distance D. Inserting the linear combinations for $\Phi_{l\,I}$ and $\Phi_{u,J}$ into (5) yields

$$S_{IJ} = \sum_\mu \sum_\nu c_{\mu I} c_{\nu J} S_{\mu\nu} \, , \tag{6}$$

where $S_{\mu\nu}$ stands for the overlap integral $S_{\mu\nu} = \langle \phi_\mu | \phi_\nu \rangle$ between two $2p_z$ atomic orbitals of M_l and M_u respectively. The latter overlap integrals $S_{\mu\nu} = S_{\mu\nu}(R_{\mu\nu}, \theta_{\mu\nu})$ depend both on the distance $R_{\mu\nu}$ and on the angle $\theta_{\mu\nu}$, which the $2p_z$ orbital axes make with the line joining the centres μ and ν of the lower and upper deck, respectively. For D = 0 we must have $S_{JJ} = 1$ if the orbitals $\Phi_{r,J}$ are required to be normalized [34]. However, this is not the case if the coefficients $c^o_{\mu J}$ of the HMO°s (4) are used in (6), because the latter have been normalized under the assumption $S_{\mu\mu'} = \delta_{\mu\mu'}$. It is therefore necessary to renormalize them through multiplication by a factor

$$N_J = \left(\sum_\mu \sum_{\mu'} c^o_{\mu J} c^o_{\mu' J} S_{\mu\mu'} \right)^{-1/2} \tag{7}$$

This yields the orbitals

$$\Phi_{r,J} = N_J \Phi^o_{r,J} = \sum_\mu c_{\mu J} \phi_\mu \tag{8}$$

with $c_{\mu J} = N_J c^o_{\mu,J}$. If Slater 2p-orbitals with atomic orbital exponents of 1.625 are used for the computation of the $S_{\mu\nu}$, then the renormalization coefficients N_J given in Table 9 [34] are obtained.

Note that two different molecular orbitals $\Phi_{1,I}$, $\Phi_{u,J}$ belonging to the same irreducible representation within the local symmetries of M_I or M_μ are no longer strictly orthogonal according to (5) and (6), even if two planar, eclipsed moieties at distance D are assumed. However the S_{IJ} values will be very small and can thus be neglected for all practical purposes.

If M_1 and M_r are no longer eclipsed, but shifted and twisted with respect to each other, e.g. in 34, 38, 39, 40, 41 or in the metacyclophane-type systems, formula (6) still applies. As an example we show in Fig. 12 the dependence of S_{IJ} on the twist angle α for two parallel naphthalene moieties with common z-axis and separated by D = 300 pm, as present in a first approximation in 38 and 39, the projections of which are shown in the following diagrams [34]:

$$\alpha \approx 55° \qquad 38 \qquad \alpha \approx 40° \qquad 39 \tag{9}$$
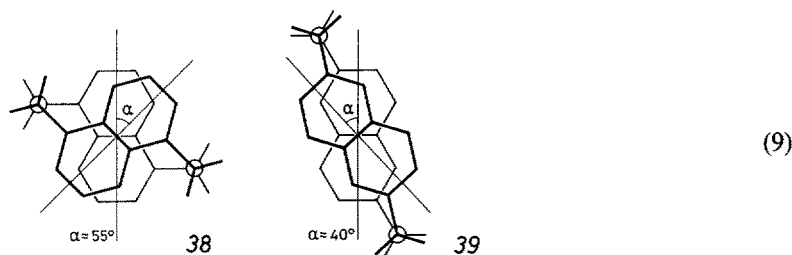
The basis energies $A(O_r)$, $A(S_r)$ and $A(A_r)$ given in Table 9 for the benzene π-HMOs in the cyclophanes 1 to 34, 43 and 61 to 71 are carried over from previous work [17,19]. There it has been shown that it is appropriate to correct the values $A°(S_r) = A°(A_r) = -9.25$ eV of the frontier orbitals of benzene, derived by applying Koopmans' theorem in reverse to the corresponding observed ionization energy,
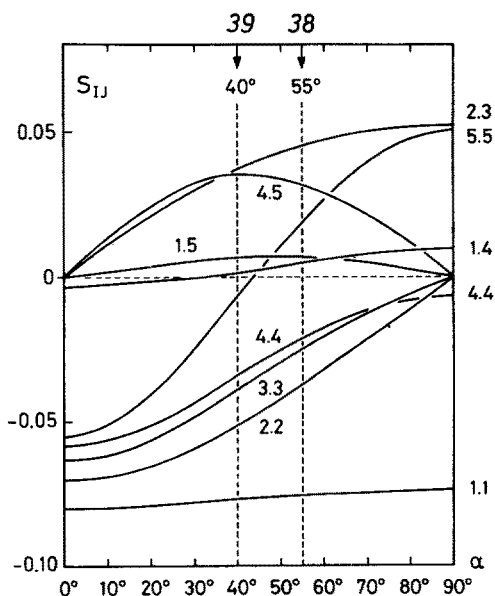
Fig. 12. Dependence of the Overlap Integral S_{IJ} (5) (6) on the Twist Angle α Around the z-Axis for Two Parallel Naphthalene Moieties Separated by D = 300 pm. The dotted vertical lines at $\alpha = 55°$ and $\alpha = 40°$ refer to compounds 38 and 39 respectively, in the conformations given in (9)

by $+0.25$ eV, to absorb roughly the neglected destabilizing effects which occur when a basis π-orbital is imbedded in the cyclophane system. In analogy, the π-orbital basis energies $A(N_2)$ to $A(N_5)$ of the naphthalene moieties in the cyclophanes *33* to *40* and *44, 45* are postulated to be equal to the negative vertical ionization energies of the first four π-bands in the photoelectron spectrum of naphthalene [35] corrected again by $+0.25$ eV. However the position of the fifth π-band is not exactly known. Therefore the value $A(N_1)$ has been extrapolated using linear regressions of $A(N_2)$ to $A(N_5)$ vs. the corresponding computed π-orbital energies [36] and the π-orbital energy of N_1 obtained by the same theoretical procedure.

4.2 Basis σ-Orbitals for the Bridging Alkyl Chains

The second set of basis orbitals needed are those of the ethano groups bridging the positions μ, μ' of the two decks in the major part of the systems under consideration, or those of the longer alkyl chains, e.g. in *61* to *64*.

The five doubly occupied semi-localized orbitals of each ethano-group (discounting the two σ-bonds which link it to the benzene moieties) can be represented in equivalent orbital diagrams as follows (μ = position of attachment):

$$\begin{array}{ccccc} \varphi_\mu^{(1)} & \varphi_\mu^{(2)} & \varphi_\mu^{(3)} & \varphi_\mu^{(4)} & \varphi_\mu^{(5)} \\ s & a & s & a & s \end{array}$$

$$\text{ascending orbital energy} \longrightarrow$$

(10)
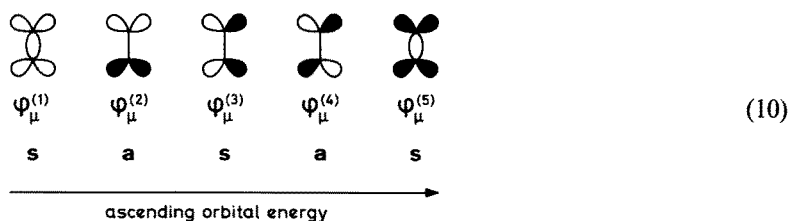
A crude estimate of the orbital energies is obtained by applying a Hückel-type model proposed recently [37]. This model uses localized bond orbitals λ_{CC} and λ_{CH}, and takes only geminal interactions into account. With the basis energies $A_{CC} \approx A_{CH} \approx -17$ eV and $B_{gem.} \approx -2$ eV the eigenvalues $\varepsilon_1 \approx -22$ eV, $\varepsilon_2 \approx -19$ eV, $\varepsilon_3 = \varepsilon_4 \approx -15$ eV and $\varepsilon_5 \approx -14$ eV are calculated.

By the same treatment we can derive the nodal properties and rough approximations for the orbital energies of the $CH_2CH_2CH_2$ bridge orbitals, e.g. of *62*. The 8 σ-orbitals so obtained exhibit the following symmetry behaviour:

$$\begin{array}{cccccccc} \eta_\mu^{(1)} & \eta_\mu^{(2)} & \eta_\mu^{(3)} & \eta_\mu^{(4)} & \eta_\mu^{(5)} & \eta_\mu^{(6)} & \eta_\mu^{(7)} & \eta_\mu^{(8)} \end{array}$$

$$\text{ascending orbital energy} \longrightarrow$$

(11)
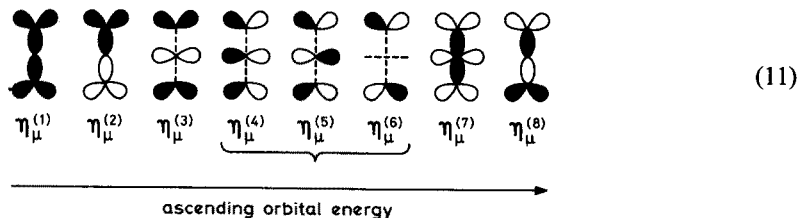
The corresponding orbital energies are $\varepsilon_1 \approx -24$ eV, $\varepsilon_2 \approx -20.5$ eV, $\varepsilon_3 \approx -19$ eV, $\varepsilon_4 = \varepsilon_5 = \varepsilon_6 \approx -15$ eV, $\varepsilon_7 \approx -14$ eV and $\varepsilon_8 \approx -13.5$ eV.

25

Although this assessment of the orbital energies for $\varphi_\mu^{(j)}$ and $\eta_\mu^{(j)}$ is rather crude, the ε_j values obtained are of sufficient quality for the purpose of the ensuing discussions. In addition the most important feature of these orbitals, i.e. their symmetry behaviour, is faithfully reproduced.

4.3 "Through Space" π-π Interaction

The orbital interaction pattern in *1* was first analysed in terms of "through-space" and "through-bond" interactions [10] by Gleiter [16]. Later Boschi and Schmidt [15] provided a semi-quantitative assessment of the magnitude of the "through-space" coupling parameter

$$\tau_{IJ} = \langle \Phi_{l,I} | \hat{H} | \Phi_{u,J} \rangle \tag{12}$$

between two highest occupied basis π-orbitals of the lower and upper deck, by using the PE-spectroscopic data of *1, 25, 31* and *43*. Although the theoretical procedure used for the computation of the coupling parameter τ_{IJ} and thus its exact meaning remained undefined (cf. footnote 11 in Ref. [15]), the results clearly demonstrated that τ_{IJ} decreases with increasing mean interdeck distance D. This was supported by the more detailed analysis of the photoelectron spectra of compounds *1, 23, 25, 26, 29* and *30* [19] for which the mean interdeck distances D are known from x-ray structure data: D (*1*) = 299.5 pm [1]; D (*23*) = 337 pm; D (*25*) = 279.5 pm; D (*26*) = 293.5 pm; D (*29*) = 270.5 pm; D (*30*) = 263 pm [38]. As discussed in Ref. [19] the "through-space" coupling parameter

$$\tau = \langle A_l | \hat{H} | A_u \rangle = \langle S_l | \hat{H} | S_u \rangle \tag{13}$$

of the [2$_n$]cyclophanes, assuming parallel, eclipsed decks, can be directly read off the PE-spectra. Matching τ and D yielded the linear regression

$$\left(\frac{\tau}{eV} \right) = 4.9 - 0.0132 \left(\frac{D}{pm} \right) \tag{14}$$

valid for the interval 260 pm < D < 350 pm (see Fig. 13, A).

In the following we shall assume that the "through-space" interaction parameter τ_{IJ} (12) is proportional to the overlap S_{IJ} (5), (6) between the two basis orbitals involved, i.e.

$$\tau_{IJ} = -\tau_0 \cdot S_{IJ} = -\tau_0 N_I N_J S_{IJ}^0 \tag{15}$$

Accordingly, τ_{IJ} is a function of the distance D between the two moieties M_l and M_u, of their relative orientations and of their relative shifts in the x and/or y direction. If the z-axis is oriented as shown in (1) and if the phases of all $2p_z$ atomic orbitals ϕ_μ of the basis π-orbitals $\Phi_{r,j}$ are the same with respect to this orientation, then the overlap integrals S_{II} between two orbitals $\Phi_{l,I}$ and $\Phi_{u,I}$ of same type, will be negative for distances in the interval 260 pm < D < 350 pm, and thus the τ_{II} positive.

26
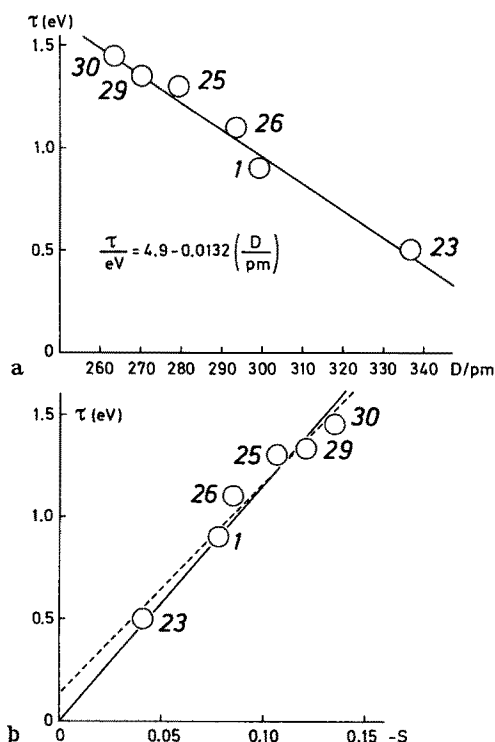
Fig. 13. Dependence of the "Through space" Coupling Parameter τ on A) the Mean Interdeck Distance D, and B) the π-Orbital Orverlap S Calculated According to (6)

If for the six cyclophanes underlying regression (14) one computes the overlaps S_{AA}, S_{SS} and S_{OO} assuming that M_l and M_u are planar, fully eclipsed (i.e. with a common sixford axis), parallel and separated by the mean inter-deck distances D given above, then the plot of $\tau = \tau_{AA} = \tau_{SS}$ vs. $S = S_{AA} = S_{SS}$ shown in Fig. 13, B yields the regression

$$-\left(\frac{\tau}{eV}\right) = (0.13 \pm 0.10) + (10.25 \pm 1.04) \cdot S, \tag{16}$$

where the first term is not significantly different from zero. If the regression is forced through the origin $S(\infty) = 0$, $\tau = 0$, then a least squares treatment yields

$$\left(\frac{\tau}{eV}\right) = -(11.52 \pm 0.34) \cdot S(D). \tag{17}$$

This is the regression which has been used subsequently. Both (16) and (17) are displayed graphically in Figure 13, B. The τ-values derived from (17) agree rather nicely with those obtained by Koutecky and Paldus [39] by a completely independent, purely theoretical assessment.

If we restrict our attention to the basis π orbitals A_u, A_l, S_u and S_l of the $[2_n]$cyclophanes, one finds for the (assumed) planar and eclipsed moieties M_u, M_l that $\tau_{AA} = \tau_{SS} = \tau$ and $\tau_{AS} = 0$. Because of the sign convention introduced above one

27

has $\tau > 0$ and the resultant linear combinations under pure "through-space" inter-
action are

$$A_+ = (A_u + A_l)/\sqrt{2} \qquad \varepsilon(A_+) = -9\,\text{eV} + \tau$$

$$A_- = (A_u - A_l)/\sqrt{2} \qquad \varepsilon(A_-) = -9\,\text{eV} - \tau$$

$$\text{(18)}$$

$$S_+ = (S_u + S_l)/\sqrt{2} \qquad \varepsilon(S_+) = -9\,\text{eV} + \tau$$

$$S_- = (S_u - S_l)/\sqrt{2} \qquad \varepsilon(S_-) = -9\,\text{eV} - \tau$$

Attention is drawn to the fact that the plus-combinations A_+, S_+ are *antisymmetric*
(a), the minus-combinations A_-, S_- *symmetric* (s) with respect to the x, y plane
passing through the middle of the system (1) and that the degenerate pair A_+, S_+ lies
above the degenerate pair A_-, S_-. For added clarity this is graphically represented
in the following diagram.

$$\text{(19)}$$
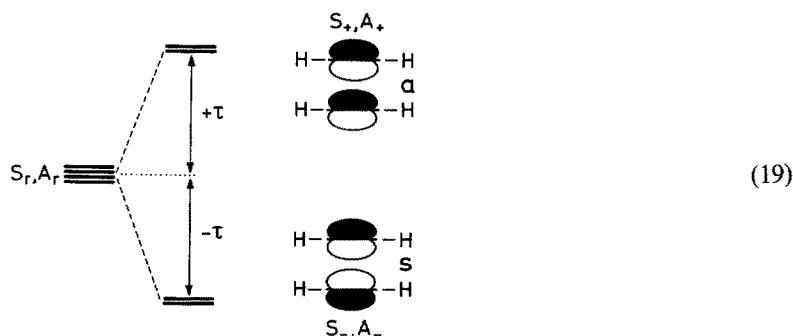
A nice verification of the relationships (14) and (17) is provided by the first
electronic transition of the benzene dimer radical cation [40,41] which may be viewed as
"zerophane" ($= $ "[0](0)cyclophane"), assuming that it has a D_{6h} structure.
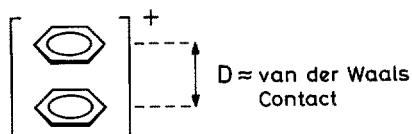
If the two benzene moieties are in van der Waals contact, i.e. $D \approx 320$ to 330 pm,
then (14) and (17) yield $\tau \approx 0.7$ to 0.5_5 eV. We predict therefore that the electronic
ground state $^2E_{1g}$ of the dimer cation and the first electronically excited state $^2E_{1u}$
are separated by $2\tau = 1.4$ to 1.1 eV and that this transition is electronically allowed.
The value observed by Bühler and Funk [41] is 1.33 eV, in complete agreement with the
one derived from our simple model.

4.4 "Through Bond" Interaction

Starting with the linear combinations A_+, A_-, S_+, S_- (18) (19), split by 2τ as a consequence of pure "through space" interaction, we now introduce in a second step their "through bond" interaction via the relay orbitals $\varphi_\mu^{(j)}$ (10). (The analogous interaction via the orbitals $\eta_\mu^{(j)}$ (11) will be discussed later in connection with the [m.n]paracyclophanes; cf. Sect. 5.4).

With reference to Fig. 14, let $X_\pm$ stand for $A_\pm$ or $S_\pm$. From the diagrams (10) of the bridge orbitals $\varphi_\mu^{(j)}$ it is obvious that their interaction with X_+ and/or X_- is severely restricted by symmetry. To begin with $\varphi_\mu^{(1)}$, $\varphi_\mu^{(3)}$ and $\varphi_\mu^{(5)}$, which are symmetric with respect to the median x,y-plane can interact only with X_-, whereas $\varphi_\mu^{(2)}$ and $\varphi_\mu^{(4)}$ which are antisymmetric interact only with X_+. However, the 2p atomic orbitals ϕ_μ (see (4) and (8)) available in positions μ have a local symmetry which prevents conjugation with $\varphi_\mu^{(3)}$ or $\varphi_\mu^{(4)}$, both of which are antisymmetric with respect to a plane containing the z-axis, the atomic orbital ϕ_μ and the CC bond of $\varphi_\mu^{(j)}$. Finally $\varphi_\mu^{(1)}$ is essentially of local σ-symmetry with respect to the bond joining the CH_2CH_2 bridge to the benzene ring and thus locally orthogonal to ϕ_μ at the point of attachment. We are left with the result that only $\varphi_\mu^{(5)}$ can interact significantly with X_- and only $\varphi_\mu^{(2)}$ with X_+. This is shown graphically in Fig. 14. The corresponding cross terms are

$$\langle \varphi_\mu^{(5)} | \hat{H} | X_- \rangle = c_{\mu X} \sqrt{2}\, B$$

$$\langle \varphi_\mu^{(2)} | \hat{H} | X_+ \rangle = c_{\mu X} \sqrt{2}\, B'$$

(20)
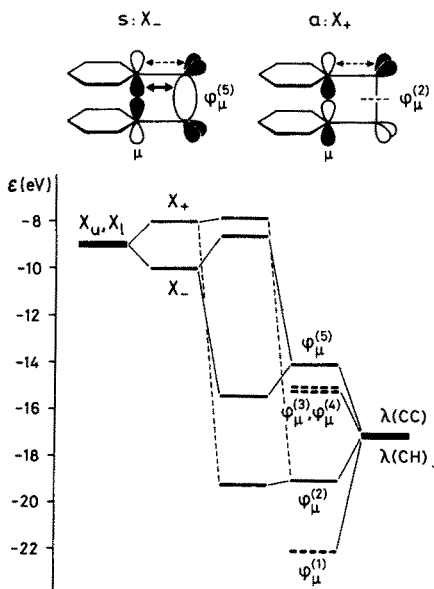
Fig. 14. Diagram Depicting the "Through Bond" Interaction in a $[2_n]$Cyclophane. The bridge orbitals $\varphi_\mu^{(1)}$ to $\varphi_\mu^{(5)}$ are shown graphically in (10)

29

where $c_{\mu X}$ is the coefficient of ϕ_μ in the linear combination (8) for X_1 (or X_u). B $\approx$ —2.4 eV, is the resonance integral which has been derived previously for the hyper-conjugative interaction of an alkyl group with a 2p atomic orbital of an unsaturated or aromatic π-system [6,42]. In contrast B' is not known, but must be much smaller than B, as implied in the top diagrams of Figure 14. A conservative guess suggests that the "through bond" induced shift of X_+ is only a tenth of that experienced by X_- [19] and can therefore be absorbed in the assumed basis energies $A(S_r)$, $A(A_r)$ (cf. Sect. 4.1).

5 Assignment and Discussion of the PE Spectra

5.1 [2_n]Cyclophanes

The key compounds for the assignment of the PE-spectra of the cyclophanes are the [2_n]cyclophanes *1*, *23* to *30*, because they form a complete set, which lends itself ideally to the usual correlation procedure [43]. They are ideally set up for "through space" and "through bond" interaction of the benzene moiety π-orbitals and it is found that the application of the approximations discussed in sections 4.1 to 4.4 yields a convincing assignment of their PE-spectra [19].

The model linear combination that has been used is

$$\psi = \sum_{J,s} a_{J,s} X_{J,s} + \sum_\mu b_\mu \varphi_\mu^{(5)} \tag{21}$$

where $X_{J,s}$ stands for $X_{1,s} = A_s$, $X_{2,s} = S_s$, $X_{3,s} = O_s$ with the sign s equal to either "+" or "—" (cf. (8)). Note that this model is based on a series of simplifying assumptions. The basis set takes into account only the occupied π-orbitals of M_l and M_u, and only the bridge orbitals $\varphi_\mu^{(5)}$, for reasons explained in Section 4.4. Furthermore the model neglects the influence of the buckling and the relative tilt of M_l and M_u, assuming that they are parallel and eclipsed with a mean interdeck distance D which, however, changes from compound to compound (cf. Sect. 4.3).

Under these conditions the linear combinations A_+ and S_+ (18) are a degenerate pair of eigenfunctions of our model. With the possible exception of *23*, which has a pronounced open-clam-like structure [38], the pair of orbitals A_+, S_+ are the HOMOs of the [2_n]cyclophanes. Consequently the positions $I_1^m = I_2^m$ of the first double band ① ② in their PE-spectra yield according to (3) and (18) the "through-space" coupling parameter τ, i.e.

$$\tau = 9\ eV - I_1^m \tag{22}$$

This relationship has been used to establish the correlations (14), (16) and (17) (see Fig. 13).

Using the parameters presented in the previous chapter 4, the following assignment for the first four bands of the $[2_n]$cyclophanes has been derived:

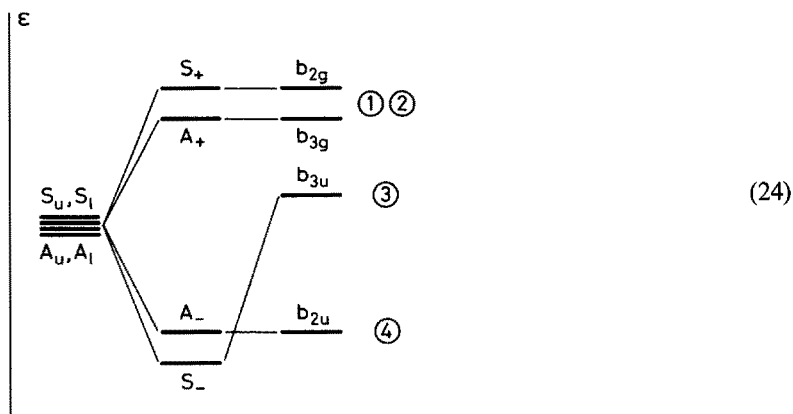|	①		②		③		④	
1	$b_{2g}(S_+)$	8.10	$b_{3g}(A_+)$	8.10	$b_{3u}(S_-)$	8.50	$b_{2u}(A)_-)$	9.90
23[a]	$a_1(S_-)$	8.24	$b_1\ (A_-)$	8.46	$b_2\ (S_+)$	8.50	$a_2\ (A_+)$	8.50
24	$a''(S_+)$	8.00	$a''(A_+)$	8.00	$a'\ (S_-)$	8.36	$a'\ (A_-)$	9.41
25	$e''(S_+;A_+)$	7.80			$e'(S_-;A_-)$	9.04		(23)
26	$a_2\ (S_+)$	8.00	$b_2\ (A_+)$	8.00	$b_1\ (S_-)$	8.31	$a_1\ (A_-)$	8.67
27[b]	$b_2\ (S_+)$	7.70	$a_2\ (A_+)$	7.70	$a_1\ (S_-)$	8.49	$b_1\ (A_-)$	9.12
28[c]	$b_{2g}(S_+)$	7.70	$b_{3g}(A_+)$	7.70	$b_{2u}(A_-)$	8.28	$b_{3u}(S_-)$	9.46
29[d]	$b_2\ (S_+)$	7.70	$a_2\ (A_+)$	7.70	$b_1\ (A_-)$	8.28	$a_1\ (S_-)$	8.75
30	$e_{1g}(S_+;\ A_+)$	7.60			$e_{1u}(S_-;A_-)$	8.36		

To make optimal use of the symmetries of the basis π-orbitals $S_\pm$, and $O_\pm$, the calculated models carry the bridging groups in the following positions: a) *23*(1,2,6); b) *27*(1,2,4,6); c) *28*(2,3,5,6); d) *29*(1,2,4,5,6). In (23) the symmetry symbol (with reference to the axes defined in Sect. 3.2) are followed by the dominant combination (18) of the benzene π-orbitals (in parenthesis) and the calculated orbital energy in eV. As can be seen by comparison with the experimental data of Table 3, the agreement is very satisfactory. Obviously the sequence of the two orbitals correlated with the maxima ① ② is arbitrary, but as we shall see there are indications that in the parent compound *1* the HOMO is the one associated with the linear combinations S_+.

In the preceeding discussion we have neglected changes in the basis energy A (cf. Sect. 4.1) due to the bending of the benzene π-systems. According to traditional views such a departure from planarity should entail loss of "aromaticity". However, as mentioned in the Introduction it would be an open question whether this will raise the basis energy A or lower it. In fact, previous experience with bent π-systems (double bonds [7], triple bonds [8,43] cyclic π-systems [4,44]) shows that out-of-plane (or out-of-line) deformations of the size encountered in the cyclophanes will not change the ionization energies by significant amounts, relative to the values for the corresponding planar (or linear) system. This observation is supported and explained by theoretical calculations on "superphane" by Iwamura et al. [45] and on bent and twisted ethene [9].

On the other hand, the assumption that the "through space" coupling parameter τ is the same for all linear combinations (18) (see also (22)), depending only on the mean inter-deck distance D, is of course only true if the benzene moieties are strictly planar, parallel and eclipsed. A more precise estimate of individual τ values involves the computation of the overlap integrals S_{IJ} (6) between upper and lower benzene π-orbitals [21]. One of the consequences will be, that the accidental degeneracy of the orbitals S_+ and A_+ suggested by our simple model is lifted. In particular, in the case *1* the distance between the bridged centers is only 278 pm, between the others 309 pm [1]. As a consequence the overlap integral and thus the parameter τ (cf. (14)) between S_u and S_l is necessarily larger than between A_u and A_l, because the coefficients $c_{\mu J}$ at the bridged centres 1 and 4 are of absolute size $1/\sqrt{3}$ for the former and

zero for the latter. This means that S_+ and S_- are split more by "through space" interaction than A_+ and A_- as shown in the following diagram.

(24)

If this is taken into account the sequence of states of the [2.2](1,4)cyclophane radical cation 1^+ is:

$$\text{Band:} \quad ① \qquad ② \qquad ③ \qquad ④$$
$$1^+ \text{ States:} \quad {}^2B_{2g} \qquad {}^2B_{3g} \qquad {}^2B_{3u} \qquad {}^2B_{2u} \qquad (25)$$

Support of this assignment is provided by the electronic (absorption) spectrum of the radical cation 1^+ which has been recorded and interpreted [40] by Badger and Brocklehurst. This spectrum (n-butylchloride/isopentane matrix at 77 K) shows a first intense band with onset ~ 0.7 eV (maximum ~ 1.0 eV) and a second weaker band with onset 2.1 to 2.2 eV (maximum ~ 2.4 eV). As discussed in Ref. [19], the intense band corresponds to the z-polarized ${}^2B_{3u} \leftarrow {}^2B_{2g}$ transition (energy difference $\approx I_3^m - I_1^m$), whereas the weak band is assigned to a transition from the ${}^2B_{2g}$ ground state to a state related to the highest $3e_{2g}$ σ-orbitals of the benzene moieties (energy difference $\approx I_5^m - I_1^m$). Note that the transitions ${}^2B_{3g} \leftarrow {}^2B_{2g}$ and ${}^2B_{2u} \leftarrow {}^2B_{2g}$ are forbidden.

That band ⑤ in the PE-spectrum of 1 should thus correspond to the removal of an electron from a σ-orbital (e.g. some combination dominated by the $3e_{2g}$ benzene orbitals) is also suggested by a comparison of the PE-spectra of 1 and 28 with those of their reduction products 65 and 66 (cf. data in Table 8). In the PE-spectra of 65 [31] and 66 [19] the four π^{-1} bands occupy the range of 8.3 eV to 8.8 eV for 65 and 8.8 eV to 8.5 eV for 66 (cf. Table 8). Therefore the fifth band observed at $I_5^m = 10.5$ eV for 65 and $I_5^m = 9.7_5$ eV for 66 must be due to electron ejection from a σ-type orbital. These values, which are valid approximations for the lower limits of the σ-band positions in the PE-spectra of 1 and 28 respectively, identify the bands

labeled ⑤ at $I_5^m = 10.3$ eV for 1 and $I_5^m = 9.8$ eV for 28 as the first σ-bands. In particular, the above comparison makes it highly improbable that band ④ in the PE-spectra of 1 to 32 could be due to electron ejection from a σ orbital as suggested in [20], and that the broad feature labeled ① ② ③ in the PE-spectrum of 1 (Fig. 1) should correspond to the four bands related to the four states listed in (25).

Further support for the assignment (25) is provided by the analysis of the PE-spectra of other cyclophanes to be discussed in the next sections.

A surprising result is that "superphane" does not have as low an ionization energy as one might have expected. Indeed the effects mentioned in the Introduction could have been invoked in predicting that 30 should be, for its size, one of the hydrocarbons with lowest first ionization energy. Indeed, leaving aside the negligible influence of the non-planarity of the π-systems, one might have expected that the inductive or hyperconjugative effect of the ethano-bridges and the "through space" interaction would operate as follows.

It is known that the mean ionization energy $\overline{I}^m(e_{1g})$ for the two HOMOs of methylsubstituted benzenes (as defined in Ref. [6]) decreases linearly with increasing number N of methyl groups [6,46] as shown in Figure 15. The same effect could be expected to operate in the cyclophane series and it could even be argued that its dependence on N should be a bit steeper than in the benzene case. If in addition the mean interdeck distance D decreased roughly in proportion to the same number N of bridging groups, one would have predicted by rather naive linear extrapolation that the photoelectron spectrum of superphane 30 should have its first maximum close to 6 eV, if we use [2.2]paracyclophane 1 and [2.2](1,3,5)cyclophane 25 as reference compounds (cf. Fig. 15). Quite obviously such an expectation is widely off the mark. It is a pleasing feature of our model that it permits a straightforward rationalization of the observed trend in the first ionization energies ($I_1^m \approx I_2^m$) of the cyclophanes.

Because the two highest occupied molecular orbitals of the cyclophanes correspond to the linear combinations S_+ and A_+ which are antisymmetric with respect to the
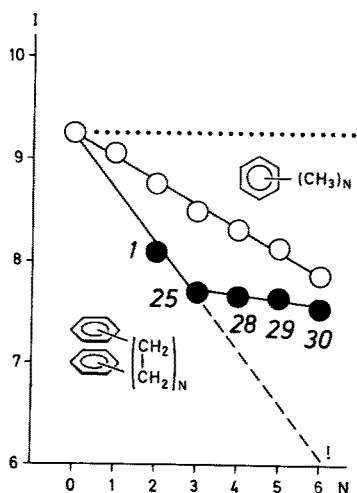

Fig. 15. Dependence of the Mean A^{-1}, S^{-1} Ionization Energy of Methylsubstituted Benzenes and of the A_-^{-1}, S_-^{-1} Ionization Energies of [2$_n$]Cyclophanes on the Number N of Substituting Groups

xy-plane, the only bridge orbital of the set (10) which could interact with them is $\varphi_\mu^{(2)}$. (Interaction with $\varphi_\mu^{(4)}$ is forbidden by the local symmetry of the 2p orbitals ϕ_μ, $\phi_{\mu'}$). However $\varphi_\mu^{(2)}$ is a very low lying orbital and its crossterms with S_+ and A_+ are small. The resulting shift has been neglected in our model, and the observation that the split between the bands ① and ② is too small to be detectable in the case of 1 and 23 to 30 justified this simplification. As a result we are in the presence of a case of symmetry forbidden hyperconjugation, as far as the S_+ and A_+ orbitals are concerned. Such restrictions, conditioned by symmetry are nothing new, and have been observed and discussed before, e.g. in Ref. [10,47].

It is perhaps worthwhile to discuss the situation in slightly more detail. In the case of a methylsubstituted benzene, one of the two pseudo-π orbitals of a methyl group is available for hyperconjugation with the benzene π-orbitals.

$$(25)$$
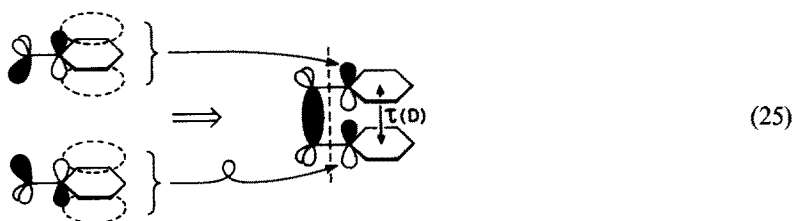
If more than one position are substituted, the effects are additive. In the cyclophane the two pseudo-π-orbitals of the original methyl groups are solidly linked *in-phase* by the newly formed CC-σ-bond. On the other hand, the rather large positive through space matrix element τ between the upper and lower π orbitals demands that the highest occupied orbitals S_+, A_+ in the cyclophane are *antisymmetric* with respect to the x,y-plane. This decouples hyperconjugation. With respect to Figure 15 a prediction of the first ionization energy can therefore not be obtained by referring to the regression line of the methylbenzenes and by adding the through space contribution, but by taking only the latter into account, relative to a fixed basis value indicated in Fig. 15 by a dotted line at 9.2_5 eV. As has been shown in Fig. 15, τ depends almost linearly on D in the interval of interest and thus explains the observed trend.

5.2 Methyl-substituted [2.2]Paracyclophanes

It is of interest to investigate the consequences of methyl substitution on the ionization energies of 1, because this allows a direct comparison of the influence of the bridging CH_2CH_2 groups which is severely restricted by symmetry, with that of the methyl groups which lack such restrictions, as explained in the previous Section 5.1.

The correlation diagram of Fig. 3 draws attention to the rather regular evolution of the band positions as a function of the number n of methyl substituents (cf. Table 1). This is especially evident if the methyl groups are evenly distributed over the rings, i.e. n/2 per benzene moiety, as shown in Fig. 16, in which the means of the
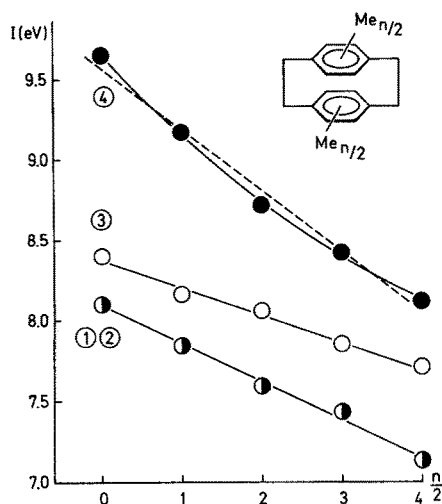
Fig. 16. Regression of Mean Ionization Energies as a Function of n/2, the Number of Methyl Groups per Ring. The solid lines numbered ①, ② and ③ correspond to the regressions (26) and (27). The broken line ④ corresponds to the linear regression (28), the solid line to a quadratic regression

ionization energies listed in the legend are plotted against the number n/2 of methyl groups in each ring. The corresponding linear regressions are:

$$\bar{I}^{m}[①②] = \left[(8.09 \pm 0.03) - (0.24 \pm 0.01)\frac{n}{2}\right] eV \tag{26}$$

$$\bar{I}^{m}[③] = \left[(8.37 \pm 0.03) - (0.17 \pm 0.01)\frac{n}{2}\right] eV \tag{27}$$

$$\bar{I}^{m}[④] = \left[(9.58 \pm 0.07) - (0.38 \pm 0.03)\frac{n}{2}\right] eV \tag{28}$$

(The reason for the larger standard errors in (28) is that this regression neglects the significant quadratic term; cf. Fig. 16). Comparison with the linear regression

$$\bar{I}^{m}(e_{1g}) = [(9.24 \pm 0.03) - (0.23 \pm 0.01) N] eV \tag{29}$$

of the mean e_{1g}^{-1} ionization energies of the set of methylsubstituted benzenes from toluene to hexamethylbenzene shown in Fig. 15 leads to the conclusion [21] that in a first approximation the influence of substitution by methyl groups on the ionization energies of 1 is both qualitatively and quantitatively the same as in benzene.

As reported in Ref. [21] a detailed discussion of the PE-spectra of the [2.2]para-cyclophanes 2 to 14 is somewhat difficult, mainly for two reasons. Firstly, in those cases where the molecules depart strongly from an idealized D_{2h} symmetry, considerable mixing of the formerly orthogonal $A_{\pm}$ and $S_{\pm}$ linear combinations can occur. An example is provided by the molecule 8, where the resultant molecular orbitals are best described by combinations of $A_{\pm}$ and $S_{\pm}$ orbitals which are rotated by 60° with respect to their orientation in the D_{2h} systems 1 or 13. This rotation, induced by the four methyl groups in positions 2, 2', 5 and 5' should lead to a split of ~ 0.4 eV between the first two ionization energies. It is perhaps more than

35
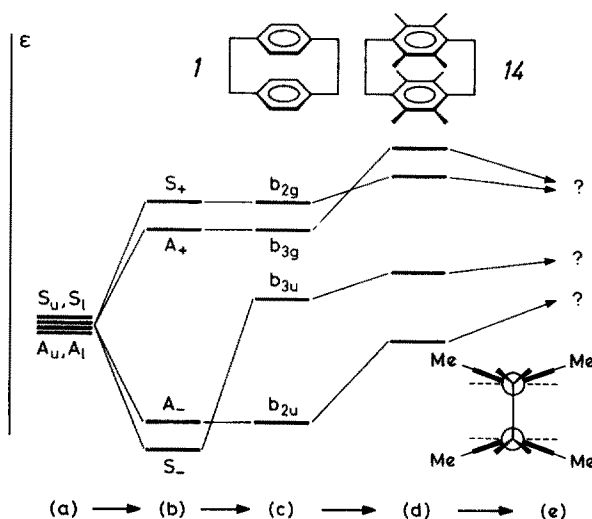
Fig. 17. Qualitative Diagram Showing the Influence of Methyl-Substitution and of the Bending of the Benzene Nuclei on the Spacing and Sequence of the [2.2]Paracyclophane π-Orbitals

a simple coincidence, that the shape of the first feature in the PE-spectrum of *8* (see Fig. 2) departs significantly from the shapes observed in the spectra of the other cyclophanes. A second, perhaps more important complication is the change in structure of the [2.2]cyclophane skeleton under the influence of the methyl substituents. From the structure analysis of *1* [1] it is known that two opposed CH bonds in positions μ, μ' of the benzene rings point slightly towards each other. Thus the distance of two H atoms is less than 309 pm and this would lead a fortiori to an even shorter distance between two methyl group centres in a molecule such as *14* i.e. much less than the sum of the van der Waals radii which is ~ 400 pm. Consequently we expect that in all cases where pairs of methyl groups occupy positions of same index μ, μ' in the two rings, the substituted centres are bent away from each other, as shown by the Newman projection in the bottom right corner of Fig. 17. A recent x-ray structure analysis of the octamethyl derivative *14* [48] has shown that this is essentially correct.

5.3 [2.2]Phanes Involving Higher Aromatic Systems

"Through space" interaction in the [2.2]phanes (cf. Table 4) is again dealt with according to the model described in Sections 4.1 and 4.3. In the absence of reliable x-ray data, a standard mean interdeck distance of D = 300 pm has been assumed, for instance in the examples *38, 39* shown in (9) or the model underlying Fig. 12 [34]. The treatment of "through bond" interaction follows closely the one used in the previous sections 5.1, 5.2, in as far as we are going to assume that only a single ethano-bridge orbital has the proper symmetry and shape to interact appreciably with the relevant linear combinations of the π-orbitals $\Phi_{r,J}$ (8). However, some of the systems have lower symmetry and the points of attachment of a given bridge are not the same in M_l and M_u. Accordingly we relabel the bridge orbital linking the

centre μ of M_l with ν of M_u as $\varphi_{\mu\nu}$. Its interaction cross term with the π-orbitals $\Phi_{l,\,l}$ and $\Phi_{u,\,j}$ is postulated to be well represented by

$$\varkappa_{l,\,\mu} = \langle \Phi_{l,\,l} | \hat{H} | \varphi_{\mu\nu} \rangle = \pm c^o_{\mu l} \cdot B$$

$$\varkappa_{j,\,\nu} = \langle \Phi_{u,\,j} | \hat{H} | \varphi_{\mu\nu} \rangle = \pm c^o_{\nu j} \cdot B$$

(30)

where $c^o_{\mu l}$ and $c^o_{\nu j}$ are the LCAO coefficients of ϕ_μ or ϕ_ν in the Hückel molecular orbitals (4) at the points attachment of the bridge orbital $\varphi_{\mu\nu}$. The sign of $\varkappa_{l\mu}$ and $\varkappa_{j\nu}$ depends on the local phase relationship between $\Phi_{l,\,j}$ or $\Phi_{u,\,j}$ and $\varphi_{\mu\nu}$. B is the same resonance integral as in (20), and is assumed to be a transferable parameter. Finally the basis energies listed in Table 9 have been used for the [2.2]phanes containing benzene and/or naphthalene moieties. (For the [2.2]azulenophanes 41, 42 a set of basis energies has been proposed in Ref. [27]).

Comparison of the observed (Table 4) and calculated band positions leads to the tentative assignment of the bands presented in Table 10. Needless to say that in view of the complexity of the systems 33 to 42 and because of the crudity of our model, such assignments should be taken with a grain of salt, even if the regression of the complete set of calculated vs. observed ionization energies I^m_j looks rather respectable (cf. Fig. 5 of Ref. [34]).

Although model calculations lead one to expect that the PE-spectra of the two isomeric [2.2]azulenophanes 41 and 42, shown in Fig. 7, should be similar, their almost complete congruence is rather striking and perhaps surprising. In particular one might have expected that linking positions 2, 2' and 6, 6' would lead to a significant change in the "through bond" interaction relative to linking 2 to 6' and 6 to 2'. However, even if the coefficients $c^o_{\mu l}$ of the molecular orbital Φ^o_l are calculated according to the standard Hückel treatment, we observe that the "through bond" destabilization of the linear combination $(\Phi^o_{4,\,upper} - \Phi^o_{4,\,lower})/\sqrt{2}$ which dominates $4a_g$ of 41 and $5a_1$ of 42 (cf. Table 10), differs by only 11 percent in these two systems. This difference is very small, considering that the standard Hückel treatment grossly overestimates the polarity of the azulene π-system. As is well known that the azulene

Table 10. Assignment of Bands in the PE-Spectra of [2.2]Phanes Involving Higher Aromatic Systems. (Cf. Table 4, Figs. 6 and 7)

Compound No.	Symmetry	Bands						
		①	②	③	④	⑤	⑥	⑦
33	C_s	4a''	6a'	3a''	5a'	2a'	4a'	
34	C_2	5a	5b	4a	4b	3b	2b	
35	C_{2v}	$2a_2$	$3b_1$	$3b_2$	$1a_2$	$4a_1$	$2b_2$	$2b_1$
36	C_{2h}	$3a_u$	$2b_g$	$4a_g$	$3b_u$	$1b_g$	$2a_u$	$3a_g$
37	C_{2h}	$3a_u$	$4a_g$	$2a_u$	$2b_g$	$3a_g$	$3b_u$	$1b_g$
38	D_2	4a	$3b_1$	$2b_1$	3a	$2b_2$	$3b_3$	$1b_2$
39	D_2	4a	$3b_1$	3a	$2b_1$	$2b_3$	$2b_2$	$2b_3$
41	C_{2h}	$2a_u$	$2b_g$	$4b_u$	$4a_g$	$1b_g$		
42	C_{2v}	$2a_2$	$2b_1$	$3b_2$	$5a_1$	$1a_2$		

π-system behaves almost as a [10]annulene π-system because of the relatively weak coupling across the 9, 10 bond, the above difference must necessarily be an upper limit. In fact, if pure [10]annulene π-orbitals had been used in our model, the difference would have been zero for symmetry reasons. Thus, the very close resemblance of the photoelectron spectra of *41* and *42* may be taken as one more indication that azulene itself is best described as a perturbed [10]annulene.

5.4 [m.n]Paracyclophanes

The major problem concerning the interpretation of the PE-spectra of [m.n]paracyclophanes with m,n $\geq$ 3 is the lack of information concerning their structure and/or their conformational equilibria. An exception is [3.3]paracyclophane *62*. In the crystal the molecule assumes a chair conformation *62a* [49] in which the two benzene moieties are separated by a mean interdeck distance D = 352 pm and are no longer eclipsed, but shifted with respect to each other by 19 pm along the x- and by 44 pm along the y-axis (axes as defined for *1*). In solution a conformational equilibrium *62a* $\rightleftharpoons$ *62b* (ratio 1:2) has been demonstrated to exist [50] and the same is probably true in the gas phase.

62a   *62b*
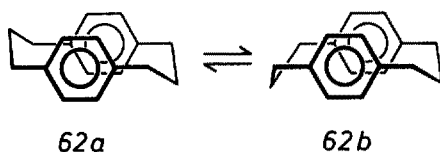
Assuming that the relative position of the benzene rings in *62b* is the same as in *62a*, the "through space" coupling parameters are calculated via formulae (6) and (16), and a mean value of $\bar{\tau} \approx 0.5$ eV is obtained [34]. The assessment of "through bond" interaction in *62* involves the basis orbitals $\eta_\mu^{(j)}$ shown in (11). Assuming, for the sake of an argument a mean "statistical" symmetry of D_{2h} (as for *1*) and applying the same reasoning as in the cases of the [2_n]cyclophanes (Sect. 5.1) we find that $\eta_\mu^{(1)}$ to $\eta_\mu^{(6)}$ will not interact appreciably with the benzene π-orbitals. This leaves $\eta_\mu^{(8)}$ and $\eta_\mu^{(7)}$ as potential relay orbitals. An important difference to the [2_n]cyclophanes is that $\eta_\mu^{(8)}$ now provides "through bond" coupling to the out-of-phase linear combination S_+, leading to a splitting of the first two bands ①, ② in the photoelectron spectrum of *62* in addition to the splitting of bands ③ and ④, which was the only one observed in the [2_n]cyclophanes. The magnitude of the splits between ①, ② and ③, ④ is difficult to predict, but qualitatively we expect to find four well separated bands spanning the interval from 7.5 to 9.5 eV. This is born out by the experimental results reported in Fig. 11 and Table 8 which are summarized in Fig. 18, together with a self-explanatory rationalization [34]. (Because of the size of the alkyl-bridges, a basis orbital energy of $A(e_{1g}^-) = -8.7$ eV instead of -9.0 eV seems appropriate to account for the destabilizing influence of the bridge orbitals $\eta_\mu^{(1)}$ to $\eta_\mu^{(6)}$).

A consequence of the rationalizations presented for the [2.2]- and [3.3]paracyclophane PE-spectra is, that the band positions I_j^m (j = 1 to 4) observed for [2.3]paracyclophane *61* [51] (cf. Fig. 11 and Table 8) should roughly be the mean
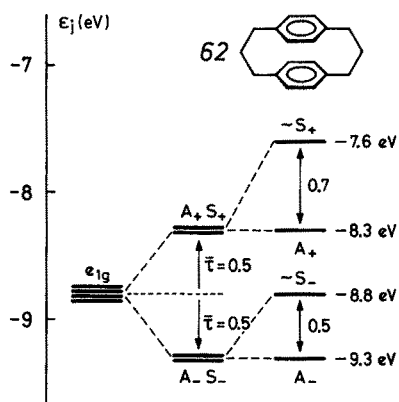
Fig. 18. "Through space" and "Through bond" Interactions in [3.3]Paracyclophane *62*

of the corresponding I_j^m values of *1* and *62*, at least in a first approximation. This is indeed the case, as shown in the correlation diagram of Fig. 19.

However, this is where useful correlations within this series, *1, 61* to *64*, ends. The PE-spectra of the higher homologues *63* and *64* can no longer be interpreted in a simple fashion. Consequently the correlation lines drawn in Fig. 19 are guesswork and do not allow for a simple rationalization, as long as the structure of the possible conformers and their relative populations are unknown.
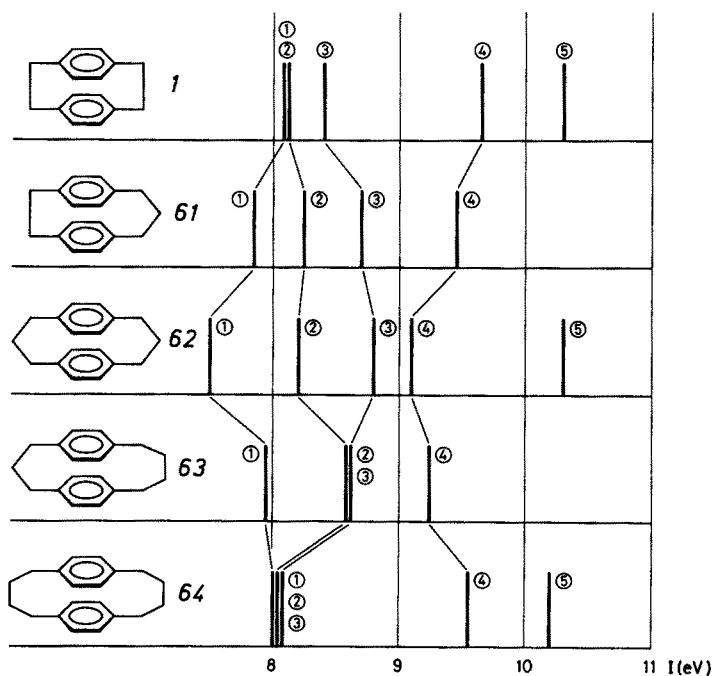
Fig. 19. Correlation Diagram for the Band Positions in the PE-Spectra of [m.n]Paracyclophanes *1* and *61* to *64*

5.5 Phanes with Unsaturated Bridges

Because of their high (D_{3h}) symmetry, the pair *25* and *31* are ideal for a discussion of the changes which occur in the photoelectron spectrum of a [2$_n$]cyclophane when the CH_2CH_2 bridges are replaced by $CH=CH$ groups.

In Fig. 20 are shown bar diagrams of the photoelectron spectra of *25* and *31* as well as the assignment proposed by Boekelheide and Schmidt [25]. The mean interdeck distance D is practically the same in *25* and *31*, namely 279.5 pm and 281 pm respectively [52]. Thus, according to (6), the „through space" coupling parameters τ should be the same in both molecules, i.e. τ = 1.2 eV. It follows that position differences of corresponding bands in the photoelectron spectra of *25* and *31* must necessarily be due to changes in the π basis energies and/or in the "through bond" coupling.

So far we have assumed a basis energy $A(e_{1g}) = -9.0$ eV to take into account neglected interactions with low lying bridge orbitals. As these interactions become even smaller in *31* because of the sp^2 character of the bridge carbon centres, $A(e_{1g}) = -9.25$ eV, (i.e. the negative first ionization energy of benzene) seems to be an appropriate choice. Combining this basis energy and the "through space" coupling term τ, yields the orbital energies $A(e_{1g}) \pm \tau$ for the out-of-phase and in-phase linear combinations e'_+ and e'_- shown in the correlation diagrams of the lower part of Fig. 20.

The basis π-orbital energy of the three bridging double bond orbitals in *31* must lie well above — 10.5 eV, i.e. the ethylene π-orbital energy, because of interaction with the σ-orbitals of the two benzene moieties. It has been argued in Ref. [34] that
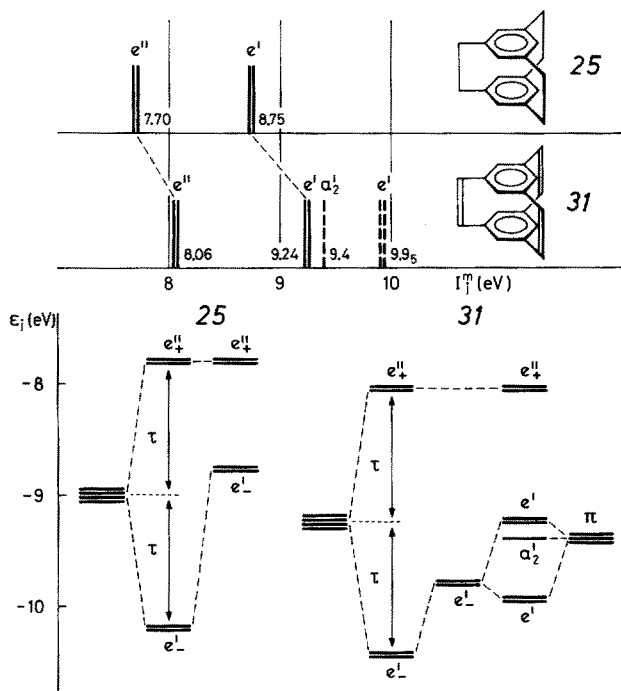

Fig. 20. Comparison and Rationalization of the Band Positions in the PE-Spectra of [2.2.2](1,3,5)Cyclophane *25* and its Corresponding Triene *31*

—9.4 eV is a reasonable choice. Because of the large distance between the double bonds (~ 500 pm), their "through space" interaction must be practically zero and all three linear combinations of A_2' and E' symmetry have approximately the same energy, as indicated in the lower right-hand side of Fig. 20.

The two bands at 9.24 eV and 9.95 eV in the photoelectron spectrum of *31* must necessarily belong to the removal of an electron from one or the other of the two pairs of e' orbitals. Consequently the in-phase combination of the benzene e_{1g} orbitals after „through bond" interaction with the linear combination of E' symmetry of the bridge σ-orbitals must be close to —9.8 eV, as shown in Figure 20. From this we deduce that the „through bond" interaction is only 0.65 eV in *31*, as compared to 1.45 eV in *25*. Such a reduction was to be expected, because the bridge σ-orbitals lie at much lower energies in *31* than in *25* due to their higher 2s-character and because the conjugation parameter is somewhat smaller.

The information derived from the pair of compounds *25* and *31* yields instant insight into the relationship between the photoelectron spectra of *1*, *15* and *16*. The mean inter-deck distance D is 299.5 pm for *1* [1)] and 302.5 pm for *16* [53)], which leads us to expect an intermediate value for *15*. Consequently the same "through space" coupling constant $\tau \approx 0.9_5$ eV applies in all three cases. This is nicely born out by the observation that $I_1^m \approx I_2^m$ are almost the same for *1*, *15* and *16* as is evident from Fig. 21. The systematic shift of I_3^m towards higher energies, going from *1* to *16*, is again due to the reduced propensity of the CH=CH bridges for "through bond" coupling. Finally, we observe in the PE-spectra of *15* and *16* the band(s) due to the ejection of an electron from orbitals which are mainly centred on the bridge π-orbitals.

Because of the size of the naphthalene moieties in the [2.2]phanes *39* and *40*, the importance of "through bond" interaction is less than in the cyclophanes discussed. Consequently, only small differences are expected as far as the positions of the π-bands in the photoelectron spectra of *39* and *40* are concerned. The only notable difference in these spectra should be the presence of additional bands in the photoelectron spectrum or *40* close to ~ 9.5 eV, which are due to ejection of an electron from the orbitals associated mainly with the two double bond π-orbitals, destabilized by interaction with the naphthalene σ-orbitals. These expectations are nicely borne out by the
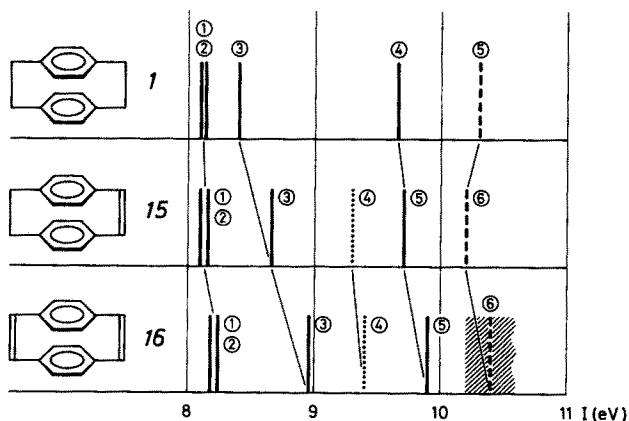

Fig. 21. Correlation Diagram for the Band Positions in the PE-Spectra of [2.2]Paracyclophane *1*, its Monoene *15* and its Diene *16*

41

experiment, as is evident from the data in Table 4 and the spectra presented in Fig. 6 [22].

In compound *32* only one of three bridges is unsaturated and we therefore expect only slight changes in the PE spectrum, relative to that of *24*. This expectation is confirmed by the data listed in Table 3. Note that band ⑤ (9.61 eV) in the spectrum of *32* is again associated with the presence of a double bond.

Although [1:2, 9:10]bismethano [2.2]paracyclophane *17* exhibits saturated bridges, its inclusion in this section is justified by the well known almost double-bond-like behaviour of cyclopropane moieties [54]. This is of particular interest in the present case, because the Walsh orbitals of the two three-membered rings [55] are well aligned for interaction with the benzene π-orbitals. If we follow the interpretation of the PE spectrum of *17* by Gleiter et al. [24], we have to conclude that "through bond" interaction in the latter compound is enhanced with respect to *1*, rather than reduced, as has been observed in *15*, *16*, *31* and *40*.

In contrast to the ethano bridges (cf. diagrams (10)) we have now seven semi-localized group orbitals $w_\mu^{(i)}$ for each of the cyclopropane moieties of *17*, which exhibit in a first approximation the following phase relationships, if expressed in terms of localized CC-banana- and CH-bond orbitals [56]:

$$\underset{w_\mu^{(1)} \quad w_\mu^{(2)} \quad w_\mu^{(3)} \quad w_\mu^{(4)} \quad w_\mu^{(5)} \quad w_\mu^{(6)} \quad w_\mu^{(7)}}{} \tag{31}$$
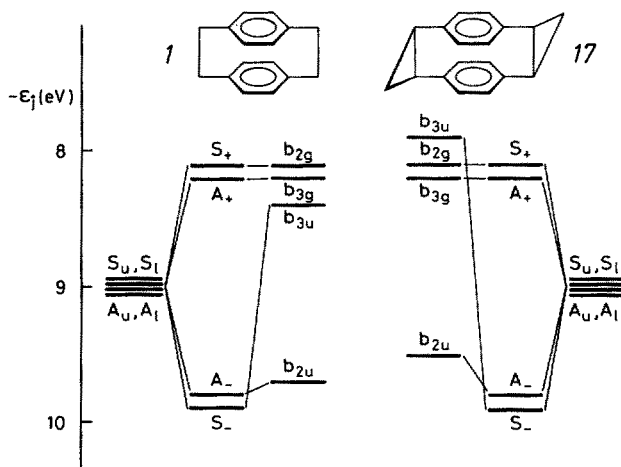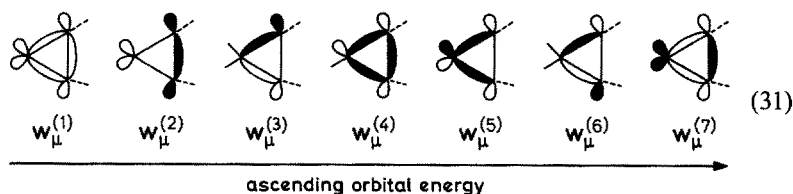
ascending orbital energy

Fig. 22. Comparison of the π-Orbital Manifolds of *1* and *17*. It has been assumed that the "through space" coupling τ is the same in both compounds. The levels of the orbitals b_{2g}, b_{3g}, b_{3u} and b_{2u} correspond to the observed band positions

(Note that only the signs of the localized bond orbitals are represented, not the size of their contribution).

Of these $w_\mu^{(4)}$ $w_\mu^{(5)}$ and $w_\mu^{(7)}$ are available as relay orbitals for "through bond" interaction of S_u and S_l, which is expected to yield a larger destabilization of S_- than in 1. In Fig. 22 is presented the rationalization of the observed spectrum (cf. Fig. 4) as proposed in Ref. [24]. Although the over-all agreement is quite reasonable, some features, such as the upwards shift of the b_{2u} orbital relative to its position in 1, demand further refinement.

5.6 Heterocyclic Phanes

Of the heterocyclic phanes only 4-aza[2.2]paracyclophane 48, 4,13-diaza- and 4,16-diaza[2_4](1,2,4,5)cyclophane, 53 and 54 (cf. Fig. 9 and 10) can be compared to the hydrocarbons discussed in the previous sections, in as far as they exhibit eclipsed and practically parallel π-systems (disregarding the replacement of CH by N). However, the interpretation of their PE spectra is by no means trivial, as has been explained in Ref. [28].

Clearly the problem of assigning the bands in the interval $8\,eV < I < 10\,eV$ is made difficult by their strong overlap, which means that a tentative assignment can only be derived on the basis of an assumed theoretical model. Such a model can be obtained by first parametrizing a Hückel-type procedure to reproduce the observed π^{-1} ionization energies of pyridine and to use these parameters in conjunction with the model described in chapter 4. One finds, based on the experimentally determined geometries of 53 [38] and 54 [57] that the positions of the first four π-bands in the PE-spectra of both compounds should be the same within rather narrow limits of error, namely for 53 a_2, -8.28; b_1, -8.57; b_2, -8.66; a_1, -10.29 eV and for 54 b_g, -8.27; a_u, -8.57; a_g, -8.71; b_u, -10.03 eV. In other words, the relative orientation of the two pyridine rings in the molecules 53 and 54 is predicted to have only a negligible influence on the π-orbital energies, in analogy to what has been observed in the case of the syn- and anti[2.2](1,6)azulenophanes $41, 42$. Accepting this result at face value, it is then possible to locate by a subtraction procedure the bands due to electron ejection from the lone-pair orbitals. It is found that they are split by roughly 0.8 eV in the case of the 4,13-diaza isomer 59 (band positions ~ 8.1 eV and ~ 8.9 eV), whereas no split can be detected in the case of the 4,16-diaza isomer 54 (band position ~ 8.5 eV). The resulting assignment is summarized in Table 11.

The same, somewhat naive model applied to 4-aza[2.2]paracyclophane 48, assuming that its geometry is the same as that of the parent compound 1 predicts π-bands in positions 8.3, 8.5, 9.0 and 10.3 eV, to which one has to add the lone-pair band due to electron ejection from the nitrogen lone pair orbital n. The latter is expected to lie close to 9.2_5 eV, i.e. at the same position as in 2,5-dimethylpyridine [58]. Obviously this yields a fair representation of the four maxima observed for the low energy band system in the PE spectrum of 48 (cf. Fig. 9 and Table 6).

All the other heterocyclic phanes investigated are either related to [2.2]metacyclophane 43 (cf. 55 to 60; Table 7), or hold a position intermediate between a [2.2]para- and a [2.2]metacyclophane (cf. 46 to 52; Table 6). Of these the PE spectra of

Table 11. Tentative Assignment and Ionization Energies of the PE-Spectra of *53, 54* and, for Comparison, of *28*

	53			*54*			*28*	
	Orb.[a]	I^m/eV		Orb[a]	I^m/eV		Orb.[a]	I^m/eV
①	$a_2(\pi)$		①	$b_g(\pi)$	8.1	①	$b_{3g}(\pi)$	
②		} ~8.2	②	$a_u(\pi)$		②	$b_{2g}(\pi)$	} 7.7
③	$b_1(\pi); b_2(n)$		③		} 8.6			
④	$a_1(n)$	} 8.9	④	$a_g(n); b_u(n)$		③	$b_{2u}(\pi)$	8.1
⑤	$b_2(\pi)$					④	$b_{3u}(\pi)$	8.8
			⑤	$a_g(\pi)$	9.3	⑤		9.8
⑥	$a_1(\pi)$	9.7	⑥	$b_u(\pi)$	9.8			
⑦		10.5	⑦		10.5			

[a] The coordinate systems are defined as follows:
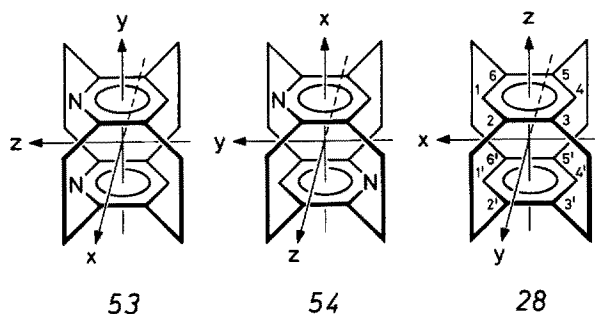
anti[2.2](2,6) pyridinophane *55* [29)], of furanophane *58*, thiophenofuranophane *59* and thiophenophane *60* [30)] have been recorded and assigned by Bernardi et al. [29, 30)]. Such assignments are rendered rather difficult due to the lack of structural information (which is presumably more important in these cases than in the ones discussed so far) and to the fact that one is much more dependent on the choice of a theoretical model. For details the reader is referred to the publications by Bernardi et al., mentioned above.

5.7 Substituted [2.2]Paracyclophanes

Figure 23 shows a correlation diagram for the first four π bands in the PE spectra of *1, 18* [23)] and *19* [17)] i.e. for [2.2]paracyclophane and its bromo- and aminoderivative. It is seen that substitution by bromine in position 2 (our numbering) yields small or even negligible shifts of the bands, whereas substitution by an amino group leads to more important changes in the ionization energies. In fact the maxima of all four
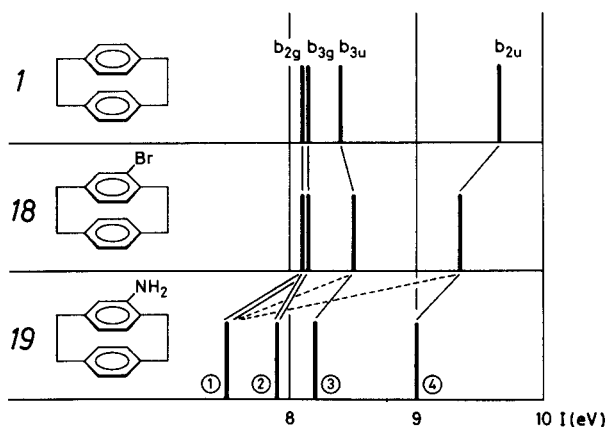
Fig. 23. Correlation Diagram for the π-Bands in the PE-Spectra of [2.2]Paracyclophane *1* and its Monobromo- and Monoamino-Derivatives *18* and *19*

π^{-1} bands are nicely separated, in the PE spectrum of *19*, confirming once more that the assignment proposed for the parent compound *1* is reasonable.

Model calculations using a parametrized Hückel-type model based on the π^{-1}-band shifts observed in the PE spectra of bromobenzene and aniline [59] (relative to the the spectrum of benzene) yield a fair rationalization of the correlation presented in Fig. 23 [51]. However, there is a complicating factor, especially in the case of *19*, to which attention has been drawn in a previous communication [17]. Under the influence of a strongly conjugating substituent, e.g. an amino group, the π-orbital linear combinations $S_{\pm}$ and $A_{\pm}$ as defined for *1* mix to a considerable extent. As a result the two highest occupied orbitals of *19* look in a first approximation as shown in the following qualitative diagrams:
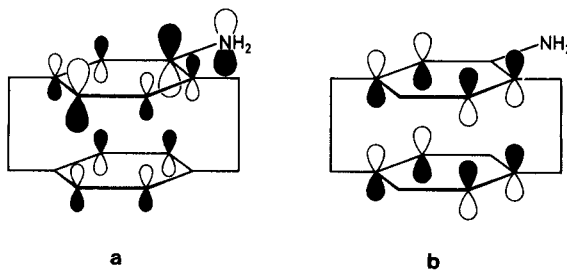
In other words it is now the substituent which primarily determines the positions of the nodes of the upper deck π-orbitals of the out-of-phase linear combinations, so that these orbitals are switched by 60° with respect to their orientation in *1*. Accordingly the parentage of these mixed orbitals is no longer well defined, as indicated in Figure 23 by the solid and dotted correlation lines. On the other hand the orbitals associated with bands ③ and ④ are dominated by the contributions of b_{3u} and b_{2u} respectively. With respect to these effects, the PE spectrum of *18* assumes an intermediate position. Of course it should be realized that the introduction of a bulky substituent, such as bromine, will also affect the geometry of the molecule and thus the "through space" coupling.

45

In Fig. 24 are correlated the PE spectra of those [2.2]paracyclophanes which carry substituents in the bridging groups (cf. Table 2). Replacement of a methylene by a carbonyl group, to yield 20, shifts all bands towards higher energy, with respect to their position in the PE spectrum of 1. In addition there is a band at 9.4_5 eV, which is due to the ejection of an oxygen lone pair electron, in good agreement with the position of the lone-pair bands in the PE spectra of acetophenone and methyl-substituted acetophenones [60]. The higher energy part of the PE spectrum of the tetra-bromo derivative 22, i.e. the one following the fourth band at 10 eV, is obliterated by the strong bands due to electron ejection from the bromine lone pairs. It is therefore impossible to locate the first σ band in the PE spectrum of 22, which would correspond to that at 10.3 eV in the spectrum of 1. The band labeled ③ in the PE spectra of 20 and 22 corresponds to the b_{3u}^{-1} band in the spectrum of 1. The observation that they are shifted towards higher energies indicates that the bridge orbitals are no longer as suitable for "through bond" coupling as those of the ethano bridges depicted in (10).

An extreme example of the latter tendency is provided by the octafluoro derivative 21, in which the four methylene groups of 1 are replaced by four difluoromethylene units. Assuming that no dramatic change in geometry occurs as a consequence of this substitution, "through space" coupling parameters τ will remain unchanged.

From the PE spectra of trifluoromethylbenzene, p-ditrifluoromethylbenzene and of related trifluoromethyl substituted benzene derivatives [59, 60] it is known that the $e_{1g}(\pi)$ orbitals of benzene are stabilized by roughly -0.5 eV per trifluoromethyl substitutent and that no split occurs, presumably because of an accidental cancellation of inductive and conjugative effects [61]. On the other hand it has been shown that σ-orbitals such as $\varphi_\mu^{(5)}$ (cf. (10)) are depressed considerably if the hydrogen
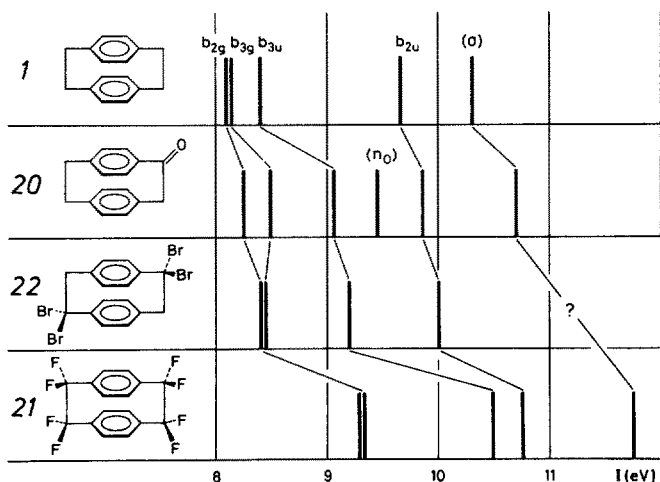

Fig. 24. Correlation Diagram for the π-Bands and the First σ-Band in the PE-Spectra of [2.2]Paracyclophane 1, the Corresponding Ketone 20, the Tetrabromo Derivative 22 and the Octafluoro Derivative 21

atoms are replaced by fluorine [62]. Depending on the type of CC-bond this depression can easily exceed —5 eV. Consequently we have to expect a large increase of the energy gap between the benzene π-orbitals $A_\pm$, $S_\pm$ and the bridge orbitals $\varphi_\mu^{(i)}$ in *21*, which in turn will lead to a sizeable reduction of through bond interaction in the latter molecule. In other words, we can effectively "turn off" through bond interaction by lowering the orbital energy of the σ-orbitals "out of reach" of the interacting π-orbitals.

This special type of fluoro-effect is nicely demonstrated by the PE spectrum of *21* as shown in the correlation diagram of Fig. 24. The fluorine induced ionization energy shifts are 1.0 to 1.3 eV for the bands corresponding to the orbitals $b_{2g}(\pi)$, $b_{3g}(\pi)$ and $b_{2u}(\pi)$ but 2.1 eV for the $b_{3u}(\pi)$ band. Thus the analysis of these spectra leads to the recognition of a novel consequence of the "fluoro-effect" concerning the competition of "through space" and "through bond" interactions in molecules such as *1*.

6 Concluding Remarks

6.1 The Influence of π-System Deformations on Ionization Energies

It is an experimental fact that π-systems have to be bent and/or twisted rather severely before a noticeable shift of their π^{-1} ionization energy (towards higher energies) occurs [7]. For example the two π-bands in the PE spectrum of cyclooctyne *72* merge to form a single narrow band ($I_\pi^m = 9.2$ eV) [7] and only if the triple bond is incorporated in a seven membered ring, e.g. in 3,3,7,7-tetramethylcycloheptyne *73* are the two bands slightly split by 0.3 eV as shown by Schweig et al. [8]. The two hydrocarbons *72* and *73* are ideal test cases because only the in-plane π-orbital is affected by the bending, whereas the other, out-of-plane π-orbital serves as a reference.

72   *73*   *74* (n)
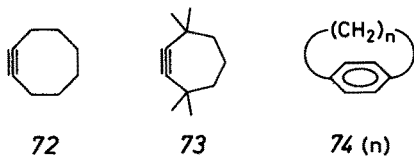
Recent model calculations [9] using localized orbitals [63] derived from an STO-3G model [64] have shown that out-of-plane deformations of ethene have a negligible influence on its π^{-1} ionization energy, as long as they do not exceed certain limits, typically $\sim 20°$ for bending and/or twisting modes. A simple rationalization of this

observation is suggested by the contour plots of the deformed π-orbitals, e.g. for a 14° out-of-plane bend of the two methylene groups of ethene:
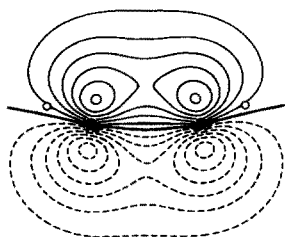
As can be seen, the π-orbital bulges outwards and one of the consequences is a reduction of the interaction of the two 2 p atomic basis orbitals, i.e. a smaller resonance integral β if we wanted to express this in Hückel language. This would lead to a reduction of the ionization energy if it were not compensated by the necessary admixture of low-lying 2s atomic orbitals to accomodate the bulge, an effect which by itself would tend to increase the ionization energy. A similar result has been obtained by Iwamura et al. [45] for the type of bending present in "superphane" 30. From the experimental side, Gleiter et al. [4] have shown that the amount of bending induced in the benzene rings of [6]- and [7]paracyclophane 74 (6) and 74 (7) by the bridging C_6- and C_7-chains does not affect the π^{-1} ionization energies significantly, in contrast to a prior claim [65], because the same split between the PE bands associated with the benzene orbitals A and S is observed for 69 ≡ 74 (8) and 70 (cf. Table 8), where the bending must be very small indeed. This is also in agreement with the data listed in the same Table for the dione 71 [23]. Finally the results summarized in the preceeding chapter provide additional support for this lack of sensitivity of ionization energies with respect of π-system bending, as do the PE spectroscopic studies mentioned in the next Section.

However, it should be remembered that deforming two π-systems in closer than van der Waals contact will affect their "through space" interaction, and that this will result in orbital energy and thus in ionization energy shifts which are much larger than those due to the bending itself. This has been discussed above in Sections 5.1 and 5.2 for the [2_n]cyclophanes and the methyl substituted [2.2]paracyclophanes. Presumably one of the larger errors in the simple orbital model we have used (cf. chapter 4) stems from the incomplete knowledge of the individual inter-ring distances in our molecules and thus of the individual values of the "through space" coupling parameters τ_{ij} defined in (12).

6.2 Cyclophane-Type Interaction between Two-Centre π-Systems

For obvious reasons the hydrocarbons 75 [66] and 76 [67] are the analogues to "superphane" 30, because two identical π-systems are sandwiched against each other by the maximum number of bridging ethano groups.

75   76
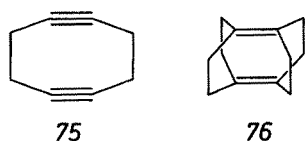
Applying the principle of symmetry conditioned competition between "through space" and "through bond" interaction used so far, leads in both cases to a transparent rationalization of the observed PE spectra.

This has been discussed in detail for 1,5-cyclooctadiyne 75 in Ref. [68], where it has been shown that the four π bands ① $9,16$ eV, ② 9.3_0 eV, ③ 9.7_5 eV (shoulder) and ④ $10,07$ eV can be assigned to the states $2b_{2g}^{-1}$, $6b_{1u}^{-1}$, $7a_g^{-1}$ and $2b_{3u}^{-1}$ respectively. This sequence, suggested by semi-empirical calculations, can be interpreted in a straightforward and transparent manner as shown in Fig. 25, which is self explanatory. The basis π-orbitals are either in-plane, $\pi_{||} \equiv \pi_z$, or out-of-plane, $\pi_\perp \equiv \pi_x$, with reference to the coordinate system defined in the top right formula of Fig. 25. It is obvious that the in-plane orbitals $\pi_{||}$ will overlap more strongly than the $\pi_\perp$ orbitals, which leads to a larger τ-value for the former and thus to a larger split between their in-phase and out-of-phase linear combinations $\pi_{||, i.p.}$, $\pi_{||, o.o.p.}$.

Except for the linear combination $\pi_{||, o.o.p.}$, all others are set up for "through bond" interaction with the $\varphi_\mu^{(i)}$ orbitals (10) of the bridging groups. Depending on the size of this hyperconjugative interaction, the resulting molecular orbitals will be shifted more or less towards higher energies, as shown in the qualitative diagram of Fig. 25, where the resulting orbitals are also depicted.

The hydrocarbon 76 with the forbidding name tricyclo-[4.2.2.2.^{2,5}]dodeca-1(2),5(6)-diene yields the PE spectrum presented in Fig. 26 [69]. It can be shown that the first
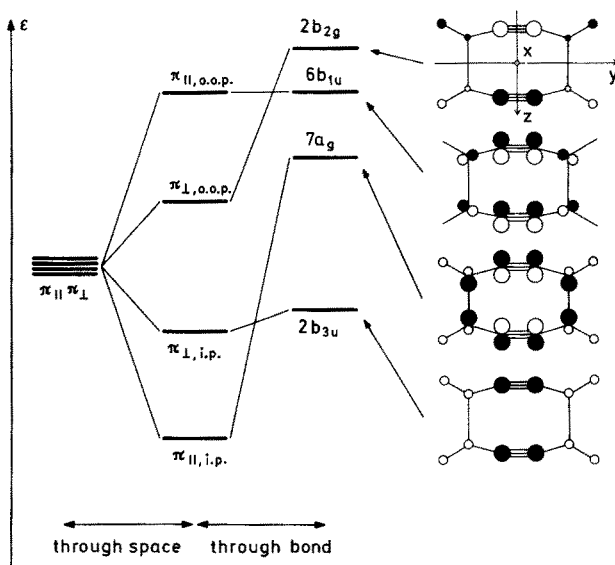

Fig. 25. Orbital Sequence and Orbital Diagrams of the Four Highest Occupied Orbitals of 1,5-Cyclooctadiyne
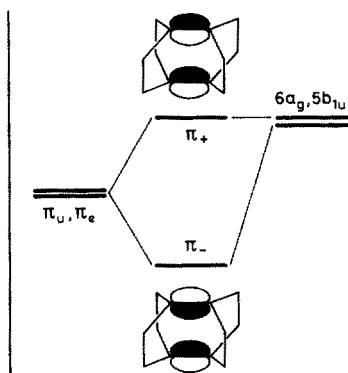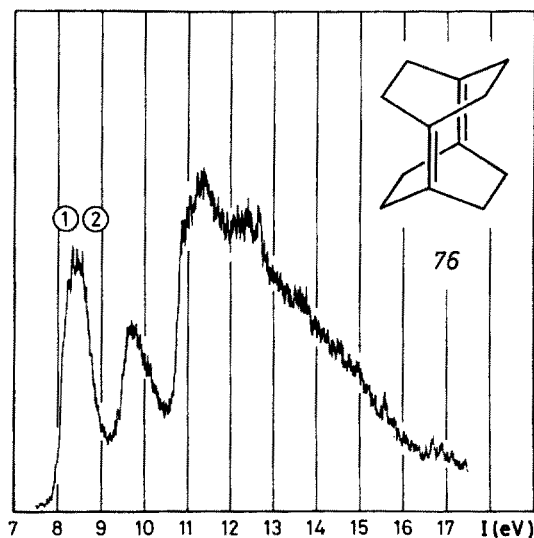
Fig. 26. PE-Spectrum and Rationalization of its First Double Band of the Tetra-bridged Diene 76

feature labeled ① ② is due to the superposition of two bands, caused by electron ejection from two orbitals which are close in energy and of A_g and B_{1u} symmetry, respectively. (The z-axis is assumed to pass through the centres of the two double bonds). Again, this result has to be explained according to the diagram at the bottom of Fig. 26. "Through space" interaction splits the symmetric and anti-symmetric linear combinations $\pi_- = (\pi_u - \pi_l)/\sqrt{2}$ and $\pi_+ = (\pi_u + \pi_l)/\sqrt{2}$ by about 3.2 to 3.4 eV. Whereas π_+ can not interact (or only very little) with the orbitals $\varphi_\mu^{(i)}$ (10) of the four bridging ethano groups, π_- is destabilized by an amount equal to the original split, so as to coincide in energy with π_+. This interpretation is supported by detailed ab initio calculations and by cross-reference to the cyclo-phanes discussed in this publication. From a quantitative side the agreement is also satisfactory, demonstrating that the model developed in chapter 4 and calibrated with respect to the [2_n]cyclophanes (cf. Sect. 5.1) extrapolates nicely to other compounds posessing two π-systems in close contact.

As in the previous case, these examples demonstrate once more that the bending of the triple bonds in *75* or of the two ethene moieties in *76* has only a negligible influence on the π-orbital basis energies.

6.3 Comment of the Inductive vs. Hyperconjugative Effect of Alkyl Groups

It is worthwhile to consider in more detail the message embodied in Fig. 15. The result of the analysis presented in Section 5.1. was that the trend in the first ionization energies of the [2$_n$]cyclophanes was due entirely to the changes in "through space" coupling τ (cf. Sect. 4.3) between A_u and A_l, or S_u and S_l respectively. In other words, if by an act of God the „through space" coupling parameter τ could be reduced to zero, all the [2$_n$]cyclophanes would have, within the limits of error, essentially the same ionization energies associated with the ejection of an electron from either of the two orbitals of A_+ or S_+ parentage. This means that contrary to expectation the presence and number of the bridging groups would have no influence on these particular ionization energies under the assumed condition τ = 0.

However, such a statement is equivalent to saying that these alkyl groups do not exert an "inductive" effect, at least as far the PE-spectroscopic results are concerned. Obviously this needs a comment, which we now provide using again a Hückel-type language. Consider the influence of methyl substitution of a π-system on its ionization energy (e.g. ethylene, benzene). In accord with other chemical evidence this substitution increases the basicity of the π-system, i.e. it becomes easier to remove one of its π-electrons, and therefore the π^{-1}-ionization energy is reduced. Within Koopmans' approximation, the methyl substituent has shifted the π-orbital energy upwards, i.e. towards less negative energies. Two possible explanations offer themselves within the framework of the Hückel formalism.

a) As shown symbolically in the top part of diagram (32) the observed π-orbital shift could be the result of an induced negative charge at the point of substitution and a concomitant increase in the shielding of the 2p electron(s).

$$(32)$$
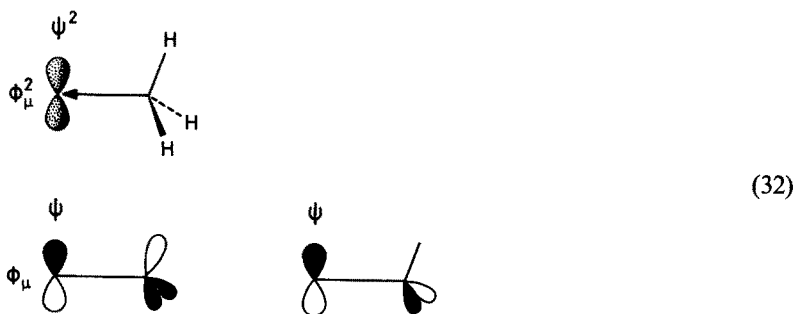
The consequence is a positive change δα of the Coulomb integral α_μ of the 2p basis function ϕ_μ (cf. formula (4)). According to first-order perturbation theory the shift of the orbital energy ε_j of Φ_j is given by

$$\delta\varepsilon_j = c_{\mu j}^2 \delta\alpha \ . \tag{33}$$

b) An alternative mechanism is the hyperconjugative interaction of the methyl group pseudo-π-orbital with the molecular orbital Φ_J, shown symbolically in the bottom part of (32). Of the two components of the degenerate pseudo-π-orbitals only the one depicted on the left has the proper symmetry to interact with ϕ_μ. The antibonding interaction shown will raise the π-orbital energy ε_J by an amount

$$\delta\varepsilon_J \approx c_{J\mu}^2 \beta'^2/(\varepsilon_J - \varepsilon_{Me}) \,, \tag{34}$$

where β' is the resonance integral for hyperconjugative interaction and ε_{Me} the basis energy of a methyl group pseudo-π-orbital.

Comparing (33) with (34) we see that $\delta\varepsilon_J$ depends in both cases on $c_{J\mu}^2$, which in turn depends on J and μ. On the other hand $\delta\alpha$ in (33) is a constant typical for a methyl group (or in general for an alkyl group) and $\beta'^2/(\varepsilon_J - \varepsilon_{Me})$ is almost a constant because $\varepsilon_J - \varepsilon_{Me}$ is usually very large compared to the variations of the orbital energy ε_J, which refers to the HOMO of a π-system. Thus it becomes almost impossible to differentiate between the mechanisms a) and b) on the basis of the observed ionization energies of the usual alkyl substituted π-systems, which could be explained according to (33) or (34), or a combination of both, if we assume that $\delta\alpha \approx \beta'^2/(\varepsilon_J - \varepsilon_{Me})$.

However, there is a fundamental difference between the two mechanisms worth emphasizing. Whereas the inductive mechanism depends on ψ^2, i.e. the electron density, the hyperconjugative mechanism depends on ψ, i.e. the wavefunction and thus on its nodal and symmetry properties. As a consequence the inductive mechanism a) does not depend on (local) symmetry whereas the hyperconjugative mechanism b) is fully subject to the restrictions imposed by (local) symmetry conditions.

Our analysis of the PE-spectra of the [2$_n$]cyclophanes, in particular the diagram of Fig. 15 has shown that the observed behaviour is only compatible with the hyperconjugative mechanism b) and that the inductive mechanism a) plays only a very minor role.

6.4 Breakdown of the Symmetry Restriction of Hyperconjugation

In this last section we want to point out very briefly an obvious consequence of the facts discussed in the previous one and in Section 5.1.

The symmetry conditioned lack of hyperconjugation in the cyclophanes possessing an interdeck symmetry plane demands as a corollary that this restriction is released in systems where such a symmetry plane is missing. This is indeed the case, as exemplified by the phanes 67 and 68, where one benzene moiety is replaced by a cyclo-octatetraene ring [70].

In Fig. 27 is shown the PE-spectrum of 67. In the range of 7.5 eV to 10.5 eV one observes two single bands ①, ②, followed by a broad feature of three overlapping bands ③ ④ ⑤. Because of the lack of symmetry (cf. the formula shown on top of Fig. 28) one expects that hyperconjugation is no longer symmetry forbidden and that the influence of the two alkyl bridges should be about the same as for the similarly substituted parent compounds, i.e. the 1,6-pentamethylene-bridged cyclo-octatetraene 71 [71] and the cyclophane 69 [4] shown in the same Figure. Consequently
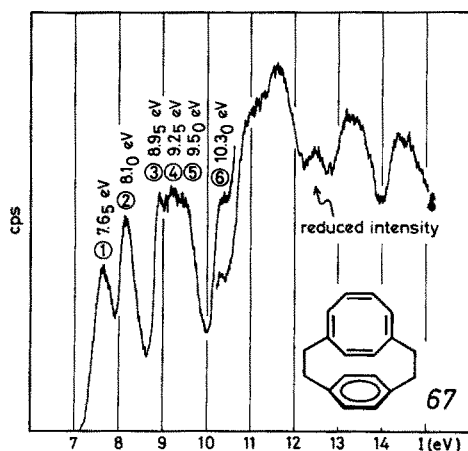
Fig. 27. PE-Spectrum of [2.2](1,4)Cycloocta-tetraeno-paracyclophane 67
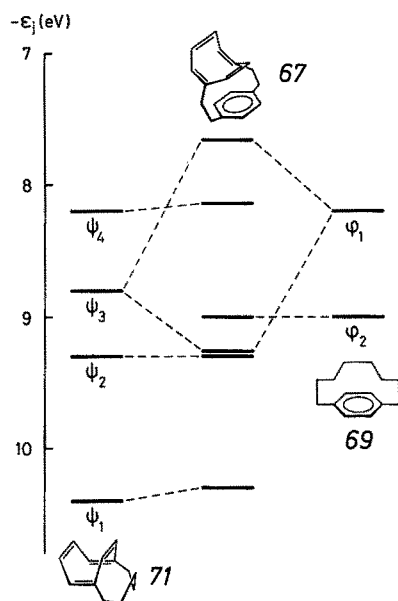
Fig. 28. Correlation Diagram for the Assignment of the PE-Spectrum of [2.2](1,4)Cyclooctatetraeno-para-cyclophane

the band positions in 67 should be the same as in 77 and 69, except for those two bands which are due to electron ejection from the two orbitals of proper symmetry and nodal properties for extensive "through space" interaction. As can be seen from the correlation diagram of Fig. 28, this is indeed the case.

7 Acknowledgements

53

8 References

1. Lonsdale, K., Milledge, H. J., Rao, K̄. V. K.: Proc. Roy. Soc. *A555*, 82 (1960); Hope, H., Bernstein, J., Trueblood, K. N.: Acta Crystallogr. *B28*, 1733 (1972)
2. Robertson, J. M.: Organic Crystals and Molecules, Cornell Univ. Press, Ithaca, 1953
3. Klessinger, M.: Angew. Chem. *84*, 544 (1972); Angew. Chem. Int. Ed. Engl. *11*, 525 (1972)
4. Gleiter, R. et al.: Chem. Ber. *113*, 3401 (1980)
5. Taft, R. W.: Separation of Polar, Steric and Resonance Effects in Reactivity, in: Steric Effects in Organic Chemistry (ed. Newman, M. S.), New York, Chapman and Hall 1956; Johnson, C. D.: The Hammett Equation, Cambridge, Cambridge Univ. Press 1973
6. Heilbronner, E., Maier, J. P.: Some Aspects of Organic Photoelectron Spectroscopy, in: Electron Spectroscopy, Theory, Techniques and Applications (ed. Brundle, C. R., Baker, A. D.) Vol. 1, London, Academic Press 1977
7. Batich, Ch. et al.: Angew. Chem. *85*, 302 (1973); Angew. Chem. Int. Ed. *12*, 312 (1973); Batich, Ch. et al.: Helv. Chim. Acta *59*, 512 (1976)
8. Schmidt, H., Schweig, A., Krebs, A.: Tetrahedron Letters *1974*, 1471
9. Honegger, E., Schmelzer, A., Heilbronner, E.: J. Electron Spectrosc. in press.
10. Hoffmann, R.: Accounts Chem. Res. *4*, 1 (1971)
11. Turner, D. W., Al-Joboury, M. I.: J. Chem. Phys. *37*, 3007 (1963); Al-Joboury, M. I., Turner, D. W.: J. Chem. Soc. *37*, 5154 (1963)
12. Koenig, T. et al.: J. Am. Chem. Soc. *97*, 3225 (1975)
13. Allan, M., Heilbronner, E., Kaupp, G.: Helv. Chim. Acta *59*, 1949 (1976)
14. Pignataro, S. et al.: Chem. Commun. *1971*, 142
15. Boschi, R., Schmidt, W.: Angew. Chem. *83*, 408 (1073); Angew. Chem. Int. Ed. *12*, 402 (1973)
16. Gleiter, R.: Tetrahedron Letters *1969*, 4453
17. Heilbronner, E., Maier, J. P.: Helv. Chim. Acta *57*, 151 (1974)
18. Koenig, T., Tuttle, M., Wielesek, R. A.: Tetrahedron Lett. *29*, 2537 (1974)
19. Kovač, B. et al.: J. Am. Chem. Soc. *102*, 4314 (1980)
20. Duke, C. B. et al.: J. Chem. Phys. *63*, 1758 (1975)
21. Yang, Z.-z. et al.: Helv. Chim. Acta *64*, 1991 (1981)
22. Kovač, B. et al.: J. Electron Spectrosc. *19*, 167 (1980)
23. Unpublished results from this laboratory
24. Gleiter, R. et al.: Chem. Ber., submitted
25. Boekelheide, V., Schmidt, W.: Chem. Phys. Letters *17*, 410 (1972);
26. Koenig, T., Tuttle, M.: J. Org. Chem. *39*, 1308 (1974)
27. Kovač, B. et al.: J. Electron Spectrosc. *22*, 327 (1981)
28. Yang, Z.-z. et al.: Helv. Chim. Acta *64*, 2029 (1981)
29. Bernardi, F. et al.: Chem. Phys. Letters *36*, 539 (1975)
30. Bernardi, F. et al.: Z. Naturforsch. *33a*, 959 (1978)
31. Gleiter, R.: private communication
32. Boekelheide, V., Heilbronner, E., Yang, Z.-z.: to be published
33. Coulson, C. A., Streitwieser, A., Jr.: Dictionary of π-Electron Calculations, in: Supplemental Tables of Molecular Orbital Calculations, Vol. II, Oxford, Pergamon Press 1965
34. Kovač, B., Allan, M., Heilbronner, E.: Helv. Chim. Acta *64*, 430 (1981)

35. Clark, P. A., Brogli, F., Heilbronner, E.: Helv. Chim. Acta *55*, 1415 (1972);
    Boschi, R., Clar, E., Schmidt, W.: J. Chem. Phys. *60*, 4406 (1974);
    Schmidt, W.: J. Chem. Phys. *66*, 829 (1977)
36. Brogli, F., Heilbronner, E.: Theor. Chim. Acta *26*, 289 (1972);
    Baird, N. C., Dewar, M. J. S.: Theor. Chim. Acta *9*, 1 (1967)
37. Heilbronner, E., Schmelzer, A.: Helv. Chim. Acta *58*, 936 (1975);
    Herndon, W. C.: Chem. Phys. Letters *10*, 460 (1971);
    Gimarc, B. M.: J. Am. Chem. Soc. *95*, 1417 (1972);
    Bieri, G. et al.: Helv. Chim. Acta *60*, 2234 (1977) and references therein
38. Hanson, A. W.: private communication
39. Koutecky, J., Paldus, J.: Coll. Czechoslov. Chem. Commun. *27*, 599 (1962)
40. Badger, B., Brocklehurst, B.: Trans. Faraday Soc. *65*, 2582 (1969); *66*, 2939 (1970)
41. Bühler, R. E., Funk, W.: J. Phys. Chem. *79*, 2098 (1975)
42. Heilbronner, E., Maier, J. P.: Helv. Chim. Acta *57*, 151 (1974)
43. Bieri, G. et al.: Helv. Chim. Acta *57*, 1265 (1974)
44. Boschi, R., Schmidt, W., Gfeller, J.-C.: Tetrahedron Letters *1972*, 4107;
    Batich, Ch., Heilbronner, E., Vogel, E.: Helv. Chim. Acta *57*, 2288 (1974)
45. Iwamura, H., Katoh, M., Kihara, H.: Tetrahedron Lett. *1980*, 1757
46. Klessinger, M.: Angew. Chem. *84*, 544 (1972); Angew. Chem. Int. Ed., Engl. *11*, 525 (1972);
    Maier, J. P., Turner, D. W.: Faraday Trans. II *69*, 196 (1973);
    Wielesek, R. A., Koenig, T.: Tetrahedron Letters *1974*, 2424;
47. Gleiter, R.: Angew. Chem. *86*, 770 (1974);
    Hoffmann, R., Mollère, Ph. D., Heilbronner, E.: J. Am. Chem. Soc. *95*, 4860 (1973)
48. Nagel, M., Allmann, R., Eltamany, S. E., Hopf, H.: submitted
49. Gantzel, P. K., Trueblood, K. N.: Acta Crystallogr. *18*, 958 (1965)
50. Anet, F. A. L., Brown, M. A.: J. Am. Chem. Soc. *91*, 2389 (1969)
51. Yang, Z.-z., Heilbronner, E.: unpublished
52. Hanson, A. W., Röhrl, M.: Acta Crystallogr. *B28*, 2287 (1972)
53. Coulter, C. L., Trueblood, K. N.: Acta Crystallogr. *16*, 667 (1963)
54. Walsh, A. D.: Nature *159*, 167, 712 (1947); Trans. Faraday Soc. *45*, 179 (1949);
    See also: Sugden, T. M.: Nature *160*, 367 (1947)
55. Förster, Th.: Z. phys. Chem. B *43*, 58 (1939)
56. Honegger, E., Heilbronner, E., Schmelzer, A., Wang, J.-Q.: Israel J. Chem. *22*, 3 (1982)
57. Hanson, A. W.: Cryst. Struct. Comm. *10*, 313 (1981)
58. Heilbronner, E., Hornung, V., Pinkerton, F. H., Thames, S. F.: Helv. Chim. Acta *55*, 289 (1972)
59. Turner, D. W., Baker, C., Baker, A. D., Brundle, C. R.: Molecular Photoelectron Spectroscopy,
    Wiley-Interscience, London 1970;
    Kimura, K. et al.: Handbook of HeI Photoelectron Spectra of Fundamental Organic Molecules,
    Japan Scientific Societies Press, Tokyo, Halsted Press, New York 1981
60. Centineo, G. et al.: J. Mol. Struct. *44*, 203 (1978);
    Baker, A. D., May, D. P., Turner, D. W.: J. Chem. Soc. *B 1968*, 22
61. Caldow, G. L., Harrison, G. F. S.: Tetrahedron *25*, 3429 (1969)
62. Brundle, C. R., Robin, M. B., Kuebler, N. A., Basch, H.: J. Am. Chem. Soc. *94*, 1451 (1972);
    Brundle, C. R., Robin, M. B., Kuebler, N. Y.: J. Am. Chem. Soc. *94*, 1466 (1971);
    Narayan, B., Murrell, J. N.: Mol. Physics *19*, 169 (1970)
63. Foster, J. M., Boys, S. F.: Rev. Mod. Phys. *32*, 300 (1960)
64. Hehre, W. J., Stewart, R. F., Pople, J. A.: J. Chem. Phys. *51*, 2657 (1969);
    Hehre, W. J. et al.: Program. No. 236, QCPE Bloomington, Indiana;
    Pople, J. A., Beveridge, D. L.: Approximate Molecular Orbital Theory, McGraw-Hill Book
    Company, New York 1970
65. Schmidt, H., Schweig, A., Thiel, W., Jones, M., jr.: Chem. Ber. *111*, 1958 (1978)
66. Kloster-Jensen, E., Wirz, J.: Angew. Chem. *85*, 723 (1973); Angew. Chem. Int. Ed. *12*, 671 (1973)
67. Wiberg, K. B., Matturo, M., Adams, R.: J. Am. Chem. Soc. *103*, 1600 (1981)
68. Bieri, G. et al.: Helv. Chim. Acta *57*, 1265 (1974)
69. Honegger, E. et al.: to be published
70. Yang, Z.-z. et al.: to be published
71. Batich, C., Bischof, P., Heilbronner, E.: J. Electron Spectrosc. *1*, 333 (1972/73)

Radical Ions of Phanes,
as Studied by ESR and ENDOR Spectroscopy

Fabian Gerson

Physikalisch-Chemisches Institut der Universität Basel, Klingelbergstraße 80, CH-4056 Basel, Switzerland

Table of Contents

A Introduction

Electron Spin Resonance (ESR) spectroscopy of the radical ions of phanes is an intriguing field of research, because it is a tool of choice for the study of intramolecular electron transfer between the non-directly bonded aromatic moieties. Apart from the radical cations of a few substituted [2.2]paracyclophanes and [2.2]-(9,10)anthracenophane, the studies have involved radical anions which were generally prepared by alkali metal reduction in an ethereal solvent. Under these conditions, the frequency of the intramolecular electron spin transfer is tied in with the rate of the concomitant migration of the counterion between its preferred sites at the radical anion [1]. When such sites are indistinguishable by symmetry, which is the case for cyclophanes with two equivalent aromatic moieties, the ESR spectra are expected to respond sensitively to this migration rate and thus yield information about the ion pairing and therewith on the electron spin transfer.

The studies, which were originally restricted to structurally simple phanes, have been extended later to more complex compounds, owing to the potential of the Electron Nuclear Double Resonance (ENDOR) spectroscopy. Both ESR and ENDOR techniques have now reached a mature stage where a nodding acquaintance can be taken as granted. For those readers who desire to deepen their knowledge, a number of books on ESR spectroscopy can be recommended [2-8]. Nearly all of these books also contain sections on the ENDOR technique. In addition, two books largely devoted to this technique have recently appeared [9, 10].

The present review gives an account of papers which, to the author's knowledge, were published before summer 1982.

The nomenclature of the phanes and the numbering of the individual positions follows the widely accepted proposal of Vögtle and Neumann [11]. The formulas of the compounds are given at the head of each section dealing with their radical ions. References below these formulas indicate the papers in which the syntheses of the compounds have been described.

Assignments of proton coupling constants are taken from the original papers to which, in most cases, the reader is referred for arguments justifying them. With one exception (radical anion of an octadeuterio[2.2]paracyclophane), hyperfine data for the deuteriated derivatives are not explicitly given. Wherever g factors have been reported, they are included either in the text or in the tables.

Conventional abbreviations are used for the solvents: DME = 1,2-dimethoxy-ethane; THF = tetrahydrofuran; MTHF = 2-methyltetrahydrofuran; HMPT = hexamethylphosphoric acid triamide; DMF = N,N-dimethylformamide; DEE = diethylether.

B [2.2]Paracyclophane

The status of [2.2]paracyclophane (*1*) within the class of phanes is comparable to that of benzene among the aromatic compounds. It is therefore not surprising that the first study of *1* dates back to 1958, the early period of ESR spectroscopy of radical ions. This study [16], like a great deal of other pioneering work in this area, was performed by Weissman; DME and K were used as the solvent and the
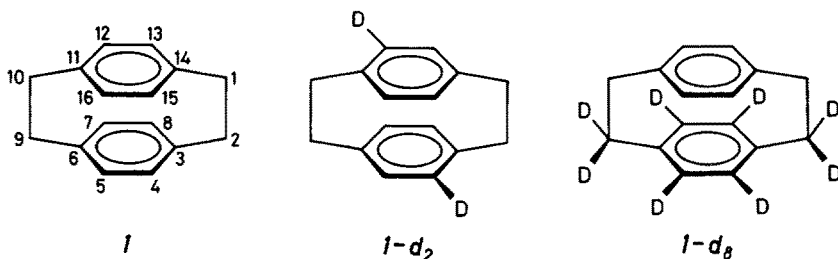
(Syntheses: 1 [12,13], $1-d_2$ [14], $1-d_8$ [15].)

reducing agent, respectively. It has been stated that the frequency of electron exchange between the two benzene π-systems in $1^{\overline{\cdot}}$ is higher than $1.5 \cdot 10^7$ s^{-1}, but a detailed analysis of the ESR spectrum was not reported. A further attempt to characterize $1^{\overline{\cdot}}$ by its hyperfine data was made 1967 by Ishitani and Nagakura [17] who used THF instead of DME. Both the analysis of the partly resolved ESR spectrum and the assignments of the proton coupling constants were in error. The next study of $1^{\overline{\cdot}}$, reported in 1969 [14], presented highly resolved ESR spectra of $1^{\overline{\cdot}}$ in a variety of solvents (Fig. 1). Assignments of the proton coupling constants
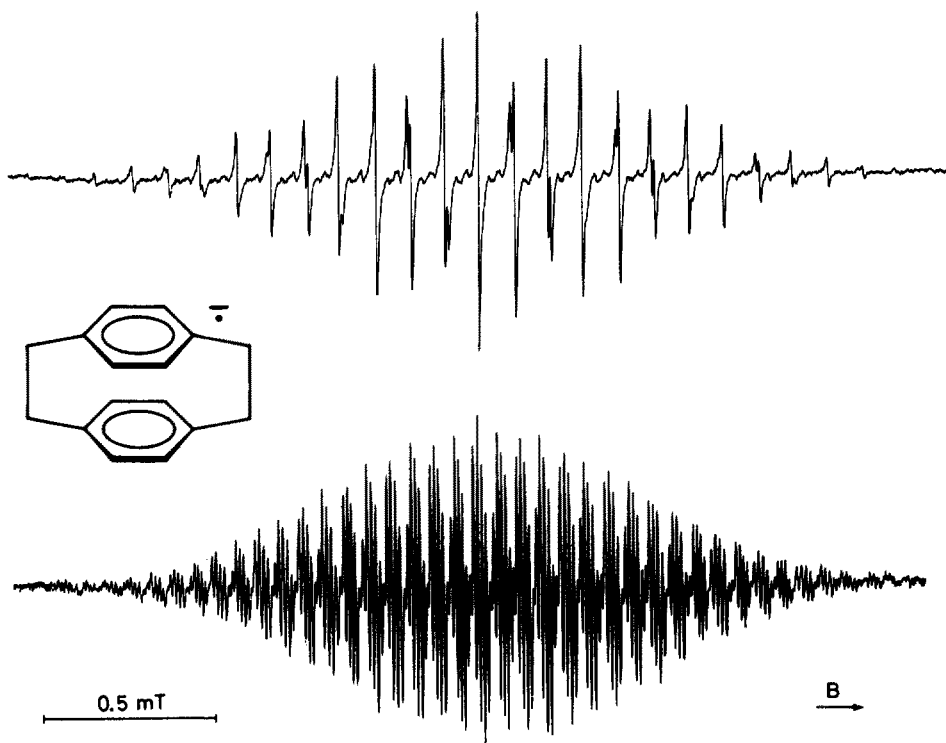
Fig. 1. ESR spectra of the radical anion of [2.2]paracyclophane (1). Top: solvent DME/HMPT ($\sim$40:1), counterion K$^+$, temperature 188 K. Bottom: solvent THF, counterion K$^+$, temperature 178 K. Reproduced by permission of J. Am. Chem. Soc. [14]
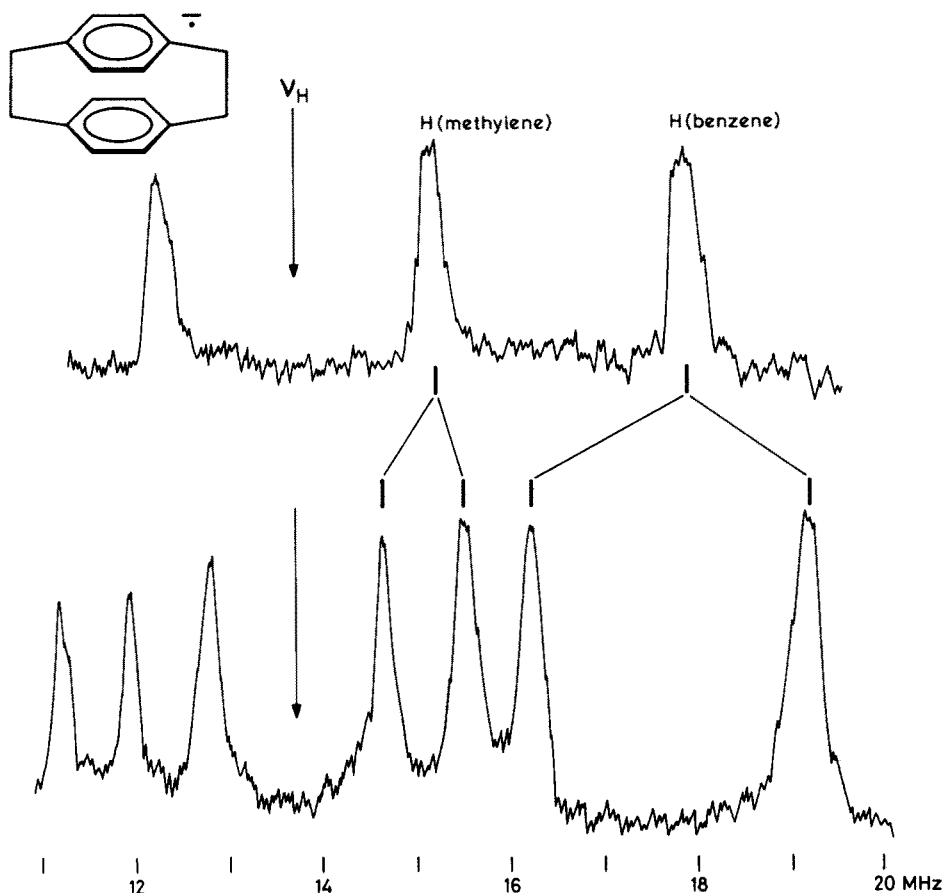
Fig. 2. Proton ENDOR spectra of the radical anion of [2.2]paracyclophane (1) [22]. Top: solvent DME/HMPT (10:1), counterion K^+, temperature 188 K. Bottom: solvent MTHF, counterion K^+, temperature 163 K. v_H = frequency of the free proton

were based on the deuteriation in the 4,12-positions ($1 - d_2$). This study was complemented by further ESR and ENDOR investigations [15, 18-23] (Fig. 2) so that an appreciable amount of experimental data has been amassed.

In an ethereal solvent, 1 reacts with K or Cs to yield the radical anion $1^{\bar{\cdot}}$. It can be also reduced to $1^{\bar{\cdot}}$ electrolytically in DME [23] or DMF [22,24] with a tetraalkyl-ammonium perchlorate as the supporting salt. The electron affinity of 1 in solution is thus considerably higher than that of benzene or p-xylene. The half-wave reduction potentials $E_{1/2}$ of 1 and benzene have been indirectly determined as -3.05 ± 0.12 and -3.31 ± 0.12 V (vs. SCE), respectively [23]. The former value agrees with a recent direct measurement giving -3.00 ± 0.05 V [24]. The radical anion $1^{\bar{\cdot}}$ is persistent below 200 K. Raising the temperature leads to a decay of $1^{\bar{\cdot}}$ so that the intensity of its ESR spectrum becomes very low above 240 K.

The spectra at the top of Figs. 1 and 2 are characteristic of a "free" or loosely associated radical anion, while those at the bottom of these figures arise from a radical

anion which is tightly paired with its counterion K^+. The "free" radical anions are obtained in relatively polar solvents such as mixtures of DME with HMPT (or in DMF, when $I^{\cdot-}$ is generated electrolytically, and Et_4N^+ is the counterion [22]). The tight ion pairs are formed in solvents of lower solvating power like THF and MTHF. On passing from a "free" to a tightly paired radical anion, the effective symmetry is reduced from D_{2h} to C_{2v}, and each of both sets of eight equivalent protons separates into two sets of four. The two four-proton coupling constants and the one eight-proton coupling constant are related in such a way that the average value of the former is close to the value of the latter (Table 1).

Table 1. Coupling constants, in mT, for the radical anion of [2.2]paracyclophane (I) [14 15, 18-22]. Counterion K^+. $g = 2.0028^a$

Solvent Temp., K		DME/HMPT 188	DME[b] 183	DME[b] 183	THF 178	MTHF 163
Benzene protons	4, 5, 7, 8[c] 12,13,15,16	0.297 (8H)	0.295 (8H)	{ 0.367 (4H) 0.204 (4H)	0.379 (4H) 0.193 (4H)	0.388 (4H) 0.178 (4H)
Methylene protons	2, 9[c] 1,10	0.103 (8H)	0.100 (8H)	{ 0.121 (4H) 0.079 (4H)	0.125 (4H) 0.070 (4H)	0.128 (4H) 0.067 (4H)
$^{39}K^a$				d	0.012 (1K)	0.013 (1K)

a In THF, with Cs^+ as the counterion, $g = 2.0020$ and the ^{133}Cs coupling constant is 0.038 and 0.016 mT, at 183 and 163 K, respectively.
b Concurrently observed, cf. text.
c Positions.
d Not resolved.

It is reasonable to assume that the larger of the two four-proton coupling constants is associated with that moiety of $I^{\cdot-}$ which is proximate to the counterion in the ion pair (vide infra). In addition to the proton hyperfine pattern, splitting from the nucleus (^{39}K or ^{133}Cs) of the counterion is usually found for the tight ion pairs.

In THF or MTHF the life-time of an ion pair $I^{\cdot-}-K^+$, which is inversely proportional to the rate k of migration of the counterion between the two equivalent sites at the radical anion, must be long on the hyperfine time-scale ($k < 10^6\ s^{-1}$). By contrast, in DME/HMPT mixtures, the migration is fast on this scale ($k > 10^8\ s^{-1}$) and, thus, a "free" or loosely associated radical anion is observed, along with the averaged values of the coupling constants. In DME/THF mixtures ion pairs $I^{\cdot-}-K^+$ occur, for which the rate k must be comparable to the hyperfine time-scale ($k \approx 10^7\ s^{-1}$), as indicated by line-width effects in the ESR spectra [14]. As for pure DME, it has recently been found that a tight ion pair $I^{\cdot-}-K^+$ and a "free" or loosely associated radical anion give rise concurrently to superimposed signals in ESR and ENDOR spectra [20-22]. This finding casts some doubt on the simple model in which both species differ only in the rate k of exchange.

The structure of the tight ion pair $I^{\cdot-}-K^+$ in THF has been derived from an ESR study of the half-deuteriated radical anion $I-d_8^{\cdot-}$ [15]. The results of this study are consistent with the counterion K^+ taking a position outside the carbon framework of $I^{\cdot-}$, above or below one of the benzene rings (Fig. 3). The observed ESR
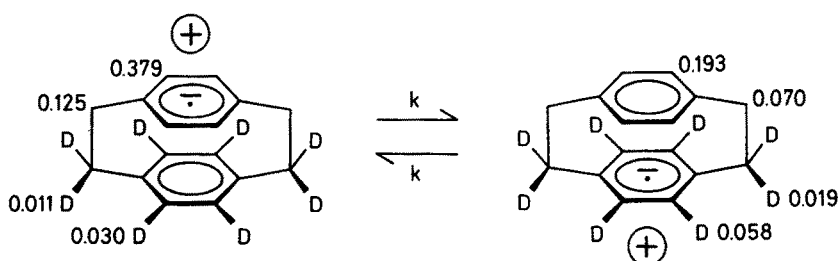
Fig. 3. Proton and deuteron coupling constants, in mT, for the ion pairs formed by the radical anion of the octadeuterio[2.2]paracyclophane $1-d_8$ with K^+ in THF [15]

spectrum arises from a $1:1$ mixture of two radical anions which have the indicated proton and deuteron coupling constants and for which the interconversion is slow on the hyperfine time-scale.

A number of theoretical models of $1^{\overline{\cdot}}$ have been described [14,17,25-27]. It is now generally accepted that the singly occupied MO of $1^{\overline{\cdot}}$ can be represented as the B_{1g} combination of the "antisymmetric" benzene LUMO's ψ_A (Fig. 4).
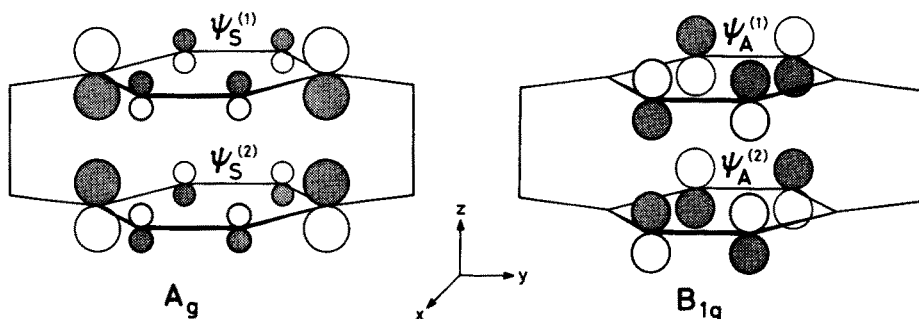
Fig. 4. A_g and B_{1g} combinations of the "symmetric" (ψ_S) and "antisymmetric" (ψ_A) LUMO's of benzene, respectively. "Symmetric" and "antisymmetric" refer to the mirror plane yz. Reproduced by permission of Helv. Chim. Acta [27]

C Derivatives of [2.2]Paracyclophane

1 Methyl Derivatives

The ionization potential of [2.2]paracyclophane (*1*) in the gas phase decreases steadily on successive methyl substitution on the benzene rings [34]. Accordingly, generation of the radical cations in solution becomes practical for derivatives bearing at least four methyl substituents. Whereas oxidation of the tetramethyl derivatives has to be carried out under rather rigorous conditions, such as dissolution in molten unpurified $SbCl_3$ (in which the oxidizing agent is thought to be $SbCl_5$ [35]) or reaction with $AlCl_3$ in CH_2Cl_2 or $MeNO_2$ above 333 K [19,22], the radical cations of the hexa- and octamethyl[2.2]paracyclophanes *5* and *6* form readily by electrolysis at 193 K [36]. Table 2 lists the proton coupling constants for $2^{\overline{+}}$, $5^{\overline{+}}$ and $6^{\overline{+}}$.

2-d₄ → $2-d_4$ 2-d₈ → $2-d_8$

Structure labels: 2, $2-d_4$, $2-d_8$, 3, 4, 5, 6
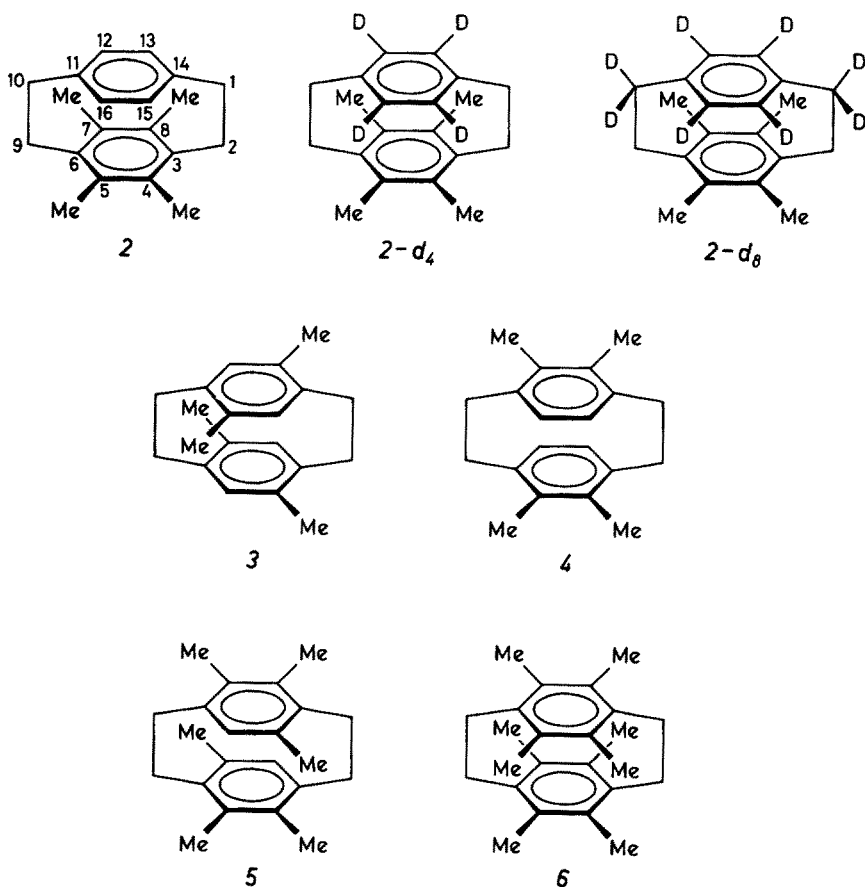
(Syntheses: 2 [28,29]; $2-d_4$ and $2-d_8$ [19]; 3 [30,31]; 4 and 5 [32]; 6 [32,33].)

Table 2. Coupling constants, in mT, for the radical cations of the tetra-, hexa- and octa-methyl-substituted [2.2]paracyclophanes (2, 5, and 6, respectively) [19,36]. $g = 2.0024$ for 2^+, and 2.0026 for 5^+ and 6^+

	2^+		5^+		6^+
Solvent	SbCl$_3$		CH$_2$Cl$_2$/CF$_3$COOH/ (CF$_3$CO)$_2$O (10:1:1)		CH$_2$Cl$_2$/CF$_3$COOH/ (CF$_3$CO)$_2$O (10:1:1)
Temp., K	323		193		193
Methyl protons		0.574 (12H)	4, 12[a] 5, 13 7, 15	0.660 (6H) 0.111 (6H) 0.542 (6H)	0.435 (24H)
Benzene protons		0.112 (4H)		<0.03 (2H)	
Methylene protons	1, 10[a] 2, 9	<0.01 (4H) 0.188 (4H)		<0.03 (4×2H)	0.008 (8H)

a Positions.

The corresponding values for $3^{\ddot{+}}$ and $4^{\ddot{+}}$ were found to be identical [21,22] with those previously reported for $2^{\ddot{+}}$ [19]. Clearly, under the rigorous conditions used for the oxidation of 2, 3 and 4, transannular migration of the methyl groups takes place, as has, in the meantime, also been found by experiments using $TiCl_4/HCl$ [37]. In view of the equal multiplicities for the sets of equivalent protons in $2^{\ddot{+}}$, $3^{\ddot{+}}$ and $4^{\ddot{+}}$, the identity of the radical cation giving rise to the observed spectrum is uncertain. Nevertheless, the original attribution [19] to $2^{\ddot{+}}$ might still hold, in view of the expected greater stabilization of the positive charge in $2^{\ddot{+}}$ relative to $3^{\ddot{+}}$ and $4^{\ddot{+}}$. The studies of the radical cations from $2-d_4$ and $2-d_8$ seem to support this attribution, although partial dedeuteriation occurring upon oxidation [19] impairs a straightforward conclusion.

It is evident from Table 2 that the major coupling constants are due to the protons in the methyl substituents. This result indicates that the methyl groups are considerably more effective than the ethano bridges in delocalizing positive charges in the radical cations of cyclophanes, as has been concluded from the gas phase ionization potentials of these compounds [34,38].

When 2 and its deuterio derivatives, $2-d_4$ and $2-d_8$, are oxidized under relatively mild conditions, such as electrolysis in $CH_2Cl_2/CF_3COOH/(CF_3CO)_2O$ (10:1:1) at 193 K [39], dimeric radical cations $(2)_2^{\ddot{+}}$, $(2-d_4)_2^{\ddot{+}}$ and $(2-d_8)_2^{\ddot{+}}$ are obtained [40].

Table 3. Coupling constants, in mT, for the dimer radical cation [40] and the radical anion [19] of 4,5,7,8-tetramethyl[2.2]paracyclophane (2). g = 2.0024 for $(2)_2^{\ddot{+}}$, and 2.0026[a] for $2^{\ddot{-}}$

		$(2)_2^{\ddot{+}}$	$2^{\ddot{-}}$
Solvent		$CH_2Cl_2/CF_3COOH/$ $(CF_3CO)_2O$ (10:1:1)	DME/THF (1:1)
Temp., K		193	163
Methyl protons		0.223 (24H)	0.099 (12H)
Benzene protons		0.035 (8H)	0.295 (4H)
Methylene protons	1, 10[b]	0.018 (8H)	0.168 (4H)
	2, 9	0.168 (8H)	0.015 (4H)
^{39}K[a]			0.102 (1K)

a Counterion K^+. With Cs^+, g = 2.0014 and the ^{133}Cs coupling constant is 0.596 mT.
b Positions.

The hyperfine data for $(2)_2^{\ddot{+}}$ (Table 3) are consistent with the structures A and B of symmetry D_{2h} (Fig. 5) or with their D_{2d} counterparts in which one molecule is twisted by 90° relative to the other.

In the case of 2, $2-d_4$ and $2-d_8$, the radical anions could also be produced by reaction with K or Cs in DME/THF (1:1) at 163 K [19]. The hyperfine data for $2^{\ddot{-}}$ (Table 3) indicate that the spin population is substantially localized on the unsubstituted benzene ring. The large hyperfine splittings from the ^{39}K and ^{133}Cs nuclei are noteworthy.
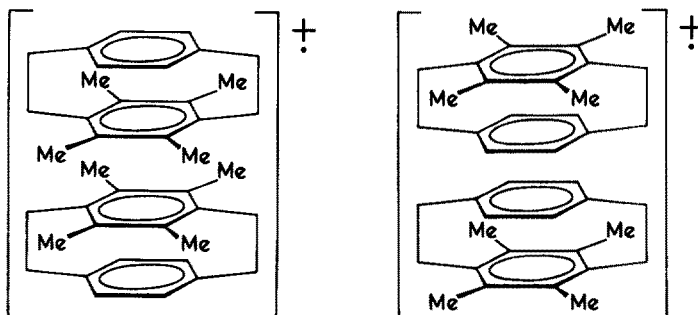
Fig. 5. Structures of symmetry D_{2h} for the dimer radical cation of 4,5,7,8-tetramethyl[2.2]-paracyclophane (2). Reproduced (in part) by permission of Helv. Chim. Acta [40]

2 Derivatives with Functional Substituents

In the radical anion of 4-nitro[2.2]paracyclophane (7), the spin population is largely localized on the nitro substituted benzene ring [48a,49] and is distributed in a way resembling the radical anion of nitrobenzene [50]. The coupling constants for $7^{\bar{\cdot}}$ generated electrolytically in DMF at 300 K are [48a]: 0.880 (1N), and 0.436, 0.655 and 0.222 mT (1H each; positions 5, 7 and 8, respectively). The spin distribution pattern of $7^{\bar{\cdot}}$ is not markedly altered by an introduction of a CN group in the unsubstituted ring of $7^{\bar{\cdot}}$ to yield $8^{\bar{\cdot}}$ [49]. On the other hand, the spin population in the radical anion of 4,12-dinitro[2.2]paracyclophane (9) seems to be evenly divided between the two rings when $9^{\bar{\cdot}}$ is generated electrolytically in a polar solvent like DMF or Me$_2$SO (coupling constant of 0.472 mT for two equivalent ^{14}N nuclei in DMF at 300 K [48b]).

Spin delocalization over both aromatic moieties is, in general, observed for the radical anions $10^{\bar{\cdot}} - 16(R)^{\bar{\cdot}}$ prepared electrolytically (supporting salt Et$_4$N$^+$ClO$_4^-$) or by reaction with K in DME from the respective derivatives of [2.2]paracyclophane [51]. With the exception of 14, all these compounds contain two equivalent aromatic moieties. Comparison of the hyperfine data for $10^{\bar{\cdot}}$, $11^{\bar{\cdot}}$, $12^{\bar{\cdot}}$, $13(R)^{\bar{\cdot}}$, $15^{\bar{\cdot}}$ and $16(R)^{\bar{\cdot}}$ with those for the radical anions of analogously substituted benzene derivatives [51] indicates that the most prominent coupling constants are roughly halved on passing from the latter to the former. Localization of the spin population, as a consequence of ion pairing is found only for $13(iPr)^{\bar{\cdot}}$ and $13(tBu)^{\bar{\cdot}}$ in DME with K$^+$ as the counterion [51]. This finding suggests that the migration of K$^+$ between two preferred sites at the radical anion is slowed down by the bulky alkyl ester groups.

A selection of hyperfine data determined by ESR and ENDOR spectroscopy for the symmetrically tetra-substituted radical anions $12^{\bar{\cdot}}$, $13(tBu)^{\bar{\cdot}}$; $15^{\bar{\cdot}}$ and $16(H)^{\bar{\cdot}}$ is given in Table 4. For a complete set of values, including those for $10^{\bar{\cdot}}$, $11^{\bar{\cdot}}$ and $14^{\bar{\cdot}}$, the reader is referred to the original paper [51].

Introduction of two electron-donating OMe substituents into 4,5,7,8-tetramethyl-[2.2]paracyclophane (2) to yield the 12,15-dimethoxy-derivative 17 decreases considerably the ionization potential so that 17 is oxidized to its radical cation with AlCl$_3$ or CF$_3$COOH in CH$_2$Cl$_2$ below 293 K [49]. The proton coupling constants for 17^{+}
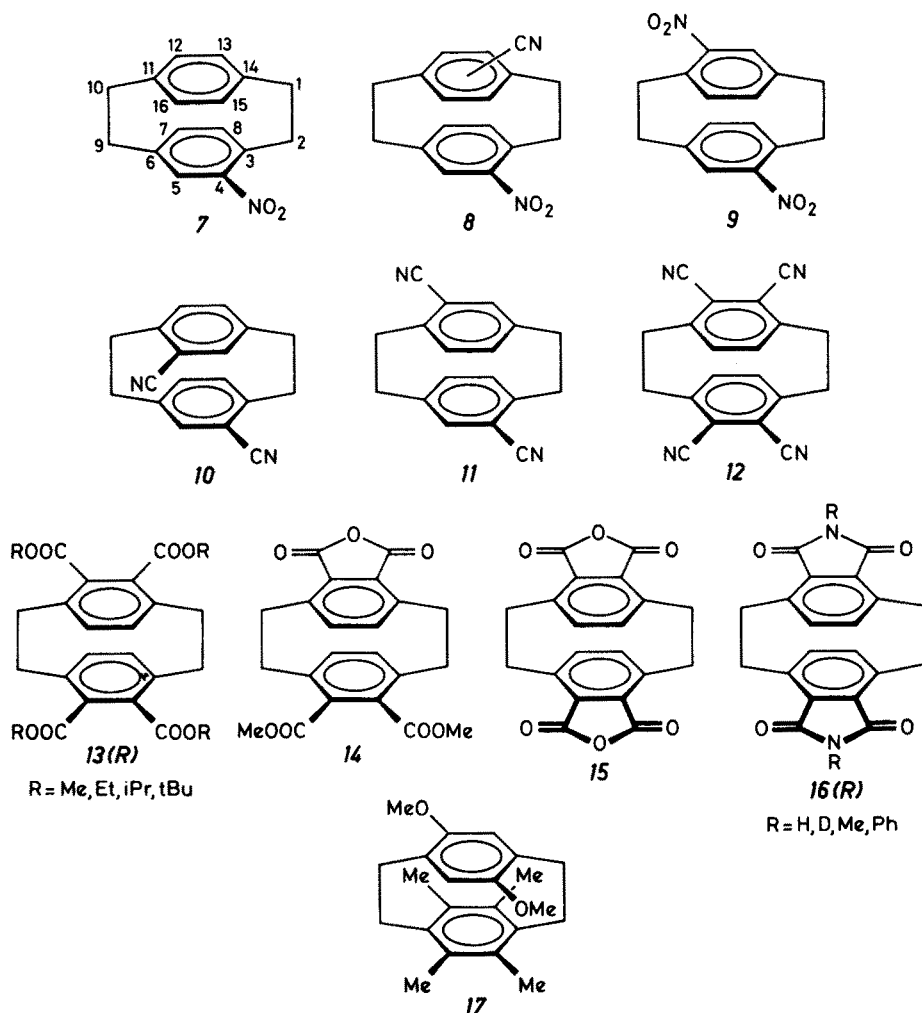
(Syntheses: 7[41]; 8[42]; 9[31,43]; 10 and 11[31]; 12[44]; 13 (R)[44-46]; 14[46]; 15 and 16 (R)[47]; 17[29].)

derived from its ENDOR spectrum are: 0.221 (6H), 0.190 (6H), 0.082 (6H), 0.041 (2H) and 0.020 mT (2H); the remaining values are smaller than 0.01 mT. The assignment to protons in specific positions would require studies of deuteriated derivatives.

3 1,1,2,2,9,9,10,10-Octafluoro[2.2]paracyclophane

Due to the octafluoro substitution of the two ethano bridges, the cyclophane 18 is considerably more easily reduced than the parent compound 1 but the resulting radical anion 18⁻ has only a low persistence. The ESR spectrum of 18⁻ could be observed by continuous electrolysis of a concentrated solution of 18 in DME below

Fabian Gerson

Table 4. Coupling constants, in mT, for the radical anions of some 4,5,12,13-tetrasubstituted [2.2]paracyclophanes[51]. g = 2.0027 for 12^{-}, 2.0034 for $13\,(tBu)^{-}$; 2.0038 for 15^{-} and 2.0040 for $16\,(H)^{-}$

		12^{-}	$13\,(tBu)^{-}$		15^{-}	$16\,(H)^{-}$
Solvent		DME	DMF	DME	DME	DME
Counterion		K⁺	Et₄N⁺	K⁺	K⁺	K⁺
Temp., K		183	213	183	183	183
Benzene protons	7, 8ᵃ 15, 16	0.213 (4H)	0.192 (4H)	0.276 (2H) 0.132 (2H)	0.156 (4H)	0.154 (4H)
Methylene protons	2, 9ᵃ 1, 10	0.053 (4H)	0.064 (4H)	0.114 (2H) 0.018 (2H)	0.015 (4H)	0.013 (4H)
	2, 9 1, 10	0.040 (4H)	0.031 (4H)	0.057 (2H) 0.004 (2H)	0.006 (4H)	0.005 (4H)
Nuclei in substituents		0.094 (4N)				0.101 (2N) 0.013 (2H)

a Positions
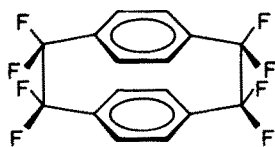
18

(Synthesis: *18* [52].)

200 K [27]. The eight ^{19}F nuclei exhibit a large coupling constant of 3.35 mT, while the eight protons give rise to an unresolved splitting which was estimated as 0.10 mT. Line-width alternation in the ESR spectrum indicates that the rate of migration of the counterion Bu_4N^+ between two equivalent sites at the radical anion is comparable to the hyperfine time-scale. The energy barrier to the migration was determined as 14 ± 2 kJ/mol.

The hyperfine data for *18*⁻ are qualitatively accounted for by an INDO [53] model, in which the singly occupied orbital is represented as the A_g combination of the "symmetric" benzene LUMO's ψ_S (Fig. 4) with a substantial delocalization onto the fluorine 2s-AO's.

4 [2.2]Paracyclophane-1,9-diene
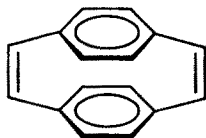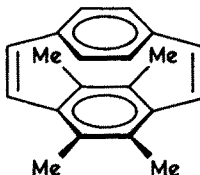
19   *20*

(Syntheses: *19* [54]; *20* [55].)

The radical anion *19*⁻ prepared by reaction of [2.2]paracyclophane-1,9-diene with K in DME at 193 K undergoes a facile conversion to *1*⁻ by a formal abstraction of four hydrogen atoms from the solvent [55]. Cleavage of one bridge and formation of the radical anion of trans-4,4'-dimethylstilbene [55] was also observed at higher temperature.

The presence of the double bonds in the ethano bridging groups has dramatic consequences on the spin distribution in the radical anion. The major and essentially temperature independent coupling constant of 0.425 mT is due to the four equivalent olefinic protons, while minor hyperfine splittings arise from the eight aromatic protons. At 183 K, these splittings are 0.046 and 0.020 mT, each for a set of four protons. They average to 0.013 mT above 253 K, at which temperature the eight protons become equivalent. Thus the two values must have opposite signs: $\frac{1}{2}(\pm 0.046 \mp 0.020)\,mT = \pm 0.013\,mT$. The non-equivalence of the aromatic protons

at low temperature is unlikely to be caused by tight ion pairing, since the ESR spectrum of $19^{\bar{\cdot}}$ is not greatly affected by changes in the solvent (addition of HMPT or THF to DME) and/or the counterion (replacement of K^+ by Li^+ through introducing an excess of LiCl salt into the solution). An alternative rationalization is in terms of slight distortions of the molecular framework so that the symmetry is lowered from D_{2h} to C_{2h} or D_2.

In the radical anion of the tetramethyl derivative 20, the olefinic protons are only pairwise equivalent and exhibit coupling constants of 0.57 and 0.34 mT [55]. The hyperfine splittings from the aromatic and methyl protons could not be resolved.

D Miscellaneous Paracyclophanes

1 [m.n]Paracyclophanes with [m.n] $\neq$ [2.2]

$(CH_2)_m$ $(CH_2)_n$ $21[2.2] = 1$

21 [m.n]
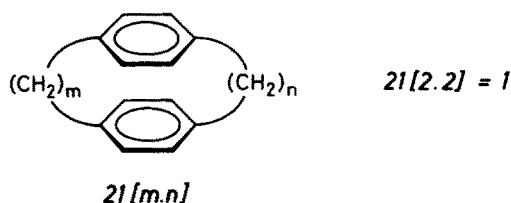
(Syntheses: $21[1.8]$ [56, 57]; $21[3.3]$ [58]; $21[3.4]$ [58, 59]; $21[4.4]$ [58, 60]; $21[6.6]$ [56].)

Along with the first report on $1^{\bar{\cdot}}$ ($= 21[2.2]^{\bar{\cdot}}$), the note by Weissman [16] included a brief statement on the radical anions prepared from several [m.n]paracyclophanes ($\neq 21[2.2]$) by reaction with K in DME. The frequency of the electron exchange between the two benzene rings was found to be lower than $3 \cdot 10^6 \ s^{-1}$ for [m.n] = [4.4] and [6.6], but higher than $1.5 \cdot 10^7 \ s^{-1}$ for [m.n] = [1.8]; an intermediate rate applied to [m.n] = [3.4]. No hyperfine data were reported. A more detailed study was carried out later [14] on the radical anions of [3.3]- and [4.4]paracyclophanes ($21[3.3]$ and $21[4.4]$) under conditions similar to those used in the first investigation. The ESR spectrum of $21[4.4]^{\bar{\cdot}}$, which exhibits a coupling constant of 0.535 mT, due to four equivalent protons of one benzene ring, is comparable to those of the radical anions of p-dialkylbenzenes [61]. Thus the spin population appears localized on one aromatic moiety. By contrast, the hyperfine data for $21[3.3]^{\bar{\cdot}}$, which are consistent with either a C_{2h} or a C_{2v} conformation, have been attributed to an even distribution of the spin population over both π-systems [14]. These data are 0.395 and 0.188 mT, each for a set of four equivalent aromatic protons, and 0.058 and 0.019 mT, each for a set of four equivalent protons in the methylene groups adjacent to the benzene rings.

The ESR studies on the radical anions of [m.n]paracyclophanes [14, 16] thus bear out the expectation that the frequency of electron exchange between the two benzene rings is lowered with the increasing numbers m, n of the methylene groups in the bridging chains. Since the exchange frequency is determined by the rate of migration of the counterion between two equivalent sites at the radical anion, every consideration of the relationship between the numbers m, n and this frequency must

be based on identical experimental conditions. For the solvent DME (with a small amount of HMPT), the counterion K^+ and temperature range 178–203 K, it appears that both numbers m and n must be equal or larger than 4 in order to slow down the migration rate k of the cation and therewith the exchange frequency of the electron spin below the hyperfine time-scale $(k < 10^6 \text{ s}^{-1})$ [14, 62].

2 Multiply Layered [2.2]Paracyclophanes
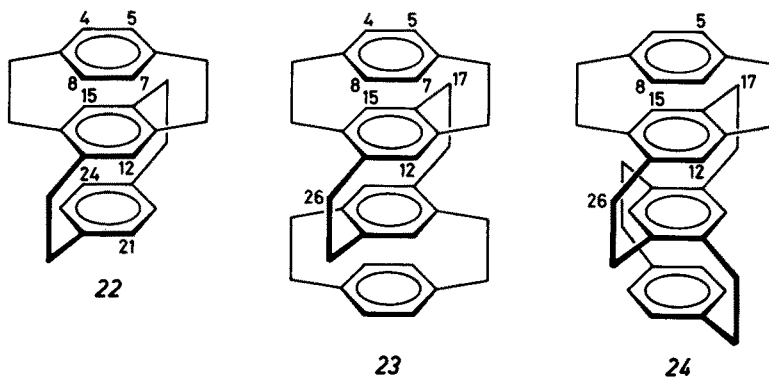
(Syntheses: 22, 23 and 24 [63].)

The triply (22) and quadruply layered paracyclophanes (23 and 24) were reduced by K, Cs, or Na/K alloy in ethereal solvents to their radical anions which proved to be less persistent than $I^{\overline{.}}$ and could be studied by ESR and/or ENDOR spectroscopy only at temperatures below 173 K [64]. No spectra attributable to primary radical anions $22^{\overline{.}}$, $23^{\overline{.}}$ and $24^{\overline{.}}$ were observed with DME or DME/HMPT, but use of DME/THF (1:1), THF, MTHF and DEE led to hyperfine patterns compatible with such species. With the exception of $22^{\overline{.}}$ in DME/THF and partly in THF (vide infra), all three radical anions give rise to ESR spectra which exhibit three broad bands spaced by ca. 0.6 mT, due to an interaction with two equivalent protons. This finding was rationalized in terms of tight or slowly exchanging ion pairs in which the counterion is situated above (or below) an outer benzene ring. The structures of such ion pairs are thus analogous to that of $I^{\overline{.}} - K^+$ (Fig. 3) [15].

The large coupling constant, responsible for the spacing in the ESR spectra, was assigned by means of simple HMO-type calculations to the two protons in the positions 4 and 7 of the benzene ring proximate to the counterion. With K^+, this value amounts to 0.613 (MTHF) and 0.648 (DEE) for $22^{\overline{.}}$, to 0.628 (DME/THF), 0.640 (THF), 0.654 (MTHF) and 0.662 mT (DEE) for $23^{\overline{.}}$, and to 0.620 (DME/THF) and 0.630 mT (THF) for $24^{\overline{.}}$. In addition, minor coupling constants were determined with the use of ENDOR spectroscopy. Only the largest values, two for $22^{\overline{.}}$ and three for $23^{\overline{.}}$ and $24^{\overline{.}}$, were assigned (Table 5) [64].

A different ESR spectrum was observed for $22^{\overline{.}}$ in DME/THF (1:1) (counterion K^+). Its main feature is a spacing into seven groups of lines, as expected for a major interaction with six protons. Occurrence of loose or fast exchanging ion pairs $22^{\overline{.}} - K^+$ was assumed in this case, and the observed major coupling

Table 5. Coupling constants, in mT, observed by ENDOR spectroscopy for the radical anions of triply (*22*) and quadruply layered paracyclophanes (*23* and *24*) [64]. Solvent MTHF (*22*⁻ and *23*⁻) and THF (*24*⁻), counterion K^+, temperature 156 (*22*⁻) and 159 K (*23*⁻ and *24*⁻)

22⁻		*23*⁻		*24*⁻	
5, 8[a]	0.134 (2H)	5, 8[a]	0.199 (2H)	5, 8[a]	0.126 (2H)
12, 15	0.147 (2H)	12, 15	0.134 (2H)	12, 15	0.170 (2H)
[b]	0.123 (2H)	17,26	0.084 (2H)	17, 26	0.126 (2H)
[b]	0.075 (2H)	[b]	0.059[c]	[b]	0.072[c]
[b]	0.064 (2H)	[b]	0.049[c]	[b]	0.052[c]
[b]	0.052 (2H)	[b]	0.017[c]	[b]	0.041[c]
[b]	0.032 (2H)			[b]	0.029[c]
[b]	0.020 (2H)			[b]	0.009[c]

a Positions.
b No assignment.
c Number of protons not indicated.

constants were assigned to protons in the positions 4,7,12,15,21 and 24, i.e., in all three benzene rings. On replacing DME/THF by pure THF, a complex spectrum appeared which might be viewed as a superposition of the seven groups of lines and the three broad bands observed with MTHF or DEE [64].

3 [2.2.2.2]Paracyclophane-1,9,17,25-tetraene
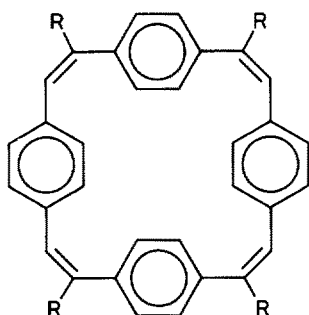
25, R = H
25-d₄, R = D

(Syntheses: *25* [65]; *25 — d₄* [66].)

Reaction of *25* and *25 — d₄* with K in DME led to relatively persistent radical anions which were studied by ESR and ENDOR spectroscopy [66]. The eight equivalent olefinic protons in *25*⁻ (g = 2.0027) have a coupling constant of 0.034 mT which is essentially temperature independent. The 16 aromatic protons give rise to coupling constants of 0.030 and 0.050 mT, each for a set of eight; the two values average to 0.040 mT at higher temperatures. Analysis of the ESR spectra in the range 193–333 K yields 36 ± 6 kJ/mol as the barrier to rotation of the phenylene

fragments. The radical anion $25^{\overline{\cdot}}$ can be considered as a non-planar species with weakly coupled aromatic and olefinic π-systems, whereby distortions from planarity reduce the coupling constant of the olefinic protons relative to the value expected for a planar molecule. In this respect $25^{\overline{\cdot}}$ bears some resemblance to the radical anion of Z-stilbene [67].

It is interesting to note that, according to their ^{1}H-NMR spectra, the corresponding diamagnetic dianion (25^{2-}) and tetraanion (25^{4-}) should be regarded as 26- and 28-π-electron derivatives of [24]annulene, respectively, since they sustain a diamagnetic (25^{2-}) or paramagnetic (25^{4-}) ring current [68]. The cyclic π-conjugation embraces the outer carbon centers of the phenylene fragments, the rotation of which is impeded.

E [2.2]Meta- and Metaparacyclophanes

1 [2.2]Metacyclophane and Its 1,9-Diene
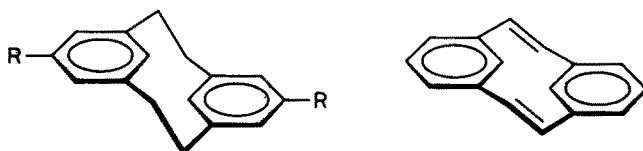
26, R = H
27, R = Me
28

(Syntheses: 26 [69]; 27 [70]; 28 [71].)

Numerous attempts to characterize the radical anion of the anti-[2.2]metacyclophanes 26, 27 and 28 failed altogether, since upon reduction of these compounds only the ESR spectra of secondary tetracyclic species were observed [14, 72, 73]. Thus reaction of 26 and 27 with K in DME [14] afforded the radical anions of 4,5,9,10-tetrahydropyrene (29) [74] and its 2,7-dimethyl-derivative (30) [21, 72], respectively (Reaction Scheme I).
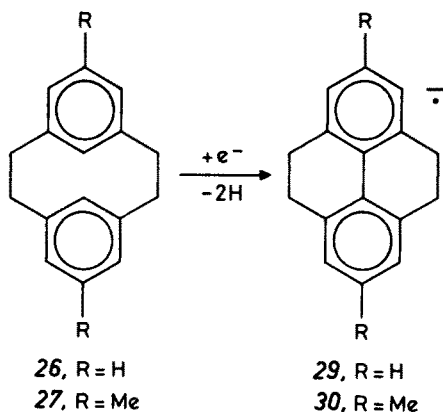
26, R = H   29, R = H
27, R = Me   30, R = Me

Reaction Scheme I

73

Analogously, reaction of the diene *28* with K in DME [72)] led to the radical anion of pyrene (*32*) [75)]. In this case, if a direct contact with the metallic mirror was avoided by using the method of solvated electrons [76)], the intermediately formed radical anion of trans-10b,10c-dihydropyrene (*31*) could also be characterized by ESR spectroscopy [72)] (Reaction Scheme II).
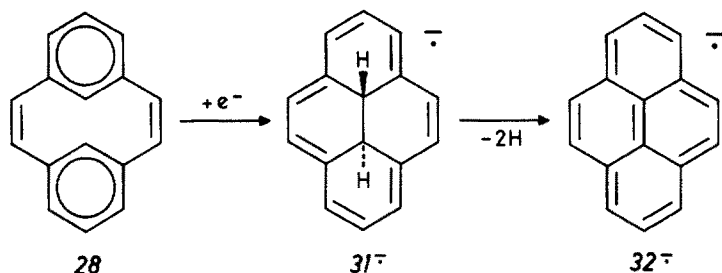
Reaction Scheme II

The dihydropyrene *31*, which is a valence isomer of the metacyclophane-diene *28*, has not been isolated in a pure form because of a facile conversion to *32* [71, 77)]. It represents an almost planar derivative of [14]annulene. The prominent feature of the ESR spectrum of *31*⁻ (Fig. 6) is a large coupling constant of 1.910 mT, due to the two inner protons of the ethano bridge [72)]. This large value points to a dominant hyperconjugative interaction between the π-perimeter LUMO and the σ-orbitals of the bridging group. (The remaining proton coupling constants for *31*⁻ will be given in Section G.3 of this review.)
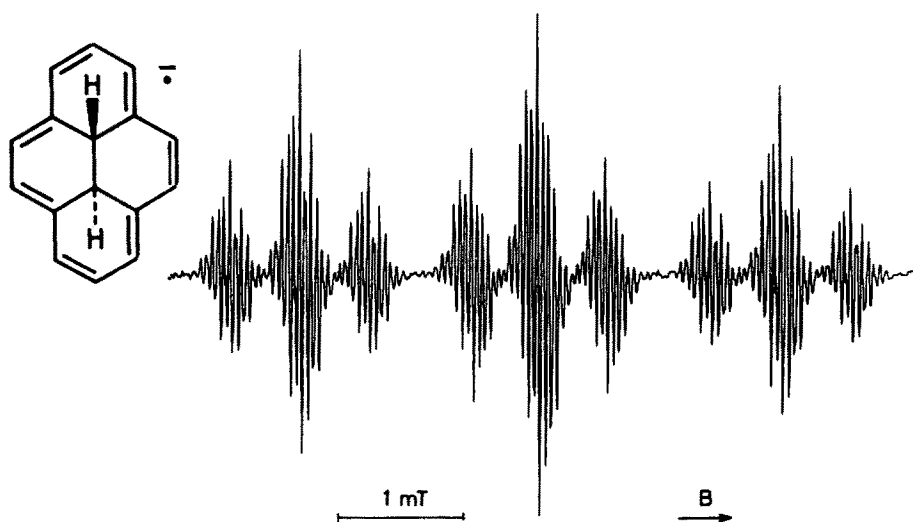
Fig. 6. ESR spectrum of the radical anion of trans-10b,10c-dihydropyrene (*31*). Solvent DME, counterion K^+, temperature 193 K. The central group of lines is broadened by unresolved second order splitting. Reproduced by permission of Helv. Chim. Acta [72)]

2 [2.2]Metaparacyclophane and Its 8-Cyano-Derivative
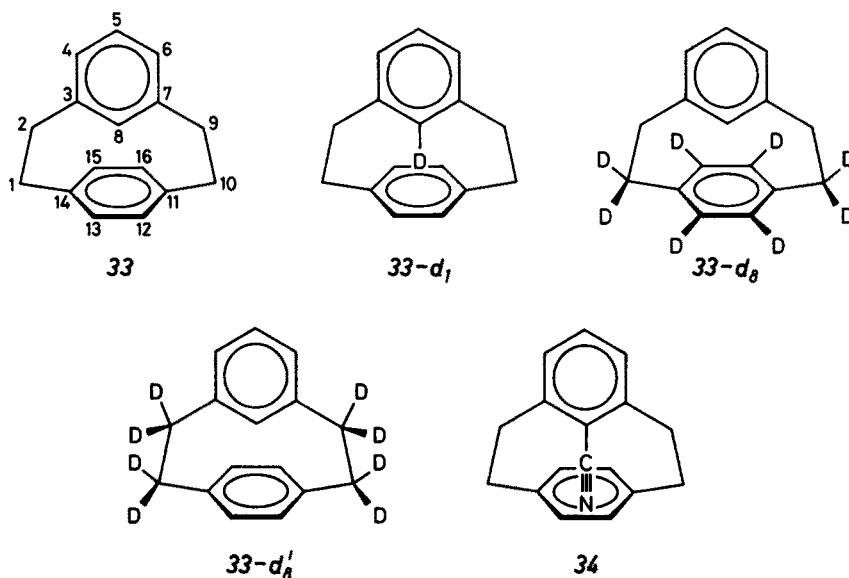
(Syntheses: 33 [78]; $33 - d_1$ [79,80]; $33 - d_8$ and $33 - d_8'$ [80]; 34 [81].)

The structure of [2.2]metaparacyclophane (33) in which the two benzene rings are perpendicular is not the preferred conformation, but a transition state for the flipping of the meta-bridged ring [82] (Fig. 7). The high temperature required for the flipping to be observed on the hyperfine time-scale is inaccessible for $33^{\bar{\ }}$ which exhibits a very poor persistence, even when prepared with K in DME/THF at a temperature as low as 163 K [80]. Although the work on this radical anion and those of its deuterio derivatives $33 - d_1$, $33 - d_8$ and $33 - d_8'$ has not yet been completed, it seems that the larger coupling constants are due to the protons in the para-bridged ring and the adjacent methylene groups. This ring thus appears to accomodate the major part of the spin population, in line with the slightly higher electron affinity of the p-xylene relative to that of m-xylene in solution [83].

The hyperfine data for the radical anion of 8-cyano[2.2]metaparacyclophane (34) [80] are similar to those for the radical anion of 2,6-dimethylbenzonitrile [80]. This finding points to substantial localization of the spin population on the meta-bridged benzene ring of $34^{\bar{\ }}$ and it allows one to make an assignment of the coupling constants in this

Fig. 7. Flipping of the meta-bridged benzene ring in [2.2]metaparacyclophane (33). Reproduced (in part) by permission of J. Am. Chem. Soc. [85]

75

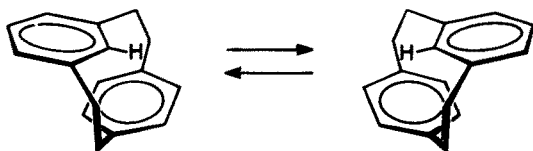radical anion: 0.203 (1N), 0.803 (1H; position 5), 0.040 (2H; positions 4, 6), and 0.243 and 0.157 mT (each 2H; 2,9-methylene); the remaining values are smaller than 0.03 mT. The experimental results for $34^{\overline{\cdot}}$, as compared with those of the unsubstituted radical anion $33^{\overline{\cdot}}$, can be rationalized by a two-fold effect of the cyano substituent, namely (1) the electron withdrawing power of the cyano group which shifts the spin population onto the meta-bridged ring, and (2) its elongated shape which enforces an almost parallel position of the two benzene rings with a concomitant reduction in the electronic interaction between the carbon atom 8 and the para-bridged ring.

3 [2.2]Metaparacyclophane-1,9-diene and Its 8-Fluoro- and 8-Cyano-Derivatives

35   35-d_1 35-d_6

36   37
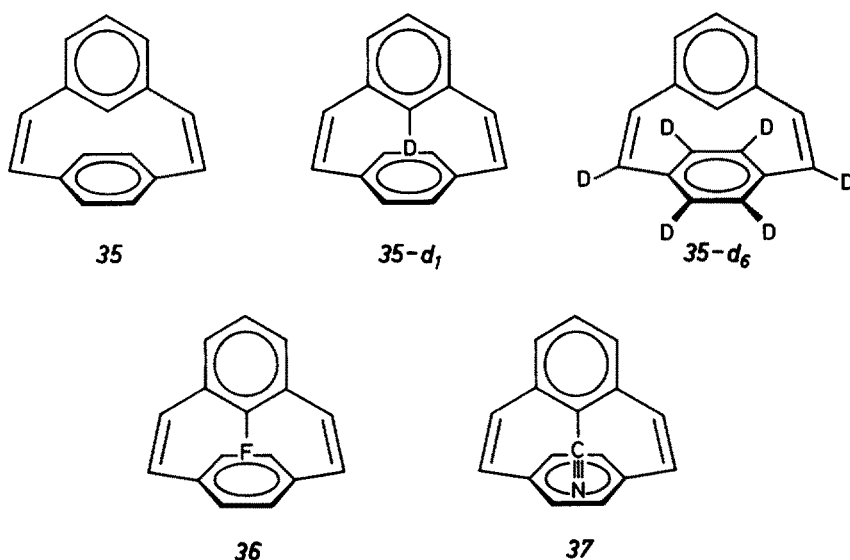
(Syntheses: 35 [84]; $35 - d_1$ [85, 86]; $35 - d_6$ [86]; 36 and 37 [81].)

The radical anion of [2.2]metaparacyclophane-1,9-diene (35) is considerably more persistent than $33^{\overline{\cdot}}$ when generated with K in ethereal solvents at low temperatures [86]. The same statement holds for the radical anions of 8-substituted derivatives of 35 relative to their analogues in the [2.2]metaparacyclophane series. Even the radical anion of 36, bearing a fluoro substituent, is sufficiently long-lived to be studied by ESR and ENDOR spectroscopy below 193 K [86]. According to the provisional results for the radical anions of 35 and its deuterio derivatives $35 - d_1$ and $35 - d_6$, the spin population in $35^{\overline{\cdot}}$ seems to be localized on the meta-divinylbenzene moiety with only little spin transfer to the para-bridged ring. Such localization is also observed for the radical anions of 36 and 8-cyano[2.2]metaparacyclophane-1,9-diene (37), although the substitutions lead to marked spin redistributions within this moiety. The substituent effects must again be due to both electronic and steric interactions.

F Multiply Bridged [2ₙ]Cyclophanes

38 (1,2,3)   38 (1,2,4)   38 (1,3,5)

39 (1,2,3,4)   39 (1,2,3,5)   39 (1,2,4,5)
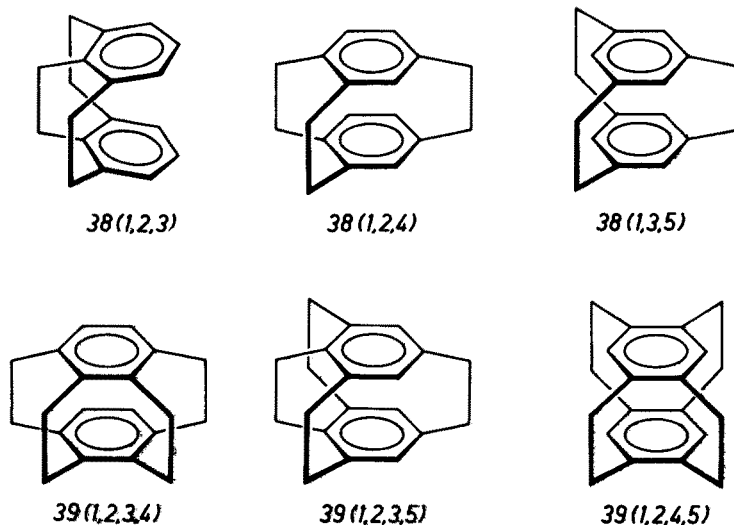
(Syntheses: *38(1,2,3)* [87]; *38(1,2,4)* [88]; *38(1,3,5)* [89]; *39(1,2,3,4)* [90]; *39(1,2,3,5)* [91]; *39(1,2,4,5)* [92].)

1 [2₃](1,2,4)- and [2₄](1,2,4,5)-Cyclophanes

All [2₃]- and [2₄]cyclophanes could be reduced in DME to their radical anions [93], either by direct contact with a K mirror or by the method of solvated electrons [76]. However, only the radical anions of [2₃](1,2,4)- and [2₄](1,2,4,5)cyclophane, *38(1,2,4)⁻* and *39(1,2,4,5)⁻*, were sufficiently persistent in solution to be studied by ESR and ENDOR spectroscopy.

Similarly to the radical anion of [2.2]paracyclophane (*1*), *38(1,2,4)⁻* [93] and *39(1,2,4,5)⁻* [20] occur as "free" or loosely associated species in DME/HMPT (counterion K^+) or in DMF (electrolysis with $Et_4N^+ClO_4^-$ as the supporting salt), while tight ion pairing with K^+ predominates in THF and MTHF. These findings are illustrated in Figs. 8 and 9 by the ESR and ENDOR spectra of *39(1,2,4,5)⁻* which is the most persistent of the [2.2]-, [2₃]- and [2₄]cyclophane radical anions and which was studied up to room temperature [20].

In pure DME, again analogously to the behavior of *1⁻*, "free" or loosely associated and tightly ion paired radical anions give rise concurrently to superimposable spectra. The coupling constants for *38(1,2,4)⁻* and *39(1,2,4,5)⁻* are listed in Tables 6 and 7, respectively. It is obvious that, on passing from the "free" or loosely associated radical anions to tight ion pairs, every set of m equivalent protons separates into two sets of m/2, as observed for *1⁻*. The average of the coupling constants for these two sets of m/2 protons in the ion pair is usually close to the corresponding value for the m protons in the "free" radical anion. By analogy to the results for *1⁻*, it is

Fig. 8. ESR spectra of the radical anion of $[2_4](1,2,4,5)$cyclophane, *39* (*1,2,4,5*). Top: solvent DMF, counterion Et_4N^+, temperature 213 K. Bottom: solvent MTHF, counterion K^+, temperature 213 K. Reproduced by permission of J. Chem. Soc. Perkin II [20]

reasonable to locate the m/2 protons having the larger of the two coupling constants in that moiety of the radical anion which is proximate to the site of the counterion.

The $[2_4](1,2,4,5)$cyclophane, *39(1,2,4,5)*, may be regarded as a counterpart of [2.2]paracyclophane (*1*), since the bridged and unbridged benzene carbon atoms are interchanged. Both cyclophanes have the same symmetry (D_{2h}) and their benzene rings undergo distortions to boats by almost the same amount, but in an opposite sense [94]. It is therefore not surprising that the radical anions $1^{\cdot-}$ and $39(1,2,4,5)^{\cdot-}$ exhibit a similar behavior on association with the counterion [20]. The large coupling constants found for the ^{39}K and ^{133}Cs nuclei in the ion pairs of $39(1,2,4,5)^{\cdot-}$ suggest merely that the association might be stronger for this radical anion than for $1^{\cdot-}$.
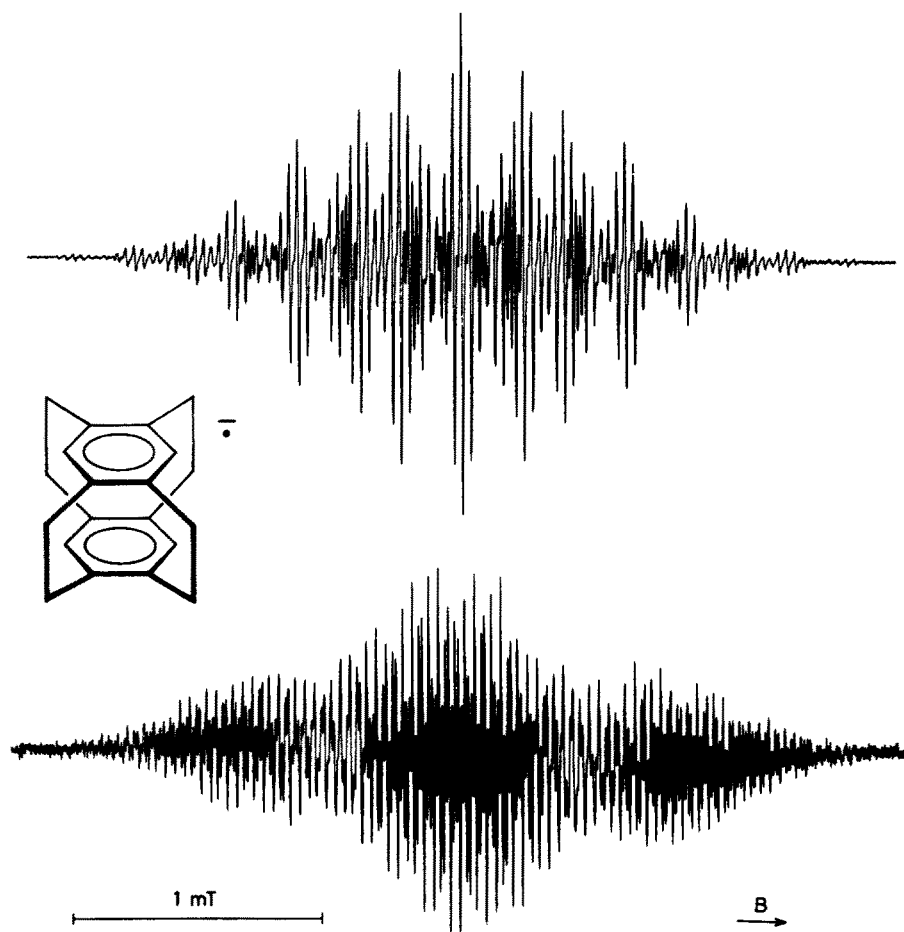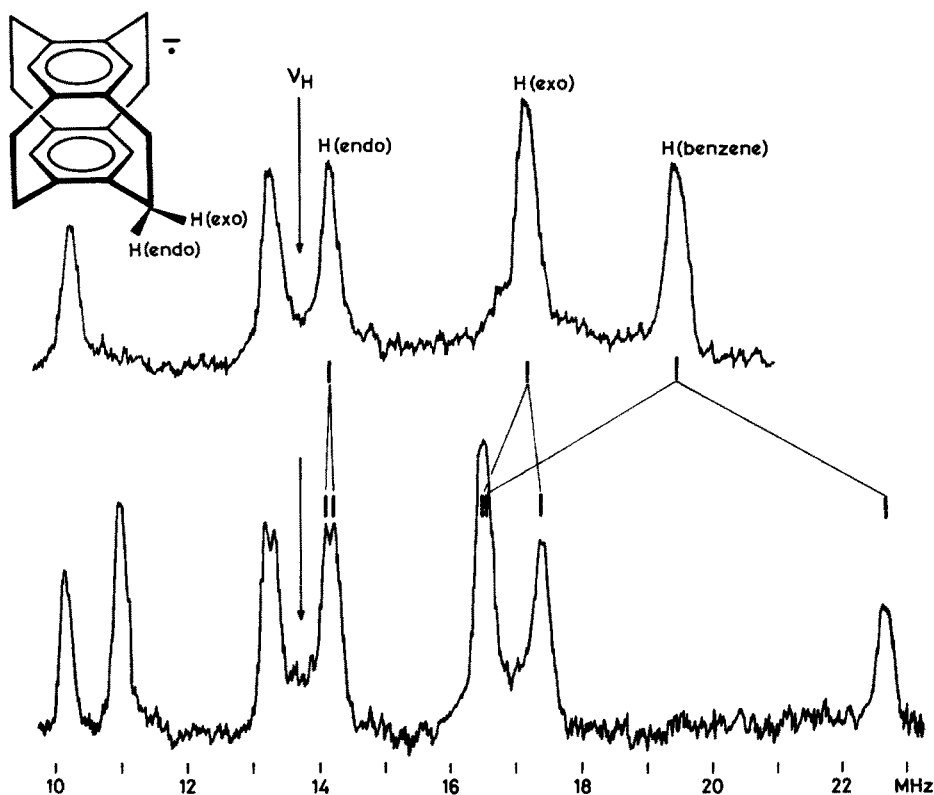
Fig. 9. Proton ENDOR spectra of the radical anion of [2₄](1,2,4,5)cyclophane, *39 (1,2,4,5)*. Top: solvent DME/HMPT (3:1), counterion K^+, temperature 153 K. Bottom: solvent MTHF, counterion K^+, temperature 153 K. ν_H = frequency of the free proton. Reproduced by permission of J. Chem. Soc. Perkin II [20]

The coupling constants of the aromatic protons in *39(1,2,4,5)*⁻, as compared with the corresponding values for *1*⁻, indicate that the singly occupied orbital in *39(1,2,4,5)*⁻ should be represented by the A_g combination of the "symmetric" benzene LUMO's ψ_S, in contrast to *1*⁻ where such an orbital is considered as the B_{1g} combination of the "antisymmetric" LUMO's ψ_A (Fig. 4). This MO description is reasonable in view of the above-mentioned interchange of bridged and unbridged benzene carbon atoms in *39(1,2,4,5)* and *1*. Proton coupling constants, calculated by the INDO procedure [53] for *39(1,2,4,5)*⁻, are in qualitative agreement with the experimental values. They support the assignment of the larger methylene proton coupling constant to the exo-positions (Fig. 9 and Table 7).

2 [2₃](1,2,3)-, [2₃](1,3,5)-, [2₄](1,2,3,4)- and [2₄](1,2,3,5)Cyclophanes

The radical anions of the two [2₃]cyclophanes, *38(1,2,3)* and *38(1,3,5)*, and of the two [2₄]cyclophanes, *39(1,2,3,4)* and *39(1,2,3,5)*, were too short-lived to give rise to observable ESR spectra [93]. Like anti-[2.2]metacyclophane (*26*) and its 5,13-dimethyl-

79

Table 6. Coupling constants, in mT, for the radical anion of [2$_3$](1,2,4)cyclophane, 38 (1,2,4)[93], g = 2.0029

Solvent	DMF	MTHF	DMF[a]	MTHF[b]	DMF[a]	MTHF[b]
Counterion	Et$_4$N$^+$	K$^+$	Et$_4$N$^+$	K$^+$	Et$_4$N$^+$	K$^+$
Temp., K	213	163	213	163	213	163
Benzene protons	0.475 (2H)	0.663 (1H) 0.289 (1H)	0.465 (2H)	0.623 (1H) 0.241 (1H)	0.330 (2H)	0.427 (1H) 0.229 (1H)
Methylene protons	0.140 (2H) 0.040 (2H)	0.211 (1H) 0.145 (1H) 0.044 (1H) 0.029 (1H)	0.140 (2H) <0.020 (2H)	0.198 (1H) 0.122 (1H) 0.029 (1H) <0.010 (1H)	0.040 (2H) <0.020 (2H)	0.052 (1H) 0.029 (1H) 0.018 (1H) <0.010 (1H)

a Continuation of the first data column.
b Continuation of the second data column.

Table 7. Coupling constants, in mT, for the radical anion of [2$_4$](1,2,4,5)cyclophane, 39 (1,2,4,5)[20], g = 2.0028[a]

Solvent	DMF	DME/HMPT	DME[b]	DME[b]	MTHF	MTHF
Counterion	Et$_4$N$^+$	K$^+$	K$^+$	K$^+$	K$^+$[a]	K$^+$[a]
Temp., K	213	178	178	178	153	213
Benzene protons	0.409 (4H)	0.407 (4H)	0.407 (4H)	0.598 (2H) 0.234 (2H)	0.645 (2H) 0.195 (2H)	0.637 (2H) 0.209 (2H)
Methylene protons endo[c]	0.033 (8H)	0.033 (8H)	0.033 (8H)	0.038 (4H) 0.028 (4H)	0.038 (4H) 0.028 (4H)	0.038 (4H) 0.028 (4H)
Methylene protons exo[c]	0.245 (8H)	0.248 (8H)	0.248 (8H)	0.259 (4H) 0.213 (4H)	0.260 (4H) 0.195 (4H)	0.253 (4H) 0.186 (4H)
^{39}K[a]				0.075 (1K)	0.085 (1K)	0.103 (1K)

a In MTHF, with Cs$^+$ as the counterion, g = 2.0020; the ^{133}Cs coupling constant is 0.625 and 0.823 mT at 153 and 213, respectively.
b Concurrently observed; cf. text.
c Cf. formula in Fig. 9.

derivative (27) (Reaction Scheme I), these compounds cyclized rapidly upon reduction to yield 4,5,9,10-tetrahydropyrenes which were identified as the corresponding radical anions by ESR and ENDOR spectroscopy [93] (Reaction Scheme III).
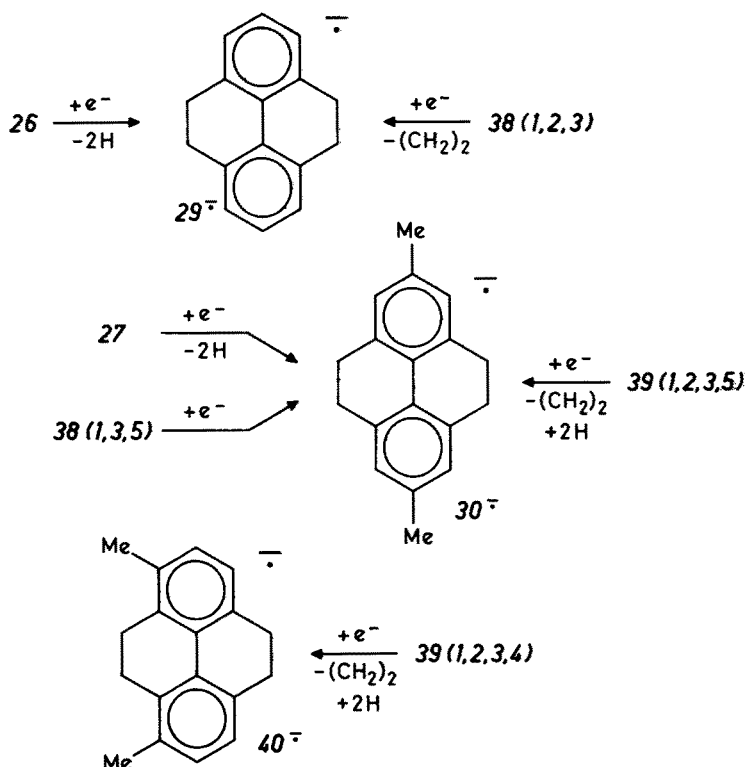
Reaction Scheme III

For 38(1,2,3), 39(1,2,3,4) and 39(1,2,3,5), in each of which three or more carbon atoms are bridged at consecutive positions (1,2,3), the cyclization to tetrahydropyrenes requires elimination of an intermediate ethano bridge (position 2). Moreover, in

Table 8. Numbers of pairs of ethano bridges in the positions ortho, meta and para of the benzene rings in [2.2]-, [2₃]- and [2₄]cyclophanes, along with the persistence of the corresponding radical anions [93]

Cyclophane	Positions			Radical anion
	ortho	meta	para	
26	0	1	0	non-persistent
1	0	0	1	persistent
38 (1,2,3)	2	1	0	non-persistent
38 (1,2,4)	1	1	1	persistent
38 (1,3,5)	0	3	0	non-persistent
39 (1,2,3,4)	3	2	1	non-persistent
39 (1,2,3,5)	2	3	1	non-persistent
39 (1,2,4,5)	2	2	2	persistent

39(1,2,3,4) and *39(1,2,3,5)*, as well as in *38(1,3,5)*, the C—C bond of one bridge undergoes a cleavage, and the methylene groups thus formed appear as methyl substituents in *30⁻* and *40⁻*.

The persistence of the radical anions of [2.2]-, [2₃]- and [2₄]cyclophanes has been related to the positions of ethano bridges at the benzene rings, these bridges being pairwise characterized by their ortho-, meta- and para-positions [93]. Thus, the radical anion is persistent when the number of the para-positioned pairs is equal to or larger than that of the meta-positioned ones (Table 8).

It is noteworthy that [2₃](1,3,5)cyclophane-1,9,17-triene *(41)* [95] reacts with K in DME [72, 73] to yield the radical anion of pyrene *(32)* [75] (Reaction Scheme IV) which is also obtained as the final product of reduction of anti-[2.2]metacyclophane-1,9-diene *(28)* (Reaction Scheme II). The cyclization of *41* to *32⁻* involves elimination of one —CH=CH— bridge.
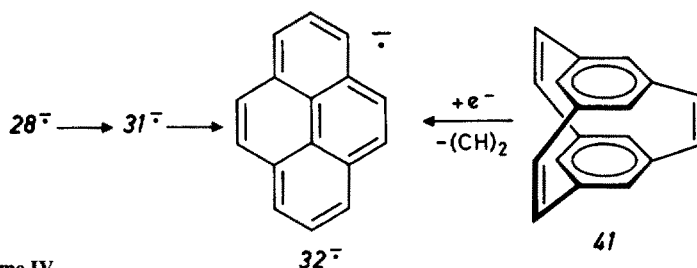
Reaction Scheme IV

G Arenophanes

1. [2]Paracyclo[2]arenophanes
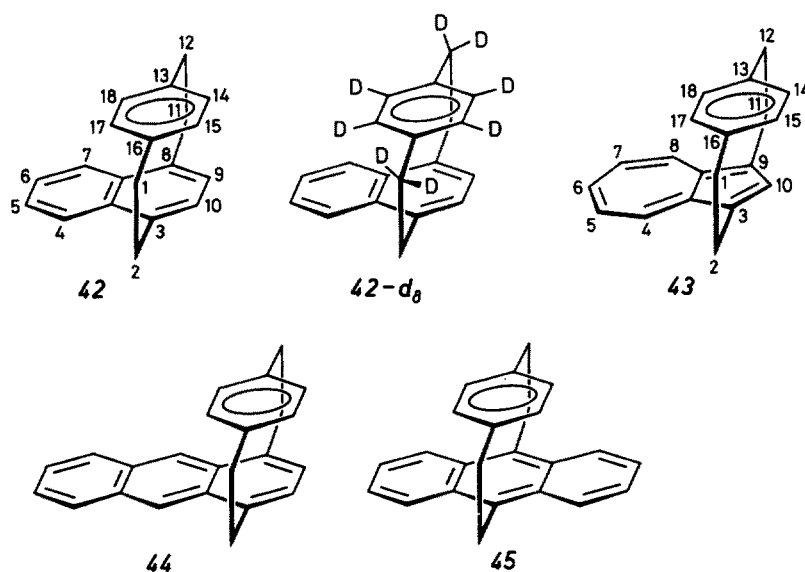
(Syntheses: *42* [96,97]; *42—d₈* [97]; *43* [98]; *44* [99]; *45* [96].)

Table 9. Coupling constants, in mT, for the radical anions of [2]paracyclo[2](1,4)naphthalenophane (*42*) [97] and [2]paracyclo[2](1,3)azulenophane (*43*) [100]

	42⁻				*43⁻*			
Solvent		DME	MTHF			DME	MTHF	
Counterion		K⁺	K⁺			Na⁺	K⁺	
Temp., K		183	183			183	178	
Naphthalene or azulene protons	4, 7[a]	0.448 (2H)	0.437 (2H)		4, 8[a]	0.575 (2H)	0.618 (2H)	
	5, 6	0.168 (2H)	0.173 (2H)		5, 7	0.107 (2H)	0.125 (2H)	
	9, 10	0.073 (2H)	0.079 (2H)		6	0.836 (1H)	0.875 (1H)	
					10	0.387 (1H)	0.361 (1H)	
Benzene protons	14, 15[a] / 17, 18	<0.005 (2×2H)	<0.005 (2×2H)		14, 15[a] / 17, 18	<0.01 (2×2H)[b]	<0.01 (2×2H)	
Methylene protons	2, 11[a]	0.412 (2H)	0.417 (2H)		2, 11[a]	0.033 (2H)	0.029 (2H)	
		0.070 (2H)	0.074 (2H)			0.024 (2H)[b]	0.022 (2H)	
	1, 12	0.014 (2H)	0.008 (2H)		1, 12	0.016 (2H)[b]	0.011 (2H)	
		<0.005 (2H)	<0.005 (2H)			<0.01 (2H)	<0.01 (2H)	

a Positions.
b Assignment different from that in the original paper [100].

Reduction with K in ethereal solvents was performed for all compounds *42–45* [97,100,101], but the ESR spectra of the radical anions of the two [2]paracyclo-[2]anthracenophanes *44* and *45* were not analyzed [101]. Hyperfine data, obtained by ESR and ENDOR spectroscopy, were reported for the radical anions of [2]para-cyclo[2](1,4)naphthalenophane (= benzo[2.2]paracyclophane; *42*) and its octadeuterio derivative *42—d*$_8$ [97]. A selection of these data is given in Table 9, along with those determined by the same techniques for the radical anion of [2]paracyclo[2](1,3)-azulenophane (*43*) [100]. Since naphthalene and azulene have substantially higher electron affinities than benzene, the spin populations in *42*⁻ and *43*⁻ are almost entirely located on the aromatic moiety with the more extended π-system, irrespective of experimental conditions. In fact, the coupling constants of the aromatic protons in *42*⁻ and *43*⁻ bear a strong resemblance to the corresponding values for the radical anions of 1,4-dimethylnaphthalene [102] and azulene [103], respectively. (The hyperfine data for the radical anion of 1,3-dimethylazulene, which is a more appropriate reference compound for *43*, have not yet been reported.)

2 [2.2](1,4)Naphthalenophanes

46   *47*
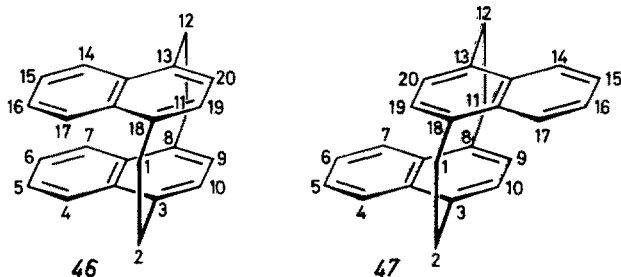
(Syntheses: *46* [104]; *47* [96,105].)

The first attempt to study the radical anion of anti-[2.2](1,4)naphthalenophane (*47*) by ESR spectroscopy was unsuccessful. The spectrum observed upon reaction of *47* with K in DME and attributed to *47*⁻ [106], stemmed from the radical anion of 1,4-dimethylnaphthalene [102], a secondary product of the reduction of *47* [18]. Shortly afterwards, the ESR spectrum of *47*⁻ was reported, but not analyzed in detail [107]. A complete set of hyperfine data for both *47*⁻ and its syn-isomer *46*⁻ was obtained by subsequent ESR and ENDOR studies [18,97] (Table 10). With the counterion K⁺, "free" or loosely associated radical anions (symmetry C$_{2v}$ for *46*⁻ and C$_{2h}$ for *47*⁻) are present in DME and THF, whereas tight ion pairs (symmetry C$_s$) form in MTHF. It is informative to compare the proton coupling constants for the tight ion pairs of *46*⁻ and *47*⁻ with the corresponding values for the radical anion of 1,4-dimethylnaphthalene [102] and, in particular, with those for the radical anion of [2]paracyclo[2](1,4)naphthalenophane (*42*) [97] (Table 9). Since, both in the ion pairs of *46*⁻ ·and *47*⁻ and in *42*⁻, the spin populations are substantially localized on one naphthalene π-system, the coupling constants for the protons in this moiety of the three species should be similar. Actually, the similarity between *42*⁻ and the ion

Table 10. Coupling constants, in mT, for the radical anions of syn- (46) and anti-[2.2](1,4)naphthalenophane (47) [18,97]. Counterion K^+, temperature 183 K

Solvent		46⁻ DME	THF	MTHF	47⁻ DME	THF	MTHF
Naphthalene protons	4, 7[a]	0.242 (4H)	0.239 (4H)	0.364 (2H)	0.300 (4H)	0.302 (4H)	0.448 (2H)
	14, 17			0.106 (2H)			0.109 (2H)
	5, 6	0.132 (4H)	0.127 (4H)	0.191 (2H)	0.098 (4H)	0.097 (4H)	0.159 (2H)
	15, 16			0.060 (2H)			0.035 (2H)
	9, 10	0.100 (4H)	0.100 (4H)	0.143 (2H)	0.060 (4H)	0.057 (4H)	0.095 (2H)
	19, 20			0.055 (2H)			0.016 (2H)
Methylene protons	2, 11[a]	0.170 (4H)	0.170 (4H)	0.232 (2H)	0.213 (4H)	0.211 (4H)	0.380 (2H)
	1, 12			0.090 (2H)			0.042 (2H)
	2, 11	0.035 (4H)	0.036 (4H)	0.050 (2H)	0.028 (4H)	0.026 (4H)	0.046 (2H)
	1, 12			0.016 (2H)			0.004 (2H)

a Positions.

pairs of *47⁻* is much more pronounced than between *42⁻* and the ion pairs of *46⁻*. This is a reasonable result, since on going from *42⁻* to the radical anion of the anti-naphthalenophane *47*, the additional benzene ring is brought into a position away from the naphthalene π-system of *42⁻* so that the spin distribution is not greatly affected by such a change. On the contrary, as the analogous annelation of *42⁻*, to yield the syn-isomer *46⁻*, places the additional ring essentially above the naphthalene π-system of *42⁻*, the spin distribution is markedly altered. In other words, due to the stronger overlap of the benzene π-clouds in *46⁻* relative to *47⁻*, the spin localization in one naphthalene moiety is less efficient in the ion pairs of the former as compared to those of the latter.

3 [2.2](2,7)Naphthalenophane and Its 1,11-Diene

48   49, R = H

49-d₂, R = D
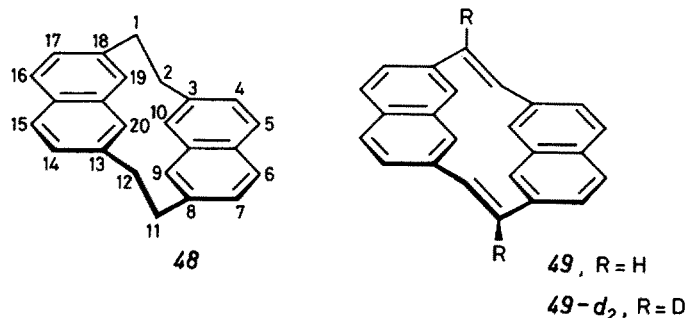
(Syntheses: *48*[108]; *49*[109,110]; *49—d₂*[110].)

While the [2.2](1,4)naphthalenophanes *46* and *47* are symmetric dibenzohomologues of [2.2]paracyclophane (*1*), anti-[2.2](2,7)naphthalenophane (*48*) can be regarded as an analogue of anti-[2.2]metacyclophane (*26*). Correspondingly, anti-[2.2](2,7)-naphthalenophane-1,11-diene (*49*) exhibits a structural relationship to anti-[2.2]meta-cyclophane-1,9-diene (*28*). In contrast to metacyclophane radical anions *26⁻* and *28⁻*, which are too short-lived to be characterized by their hyperfine data, *48⁻* and *49⁻* are sufficiently persistent to be studied by ESR and ENDOR spectroscopy[73]. The radical anions *48⁻*, *49⁻* and *49—d₂⁻* were all prepared by reaction with K in DME and, under these conditions, they displayed the full symmetry (C_{2h}) of the "free" or

Table 11. Coupling constants, in mT, for the radical anions of anti-[2.2](2,7)naphthalenophane (*48*) and its 1,11-diene (*49*)[73]. Solvent DME, counterion K⁺, temperature 193 K

		48⁻	*49⁻*
Naphthalene protons	4, 7, 14, 17[a]	0.083 or 0.104 (4H)	0.032 (4H)
	5, 6, 15, 16	0.268 (4H)	0.108 (4H)
	9, 10, 19, 20	0.194 (4H)	0.307 (4H)
Methylene or olefin protons	1, 2, 11, 12[a]	{ 0.104 or 0.083 (4H) { 0.043 (4H)	0.087 (4H)

a Positions.

86

loosely associated species. The proton coupling constants for *48*⁻ (Table 11) compare favorably with halves of the corresponding values for the radical anion of 2,7-dimethylnaphthalene [102] which is also obtained as a cleavage product, presumably via the dianion *48*= [73].

Cyclization of *48*⁻ to the radical anion of 5,6,11,12-tetrahydrocoronene, which might have been anticipated by formation of *29*⁻ upon reduction of *26* (Reaction Scheme I), was not observed [73]. By contrast, the radical anion *49*⁻ of the diene (characterized by the hyperfine data in Table 11) cyclizes in a way analogous to the conversion of *28* into *32*⁻ via *31*⁻ (Reaction Scheme II). Thus, on standing, *49*⁻ yields the radical anion of trans-12b,12c-dihydrocoronene (*50*) [73] which is subsequently transformed to that of coronene (*51*) [111] (Reaction Scheme V).
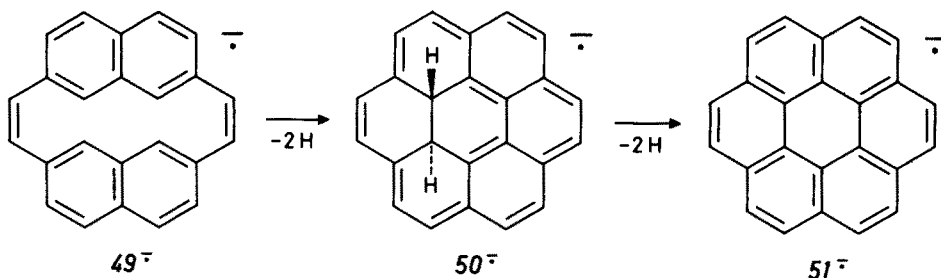
Reaction Scheme V

Compound *50* is still unknown in its neutral form. It can be viewed as trans-10b,10c-dihydropyrene (*31*) fused to the phenanthrene π-system. The structural relationship of *31*⁻ and *50*⁻ is evident from comparison of their proton coupling constants (Fig. 10).
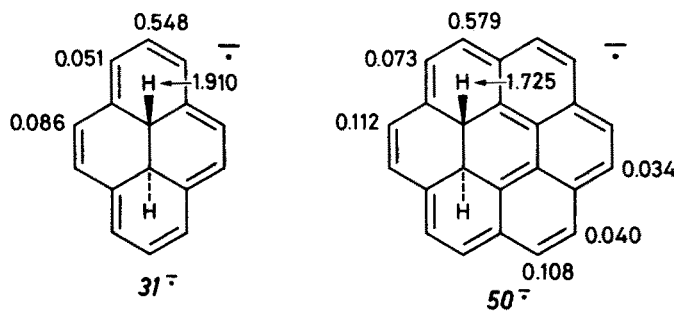
Fig. 10. Proton coupling constants, in mT, for the radical anions of trans-10b,10c-dihydropyrene (*31*) and trans-12b,12c-dihydrocoronene (*50*). Reproduced (in part) by permission of J. Am. Chem. Soc. [73]

4 [2.2](1,4)- and [2.2](9,10)Anthracenophanes

In the radical anions of syn- and anti-[2.2](1,4)anthracenophanes (*52* and *53*) prepared by reduction of the neutral compounds with Na or K in DME, THF or MTHF, the spin population is evenly distributed between the two aromatic

52

53

54

54 − d₁₆
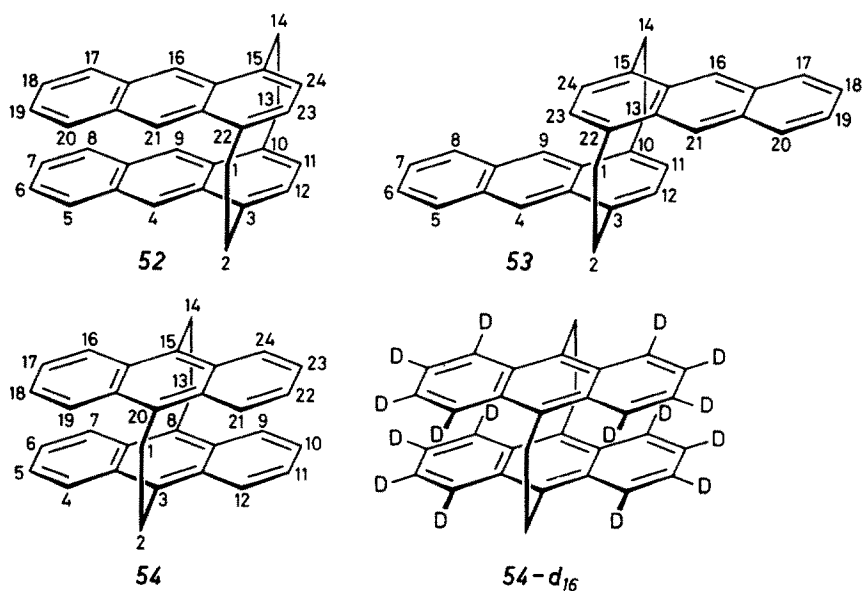
(Syntheses: 52 and 53 [112]; 54 [113]; 54 — d_{16} [107,114].)

moieties, irrespective of the alkali metal and the ethereal solvent used [115]. The coupling constants of the aromatic protons in 52⁻ and 53⁻ (Table 12) thus resemble halves of the corresponding values for the radical anion of 1,4-dimethylanthracene [115] It is noteworthy that the coupling constant of the protons in the positions 4, 9, 16 and 21 is considerably larger for 52⁻ than for 53⁻. This finding has been interpreted as evidence for the accumulation of the spin population on the overlapping part of the aromatic moieties. Furthermore, the non-equivalence of the two protons in a methylene group of 52⁻ and 53⁻, which is expected by symmetry (C_{2v} or C_{2h}, respectively), has been discussed in terms of a rocking model of the ethano bridges [115].

Table 12. Coupling constants, in mT, for the radical anions of syn- (52) and anti-[2.2](1,4)anthraceno-phanes (53) [115]. Counterion Na⁺, temperature 173 K

Solvent[a]		52⁻		53⁻	
		DME	MTHF	DME	MTHF
Anthracene protons	4, 9, 16, 21[b]	0.268 (4H)	0.273 (4H)	0.244 (4H)	0.235 (4H)
	5, 8, 17, 20	0.113 (4H)	0.112 (4H)	0.111 (4H)	0.110 (4H)
	6, 7, 18, 19[c]	0.077 (4H)	0.074 (4H)	0.079 (4H)	0.078 (4H)
	11, 12, 23, 24[c]	0.070 (4H)	0.074 (4H)	0.073 (4H)	0.072 (4H)
Methylene protons	1, 2, 13, 14[b]	0.090 (4H)	0.090 (4H)	0.168 (4H)	0.167 (4H)
		0.056 (4H)	0.054 (4H)	0.015 (4H)	0.015 (4H)

a Values for THF are very close to those for DME and MTHF.
b Positions.
c Assignment to these positions is not secured.

[2.2](9,10)anthracenophane (*54*) is of special interest, since it represents an unsubstituted phane of which both radical anion and cation have been investigated in solution and characterized by their hyperfine data.

The radical anion *54⁻*, produced by reaction of *54* with K in ethereal solvents, was studied by several research groups. The ESR spectra of *54⁻* and $54 - d_{16}^-$ were first reported in 1971 [107], but only the hyperfine splitting from the methylene protons was determined. Subsequently, all coupling constants for *54⁻* appeared in the literature [101], but one of the values for the aromatic protons was in error. Shortly afterwards, correct hyperfine data, as measured by ESR and ENDOR spectroscopy of *54⁻* [18] and $54 - d_{16}^-$ [18,114], were published (Table 13). The coupling constants, which do not markedly depend on the ethereal solvent used (DME, THF and MTHF), reflect the full symmetry (D_{2h}) of the molecule without any evidence of a tight ion pairing. The values for the aromatic protons are roughly half as large as those for the radical anion of 9,10-dimethylanthracene [116].

Table 13. Coupling constants, in mT, for the radical anion and the radical cation of [2.2](9,10)-anthracenophane (*54*) [18,114]

		54⁻		*54⁺*
Solvent		DME	THF or MTHF	$CH_2Cl_2/CF_3COOH/$ $(CF_3CO)_2O$ (20:2:1)
Counterion		K^+	K^+	CF_3COO^-
Temp., K		183	183	183
Anthracene protons	4, 7, 9,12[a] 16,19,21,24	0.126 (8H)	0.126 (8H)	0.110 (8H)
	5, 6,10,11 17,18,22,23	0.078 (8H)	0.078 (8H)	0.065 (8H)
Methylene protons	1, 2,13,14[a]	0.156 (8H)	0.155 (8H)	0.098 (8H)

a Positions.

The radical cations *54⁺* (hyperfine data in Table 13) and $54 - d_{16}^+$ were generated by dissolving the neutral compounds in $CH_2Cl_2/CF_3COOH/(CF_3CO)_2O$ (20:2:1) [114]. In Fig. 11, the coupling constants of the aromatic protons for the dimer radical cation of 9,10-dimethylanthracene (*55*) [39] are compared with those for *54⁺*. The similarity
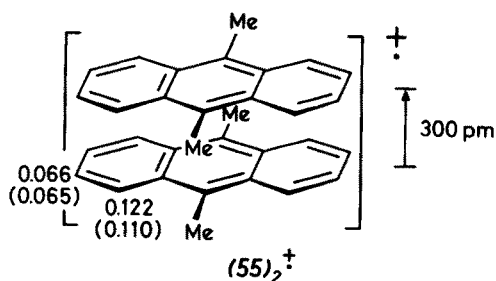

$(55)_2^{+}$

Fig. 11. Coupling constants, in mT, of the aromatic protons in the dimer radical cation of 9,10-dimethylanthracene (*55*) [39]. The corresponding values for the radical cation of [2.2](9,10)anthracenophane (*54*) [114] are given in parentheses

between the two sets of values suggests that $(55)_2^{+}$, like 54^{+}, contains two aromatic moieties in essentially eclipsed positions with a mean interplanar distance of ca. 300 pm. Such a structure has been previously proposed for the dimer radical cations of anthracene and several other aromatic hydrocarbons [117].

5 [2.2](2,7)Pyrenophane

56
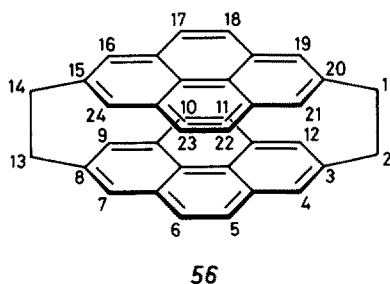
(Synthesis: 56 [118].)

Reduction of [2.2](2,7)pyrenophane (56) with Na in DME or THF yielded its radical anion which was studied by ESR and ENDOR spectroscopy [119]. The observed coupling constants of 0.225 and 0.108 mT, each for eight equivalent aromatic protons in the positions 4, 7, 9, 12, 16, 19, 21, 24 and 5, 6, 10, 11, 17, 18, 22, 23, respectively, indicated delocalization of the spin population over both pyrene moieties. They are comparable to halves of the corresponding values for the radical anion of pyrene (32) [75]. (Those for the 2,7-dimethyl-derivative of 32^{-} have not yet been reported.) The hyperfine splittings from the methylene protons in 56^{-} are very small and could not be observed [119].

## 6 "Mixed" Arenophanes

57

58
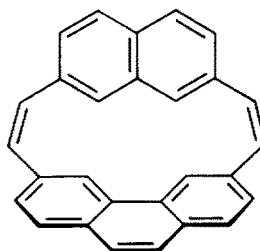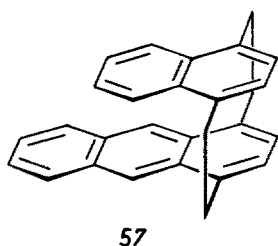
(Syntheses: 57 [99, 120]; 58 [121].)

Radical anions of syn-[2](1,4)naphthaleno[2](1,4)anthracenophane (57) [101] and [2](2,7)naphthaleno[2](3,6)phenanthrenophane-1,13-diene (58) [122] were prepared by alkali metal reduction of the neutral compounds in ethereal solvents. While no analysis was reported for the ESR spectrum of 57^{-}, all nine coupling constants,

each for a pair of equivalent protons, were determined for *58⁻* with the use of the ENDOR technique [122]. These values (solvent DME, counterion K⁺, temperature 183 K) are as follows: 0.367, 0.234, 0.155, 0.105, 0.087, 0.071, 0.046, 0.030 and 0.006 mT. Their assignment to protons in individual positions of *58⁻* is difficult without availability of deuteriated derivatives.

7 [2.2](1,3)- and [2.2](2,6)Azulenophanes

59

60   **61**
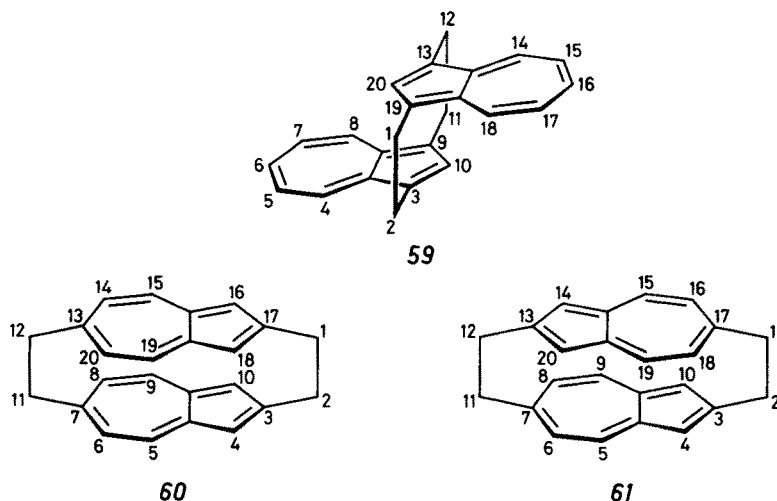
(Syntheses: *59* [123]; *60* [124]; *61* [124−126].)

Except [2]paracyclo[2](1,3)azulenophane (*43⁻*) (Section G.1), which contains one non-alternant aromatic moiety, all arenophanes dealt with so far in this review comprise two benzenoid systems. By contrast, in anti-[2.2](1,3)azulenophane (*59*), as well as in syn- and anti-[2.2](2,6)azulenophanes (*60* and *61*), both aromatic moieties are non-alternant. Recently, the radical anions *59⁻*, *60⁻* and *61⁻*, generated from the neutral compounds by reaction with K or Na in ethereal solvents, were studied by ESR spectroscopy [100]. Their persistence is lower than that of *43⁻* which, in turn, is less persistent than the radical anions of cyclophanes containing only benzenoid aromatic moieties, such as [2]paracyclo[2](1,4)naphthaleno-phane (*42*) and syn- and anti-[2.2](1,4)naphthalenophanes (*46* and *47*). Thus, the persistence decreases with the successive replacement of a benzenoid by a non-alternant π-system. The radical anions *59⁻*, *60⁻* and *61⁻* could be investigated only at temperatures below 183 K and, unlike *43⁻*, they were not persistent in DME/THF mixtures when the ratio of DME to THF exceeded 3:1. Also, in contrast to *43⁻* the concentrations of *59⁻*, *60⁻* and *61⁻* were not sufficient for the use of the ENDOR technique. The reported hyperfine data refer to the counterion K⁺ and to the solvents THF, MTHF and DME/THF (3:1) with or without addition of the 18-crown-6-ether [100]. Table 14 lists only the values for DME/THF (without the crown-ether), since their dependence on the solvent is rather small. It is obvious that, under the applied experimental conditions, tight ion pairs are observed with a sub-

Table 14. Coupling constants, in mT, for the radical anions of anti-[2.2](1,3)azulenophane (*59*), and syn- (*60*) and anti-[2.2](2,6)azulenophane (*61*) [100] Solvent DME/THF (3:1), counterion K^{+}, temperature 193 K

|	*59*[–]		*60*[–]		*61*[–]
	4,8[a]	0.610 (2H)	5,9[a]	0.557 (2H)	0.599 (2H)
Azulene	5,7	0.110 (2H)	6,8	0.251 (2H)	0.222 (2H)
protons[b]	6	0.840 (2H)	15,19	0.094 (2H)	—
	10	0.367 (2H)			
			2[a]	0.291 (2H)	0.349 (2H)
Methylene			11	0.517 (2H)	0.505 (2H)
protons[b]			12	0.050 (2H)	—

a Positions.
b Those positions for which no proton coupling constants were reported have been omitted.

stantial localization of the spin population on one azulene moiety. This effect increases in the sequence *60*[–] < *61*[–] < *59*[–], i.e., with decreasing overlap of the π-clouds of the two azulene moieties. The relationship *60*[–] < *61*[–] is analogous to that observed for *46*[–] and *47*[–] in which the spin localization on one naphthalene moiety is less effective in the syn-isomer *46*[–] than in its anti-counterpart *47*[–] (Section G.2). On the whole, radical anions of azulenophanes are more prone to association with the counterion (extent of localization 85–95%) [100] than those of naphthalenophanes (70–80%) [18, 97]. This observation is in line with the similar findings for the radical anions of azulene and naphthalene and can be rationalized by the larger polarizability of the non-benzenoid π-systems relative to the benzenoid ones [127].

H Heterophanes

1 Pyridinophanes

62   **63**   **64**
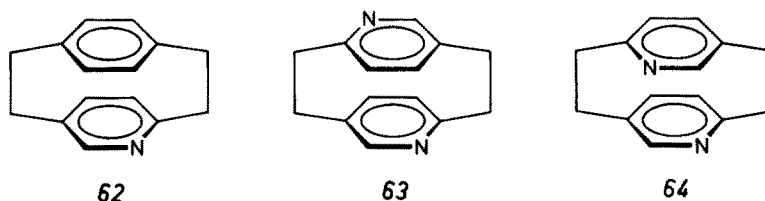
(Syntheses: *62* [128]; *63* and *64* [129].)

Reduction of [2]paracyclo[2](2,5)pyridinophane (*62*) and the two [2.2](2,5)pyridino-phanes *63* and *64* with K in DME at 193 K led to their radical anions which exhibited poorly resolved ESR spectra [49]. Tentative analysis for *62*[–] yielded the following hyperfine data: 0.45 (1N), 0.85 (1H), 0.36 (2H) and 0.06 (1H) mT. They bear some resemblance to the corresponding values for the radical anion of pyridine [130] and

thus suggest a substantial localization of the spin population on the heteroaromatic moiety, in line with its higher electron affinity relative to benzene. The ESR spectra of $63^{\bar{\cdot}}$ and $64^{\bar{\cdot}}$ were not analyzed.

2 Furanophane- and Thiophenophane-Polyenes
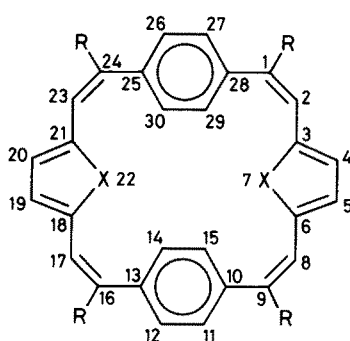
65, X = O, R = H
65-d_4, X = O, R = D
66, X = S, R = H
66-d_4, X = S, R = D
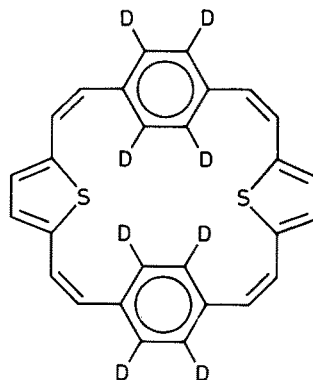
66-d_8
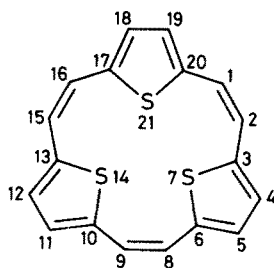
67
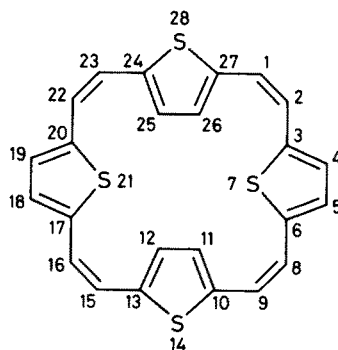
68

(Syntheses: 65 and 66 [131]; 65—d_4, 66—d_4 and 66—d_8 [66]; 67 [132]; 68 [133].)

Reduction of [2](2,5)furano[2]paracyclo[2](2,5)furano[2]paracyclophane-1,8,16,23-tetraene (65) and [2](2,5)thiopheno[2]paracyclo[2](2,5)thiopheno[2]paracyclophane-1,8,16,23-tetraene (66), as well as their deuterio derivatives 65—d_4, 66—d_4 and 66—d_8, was carried out with K in DME, and the resulting radical anions were studied by ESR and ENDOR spectroscopy [66]. Whereas for $66^{\bar{\cdot}}$ five sets, each of four equivalent protons, contribute to the hyperfine pattern, the number of sets is doubled and their multiplicities are reduced to two in the case of $65^{\bar{\cdot}}$ (Table 15). This results must be due to a strong association of $65^{\bar{\cdot}}$ with K$^+$, since addition of HMPT to DME leads to an averaging of the coupling constants, as expected for the replacement of a tight ion pair by a "free" or loosely paired radical anion. Evidently, $65^{\bar{\cdot}}$ is more closely associated with K$^+$ than $66^{\bar{\cdot}}$ under the same conditions,

93

Table 15. Coupling constants, in mT, for the radical anions of the heterophanetetraenes 65 and 66 [66]. Counterion K^+. g = 2.0026 for $65^{\bar{}}$ and 2.0038 for $66^{\bar{}}$

		$65^{\bar{}}$			$66^{\bar{}}$
Solvent		DME	DME/HMPT (2:1)		DME
Temp., K		193	193	263	193
Benzene protons	11, 12, 14, 15, 26, 27, 29, 30[a]	0.086 (2H) 0.051 (2H)	0.069 (4H)	0.051 (8H)	0.046 (4H)
		0.056 (2H) 0.007 (2H)	0.032 (4H)		0.041 (4H)
Furan or thiophene protons	4, 5[a] 19, 20	0.180 (2H) 0.031 (2H)	0.105 (4H)	0.105 (4H)	0.104 (4H)
Olefin protons	1, 9[a] 16, 24	0.099 (2H) <0.003 (2H)	0.052 (4H)	0.052 (4H)	0.089 (4H)
	2, 8 17, 23	0.068 (2H) 0.027 (2H)	0.042 (4H)	0.042 (4H)	0.058 (4H)

a Positions.

presumably due to a stronger attraction of the counterion to the O-atom of a furan moiety relative to the S-atom of a thiophene moiety. As in the radical anion of [2.2.2.2]paracyclophane-1,9,17,25-tetraene (25) (Section D.3), rotation of the phenylene parts about the bonds linking them to the olefinic fragments is slow on the hyperfine time-scale at 193 K, but becomes fast at higher temperatures. In the case of $65^{\bar{}}$ in DME/HMPT, an Arrhenius activation energy of 28 ± 4 kJ/mol was derived for such a rotation from ESR studies, whereas the analogous procedure could not be applied to $66^{\bar{}}$ because of the small difference (0.005 mT) in the pertinent coupling constants of the phenylene protons [66].

The radical anion of [2.2.2](2,5)thiophenophane-1,8,15-triene (= [18]annulene-1,4: 7,10:13,16-trisulfide; 67) was prepared by reduction of 67 with K or Na in DME or THF [134]. The ESR spectrum of $67^{\bar{}}$ which exhibits six coupling constants, each for a pair of equivalent protons, is inconsistent with the presence of a threefold symmetry axis. Since the molecule is undoubtedly non-planar, the observed lowering of the symmetry from C_{3v} to C_s can be rationalized by assuming a preferred conformation, in which not all three S-atoms lie on the "same" side of the mean molecular plane. The assignment of the coupling constants 0.440, 0.296, 0.192, 0.086, 0.061 and 0.043 mT to protons in the positions 8, 9; 1, 16; 5, 11; 18, 19; 4, 12 and 2, 15, respectively, has been based on a single occupancy of an orbital which is anti-symmetric relative to a mirror plane passing through one S-atom (21) and bisecting the opposite C—C bond (8–9).

The ESR and ENDOR spectra of the radical anion of [2.2.2.2](2,5)thiophenophane-1,8,15,22-tetraene (= [24]annulene-1,4:7,10:13,16:19,22-tetrasulfide; 68), generated by reduction of 68 with K in DME [66], exhibit four coupling constants of 0.115, 0.085, 0.058 and 0.034 mT, each for a set of four equivalent protons (g = 2.0023). By analogy with the data for $65^{\bar{}}$ and $66^{\bar{}}$, the two larger and the two smaller values have been assigned to the protons in the thiophenic and olefinic parts, respectively. The lack of a four-fold symmetry axis is unlikely to be due to association of $68^{\bar{}}$ with K^+,
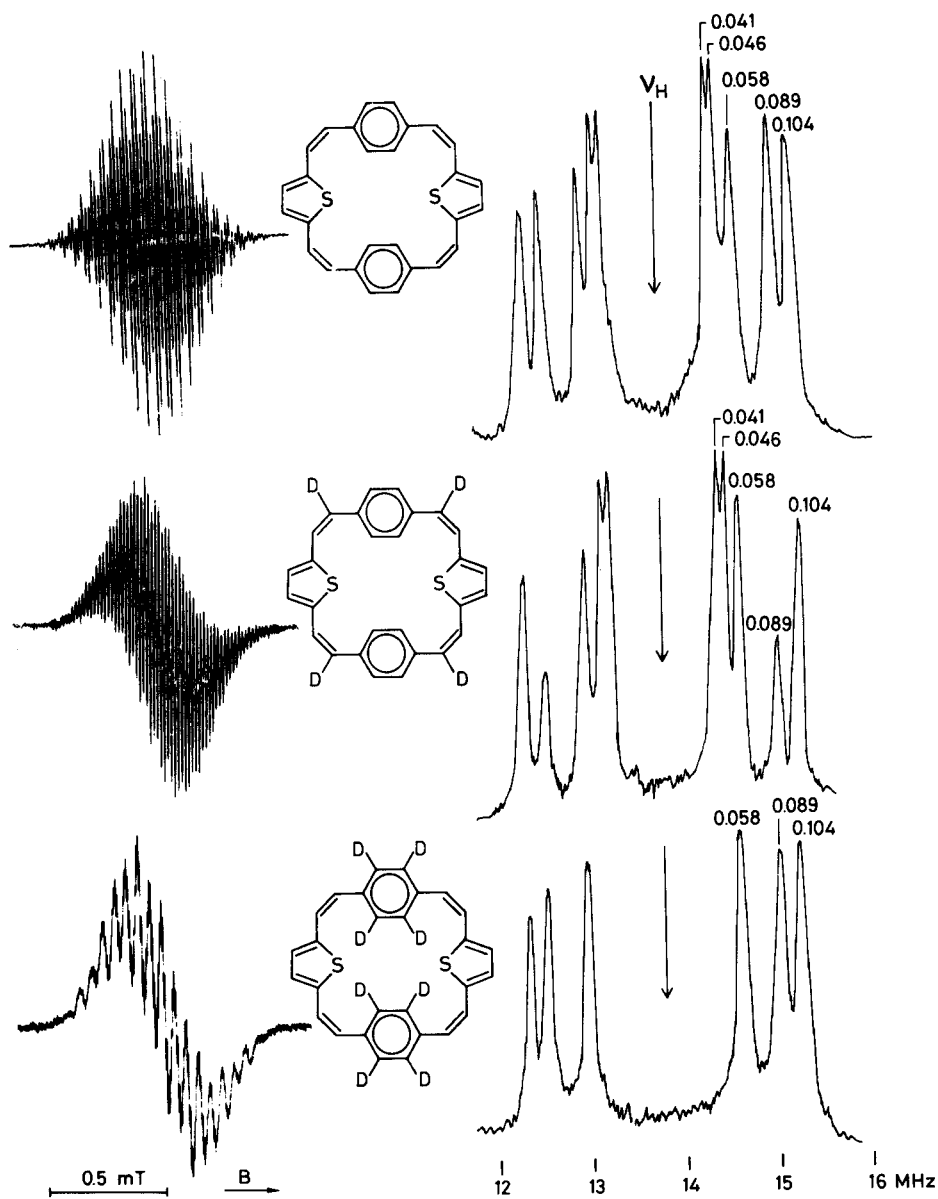
Fig. 12. ESR and proton ENDOR spectra of the radical anions of [2](2,5)thiopheno[2]para-cyclo[2](2,5)thiopheno[2]paracyclophane-1,8,16,23-tetraene (*66*) (top) and its deuterio derivatives *66-d₄* (50%-deuteriation; middle) and *66-d₈* (bottom). Solvent DME, counterion K^+, temperature 193 K. The numbers refer to proton coupling constants in mT. v_H = frequency of the free proton. Reproduced by permission of Helv. Chim. Acta [66]

since addition of HMPT to DME has only a negligible effect on the spectrum. Presumably, the molecule adopts a conformation in which the S-atoms lie alternatively in- and outwards relative to the mean molecular plane.

It seems appropriate to close this last section on the experimental results by demonstrating the potential of the ENDOR technique in unravelling complex and/or poorly resolved ESR spectra. This technique is particularly useful when combined with specific deuteration, since the introduction of deuterons leads to disappearance of the proton ENDOR signals for the labeled positions. Fig. 12 shows the ESR and ENDOR spectra of 66^{τ} (top), $66-d_4^{\tau}$ (middle) and $66-d_8^{\tau}$ (bottom) [66]. Although the ESR spectrum of 66^{τ} is well resolved and can be analyzed with some effort, the corresponding proton ENDOR signals yield the five coupling constants in a much more straightforward way. In addition, the small difference between the values 0.041 and 0.046 mT, which is unresolved in the ESR spectrum, clearly appears as a splitting of an ENDOR signal. On passing to $66-d_4^{\tau}$ the ESR spectrum becomes rather complex, the more so as the deuteration is only 50%. By contrast, a decrease by one half of the ENDOR signal associated with 0.089 mT unequivocally identifies this value as the coupling constant of the four protons in the positions 1, 9, 16 and 24. The passage from 66^{τ} to $66-d_8^{\tau}$ renders the ESR spectrum less resolved than that of $66-d_4^{\tau}$, despite the almost 100% deuteration. The absence of the ENDOR signals for 0.041 and 0.046 mT readily establishes the assignment of these values to the two sets of four phenylene protons.

I Concluding Remarks

ESR and ENDOR spectroscopy of phane radical ions have provided a wealth of experimental data which are not only informative with respect to the investigated species, but which also corroborate our current models on molecular structure and ion pairing. A few representative examples are given below.

In the particular case of phane radical anions containing two equivalent aromatic moieties in roughly parallel planes, the ESR and ENDOR studies confirm the interdependence of the electron spin transfer between these moieties and the migration of the counterion between its preferred sites at each moiety. The rate of migration, and therewith the frequency of the electron spin transfer, is determined by the strength of association of the counterion with such a site at the radical anion. This association, usually denoted as ion pairing, becomes tighter with the decreasing solvating power of the solvent, i.e., in the order DMF $\sim$ DME/HMPT, DME, THF, MTHF [135]. All other things being equal, the ion pairing is loosened when the π-systems of the two equivalent aromatic moieties are extended, e.g., on going from benzenes to naphthalenes and to anthracenes. Thus the radical anion of [2.2]paracyclophane (1) and those of the two investigated [2₃]- and [2₄]cyclophanes, 38(1,2,4) and 39(1,2,4,5), form tight ion pairs with K$^+$ in THF and MTHF, whereas "free" or loosely associated species predominate in DME/HMPT; both types of 1^{τ}, $38(1,2,4)^{\tau}$ and $39(1,2,4,5)^{\tau}$ are present in pure DME. On passing to the radical anions of syn- and anti-[2.2](1,4)naphthalenophanes (46 and 47), tight ion pairs still occur in MTHF, but are no longer observed in THF and DME. Finally, even the use of MTHF does not lead to tight ion pairing for the radical

anions of the syn- and anti-[2.2](1,4)anthracenophanes (52 and 53), and that of [2.2](9,10)anthracenophane (54); the species 52$^{\tau}$, 53$^{\tau}$ and 54$^{\tau}$ are "free" or loosely associated in all three ethereal solvents, DME, THF and MTHF. These results for the radical anions of cyclophanes, naphthalenophanes and anthracenophanes are diagrammatically presented in Fig. 13.

	DME/HMPT	DME	THF	MTHF
Cyclophanes	f	f p	p	p
Naphthalenophanes	f	f	f	p
Anthracenophanes	f	f	f	f

Fig. 13. Occurrence of "free" (or loosely associated) anions (f) and tight ion pairs (p); cf. text

The obvious loosening of ion pairing with the successive benzannellation of 1$^{\tau}$ is undoubtedly due to the more effective distribution of the negative charge over the extended π-systems.

In the ESR and ENDOR spectra, close association of the counterion with the radical anion containing two equivalent aromatic moieties manifests itself by apparent accumulation of the spin population on that moiety which is proximate to the counterion. Such "spin localization" is, in general, more pronounced for the anti-isomers than for their syn-counterparts, as exemplified by 47$^{\tau}$ and 46$^{\tau}$, and by the radical anions of anti- and syn-[2.2](2,6)azulenophanes (60 and 61). The structural feature which accounts for this behavior is obvious, since the π-clouds of the two aromatic moieties overlap more strongly in the syn- than in the anti-isomers.

In the phane radical anions with two non-equivalent aromatic moieties, the unpaired electron clearly favors the moiety having the higher electron affinity. The substantial confinement of the spin population to the π-system of this moiety, as observed irrespective of the experimental conditions, is again in full accord with expectation. It has been borne out by the studies of the radical anions of 4,5,7,8-tetramethyl[2.2]-paracyclophane (2), [2.2]metaparacyclophane (33), [2]paracyclo[2](1,4)naphthaleno-phane (42) and [2]paracyclo[2](1,3)azulenophane (43).

In many cases, structural information derived from the spectra of the radical ions can be considered as being also valid for the neutral compounds. This information is particularly valuable when the compounds themselves are not readily amenable to studies by other techniques, such as the X-ray crystallography and NMR spectroscopy. For instance, conformational information not easily available elsewhere has been provided by ESR and ENDOR investigations on the radical anions of the [2.2](1,4)anthracenophanes, 52 and 53, and those of the thiophenophanes 67 and 68.

Last but not least, conversion of some phanes into their radical ions leads to interesting secondary products which can be characterized by ESR and ENDOR spectroscopy. Prominent representatives of such products are the radical anions of trans-10b,10c-dihydropyrene (31) and trans-12b,12c-dihydrocoronene (50), which have been obtained as secondary products in solution upon reduction of anti-[2.2]-metacyclophane-1,9-diene (28) and anti-[2.2](2,7)naphthalenophane-1,11-diene (49),

respectively. While compound *31* itself could be identified by NMR spectroscopy, but was not isolated in a pure state, its higher analogue *50* is still unknown in the neutral form.

J Acknowledgements

K References

1. See, e.g., Szwarc, M., Jagur-Grodzinski, J., in: Ions and Ion Pairs in Organic Reactions, (Szwarc, M. ed.), Vol. 2, New York—London—Sydney—Toronto, J. Wiley 1974
2. Ayscough, P. B.: Electron Spin Resonance in Chemistry, London Methuen 1967
3. Carrington, A., McLachlan, A. D.: Introduction to Magnetic Resonance, New York—Evanston—London—Tokyo, Harper & Row, and J. Weatherhill 1967
4. Gerson, F.: Hochauflösende ESR Spektroskopie, Weinheim, Chemie-Verlag 1967; High Resolution ESR Spectroscopy, Weinheim—New York, Chemie Verlag and J. Wiley 1970
5. Scheffler, K., Stegmann, H. B.: Elektronenspinresonanz, Berlin—Heidelberg—New York, Springer 1970
6. Wertz, J. E., Bolton, J. R.: Electron Spin Resonance. Elementary Theory and Practical Applications, New York—St. Louis—San Francisco—London, McGraw-Hill 1972
7. Atherton, N. M.: Electron Spin Resonance, Theory and Applications, Chichester, Ellis Horwood 1973
8. Symons, M. C. R.: Chemical and Biochemical Aspects of Electron Spin Resonance Spectroscopy, New York—London—Sydney—Toronto, J. Wiley 1978
9. Kevan, L., Kispert, L. D.: Electron Spin Double Resonance Spectroscopy, New York—London—Sydney—Toronto, J. Wiley 1976
10. Dorio, M. M., Freed, J. H. (editors): Multiple Electron Resonance Spectroscopy, New York—London, Plenum Press 1979
11. Vögtle, F., Neumann, P.: Tetrahedron Lett. *1969*, 5929; Tetrahedron *26*, 5847 (1970)
12. Brown, C. J., Farthing, A. C.: Nature *164*, 915 (1949); Farthing, A. C.: J. Chem. Soc. *1953*, 3251; Brown, C. J.: ibid. *1953*, 3265
13. Cram, D. J., Steinberg, H.: J. Am. Chem. Soc. *73*, 5691 (1951); Winberg, H. E., Fawcett, F. S., Mochel, W. E., Theobald, C. W.: ibid. *82*, 1428 (1960)
14. Gerson, F., Martin, W. B., Jr.: ibid. *91*, 1883 (1969)
15. Gerson, F., Martin, W. B., Jr., Wydler, Ch.: Helv. Chim. Acta *59*, 1365 (1976)
16. Weissman, S. I.: J. Am. Chem. Soc. *80*, 6462 (1958)
17. Ishitani, A., Nagakura, S.: Mol. Phys. *12*, 1 (1967)
18. Gerson, F., Martin, W. B., Jr., Wydler, Ch.: J. Am. Chem. Soc. *98*, 1318 (1976)
19. Bruhin, J., Gerson, F., Ohya-Nishiguchi, H.: J. Chem. Soc. Perkin II, *1980*, 1045
20. Gerson, F., Lopez, J., Boekelheide, V.: ibid. *1981*, 1298

21. Lopez, J.: Ph. D. Thesis, Univ. Basel 1982
22. Bruhin, J., Lopez, J., Gerson, F., unpublished results
23. Gerson, F., Ohya-Nishiguchi, H., Wydler, Ch.: Angew. Chem. *88*, 617 (1976); Int. Edit. Engl. *15*, 552 (1976)
24. Jund, R., Lemoine, P., Gross, M.: Angew. Chem. *94*, 312 (1982); Int. Edit. Engl. *21*, 305 (1982)
25. Gleiter, R.: Tetrahedron Lett. *1969*, 4453
26. Duke, C. B., Lipari, N. O., Salaneck, W. R., Schein, L. B.: J. Chem. Phys. *63*, 1758 (1975)
27. Gerson, F., Ohya-Nishiguchi, H., Plattner, G.: Helv. Chim. Acta *65*, 551 (1982)
28. Jenny, W., Bruhin, J., Davatz, A.: Chimia *27*, 641 (1973)
29. Davatz, A.: Ph. D. Thesis, Univ. Bern 1976
30. Longone, D. T., Warren, C. L.: J. Am. Chem. Soc. *84*, 1507 (1962);
    Longone, D. T., Boettcher, F. P.: ibid. *85*, 3436 (1963);
    Longone, D. T., Chow, H. S.: ibid. *92*, 994 (1970)
31. Reich, H. J., Cram, D. J.: J. Am. Chem. Soc. *91*, 3527 (1969)
32. El-tamany, S. H., Hopf, H.: Tetrahedron Lett. *1980*, 4901
33. Longone, D. T., Simanyi, L. H.: J. Org. Chem. *29*, 3245 (1964)
34. Yang, Zhong-zhi, Kovač, B., Heilbronner, E., El-tamany, S., Hopf, H.: Helv. Chim. Acta *64*, 1991 (1981)
35. Baugham, E. C., Jones, T. P., Stoodley, L. G.: Proc. Chem. Soc. *1963*, 274;
    Gerson, F., Heinzer, J.: Helv. Chim. Acta *50*, 2471 (1977)
36. Gerson, F., Lopez, J., Hopf, H.: Helv. Chim. Acta *65*, 1398 (1982)
37. Kleinschroth, J., El-tamany, S., Hopf, H., Bruhin, J.: Tetrahedron Lett. *1982*, 3345
38. Kovač, B., Mohraz, M., Heilbronner, E., Boekelheide, V., Hopf, H.: J. Am. Chem. Soc. *102*, 4314 (1980)
39. Ohya-Nishiguchi, H.: Bull. Chem. Soc. Jpn. *52*, 2064 (1979)
40. Bruhin, J., Gerson, F., Ohya-Nishiguchi, H.: Helv. Chim. Acta *60*, 2471 (1977)
41. Cram, D. J., Allinger, N. L.: J. Am. Chem. Soc. *77*, 6289 (1955);
    Norcross, B. E., Becker, D., Crukier, R. I., Schulz, R. M.: J. Org. Chem. *32*, 220 (1967)
42. Allgeier, H., Siegel, M. G., Helgeson, R. C., Schmidt, E., Cram, D. J.: J. Am. Chem. Soc. *97*, 3782 (1975)
43. Cram, D. J., Bauer, R. H., Allinger, N. L., Reeves, W. J., Wechter, W. J., Heilbronner, E.: ibid. *81*, 5977 (1959)
44. Hopf, H., Lenich, F. Th.: Chem. Ber. *107*, 1891 (1974)
45. Hopf, H.: Angew. Chem. *84*, 471 (1972); Angew. Chem. Int. Edit. Engl. *11*, 419 (1972)
46. Hopf, H.: unpublished work
47. Böhm, I., Hermann, H., Menke, K., Hopf, H.: Chem. Ber. *111*, 523 (1978)
48. Rogers, J. W., Watson, W. H.: Texas J. Sci. *21*, 471 (1970), as quoted in Landolt-Börnstein, New Series, Magnetic Properties of Free Radicals (Fischer, H., Hellwege, K. H., eds.) Vol. 9, Part 1, Berlin—Heidelberg—New York, Springer 1980; a) p. 467; b) p. 646
49. Bruhin, J., Gerson, F.: unpublished work
50. Geske, D. H., Maki, A. H.: J. Chem. Phys. *82*, 2671 (1960)
51. Fürderer, P., Gerson, F., Ohya-Nishiguchi, H., Böhm, I., Hopf, H.: Helv. Chim. Acta *62*, 2569 (1979)
52. Chow, S. W., Pilato, A., Wheelright, W. L.: J. Org. Chem. *35*, 20 (1970)
53. Pople, J. A., Beveridge, D. L.: Approximate Molecular Orbital Theory, New York— St. Louis—San Francisco—London, McGraw-Hill 1970
54. Cram, D. J., Dewhirst, K. C.: J. Am. Chem. Soc. *80*, 3115 (1958)
55. Bruhin, J., Gerson, F.: to be published
56. Abell, J., Cram, D. J.: J. Am. Chem. Soc. *76*, 4406 (1954)
57. Cram, D. J., Antar, M. F.: ibid. *80*, 3103 (1958)
58. Cram, D. J., Allinger, N. L., Steinberg, H.: ibid. *76*, 6132 (1954);
    Cram, D. J., Helgeson, R. C.: ibid. *88*, 3515 (1966)
59. Cram, D. J., Allinger, N. L.: ibid. *76*, 2362 (1954)
60. Cram, D. J., Allinger, N. L.: ibid. *76*, 726 (1954)
61. Bolton, J. R., Carrington, A., Forman, A., Orgel, L. E.: Mol. Phys. *5*, 43 (1962)
62. Gerson, F.: Chimia *28*, 194 (1974)

63. Otsubo, T., Mizogami, S., Sakata, Y., Misumi, S.: Tetrahedron Lett. *1971*, 4803;
    Otsubo, T., Mizogami, S., Otsubo, I., Tozuka, Z., Sakagami, A., Sakata, Y., Misumi, S.:
    Bull. Chem. Soc. Jpn. *46*, 3519 (1973);
    Otsubo, T., Hirota, H., Misumi, S.: Synth. Commun. *6*, 591 (1976)
64. Iwaizumi, M., Kita, S., Isobe, T., Kohno, M., Yamamoto, T., Horita, H., Otsubo, T.,
    Misumi, S.: Bull. Chem. Soc. Jpn. *50*, 2074 (1977)
65. Thulin, B., Wennerström, O., Högberg, H.-E.: Acta Chem. Scand. *B29*, 138 (1975)
66. Gerson, F., Huber, W., Wennerström, O.: Helv. Chim. Acta *61*, 2763 (1978)
67. Gerson, F., Ohya-Nishiguchi, H., Szwarc, M., Levin, G.: Chem. Phys. Lett. *52*, 587 (1977)
68. Huber, W., Müllen, K., Wennerström, O.: Angew. Chem. *92*, 636 (1980); Angew. Chem. Int.
    Edit. Engl. *19*, 624 (1980)
69. Pellegrin, M. M.: Rec. Trav. Chim. Pays-Bas *18*, 457 (1899);
    Baker, W., McOmie, J. F. W., Norman, J. M.: Chemistry and Industry *1950*, 77; J. Chem.
    Soc. *1951*, 1114
70. Allinger, N. L., Gordon, B. J., Hu, S. E., Ford, R. A.: J. Org. Chem. *32*, 2272 (1967)
71. Boekelheide, V., Mitchell, R. H.: J. Am. Chem. Soc. *92*, 3510 (1970)
72. Elschenbroich, Ch., Gerson, F., Boekelheide, V.: Helv. Chim. Acta *58*, 1245 (1975)
73. Elschenbroich, Ch., Gerson, F., Reiss, J. A.: J. Am. Chem. Soc. *99*, 60 (1977)
74. Iwaizumi, M., Isobe, T.: Bull. Chem. Soc. Jpn. *38*, 1547 (1965)
75. Hoijtink, G. J., Townsend, J., Weissman, S. I.: J. Chem. Phys. *34*, 507 (1961)
76. Gerson, F., Moshuk, G., Schwyzer, M.: Helv. Chim. Acta *54*, 361 (1971)
77. Boekelheide, V., Mitchell, R. H.: J. Am. Chem. Soc. *96*, 1547 (1974)
78. Cram, D. J., Helgeson, R. C., Loch, D., Singer, L. A.: J. Am. Chem. Soc. *88*, 1324
    (1966);
    Hefelfinger, D. T., Cram, D. J.: ibid. *92*, 1073 (1970)
79. Sherrod, S. A., Boekelheide, V.: ibid. *94*, 5513 (1972)
80. Bruhin, J., Gerson, F.: in preparation
81. Boekelheide, V., Anderson, P. H., Hylton, T. A.: J. Am. Chem. Soc. *96*, 1558 (1974)
82. Hefelfinger, D. T., Cram, D. J.: ibid. *93*, 4767 (1971);
    Vögtle, F.: Chem. Ber. *102*, 3077 (1969);
    Akabori, S., Hayashi, S., Nawa, M., Shioni, M.: Tetrahedron Lett. *1969*, 3727
83. Lawler, R. G., Tabit, C. T.: J. Am. Chem. Soc. *91*, 5671 (1969)
84. Boekelheide, V., Anderson, P. H.: Tetrahedron Lett. *1970*, 1207;
    Hylton, T. A., Boekelheide, V.: J. Am. Chem. Soc. *90*, 6887 (1968)
85. Sherrod, S. A., da Costa, R. L., Barnes, R. A., Boekelheide, V.: ibid. *96*, 1565 (1974)
86. Bruhin, J., Gerson, F., Boekelheide, V.: in preparation
87. Boekelheide, V., Neuschwander, B.: Israel J. Chem. *20*, 288 (1980);
    Hopf, H., Kleinschroth, J., Murad, A. E. E.: ibid. 291 (1980)
88. Truesdale, E. A., Cram, D. J.: J. Am. Chem. Soc. *95*, 5825 (1973);
    Trampe, S., Menke, K., Hopf, H.: Chem. Ber. *110*, 371 (1977)
89. Boekelheide, V., Hollins, R. A.: J. Am. Chem. Soc. *95*, 3201 (1973)
90. Hopf, H., Kleinschroth, J.: Angew. Chem. *91*, 336 (1979); Angew. Chem. Int. Edit. Engl. *18*,
    329 (1979)
91. Gilb, W., Menke, K., Hopf, H.: Angew. Chem. *89*, 177 (1977); Angew. Chem. Int. Edit. Engl.
    16, 191 (1977)
92. Gray, R., Boekelheide, V.: Angew. Chem. *87*, 138 (1975); Angew. Chem. Int. Edit. Engl.
    14, 107 (1975);
    Gray, R., Boekelheide, V.: J. Am. Chem. Soc. *101*, 2128 (1979)
93. Gerson, F., Lopez, J., Boekelheide, V., Hopf, H.: Helv. Chim. Acta *65*, 1391 (1982)
94. Coulter, C. L., Trueblood, K.: Acta Crystallogr. *16*, 668 (1963);
    Manson, A.: ibid. *B33*, 2003 (1977)
95. Boekelheide, V., Hollins, R. A.: J. Am. Chem. Soc. *92*, 3512 (1970); ibid. *95*, 3201 (1973)
96. Cram, D. J., Dalton, C. K., Knox, G. R.: ibid. *85*, 1088 (1963)
97. Bruhin, J., Gerson, F., Martin, W. B., Jr., Wydler, Ch.: Helv. Chim. Acta *60*, 1915 (1977)
98. Fukazawa, Y., Aoyagi, M., Itô, S.: Tetrahedron Lett. *1978*, 1067
99. Iwama, A., Toyoda, T., Misumi, S.: Chemistry Lett. *1973*, 587
100. Iwaizumi, M., Fukazawa, Y., Kato, N., Itô, S.: Bull. Chem. Soc. Jpn. *54*, 1299 (1981)
101. Hayashi, T., Mataga, N., Sakata, Y., Misumi, S.: Bull. Chem. Soc. Jpn. *48*, 416 (1975)

102. Gerson, F., Weidmann, B., Heilbronner, E.: Helv. Chim. Acta *47*, 1951 (1964)
103. Bernal, I., Rieger, P. H., Fraenkel, G. K.: J. Chem. Phys. *37*, 1489 (1962);
     Reddoch, A. H.: ibid. *41*, 444 (1964);
     Gerson, F., Lopez, J., Metzger, A., Jutz, Ch.: Helv. Chim. Acta *63*, 2135 (1980)
104. Wassermann, H. H., Keehn, P. M.: J. Am. Chem. Soc. *91*, 2374 (1969)
105. Wassermann, H. H., Clagett, D. C.: ibid. *88*, 5368 (1966);
     Brown, G. W., Sondheimer, F.: ibid. *89*, 7116 (1967)
106. Eargle, D. H., Jr.: J. Magn. Reson. *2*, 225 (1970)
107. Williams, D. J., Pearson, J. M., Levy, M.: J. Am. Chem. Soc. *93*, 5483 (1971)
108. Baker, W., Glockling, F., McOmie, J. F. W.: J. Chem. Soc. *1951*, 1118
109. Davy, J. R., Reiss, J. A.: Tetrahedron Lett. *1972*, 3639; J.C.S. Chem. Commun. *1973*, 806
110. Davy, J. R., Reiss, J. A.: J. Austral. Chem. *29*, 163 (1976)
111. De Boer, E., Weissman, S. I.: J. Am. Chem. Soc. *80*, 4549 (1958);
     Bolton, J. R., as quoted by Lewis, I. C., Singer, L. S.: J. Chem. Phys. *43*, 2712 (1965)
112. Toyoda, T., Otsubo, I., Tetsubo, O., Sakata, S., Misumi, S.: Tetrahedron Lett. *1972*, 1731
113. Golden, J. H.: J. Chem. Soc. *1961*, 3741
114. Gerson, F., Ohya-Nishiguchi, H., Kaupp, G.: Angew. Chem. *89*, 666 (1977); Angew. Chem.
     Int. Edit. Engl. *16*, 657 (1977)
115. Nemoto, F., Ishizu, K., Toyoda, T., Sakata, Y.: J. Am. Chem. Soc. *102*, 654 (1980)
116. Bolton, J. R., Carrington, A., McLachlan, A. D.: Mol. Phys. *5*, 31 (1962)
117. Howarth, O. W., Fraenkel, G. K.: J. Chem. Phys. *52*, 6258 (1970), and references therein
118. Umemoto, T., Satani, S., Sakata, Y., Misumi, S.: Tetrahedron Lett. *1975*, 3159
119. Ishizu, K., Sugimoto, Y., Umemoto, T., Sakata, Y., Misumi, S.: Bull. Chem. Soc. Jpn. *50*, 2801
     (1977)
120. Iwama, A., Toyoda, T., Otsubo, T., Misumi, S.: Tetrahedron Lett. *1973*, 1725
121. Jessup, P. J., Reiss, J. A.: J. Austral. Chem. *30*, 851 (1977)
122. Wydler, Ch.: Ph. D. Thesis, Univ. Basel 1976
123. Fukazawa, Y., Aoyagi, M., Itô, S.: Tetrahedron Lett. *1979*, 1055
124. Kato, N., Matsumaga, M., Oeda, S., Fukazawa, Y., Itô, S.: ibid. *1979*, 2419
125. Kato, N., Fukazawa, Y., Itô, S.: ibid. *1976*, 2045
126. Luhowy, R., Keehn, P. M.: ibid. *1976*, 1043;
     Luhowy, R., Keehn, P. M.: J. Am. Chem. Soc. *99*, 3797 (1977)
127. See, e.g., Gerson, F., Hammons, J. H., in: Nonbenzenoid Aromatics (Snyder, J. P., ed.), Vol. II,
     Chapter 2, New York—London, Academic Press 1971
128. Bruhin, J., Jenny, W.: Chimia *26*, 420 (1972); Tetrahedron Lett. *1973*, 1215
129. Bruhin, J., Jenny, W.: Chimia *25*, 238, 308 (1971);
     Bruhin, J.: Ph. D. Thesis, Univ. Bern 1976
130. Myers, R. L., Talcott, C. L.: Mol. Phys. *12*, 549 (1967)
131. Thulin, B., Wennerström, O., Somai, I., Chmielarz, B.: Acta Chem. Scand. *B31*, 135 (1977)
132. Badger, G. M., Elis, J. A., Lewis, G. E.: Proc. Chem. Soc. *1964*, 82;
     Badger, G. M., Elis, J. A., Lewis, G. E.: Austral. J. Chem. *18*, 70 (1965)
133. Strand, A., Thulin, B., Wennerström, O.: Acta Chem. Scand. *B31*, 521 (1977)
134. Gerson, F., Heinzer, J.: Helv. Chim. Acta *51*, 366 (1968)
135. See, e.g., Fürderer, P., Gerson, F., Heinzer, J., Mazur, S., Ohya-Nishiguchi, H., Schroeder, A. H.:
     J. Am. Chem. Soc. *101*, 2275 (1979)

L Addendum

In the following, a brief account is given of quite recent results which have not been included so far in this review.

1 Supplement to Sections C.1 and D.2

69

70
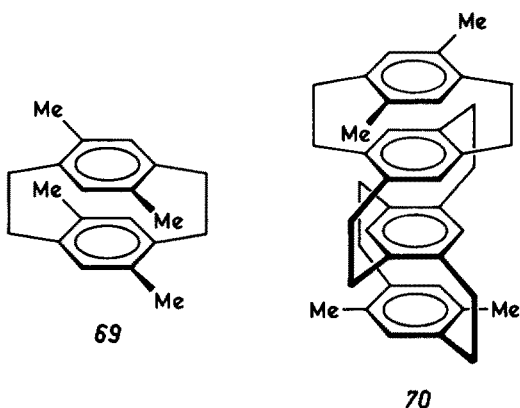
(Syntheses: 69 and 70 [63].)

A successful preparation of the monomeric radical cation of 4,7,13,16-tetramethyl-[2.2]paracyclophane (3) under relatively mild conditions was reported [136]. This radical cation, as well as that of the isomeric 4,7,12,15-tetramethyl[2.2]para-cyclophane (69), was obtained by electrolytic oxidation of the neutral compound in CH_2Cl_2/CF_3COOH (10:1) with tetra-n-butylammonium tetrafluoroborate as the supporting salt [136] (temperature 188 K for 3 and 203 K for 69). The ESR spectrum of $3^{\ddagger}$ exhibited the coupling constants of 0.649 mT for the twelve equivalent protons of the four methyl substituents, 0.049 mT for the eight methylene protons, and 0.033 mT for the four equivalent aromatic protons. The corresponding values for $69^{\ddagger}$ are 0.637, 0.041 and 0.043 mT. It is interesting to note that the hyperfine data for $3^{\ddagger}$ differ from those found for the radical cation of 4,5,7,8-tetramethyl[2.2]paracyclophane (2) (Table 2), whereas oxidation of 3 under more rigorous conditions (with $AlCl_3$ in CH_2Cl_2 above 333 K) leads to the same ESR spectrum as that of $2^{\ddagger}$ [21,22] (cf. Sect. C.1).

An ESR spectrum attributed to the dimeric radical cation $(3)_2^{\ddagger}$ was observed upon oxidation of 3 at higher concentration and lower temperature (165 K). Its analysis yields the coupling constants of 0.307 and 0.077 mT, each for twelve equivalent methyl protons, and two values of 0.018 and 0.014 mT for eight and four protons, respectively. By analogy to $(2)_2^{\ddagger}$ [40], the two molecules of 3 are assumed to be stacked face to face in $(3)_2^{\ddagger}$. The spin population seems to be distributed between the four benzene rings of the dimer in the ratio 4:1 in favor of the two inner rings.

The triply layered [2.2]paracyclophane 22 and its quadruply layered analogues 23 and 70 (a tetramethyl derivative of 24) were also oxidized to their radical cations by the same method as 3 and 69 (temperature 217 K for 22 and 288 K for 23 and 70) [136]. The ESR spectrum of $22^{\ddagger}$ was analyzed in terms of the following coupling constants: 0.079 mT due to the two equivalent protons at the central benzene ring, 0.328 and 0.305 mT tentatively assigned to the two sets of four equivalent protons

in the methylene groups adjacent to this ring, and 0.032, 0.024 and 0.009 mT for four, four, and eight protons, respectively, in the outer parts of the molecule. From these data a ratio 15:1 was estimated for the spin population in the inner benzene ring relative to that in the outer ones.

The radical cations $23^{\ddot+}$ and $70^{\ddot+}$ gave rise to unresolved ESR signals having respective widths of 0.56 and 0.45 mT.

2 Supplement to Section E.1

71
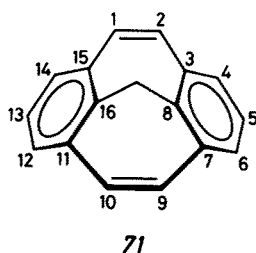
(Synthesis: 71 [137].)

Upon reduction of 8,16-methano[2.2]metacyclophane-1,9-diene (71) by the method of solvated electrons in DME a well-resolved ESR spectrum was observed [138]. This spectrum is consistent with that expected for the radical anion $71^{\bar{\cdot}}$ in which the singly occupied orbital should be similar to the corresponding MO in the radical anion of pyrene (32) [75]. The coupling constants and their assignments are as follows: 0.440 and 0.148 mT to the two sets of four equivalent protons in the positions 4, 6, 12, 14 and 1, 2, 9, 10, respectively, 0.091 mT to the two equivalent protons in the positions 5,13, and 0.015 mT to the pair of equivalent protons in the methano bridge.

The radical anion $71^{\bar{\cdot}}$ is not persistent and converts readily to the radical anion of pyrene (32) (Reaction Scheme VI).

This conversion, in which the radical anion of the cyclopropano-bridged [14]-annulene (72) is postulated as an intermediate, is analogous to the formation of

$71 \xrightarrow{+e^-}$ **71**$^{\bar{\cdot}}$ **72**$^{\bar{\cdot}}$ $\xrightarrow{-CH_2}$ **32**$^{\bar{\cdot}}$
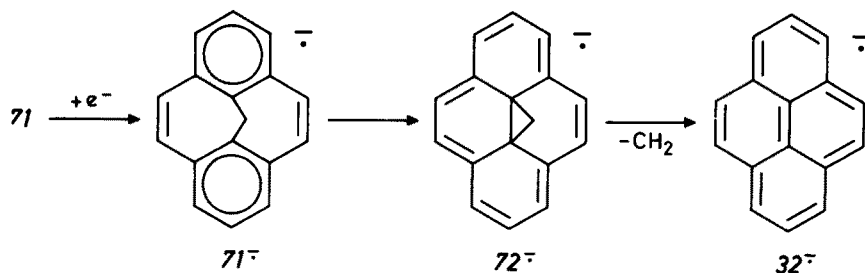
Reaction Scheme VI

32⁻ from anti-[2.2]metacyclophane-1,9-diene (*28*) via the radical anion of trans-10b,10c-dihydropyrene (*31*) [72] (Reaction Scheme II). The intermediate *72⁻*, corresponding to *31⁻*, is isomeric with *71⁻*; MO models indicate that the ESR spectrum observed upon reduction of *71* and tentatively attributed to *71⁻* could also arise from *72⁻*. A definite choice between the two alternative structures must await further studies in this field.

3 Supplement to Section F.1
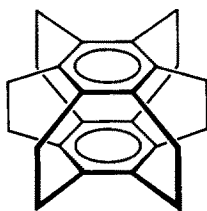
73

(Synthesis: *73* [139].)

$[2_6](1,2,3,4,5,6)$Cyclophane or "superphane" (*73*) can not be reduced to its radical anion in DME, either by a method of solvated electrons or by direct contact of the solution with a K mirror [93]. However, an ESR spectrum of *73⁻* was observed upon irradiating a solution of *73* and solvated electrons in DME with visible light at low temperatures [140]. This method proved to be effective for reducing benzene derivatives of low electron affinity [140]. The observed hyperfine pattern is due to twelve equivalent protons with a coupling constant of 0.185 mT. This result indicates that the spin population is (on the hyperfine time-scale) localized in one benzene moiety.

4 Supplement to Section G.5

Oxidation of [2.2](2,7)pyrenophane (*56*) with CF_3COOH in CH_2Cl_2 (or electrolytically) yielded the radical cation *56⁺* which was studied by ESR and ENDOR spectroscopy [141]. The coupling constants observed for *56⁺* at 188 K are 0.234 and 0.111 mT for the two sets of equivalent aromatic protons in the positions 4,7,9,12,16,19,21,24 and 5,6,10,11,17,18,22,23, respectively, and 0.032 mT for the eight equivalent methylene protons. These values compare favorably with hyperfine data for the dimeric radical cation of pyrene (*32*) [117]. The structures of *56⁺* and $(32)_2^+$ must thus be similar, with the two pyrene π-systems lying one above each other in essentially eclipsed position.

In addition to *56⁺*, the isomeric radical cations of [2](1,6)pyrenophane[2](2,7)-pyrenophane (*74*) and [2.2](1,6)pyrenophane (*75*) were also generated by the same method [141]. (Syntheses: *74* and *75* [142].) With the assistance of the ENDOR

technique, eleven coupling constants, each for a pair of equivalent protons (0.307, 0.239, 0.209, 0.209, 0.165, 0.129, 0.116, 0.084, 0.072, 0.045 and 0.013 mT), are obtained for 74^{+}, while six coupling constants, each for four equivalent protons (0.308, 0.114, 0.070, 0.063, 0.062 and 0.044 mT), can be observed for 75^{+}. Partial assignments of these values to aromatic protons is indicated by H/D exchange in CF_3COOD used instead of CF_3COOH as the oxidizing agent. The hyperfine data for 74^{+} and 75^{+} are discussed in terms of the twist angles between the two pyrene moieties; these angles have been estimated as 35° and 60°, respectively. In 74^{+}, with two non-equivalent pyrene moieties, the spin population is largely localized on the 1,6-bridged one. This finding is in line with the expected lower ionization potential of 1,6-dialkyl derivatives of pyrene relative to those substituted in the 2,7-positions.

5 Supplement to References

136. Ohya-Nishiguchi, H., Terahara, A., Hirota, N., Sakata, Y., Misumi, S.: Bull. Chem. Soc. Jpn. *55*, 1782 (1982)
137. Nakasuji, K., Katada, M., Murata, I.: Angew. Chem. *91*, 1011 (1979); Angew. Chem. Int. Edit. Engl. *18*, 946 (1979)
138. Metzger, A.: Ph.D. Thesis, Univ. Basel 1983
139. Sekine, Y., Brown, M., Boekelheide, V.: J. Am. Chem. Soc. *101*, 3126 (1979)
140. Heckendorn, R.: Ph.D. Thesis, Univ. Basel 1983; Gerson, F., Heckendorn, R.: Angew. Chem., in press.
141. Terahara, A., Ohya-Nishiguchi, H., Hirota, N., Sakata, Y., Misumi, S., Ishizu, K.: Bull. Chem. Soc. Jpn. *55*, 3896 (1982)
142. Kawashima, T., Otsubo, T., Sakata, Y., Misumi, S.: Tetrahedron Lett. *1978*, 5115

Functionalized Cyclophanes as Catalysts and Enzyme Models

Yukito Murakami

Department of Organic Synthesis, Faculty of Engineering, Kyushu University, Fukuoka 812, Japan

Table of Contents

1 Introduction

The interest in the chemistry of macrocyclic compounds with a sizable internal cavity lies in their ability to incorporate a suitably bulky substrate molecule through hydrophobic host-guest interactions. The bound substrate subsequently undergoes reaction with a functional group or groups intramolecularly located close to the hydrophobic binding site. The general kinetic behavior of macrocyclic compounds is therefore consistent with that confirmed for the enzymatic catalysis. Consequently, such species having a macrocyclic skeleton of hydrophobic nature can be regarded as catalysts which simulate enzyme functions (enzyme models).

Macrocyclic systems have some potentiality as superior enzyme models for the following reasons.

i) The macrocyclic cavity provides a stable substrate-binding site which is scarcely affected by external factors such as pH, temperature, and ionic strength.

ii) The stable binding site shows a high substrate specificity due to its intrinsic geometrical requirements for host-guest interactions.

iii) The introduction of two or more catalytically active groups into the macrocyclic skeleton in a definite, favorable spatial orientation provides an effective reaction site of cooperative polyfunctional nature.

In the past decade, we have prepared various [20]- and [10.10]paracyclophanes to explore novel enzyme model systems and investigated their catalytic efficiencies in the deacylation of carboxylic esters. Functionalized paracyclophanes show significant rate effects on the deacylation due to their hydrophobic interactions with the substrates. The most attractive observation is the bifunctional catalysis of some paracyclophanes. Such functional groups are fixed in a definite spatial orientation so that cooperative catalysis occurs.

In order to provide deeper hydrophobic cavities for the incorporation of hydrophobic substrates of various bulkiness, we have prepared azaparacyclophanes having long alkyl branches on the macrocyclic skeleton. Such octopus-like cyclophanes bind various guest molecules by their induced-fit function, even though substrate selectivity is exercised by the nature of charged substituents located at the ends of the alkyl chains. These azaparacyclophanes can be readily polyfunctionalized by introducing a functional group into each alkyl chain, and the turnover catalysis of such cyclophanes takes place in the deacylation of carboxylic esters.

If we emphasize the characteristic feature of a macrocyclic skeleton in such a way that functional groups, incorporated as structural components of the skeleton, are spatially fixed with a favorable orientation relative to each other, then the cooperative interaction among such groups becomes effective. Under such circumstances, a macrocyclic skeleton does not necessarily provide a hydrophobic binding site, and its reaction with an appropriate substrate is rather carried out in non-aqueous media. This review article describes the catalytic function of bisdihydronicotinamide-type macrocycles in the reduction of a carbonyl substrate.
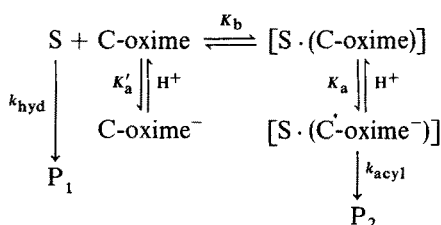
2 Hydrophobic Substrate-Binding Behavior of Paracyclophanes

2.1 Penetration-Type Incorporation

2.1.1 [20]Paracyclophanes Bearing a Hydroxyimino Group

In the presence of a paracyclophane bearing a hydroxyimino group (C-oxime), the inclusion of a p-nitrophenyl carboxylate with a long alkyl chain into the cyclic cavity of the C-oxime takes place prior to acyl transfer from the carboxylic ester to the C-oxime as represented in Scheme 1. The primary force which holds a substrate

Scheme 1:

$$
\begin{array}{ccc}
\text{S} + \text{C-oxime} & \underset{}{\overset{K_b}{\rightleftharpoons}} & [\text{S}\cdot(\text{C-oxime})] \\
\Big\downarrow k_{hyd} \quad K'_a \Big\Vert \text{H}^+ & & K_a \Big\Vert \text{H}^+ \\
\text{C-oxime}^- & & [\text{S}\cdot(\text{C-oxime}^-)] \\
\text{P}_1 & & \Big\downarrow k_{acyl} \\
& & \text{P}_2
\end{array}
$$

S: substrate
C-oxime: paracyclophanoxime
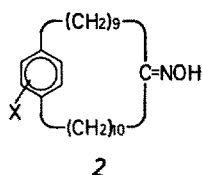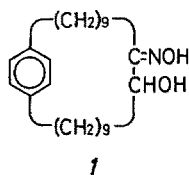P_1: carboxylate and p-nitrophenolate ions
P_2: acylated paracyclophanoxime and p-nitrophenolate ion

and a cyclic oxime together must be hydrophobic in origin as became evident from the effect of added urea and organic solvent on the kinetic behavior of the system of 1 and p-nitrophenyl dodecanoate (PNPL) [1]. The real nucleophile in the acyl transfer reaction is not the neutral hydroxyimino group but the deprotonated one in the inclusion complex. Thus, the observed first-order rate constant (k_{obsd}) is given by Eq. (1) where $[\text{S}]_T$ and $[\text{C}]_T$ are the total concentrations of substrate and cyclic oxime, respectively, and α, β, and γ are defined as $K_a/[\text{H}^+]$, $K'_a/[\text{H}^+]$, and $([\text{H}^+]/K_a) + 1$, respectively; k_{hyd} is the rate constant of alkaline hydrolysis in the absence of a cyclic oxime [2].

$$
k_{obsd} = k_{hyd} + \left(\frac{1}{\gamma} k_{acyl} - k_{hyd}\right) \frac{K_b[\text{C}]_T}{\dfrac{(1+\beta)}{(1+\alpha)} + K_b[\text{S}]_T + K_b[\text{C}]_T} \tag{1}
$$

Rearrangement of Eq. (1) gives Eq. (2).

$$
\frac{1}{k_{obsd} - k_{hyd}} = \frac{\dfrac{(1+\beta)}{(1+\alpha)} + K_b[\text{S}]_T}{\left(\dfrac{1}{\gamma} k_{acyl} - k_{hyd}\right) K_b[\text{C}]_T} + \frac{1}{\dfrac{1}{\gamma} k_{acyl} - k_{hyd}} \tag{2}
$$

1

6 : R = [CH₂]₁₀CO₂H

6 : R = $[CH_2]_{10}CO_2H$

7 : R = $[CH_2]_{10}N^+Me_3 \cdot I^-$

8 : R = $[CH_2]_{10}N^+Me_3 \cdot Br^-$

9 : R = $[CH_2]_{10}N^+Me_2(CH_2CH_2OH) \cdot Br^-$

10 : R = $[CH_2]_{10}N^+Me_2(CH_2Im) \cdot Cl^-$

11 : $2/4:[CH_2]_{10}N^+HMe_2 \cdot Cl^-$

     $2/4:[CH_2]_{10}N^+Me_2(CH_2Im) \cdot Cl$

2

X : (a) H, (b) COOH
(c) $CH_2N^+(CH_3)_3Cl^-$
(d) $CONHCH_2CH_2$

3

12

$CH_3(CH_2)_7$ $(CH_2)_8COOH$

13

4
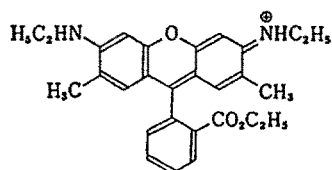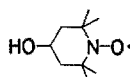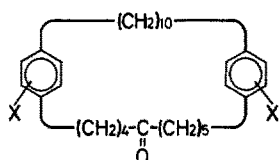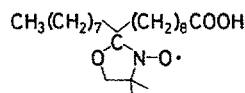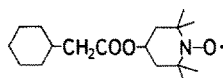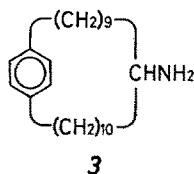
X : (a) H, (b) COOH
(c) $CH_2N^+(CH_3)_3Cl^-$
(d) $CO(CH_2)_3COOH$
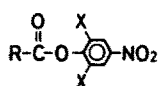
14

H_5C_2HN $N^+HC_2H_5$

H_3C CH_3

$CO_2C_2H_5$

15

5

$R-C-O-\phenyl-NO_2$

(a) R = $\bigcirc$–CH₂–, X = H

(b) R = $\bigcirc$–CH(CH₃)–, X = H

(c) R = $H_3C \bigcirc CH_2-$, X = H

(d) R = (CH₂)₉ CHCH₂–, X = H

(e) R = $H_3C \bigcirc CH_2-$, X = CH₃

16

N^+–CH=CH–$\phenyl$–N(CH₃)₂·I⁻
C_2H_5

17

18

OH
$N=N$–$\phenyl$
SO_3Na
NaO_3S
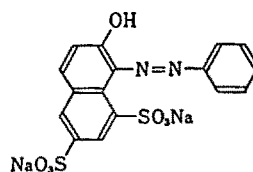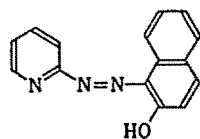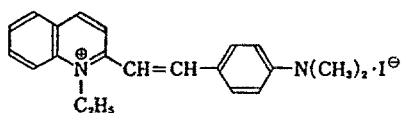
Thus, a linear relationship is obtained by plotting the left-hand side of Eq. (2) against the reciprocal initial concentration of the cyclic oxime, when the initial concentration of substrate and the pH of the reaction medium are constant. If the reasonable assumption is made that $K_a \cong K'_a$, $(1/\gamma)\,k_{acyl}$ and K_b are obtained from Eq. (2). Through evaluation of $(1/\gamma)\,k_{acyl}$ at various pH's, k_{acyl} is determined according to Eq. (3).

$$\frac{\gamma}{k_{acyl}} = \frac{[H^+]}{K_a k_{acyl}} + \frac{1}{k_{acyl}} \tag{3}$$

The constants of binding (K_b, Table 1) of paracyclophanoximes with hydrophobic carboxylic esters ($K_b \cong 10^3\text{--}10^5 \text{ mol}^{-1} \text{ dm}^3$)[2,3] are considerably larger than those for the complexes formed between phenyl esters[4--6] or azo dyes[7] and cycloamyloses ($K_b \cong 10^2\text{--}10^3 \text{ mol}^{-1} \text{ dm}^3$). The binding constant for each system (Table 1) decreases with increasing reaction temperature (negative enthalpy change) as observed for cycloamyloses[4--7]. The formation of an appreciably stable complex between a cyclic oxime and p-nitrophenyl dodecanoate (PNPL) or hexadecanoate (PNPP) is attributed to a favorable enthalpy change which is sufficiently large to compensate for an unfavorable entropy change (Table 2)[2,3].

When hydrocarbon-like molecules such as carboxylic esters with a long alkyl chain are dissolved in water, some of the structured water molecules surrounding each solute molecule are transferred to the bulk medium due to association of solute molecules. Thus, hydrophobic interactions are accompanied by an increase in entropy and possibly by a positive enthalpy change[8,9]. There are, however, a number of examples of hydrophobic association which result in negative enthalpy and entropy changes, e.g. the association of dyes[10,11] and purines[12--14]. In such cases, several factors other than the behavior of structured water molecules should be operative, e.g. attractive van der Waals dispersion forces, conformational changes of interacting molecules, and so on. There are good reasons to expect that p-nitrophenyl carboxylates bearing a relatively long alkyl chain preferably adopt a folded conformation[15,16] or a so-called self-aggregated form[17]. If this is the case, the binding process may consist of two steps, unfolding or deaggregation of a free ester (step 1) followed by complexation of the unfolded ester with a macrocyclic host molecule (step 2). The thermodynamic parameters associated with the binding process are determined by the relative importance of the two steps, and the unfolding process of PNPL and PNPP is responsible for the observed large negative entropy change. The binding efficiency follows the decreasing order: *2a* > *1* > *2b* > > *2c* (Tables 1 and 2). The lower binding efficiencies of *2b* and *2c* are presumably related to the nature of their charged substituents (carboxylate and ammonium, respectively), which are located in the vicinity of the hydrophobic binding site. Since hydrophobic interactions are accompanied by the formation of a special structure of liquid water, the effects of added salts have been interpreted in terms of their disruption of the water structure[9]. Hydrophobic interactions are inhibited by highly chaotropic ions, the resulting effect being reflected in the disordering of the water structure the extent of which is governed by the nature of chaotropic ions and their concentrations. Consequently, the structure-breaking ability of the charged substituents of *2b* and *2c* is primarily responsible for their

Yukito Murakami

Table 1. Kinetic binding constants for the incorporation of *p*-nitrophenyl carboxylates into [20]paracyclophanoximes

Host	Guest	pH	Temp. [°C]	K_b [mol^{-1} dm^3]
1[a]	PNPL[e]	10.31	43.1	2.0×10^5
		10.31	33.9	4.4×10^5
		12.37	42.1	1.1×10^5
		12.37	34.1	1.8×10^5
		12.37	24.5	3.9×10^5
1[a]	PNPP[f]	10.71	49.8	5.8×10^4
		10.71	39.9	1.5×10^5
		10.71	30.1	3.9×10^5
		11.78	49.8	3.6×10^4
		11.78	39.9	8.2×10^4
		11.78	20.2	5.1×10^5
2a[b]	PNPP[g]	11.02	33.4	6.5×10^5
		10.73	40	3.2×10^5
		10.62	48	1.4×10^5
		11.53	33.4	2.6×10^5
		11.37	40	1.2×10^5
		11.23	48	6.7×10^4
2b[c]	PNPP[g]	11.02	33.4	2.5×10^4
		10.73	40	1.5×10^4
		10.62	48	7.4×10^3
		11.53	33.4	2.9×10^4
2c[d]	PNPL[g]	11.11	20	8.8×10^3
		10.97	25	5.8×10^3
		10.82	30	4.0×10^3
		11.26	20	1.4×10^4
		11.20	25	7.7×10^3
		11.03	30	5.2×10^3
		11.65	20	2.0×10^4
		11.56	25	1.1×10^4
		11.43	30	6.7×10^3

[a] Measured in acetone-water (10.9:89.1 v/v) at $\mu = 0.10$ (KCl) and the maximum concentration of *1*, 2×10^{-5} mol dm^{-3}. [b] Measured in ethanol-acetone-water (10:1:89 v/v) at $\mu = 0.10$ (KCl) and the maximum concentration of *2a*, 2.5×10^{-5} mol dm^{-3}. [c] Measured in ethanol-acetone-water (10:1:89 v/v) at $\mu = 0.10$ (KCl) and the maximum concentration of *2b*, 8.8×10^{-5} mol dm^{-3}. [d] Measured in methanol-acetone-water (1:1:98 v/v) at $\mu = 0.10$ (KCl) and the maximum concentration of *2c*, 8.5×10^{-5} mol $\times$ dm^{-3}. [e] Initial concentration: 9.9×10^{-6} mol dm^{-3}. [f] Initial concentration: 9.6×10^{-6} mol dm^{-3}. [g] Initial concentration: 1.0×10^{-5} mol $\times$ dm^{-3}.
(Cited from Refs. [2)] and [3)])

weaker binding force. It is interesting to note that the binding constant for the *2c*-PNPL system slightly increases with increasing pH of the medium in contrast to those for the *2a*-PNPP, *1*-PNPL, and *1*-PNPP systems (Table 1). The trend observed for the *2c* system may be attributed to the counterion effect. At lower pH, the primary counterion of the ammonium group may be chloride which is added in a large excess to maintain the ionic strength of the reaction medium constant. As

Table 2. Thermodynamic parameters for the binding of p-nitrophenyl carboxylates with [20]para-cyclophanoximes[a]

Host	Guest	pH	ΔG^0_{303K} [kcal mol^{-1}]	ΔH^0 [kcal mol^{-1}]	ΔS^0 [cal mol^{-1} K^{-1}]
1	PNPL	12.37	—7.50	—14.4	—22.8
	PNPP	10.71	—7.65	—16.2	—28.2
		11.78	—7.32	—16.1	—28.9
2a	PNPP	11.00	—8.2	—26.5	—60.1
		11.50	—7.8	—28.8	—69.4
2b	PNPP	10.73	—6.3	—16.0	—32.1
2c	PNPL	11.00	—5.1	—7.2	—6.8
		11.50	—5.4	—15.6	—33.8

[a] Thermodynamic parameters were evaluated on the basis of K_b values listed in Table 1. (Cited from Refs. [2] and [3])
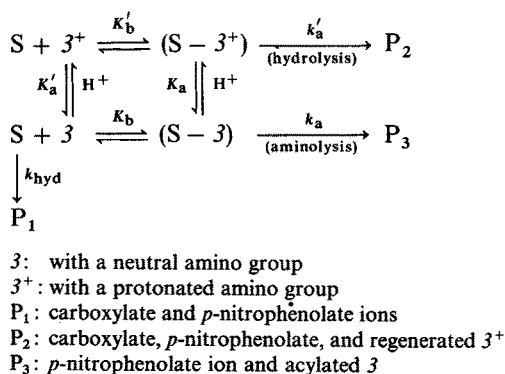
the pH increases, chloride ions surrounding the ammonium groups are gradually replaced by hydroxide ions. Hydroxide ions around the binding site of *2c* at high pH may enhance hydrophobic interactions between *2c* and PNPL since the hydroxide ion has been suggested to be structure-making [9].

There exists a considerable linear compensation effect between enthalpy and entropy for binding as exemplified by the interaction of *1* with p-nitrophenyl decanoate (PNPD), PNPL, and PNPP [2]. A very low isoequilibrium temperature ($\beta = 265$ K) suggests that the inclusion of a phenyl carboxylate with a long alkyl chain into the cavity of a cyclic oxime is certainly controlled by the entropy at ordinary temperatures.

2.1.2 [20]Paracyclophane Bearing an Amino Group [18]

10-Amino[20]paracyclophane (*3*) is characterized by two functions: a hydrophobic binding site formed by polymethylene chains and a benzene ring and a catalytic site provided by an amino group. In fact, dinitrophenylation of *3* with 2,4-dinitrofluoro-benzene, which is a potential reagent for the modification of an essential amino group of enzymes [19], resulted in the complete disappearance of the catalytic effect.

Scheme 2:

$$
\begin{array}{ccccc}
S + 3^+ & \underset{}{\overset{K'_b}{\rightleftharpoons}} & (S - 3^+) & \xrightarrow[\text{(hydrolysis)}]{k'_a} & P_2 \\[4pt]
K'_a \big\Vert \text{H}^+ & & K_a \big\Vert \text{H}^+ & & \\[4pt]
S + 3 & \underset{}{\overset{K_b}{\rightleftharpoons}} & (S - 3) & \xrightarrow[\text{(aminolysis)}]{k_a} & P_3 \\[4pt]
\big\downarrow k_{hyd} & & & & \\[4pt]
P_1 & & & &
\end{array}
$$

3: with a neutral amino group
3$^+$: with a protonated amino group
P_1: carboxylate and p-nitrophenolate ions
P_2: carboxylate, p-nitrophenolate, and regenerated *3*$^+$
P_3: p-nitrophenolate ion and acylated *3*

Formation of an inclusion complex between *3* and a hydrophobic carboxylate was confirmed by the inhibition experiment with 1-dodecanol. The catalytic efficiency exhibited by *3* gradually decreases with increasing inhibitor concentration. Since the inhibitor and substrate (PNPL or PNPP) bear hydrophobic alkyl chains of similar length, they can compete with each other in occupying the hydrophobic cavity of *3*.

Being consistent with the correlation between pH and rate and with the saturation-type kinetics, the reaction scheme is given by Scheme 2 which describes the preequilibrium complexation of *3* with a substrate at a 1 : 1 molar ratio followed by decomposition of the bound substrate through pseudo-intramolecular catalysis. The hydrolysis and aminolysis reactions are treated separately by analyzing the kinetic
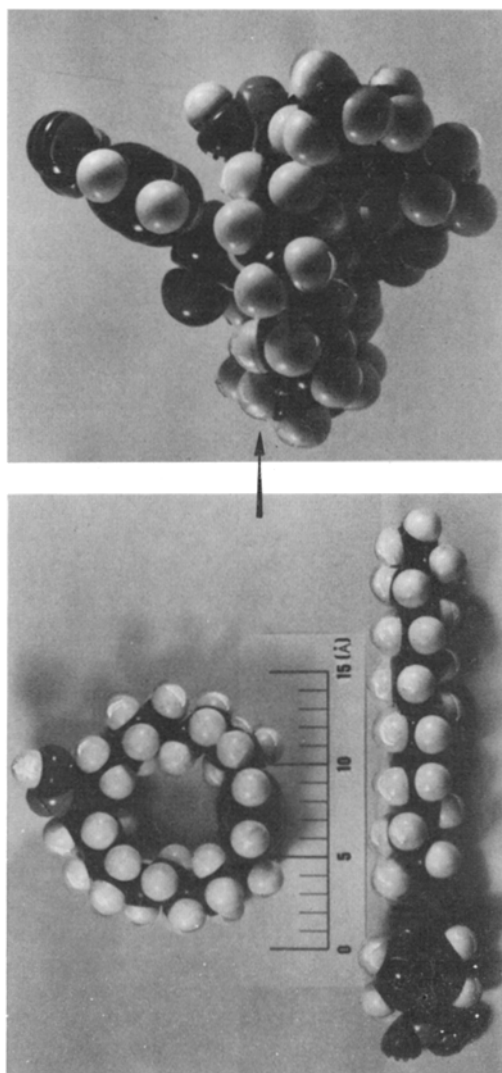

Fig. 1. CPK (Corey-Pauling-Koltum) molecular model representation of the incorporation of PNPP into the cavity of *2a*
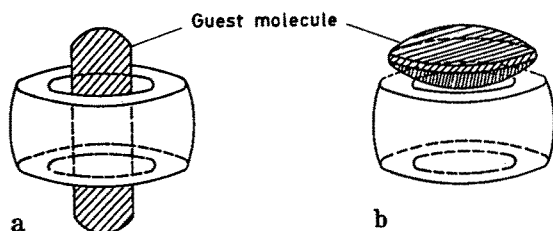
Fig. 2a and b. Schematic representation of the incorporation modes of paracyclophanes: **a** penetration mode, **b** face-to-face mode

data obtained in sufficiently low and high pH regions, respectively, relative to the pK_a values of the catalyst [pK_a 8.1–8.3 with PNPL and PNPP in ethanol-water (20.8:79.2 v/v) at 40.0 °C and $\mu = 0.10$ (KCl)]. The substrate-binding constants (K_b in Scheme 2) for aminolysis are $5.9 \times 10^4 \, mol^{-1} \, dm^3$ (at pH 9.95) and $1.0 \times 10^5 \, mol^{-1} \, dm^3$ (at pH 10.29) with PNPL and PNPP, respectively, and are comparable to those obtained for the paracyclophanoxime systems described above.

The [20]paracyclophane skeleton provides a hydrophobic cavity of 4.4–4.8 Å in diameter. This cavity size is just sufficient to incorporate a polymethylene chain in its extended conformation, since the average diameter of a polymethylene chain is 4 Å. The substrate-binding behavior of *2a* is illustrated in Fig. 1 with the aid of the CPK molecular models. This binding mode can be designated as a "penetration-type" and is schematically shown in Fig. 2. The substrate concentrations were $1.0 \times 10^{-5} \, mol \, dm^{-3}$ in most of the experiments described above. In such a high concentration range, hydrophobic substrate species are largely in the self-aggregated state [17]. Consequently, the true constant of association between a hydrophobic substrate in its monomeric form and a [20]paracyclophane must be somewhat larger than those reported here.

2.2 Face-to-Face Incorporation [20]

The rates of alkaline hydrolyses of a series of *p*-nitrophenyl carboxylates bearing an alicyclic moiety (*5a–5e*) are retarded in the presence of an excess of *4d*. The observed extent of inhibition is attributed to the formation of an association complex between *4d* and a substrate. In such a complex, the substrate ester is protected against attack by an external hydroxide ion due to the steric effect of the cyclophane skeleton and the electrostatic effect of the carboxylate groups on the macrocycle which repels approaching hydroxide ions. The paracyclophane exists in a monomeric form under the kinetic conditions employed as confirmed by surface tension measurements. In all cases saturation-type kinetics are observed with

Scheme 3:

$$S + C \underset{}{\overset{K_b}{\rightleftharpoons}} (SC) \xrightarrow{k'_{hyd}} P$$
$$\downarrow^{k_{hyd}}$$
$$P$$
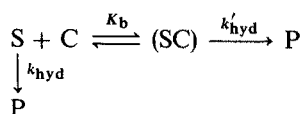
respect to cyclophane concentration, and the kinetic data are consistent with Scheme 3. Substrate S and paracyclophane C associate to yield a complex (SC) at a 1:1 molar ratio with binding constant K_b, and the free and bound substrates undergo hydrolysis with rate constants k_{hyd} and k'_{hyd}, respectively. The ratio k_{hyd}/k'_{hyd} is a direct measure of the extent of rate inhibition due to complex formation (Table 3). A qualitative correlation between k_{hyd} and k_{hyd}/k'_{hyd} has been found: the less reactive the ester in a bulk phase, the more severely inhibited is its hydrolysis in the association complex, suggesting that the reactivity of the ester in the association complex is also controlled by the steric effect.

Table 3. Kinetic parameters for the hydrolysis of p-nitrophenyl carboxylates in the presence and absence of $4d$[a]

Ester (5)[b]	k_{hyd} [s^{-1}]	k'_{hyd} [s^{-1}]	k_{hyd}/k'_{hyd}	K_b [mol^{-1} dm^3]	pH[c]	Temp. [°C]
a	3.58×10^{-3}	5.5×10^{-4}	6.5	2.3×10^3	10.8	20.0
b	3.12×10^{-4}	6.0×10^{-6}	52	2.0×10^3	10.8	20.0
c	8.67×10^{-4}	3.4×10^{-5}	26	4.3×10^3	10.8	20.0
d	8.23×10^{-4}	1.0×10^{-5}	82	2.6×10^4	10.8	20.0
e	9.88×10^{-5}	1.0×10^{-6}	99	2.8×10^4	11.8	40.0

[a] In ethanol-dioxane-water (10.9:1:88.1 v/v), $\mu = 0.15$ (KCl).

[b] Initial concentrations: 1.0×10^{-5} mol dm^{-3} for $5a$–$5c$, 1.0×10^{-6} mol dm^{-3} for $5d$, and 2.0×10^{-6} mol dm^{-3} for $5e$.

[c] Borax-carbonate buffer (0.05 mol dm^{-3}) for runs at pH 10.8 and sodium hydroxide-phosphate buffer (0.05 mol dm^{-3}) for runs at pH 11.8.
(Cited from Ref.[20])

In the hydrophobic association of [10.10]paracyclophane with the substrates, the latter are not necessarily incorporated into the macrocyclic cavity in the light of binding constants and their molecular sizes. When two methyl groups are introduced into the cyclohexane ring ($5c$) or the cyclohexane ring is replaced by cyclodecane ($5d$), the acyl moiety cannot be incorporated into the paracyclophane cavity as confirmed by the CPK space-filling molecular models. Substitution of two methyl groups on the nitrophenyl moiety ($5e$) makes it impossible to incorporate any part of the substrate molecule into the cavity. In spite of this stereochemical situation, the binding constant increases in the order: $5a < 5c < 5e$. The binding constant for $5d$ is also significantly large. On the basis of these observations, the [10.10]paracyclophane skeleton, which provides a hydrophobic cavity of 5.6–6.4 Å, undergoes host-guest interactions with various bulky and hydrophobic substrates in a face-to-face mode. The substrate-binding behavior of $4d$ is illustrated in Fig. 3 with the aid of the CPK molecular models. The schematical representation of the "face-to-face" mode is given in Fig. 2. The above finding does not exclude the possibility of strong hydrophobic interactions to occur between a [10.10]paracyclophane and a carboxylic ester bearing a long alkyl chain in a penetration-type mode.
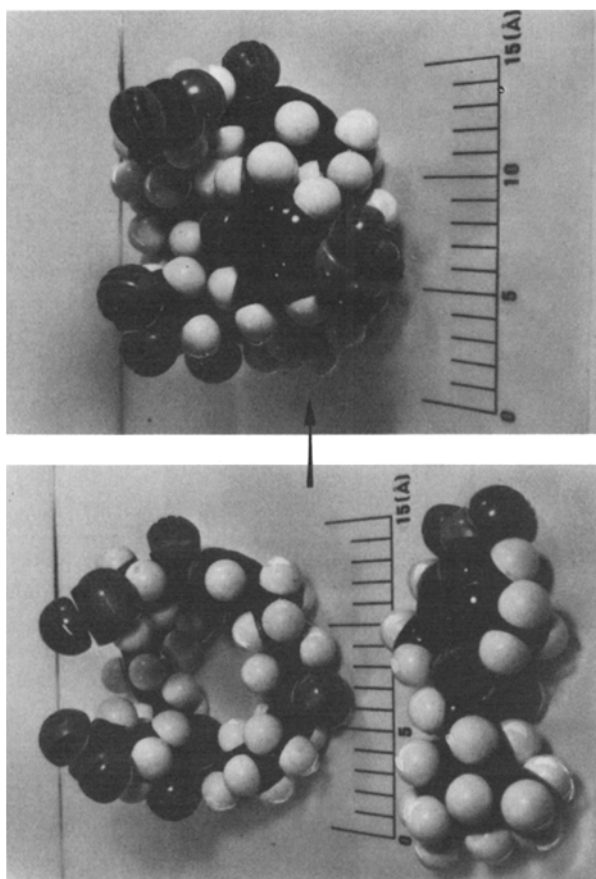
Fig. 3. CPK molecular model representation of the association of *4d* with *5e*

2.3 Induced-Fit Incorporation

Azaparacyclophanes containing amide nitrogens in the cyclic skeleton and long alkyl chains as branches of this skeleton have been prepared to investigate their ability to incorporate various hydrophobic substrates. Such a macrocycle is expected to provide a deeper and efficient hydrophobic cavity for these substrates by cooperation of alkyl chains in aqueous media. Moreover, these macrocycles may incorporate substrates of various bulkiness through an induced-fit mechanism because of the flexible character of the alkyl branches. We have prepared such octopus-like azaparacyclophanes as represented by *6–11*.

2.3.1 Substrate-Binding Ability [21, 22)

4-(Cyclohexylacetoxy)-2,2,6,6-tetramethylpiperidin-1-oxyl (*12*), 2-(8-carboxyoctyl)-5,5-dimethyl-2-octyl-3-oxazolidin-1-oxyl (*13*) and 4-hydroxy-2,2,6,6-tetramethyl-piperidin-1-oxyl (*14*) were used as moderately hydrophobic, hydrophobic, and hydrophilic spin probes, respectively, and the ESR parameters are summarized in Table 4. A correlation time for the rotational motion of a paramagnetic molecule

Table 4. Isotropic nitrogen hyperfine splitting constants (A_N) and rotational correlation times (τ_c) of nitroxide radicals at room temperature

ESR probe[a]	Host	Medium[b]	A_N [G]	$10^{11} \tau_c$ [s]
12, 5.0×10^{-5} mol dm^{-3}	None	DEW	17.03	10.8
12, 5.0×10^{-5} mol dm^{-3}	6, 1.0×10^{-3} mol dm^{-3}	DEW	17.12	21.2
12, 5.25×10^{-4} mol dm^{-3}	None	EMW	17.08	6.5
12, 5.25×10^{-4} mol dm^{-3}	8, 5.05×10^{-3} mol dm^{-3}	EMW	16.99	10.74
13, 5.66×10^{-4} mol dm^{-3}	None	EMW	15.80	21.5
13, 5.66×10^{-4} mol dm^{-3}	8, 5.05×10^{-3} mol dm^{-3}	EMW	15.78	68.3
14, 5.40×10^{-4} mol dm^{-3}	None	EMW	17.11	3.3
14, 5.40×10^{-4} mol dm^{-3}	8, 5.05×10^{-3} mol dm^{-3}	EMW	17.05	4.4

[a] Alkaline hydrolysis of 12 and 13 was not detected throughout the measurements.
[b] DEW, dimethyl sulfoxide-ethanol-water (10:1:89 v/v) at pH 10.29 and $\mu = 0.15$ (KCl); EMW, ethanol-methanol-water (5:2:95 v/v) at pH 8.34 and $\mu = 0.10$ (KCl).
(Cited from Refs. [21] and [22])

is obtained by Eq. (4) where $\Delta H_{(m=+1)}$ is the peak-to-peak line width in gauss of the derivative of the low-field absorption line; $I_{(m=+1)}$ and $I_{(m=-1)}$ are the corresponding peak-to-peak heights for the low- and high-field lines, respectively. For the calculation of

$$\tau_c = A \cdot \Delta H_{(m=+1)}[(I_{(m=+1)}/I_{(m=-1)})^{1/2} - 1] \tag{4}$$

τ_c, $A = 6.6 \times 10^{-10}$, which was obtained for di-t-butyl nitroxide, was used because it does not markedly change among various nitroxide radicals. The rotational correlation times indicate that Michaelis-type complexes are definitely formed between azaparacyclophanes and hydrophobic spin probes. In particular, the most hydrophobic probe (13) is most effectively incorporated into the hydrophobic field. On the other hand, the isotropic nitrogen hyperfine splitting constants (A_N) in the presence of azaparacyclophanes do not change to any meaningful extent, relative to those observed in the absence of these compounds. Thus, octopus cyclophanes incorporate only the hydrophobic portion of the substrates into their deep cavities while the nitroxide moiety remains exposed to the bulk phase.

Four hydrophobic alkyl chains in azaparacyclophanes may be arranged in the same direction due to their mutual hydrophobic interactions in aqueous media while in nonaqueous media they are presumably extended to minimize their mutual interactions (substrate-binding interactions are not expected in the latter state; dead state). Such hydrophobic branches may provide the deep hydrophobic cavity in aqueous media. The substrate-binding ability of 6 and 8 was studied spectrophotometrically using several organic dyes as guest molecules. The appearance of isosbestic points is consistent with the formation of inclusion complexes in 1:1 stoichiometry, and the spectral data are analyzed according to the Benesi-Hildebrand equation [23] (Table 5). Cationic dyes such as Rhodamine 6G (15) and Quinaldine Red (16) as well as a suitably bulky neutral dye, 1-(2-pyridylazo)-2-naphthol (PAN, 17), undergo complex formation with 6, while an anionic dye (Orange G, 18) and PAN with 8. On the other hand, cationic dyes (15 and 16) and an anionic

Table 5. Dissociation constants for inclusion complexes of azaparacyclophanes

Substrate[a]	Host[b]	Medium[c]	K_d [mol dm^{-3}]	λ_{iso}[d] [nm]	λ_{meas}[e] [nm]
Rhodamine 6G (10.1)	6 (0.67–6.67)	DEW	2.1×10^{-4}	535	530
Quinaldine Red (3.89)	6 (0.19–6.30)	DEW	2.2×10^{-4}	520	478
PAN (6.77)	6 (1.65–8.25)	DEW	6.78×10^{-4}	494	550
Orange G (11.3)	8 (0.89–8.85)	EMW	1.92×10^{-3}	512	480
PAN (11.5)	8 (0.89–5.34)	EMW	2.84×10^{-3}	498	470

[a] Concentrations given in units of 10^{-6} mol dm^{-3} in parentheses.
[b] Concentrations given in units of 10^{-4} mol dm^{-3} in parentheses.
[c] DEW, dimethyl sulfoxide-ethanol-water (10:1:89 v/v) at pH 10.29, $\mu = 0.15$ (KCl), and 39.4 °C; EMW, ethanol-methanol-water (5:2:95 v/v) at pH 8.70, $\mu = 0.10$ (KCl), and 30.0 °C.
[d] Observed isosbestic point.
[e] Wavelength used for measurements.
(Cited from Refs. [21] and [22])

dye (methyl orange) do not show any spectral change upon addition of 8 and 6, respectively. Furthermore, dyes having an opposite charge are incorporated into the hydrophobic cavity of azaparacyclophane more tightly than neutral ones of similar size. These results indicate that both electrostatic and hydrophobic interactions contribute effectively to the substrate-binding process of these octopus cyclophanes. It is interesting to note that Rhodamine 6G and PAN do not undergo complex formation with β-cyclodextrin under similar conditions [21]. Rhodamine 6G seems to be too bulky to be incorporated into the cyclodextrin cavity (cavity diameter 7.5 Å). The aggregation behavior of 6 was observed in dimethyl sulfoxide-water (1:9 v/v) at 16 °C, pH 10.29, and μ 0.15 (KCl), the critical aggregate concentration being 3.15×10^{-4} mol dm^{-3}. However, the incorporation of the above dyes into the cavity in 1:1 stoichiometry is not disturbed by the aggregate formation. Such aggregation behavior is not detected with 8 and 10 in ethanol-methanol-water (5:1:95 v/v) at μ 0.10 (KCl) and room temperature up to concentrations of 3.7×10^{-3} (pH 8.34) and 1.2×10^{-3} mol dm^{-3} (pH 9.04), respectively. The substrate-binding mode is schema-
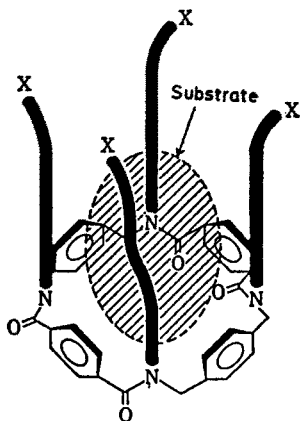
Fig. 4. Schematic representation of the substrate-binding mode of octopus cyclophane: the shaded portion refers to an incorporated guest molecule

tically shown in Fig. 4. Since these azaparacyclophanes can incorporate substrates of various molecular sizes, the induced-fit mechanism must be operative in the binding process.

An azaparacyclophane bearing an anionic carboxy group at the end of each alkyl chain (6) inhibits the alkaline hydrolysis of hydrophobic esters. In fact, the alkaline hydrolysis of p-nitrophenyl 3,5-dimethylcyclohexylacetate (5c) in dimethyl sulfoxide-dioxane-water (10:1:89 v/v) at 20.5 °C, pH 10.29, and μ 0.15 (KCl) was investigated; the rate of hydrolysis is retarded as the concentration of 6 increases. The observed saturation-type kinetics is consistent with Scheme 3 in a similar manner as observed with [10.10]paracyclophane (see Sect. 2.2), and the kinetic parameters thus evaluated are as follows: $1/K_b$, 1.79×10^{-3} mol dm^{-3}; k'_{hyd}, 1.80×10^{-6} s^{-1}. The rate of hydrolysis is retarded by 147-fold relative to the spontaneous one. The dissociation constant for the 6-PAN system is smaller than that for the 6-5c. The cavity constructed by four benzene rings of aza[3.3.3.3]paracyclophane and four alkyl branches is suitable for the incorporation of a naphthyl moiety. It should be pointed out that 6 effectively incorporates bulky guest molecules in a concentration range above and below its critical aggregate concentration. This means that the
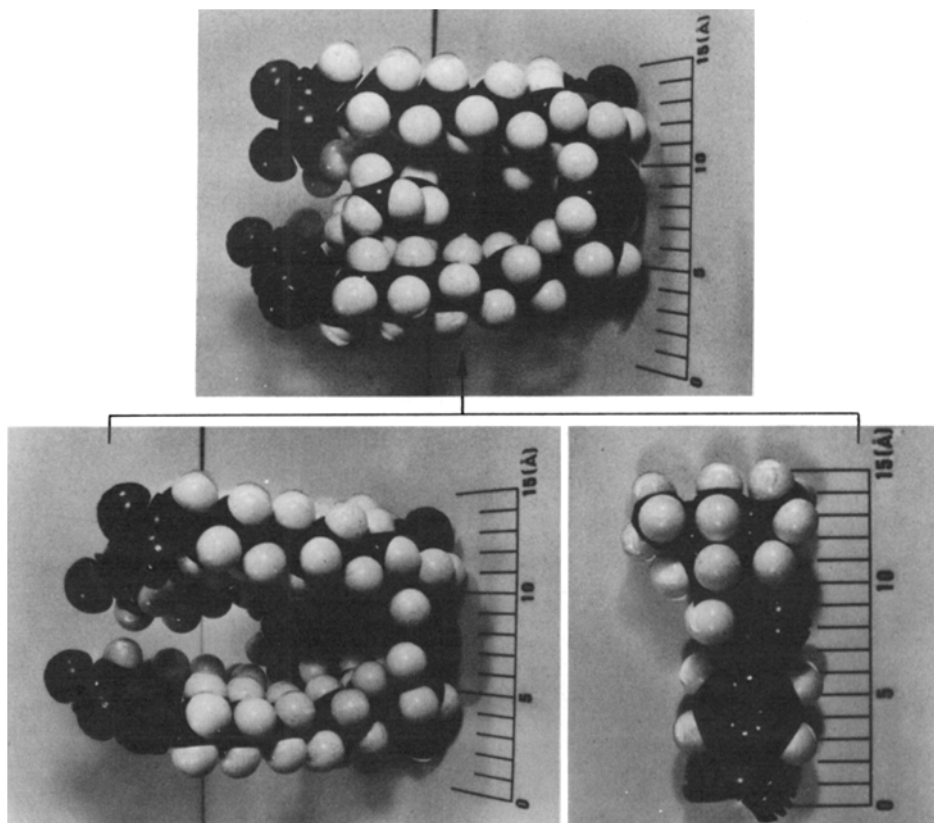

Fig. 5. CPK molecular model representation of the incorporation of 5c into the hydrophobic field of 6

azaparacyclophane itself forms an effective hydrophobic binding site and the aggregate formation has little effect on the substrate-binding process. The substrate-binding behavior of 6 is illustrated in Fig. 5 with the aid of the CPK molecular models.

2.3.2 Substrate-Selectivity in the Hydrolysis of p-Nitrophenyl Carboxylates [22]

The observed first-order rate constants (k_{obsd}) and the catalytic efficiency parameters (k_c/k_{hyd}) for the hydrolysis of eight p-nitrophenyl carboxylates, which have n-alkyl groups of various length in their respective acyl moieties, in the presence of 11 are shown in Fig. 6: k_{hyd} is the rate constant for the spontaneous alkaline hydrolysis; $k_c = k_{obsd} - k_{hyd}$. In practice, it should be possible to estimate the substrate selectivity exhibited by the azaparacyclophane from the observed rate constants. The trend of substrate selectivity does not coincide with that of catalytic efficiency. This is caused by the fact that the rate constant of the spontaneous hydrolysis under the conditions indicated in Fig. 6 decreases as the alkyl chain length of the ester increases, owing to the self-coiling property of alkyl chains in addition to molecular aggregation [17]. Therefore, one of the roles of octopus cyclophanes in catalysis must, in addition to the binding ability itself, be unfolding of the long alkyl chains of the carboxylic esters so that the ester bond is exposed to the catalytic group or groups.

From a theoretical viewpoint in general, the difference in free energy of activation between a catalytic reaction and the corresponding spontaneous one needs to be
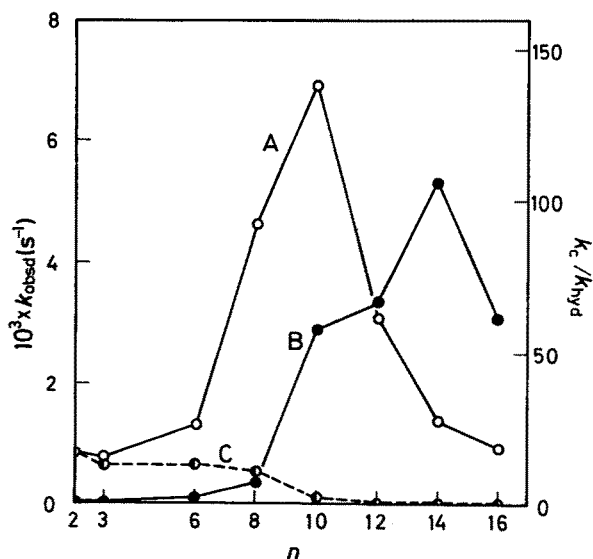

Fig. 6. Pseudo-first-order rate constant in the presence (k_{obsd}, A) and in the absence (k_{hyd}, C) of 11 and catalytic efficiency (B) as a function of the length of the alkyl chain of the substrates (n = number of carbon atoms in an acyl moiety) for the hydrolysis of p-nitrophenyl carboxylates ($NO_2C_6H_4OCO$-$[CH_2]_{n-2}CH_3$) performed in ethanol-methanol-dioxane-water (5:1:1:95 v/v) at pH 8.88, μ 0.10 (KCl), 30 °C, and the initial concentrations: 11, 5.55×10^{-5} mol dm^{-3}; substrate, 5.0×10^{-6} mol × dm^{-3} (taken from Ref. [22])

examined in order to evaluate the catalytic efficiency. On these grounds, the value of k_c/k_{hyd} must be referred to rather than the apparent rate constant (k_{obsd}) for the evaluation of catalytic and selectivity efficiency. The highest catalytic efficiency of *11* is observed with *p*-nitrophenyl tetradecanoate (Fig. 6). A similar result was obtained with another azaparacyclophane *10*. In the catalysis of octopus cyclophanes, hydrophobic interactions between the long alkyl chain of the substrate and those of the azaparacyclophane play an important role in holding the reactive sites of both species in juxtaposition ready for nucleophilic attack of the imidazolyl group. There must be a certain threshold for the length of the alkyl chain of the substrate in order to attain the most favorable arrangement of both the ester bond of an incorporated substrate and the catalytic group (or groups) of an octopus cyclophane; this is achieved for *10* and *11* with the substrate, *p*-nitrophenyl tetradecanoate. On the other hand, *N*-(imidazol-4-ylethyl)-10(11)-oxo[20]paracyclophane-22-carboxamide [24] bearing no alkyl chain and *N*-decylimidazole [16] did not show a maximum catalytic efficiency in the deacylation of the ester substrates. This again indicates that the relative geometrical arrangement of the active functional groups of the azaparacyclophane with respect to the reactive site of the ester substrate in the Michaelis-type complex is one of the most important factors of effective catalysis, as generally suggested for enzymatic reactions [25, 26].

2.3.3 Orientational Behavior of Octopus-Leg Segments [22]

The effect of pH on the substrate-binding behavior of *8* and *11* was investigated by the fluorescence technique. 1,6-Diphenylhexa-1,3,5-triene (DPH), which has no proton-dissociative group and is hydrophobic, was used as a probe. DPH shows excitation and emission maxima at 317 and 441 nm, respectively, in the absence of azaparacyclophane derivatives in ethanol-methanol-tetrahydrofuran-water (5:1:1:95 v/v). The excitation and emission maxima are shifted to 365 and 430 nm,
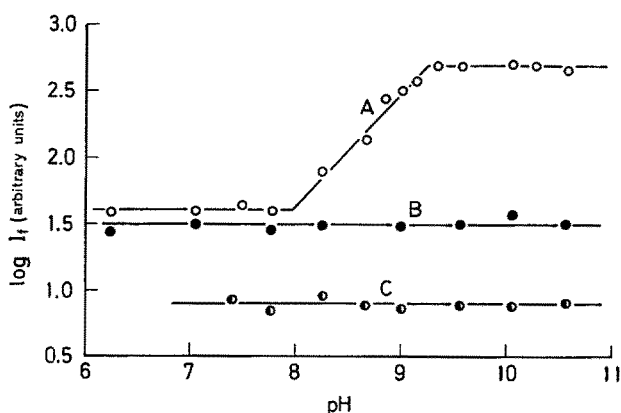

Fig. 7. Fluorescence intensity of DPH as a function of pH in the presence of *11* (A) and *8* (B) and in the absence of an azaparacyclophane derivative (C) in ethanol-methanol-tetrahydrofuran-water (5:1:1:95 v/v) at the following initial concentrations: *11*, 5.33×10^{-4} mol dm^{-3}; *8*, 4.99×10^{-4} mol × dm^{-3}; DPH, 1.08×10^{-6} mol dm^{-3} [$\mu = 0.10$ (KCl)] (taken from Ref. [22])
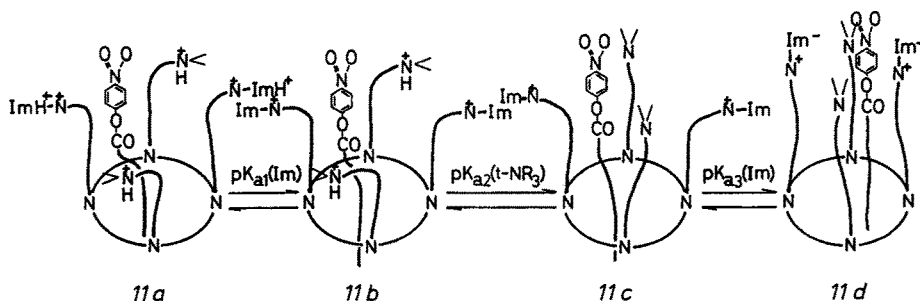
Fig. 8. Schematic representation of the variation in orientation of octopus-leg segments in *11* along with proton dissociation of the functional groups (taken from Ref. [22])

respectively, upon the addition of the octopus cyclophanes. DPH was therefore excited at 365 nm and the fluorescence intensity was measured at 430 nm with a cut-off filter for radiation below 390 nm. The relative fluorescence intensity of DPH remains the same over the whole pH region in the absence of azaparacyclophanes. The fluorescence intensity increases fivefold upon the addition of *8*, although it remains constant throughout the whole pH region examined owing to the lack of a proton-dissociative group in *8*. On the other hand, in the presence of *11* the fluorescence intensity increases above pH 8 and levels off beyond pH 9.3 (Fig. 7). The saturated fluorescence intensity is 83 times larger than that observed in the absence of *11*. This intensity is comparable to that observed in benzene. As a result, the pH value of 9.2 observed as a breaking point in Fig. 7 is referred to the pK_a for the tertiary amino group of *11*. A strong hydrophobic interaction is apparently exercised upon deprotonation of the tertiary amino group as shown in Fig. 8. The binding constant for the incorporation of DPH into the cavity of *11c* was determined at pH 9.32 according to the Benesi-Hildebrand treatment [23]; $1/K_b = (1.5 \pm 0.3) \times 10^{-5}$ mol dm^{-3}. The corresponding binding constants for *11a* and *11b*, which are present at lower pH's, were not obtained owing to the weak binding ability of these species. In reference to the data given in Fig. 7, acid dissociation of the neutral imidazolyl group seems to make little contribution to the substrate-binding ability of *11*.

3 Catalytic Behavior of Paracyclophanes in Aqueous Media

3.1 Nucleophilic—Electrostatic Bifunctional Catalysis [3]

The liberation of *p*-nitrophenoxide from PNPL and PNPP is accelerated by para-cyclophanoximes relative to spontaneous alkaline hydrolysis under the identical kinetic conditions; initial concentration of substrate ester $(1.0 \times 10^{-5}$ mol dm$^{-3})$, ionic strength (0.10 with KCl), and solvent system. The apparent first-order rate constants (k_{obsd}) determined from the initial stage of the deacylation reactions of

PNPL and PNPP follow saturation-type kinetics[1]. The results are consistent with a reaction mechanism in which preequilibrium complexation of the cyclic oxime and the substrate at a 1:1 molar ratio is followed by pseudo-intramolecular acyl transfer from the bound substrate to the hydroxyimino group of the cyclic oxime as shown in Scheme 1. The primary product of such a deacylation reaction was identified to be an acylated paracyclophane[1]. The apparent catalytic constants (k_c) and the catalytic efficiency factors (r_e) are listed in Table 6 for selected cases; thus allowing the catalytic ability of paracyclophanoximes to be evaluated. The high activity of $2c$ must be attributed to the electrostatic field effect exerted by the positively charged ammonium group in the benzene ring moiety.

Table 6. Apparent catalytic efficiency of cyclic oximes for the release of p-nitrophenol from p-nitrophenyl carboxylates

Oxime	Substrate[a]	pH	Temp. [°C]	k_c[b] $[s^{-1} mol^{-1} dm^3]$	r_e[c]
$2a$[d], 2.50×10^{-5} mol dm^{-3}	PNPP	11.02	33.4	6.6	7.2
$2a$[d], 2.50×10^{-5} mol dm^{-3}	PNPP	11.53	33.4	12.5	6.7
$2b$[d], 2.93×10^{-5} mol dm^{-3}	PNPP	11.02	33.4	0.40	1.4
$2b$[d], 2.93×10^{-5} mol dm^{-3}	PNPP	11.53	33.4	0.98	1.5
$2c$[e], 2.84×10^{-5} mol dm^{-3}	PNPP	11.03	30	313	150
$2c$[e], 2.84×10^{-5} mol dm^{-3}	PNPP	11.43	30	708	188
$2c$[e], 2.84×10^{-5} mol dm^{-3}	PNPL	10.82	30	160	77
$2c$[e], 2.84×10^{-5} mol dm^{-3}	PNPL	11.43	30	719	75

[a] Initial concentrations of PNPL and PNPP: 1.0×10^{-5} mol dm^{-3}.
[b] $k_c = (k_{obsd} - k_{hyd})/[\text{C-oxime}]$.
[c] $r_e = k_{obsd}/k_{hyd}$.
[d] Measured in ethanol-acetone-water (10:1:89 v/v) at $\mu = 0.10$ (KCl).
[e] Measured in methanol-acetone-water (1:1:98 v/v) at $\mu = 0.10$ (KCl).
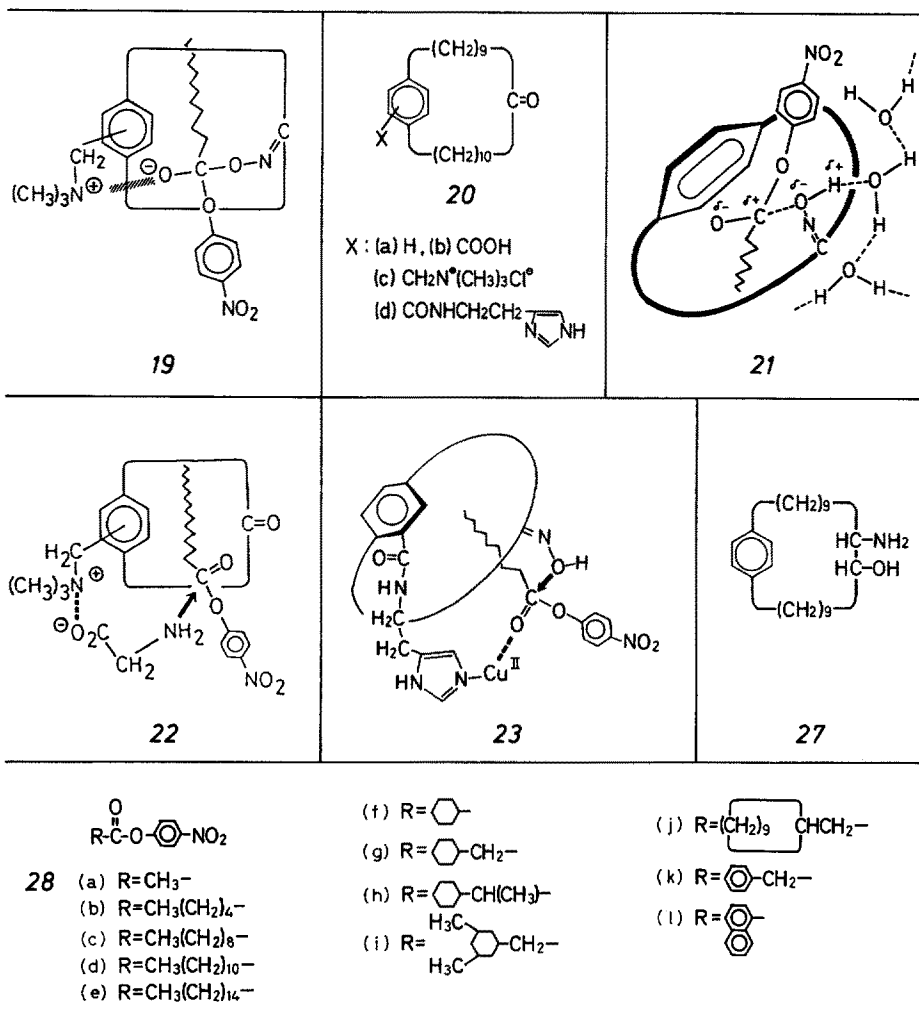(Cited from Ref. [3])

The kinetic data are analyzed by means of Eqs. (2) and (3). The acid dissociation constants for the hydroxyimino group are largely in the range of $(2-6) \times 10^{-12}$ mol^{-1} dm^3 (Table 7), and are relatively insensitive to the nature of an additional substituent introduced into the benzene ring moiety. The acyl transfer rate (k_{acyl}), on the other hand, depends on the nature of such charged substituents. The extremely high activity of $2c$ in the acyl transfer reaction is evidently related to the superacid nature of the quaternary ammonium group. Two alternative mechanisms explain these effects. (i) The hydroxide ion, a nucleophile which attacks the substrate, is concentrated around the ammonium group due to electrostatic attraction; consequently, a concentration effect facilitates the reaction concerned. (ii) The hydroxy-

---

[1] An apparent first-order rate constant determined from the initial stage of reaction between catalyst (C) and substrate (S) species increases with increasing concentration of either of the reacting species and levels off beyond a certain concentration range. This behavior is conventionally referred to "saturation-type kinetics". In such cases, the preequilibrium complexation between S and C is followed by the pseudo-intramolecular reaction of complex SC: S + C $\rightleftharpoons$ SC $\rightarrow$ products.

Table 7. Kinetic and activation parameters for acyl transfer reactions between bound p-nitrophenyl carboxylates and [20]paracyclophanoximes

Oxime	Substrate	Temp. [°C]	K_a [mol^{-1} dm^3]	pK_a	k_{acyl} [s^{-1}]	$\Delta G^{\ddagger}_{303\,K}$ [kcal mol^{-1}]	$\Delta H^{\ddagger}$ [kcal mol^{-1}]	$\Delta S^{\ddagger}$ [cal mol^{-1} K^{-1}]
1^a	PNPL^e	43	3.5×10^{-12}	11.46	1.8×10^{-2}	20.9	17.7	-10.6
		34	4.3×10^{-12}	11.37	7.8×10^{-3}			
1^a	PNPP^f	49.8	2.3×10^{-12}	11.65	1.1×10^{-1}	20.2	17.6	-8.6
		39.9	2.1×10^{-12}	11.67	4.5×10^{-2}			
		20.2	7.6×10^{-13}	12.12	9.4×10^{-3}			
$2a^b$	PNPP^g	33.4	2.4×10^{-12}	11.63	1.4×10^{-3}	21.9	16.8	-16.9
		40	5.0×10^{-12}	11.30	2.3×10^{-3}			
		48	5.9×10^{-12}	11.23	5.0×10^{-3}			
$2b^c$	PNPP^g	33.4	2.2×10^{-12}	11.66	3.0×10^{-4}			
$2c^d$	PNPL^g	20	2.1×10^{-12}	11.68	6.7×10^{-2}	18.8	19.5	2.4
		25	3.6×10^{-12}	11.44	1.0×10^{-1}			
		30	4.3×10^{-12}	11.36	2.1×10^{-1}			

[a] Measured in acetone-water (10.9:89.1 v/v) at $\mu = 0.10$ (KCl) and the maximum concentration of 1, 2×10^{-5} mol dm^{-3}.
[b] Measured in ethanol-acetone-water (10:1:89 v/v) at $\mu = 0.10$ (KCl) and the maximum concentration of $2a$, 2.5×10^{-5} mol dm^{-3}.
[c] Measured in ethanol-acetone-water (10:1:89 v/v) at $\mu = 0.10$ (KCl) and the maximum concentration of $2b$, 8.8×10^{-5} mol dm^{-3}.
[d] Measured in methanol-acetone-water (1:1:98 v/v) at $\mu = 0.10$ (KCl) and the maximum concentration of $2c$, 8.5×10^{-5} mol dm^{-3}.
[e] Initial concentration: 9.9×10^{-6} mol dm^{-3}.
[f] Initial concentration: 9.6×10^{-6} mol dm^{-3}.
[g] Initial concentration: 1.0×10^{-5} mol dm^{-3}.
(Cited from Refs. [2] and [3])

19

20

X : (a) H, (b) COOH
(c) CH2N⁺(CH3)3Cl⁰
(d) CONHCH2CH2—

21

22

23

27

$$R-\overset{O}{\overset{\|}{C}}-O-\!\langle\bigcirc\rangle\!-NO_2$$

28 (a) R=CH3–
(b) R=CH3(CH2)4–
(c) R=CH3(CH2)8–
(d) R=CH3(CH2)10–
(e) R=CH3(CH2)14–

(f) R=◯–
(g) R=◯–CH2–
(h) R=◯–CH(CH3)–
(i) R= (CH3)2◯–CH2–

(j) R=(CH2)9 ⏌CHCH2–
(k) R=◎–CH2–
(l) R=◎◎–

imino group and the ammonium group, a nucleophile and a superacid, respectively, cooperate in the catalytic process (bifunctional catalysis), and a negative charge developing on the carbonyl oxygen of the substrate in the transition state, which is formed by nucleophilic attack of the deprotonated hydroxyimino group on the acyl carbon of the substrate, is stabilized through tight ion-pair formation with the positive ammonium group as shown in *19*. These two mechanisms differ from each other in the way in which the hydroxyimino group participates in the transition state. However, the former mechanism may be ruled out on the basis of kinetic data obtained in the presence of ammonium salt *20c* which lacks a nucleophilic center. The observed first-order rate constant for deacylation of PNPP at 30 °C in the presence of *20c* (2.60×10^{-5} mol dm^{-3}) is 9.89×10^{-4} s^{-1}. Even though this value is somewhat larger than that for the spontaneous hydrolysis (1.07×10^{-4} s^{-1}), the catalytic efficiency of *20c* is negligibly small (Table 8). The local concentration

Table 8. Effect of some quaternary ammonium species on the deacylation of PNPP[a]

Catalyst[b]	Medium[c]	pH	Temp. [°C]	k_{obsd} [s^{-1}]
$2a$ (8.34×10^{-6})	EAW	11.53	33.4	2.68×10^{-4}
$2a$ (8.34×10^{-6}) + Me$_4$N$^+$Cl$^-$ (0.1)	EAW	11.53	30	2.15×10^{-4}
CTAB[d] (4×10^{-5})	EAW	11.53	30	1.63×10^{-3}
$2a$ (8.34×10^{-6}) + CTAB (4×10^{-5})	EAW	11.53	30	1.48×10^{-3}
$2c$ (2.84×10^{-5})	MAW	11.43	30	2.02×10^{-2}
$20c$ (2.60×10^{-5})	MAW	11.43	30	9.89×10^{-4}
None	MAW	11.43	30	1.07×10^{-4}

[a] Initial concentration of PNPP: 1.0×10^{-5} mol dm^{-3}.
[b] Concentration of each species (in mol dm^{-3}) is given in parentheses.
[c] EAW, ethanol-acetone-water (10:1:89 v/v) at $\mu = 0.10$ (KCl); MAW, methanol-acetone-water (1:1:98 v/v) at $\mu = 0.10$ (KCl).
[d] CTAB, hexadecyltrimethylammonium bromide.
(Cited from Ref. [3])

effect of hydroxide ion plays only a minor role. The absence of catalytic activity of $20c$ in the reaction seems to indicate that both $2c$ and $20c$ must exist primarily in a monomeric form different from typical cationic surfactants for which aggregation behavior is generally observed [27].

Electrostatic attraction between the ammonium and hydroxyimino groups of $2c$ may facilitate nucleophilic attack of the latter group on the bound substrate on the one hand, and the former group may stabilize the transition state by its electrostatic field effect on the other hand. These effects may reduce the free energy of activation appreciably. The opposite situation occurs in the $2b$ system since this cyclic oxime bears a negatively charged carboxylate group and, therefore, destabilizes the negatively charged transition state. This type of electrostatic charge effect is rarely observed in common bimolecular ionic reactions in aqueous media. This is partly due to the exceptional charge-solvating ability of water and partly and more significantly because the interaction of a charged species with a dipolar neutral substrate is not large enough to compensate for an appreciable entropy loss which would be brought about by a bimolecular association. To make this point clear, catalytic activities of some quaternary ammonium species in the deacylation of PNPP were examined (Table 8). The addition of tetramethylammonium chloride to the $2a$ system does not result in any significant effect on the reaction rate because of the absence of an intrinsic affinity of the salt for PNPP. On the other hand, hexadecyltrimethylammonium bromide (CTAB) shows a noticeable catalytic effect even in a concentration range below its critical micelle concentration. It is important, however, to note that no cooperative acceleration is detected by the combination of CTAB (an electrostatic catalyst) and $2a$ (a nucleophilic catalyst). It should be emphasized that the significant, bifunctional catalysis of $2c$ is caused by fixation of the ammonium and hydroxyimino groups in a favorable orientation for simultaneous interaction with the bound substrate. A plausible structure of the $2c$-PNPL complex is illustrated in Fig. 9. It has been pointed out that the rates of some amide hydrolyses [28], lactonizations [29], and esterifications [29] which occur via intramolecular processes are surprisingly sensitive to the orientation of reacting groups.
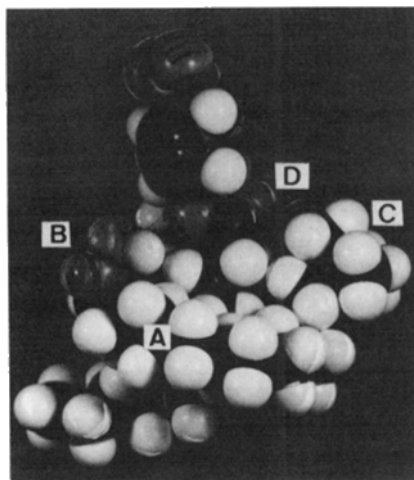
Fig. 9. CPK molecular model of the inclusion complex formed between cyclic oxime *2c* and PNPL: **A**, paracyclophane skeleton; **B**, hydroxyimino oxygen; **C**, ammonium group; **D**, carbonyl oxygen of PNPL (taken from Ref. [3])

Nucleophilic attack of the hydroxyimino group on the substrates results in a transition state in which the substrate-carbonyl develops a partial negative charge. This polar transition state would then require appreciable solvation by water molecules as characterized by a negative entropy change (Table 7). On the other hand, the developed negative charge in the transition state of the *2c*-PNPL system would be neutralized through a tight ion-pair association with the positively charged ammonium group (see *19*). This transition state thus requires less solvation by water molecules, relative to that for the *2a*-PNPP system as reflected in the activation entropy change (ΔS^+). The acyl transfer rate for the system of *1*-PNPP is much greater than that for *2a*-PNPP (Table 7). The higher catalytic effectiveness of *1* is apparently related to the entropy effect: $\Delta\Delta S^+ = \Delta S^+_{(1)} - \Delta S^+_{(2a)} = 8.3$ cal mol^{-1} K^{-1}. By extending the above argument for the characterization of the transition state of the *2c*-PNPL system, the hydroxy group of *1* would neutralize in part a negative charge on the carbonyl oxygen of the substrate in the transition state through hydrogen bonding interaction.

3.2 Nucleophilic—Hydrophobic Bifunctional Catalysis [30]

p-Nitrophenyl decanoate and hexadecanoate are deacylated in a neutral to acidic pH region by *2a* and *2b* in dioxane-water (1:9 v/v) or methanol-water (1:9 v/v). In the absence of *2a* or *2b*, the *p*-nitrophenyl carboxylates are inactive in such a pH region. A large excess of acetoxime fails to deacylate *p*-nitrophenyl acetate (PNPA) to any detectable extent under the same reaction conditions. The pH-rate profiles for the deacylation of PNPP in the presence of various [20]paracyclophanes are shown in Fig. 10. The hydroxyimino group of the paracyclophane macrocycles certainly provides an effective nucleophilic center in the deacylation in the light of the following results: replacement of the hydroxyimino group in *2b* by an oxo group, which affords *20b*, results in the complete disappearance of reactivity, and *2a* is acylated with PNPD at its hydroxyimino group as confirmed by product analysis.

The kinetically determined pK_a values for the hydroxyimino groups of $2a$–$2c$ are in a range of 11.2–11.7 [3]. Thus, the hydroxyimino group intramolecularly located on the macrocyclic skeleton exists in a completely protonated form in the neutral to acidic pH range. Although the nucleophilicity of anionic oxygen groups is generally large, protonation reduces their nucleophilic reactivity appreciably. The intrinsic nucleophilicity of an unionized hydroxyimino group is so weak that even a large excess of acetoxime does not undergo reaction with PNPA at a measurable rate. The reactivity of $2c$ toward PNPP is markedly reduced in the neutral to acidic region in a manner similar to that of normal oximes. On the other hand, the unfavorable electrostatic effect of the negatively charged carboxylate group of $2b$ reduces the nucleophilic reactivity of the anionic hydroxyimino group in the alkaline region. The pH-rate profile (Fig. 10) indicates that $2b$ is reactivated in a lower pH region where its carboxylate group is completely protonated. The kinetic pK_a value of 7.1 must be due to the dissociation of the carboxy proton. The large pK_a value of the carboxy group is presumably attributed to the hydrophobic field effect provided by the inclusion complex. Among paracyclophanoximes $2a$–$2c$, the catalytic activity toward carboxylic esters decreases in an alkaline region in the order: $2c \gg 2a > 2b$ [3]. However, $2a$ and $2b$ show comparable catalytic efficiency but $2c$ exhibits a markedly low reactivity in the neutral to acidic region.

The primary factor which differentiates the reaction behavior of $2a$ and $2b$ from that of normal oximes such as acetoxime is the hydrophobic field effect provided by the former species. The special feature of water molecules surrounding the hydrophobic paracyclophane skeleton seems to facilitate in an unusual way the nucleophilic attack of the neutral hydroxyimino group on the incorporated substrate. On the basis of the concept of hydrophobic interactions, water molecules in the neighborhood of a nonpolar species would be highly structured [8,31]. The flickering cluster model of liquid water is provided by extensive hydrogen bonding interactions, and water molecules become ordered around a nonpolar organic molecule with an increase in hydrogen bonding in this region. It has been postulated that the hydrogen
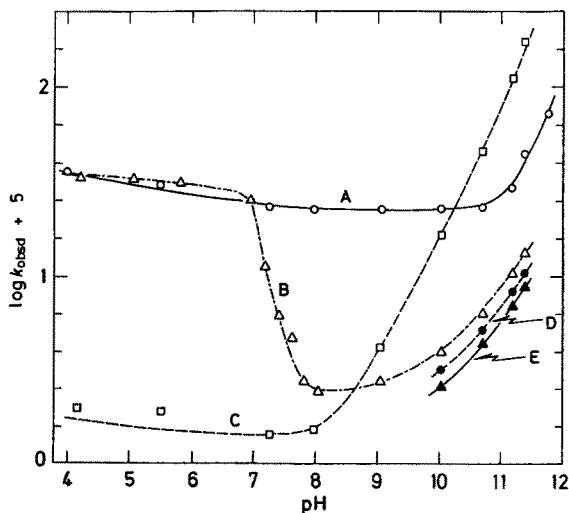

Fig. 10. Dependence of the rate of the deacylation of p-nitrophenyl hexadecanoate on pH in the presence and absence of various [20]paracyclophanes at 40 °C and $\mu = 0.20$ (KCl): A, $2a$ (8.34×10^{-6} mol dm^{-3}); B, $2b$ (8.79×10^{-6} mol dm^{-3}); C, $2c$ (8.52×10^{-6} mol dm^{-3}); D, no catalyst; E, $20b$ (1.26×10^{-5} mol × dm^{-3}); initial PNPP concentration, 1.00×10^{-5} mol dm^{-3}. Values of k_{obsd} are in s^{-1} (taken from Ref. [30])

bonding interaction enhances both acidity and basicity of water molecules [31]. This view was supported by *ab initio* MO-SCF calculations on linear water trimers [32]. Furthermore, the enhanced basicity of structured water molecules has been confirmed by an NMR study of the chloroform—water system [33] and by kinetic investigation of water-catalyzed detritiation of malononitriles [34]. On the basis of these views, the water molecules around the present hydrophobic inclusion complexes must be highly structured and act as favorable proton acceptors due to the enhanced basicity. The direct involvement of water molecules in the transition state of acyl transfer was confirmed by the appreciable solvent isotope effects. The k_{H_2O}/k_{D_2O} values observed for reactions of PNPP with *2a* and *2b* are in the range 4.5–5.0. These values are even larger than those reported for some water-catalyzed hydrolyses of reactive esters: acetic anhydride (2.9) [35], *p*-nitrophenyl dichloroacetate (3.15) [36], *p*-methoxyphenyl dichloroacetate (3.24) [36], and bis(*p*-nitrophenyl) carbonate (2.88) [37].

The acyl transfer reaction proceeds most plausibly by a three-step mechanism:

i) The preequilibrium complex formation takes place between an acyl substrate bearing a long alkyl chain and a paracyclophanoxime (*2a* or *2b*);

ii) the bound substrate is subjected to nucleophilic attack by the neutral hydroxyimino group of a paracyclophanoxime under the influence of the proximity effect, and consequently, an active tetrahedral intermediate (*21*) is formed;

iii) the hydroxyimino proton is abstracted by the structured water molecules around the inclusion complex which is the rate-determining step.

The much lower reactivity of *2c* relative to *2a* and *2b* must be due to the presence of the positively charged ammonium group in its benzene ring moiety. Since, due to the structure-breaking ability of this group, the hydrogen bonds of the water molecules surrounding the hydrophobic paracyclophane skeleton are disrupted, novel water catalysis may not be expected to occur in the acyl transfer reaction. Since the hydrophobic inclusion complex formed between an acyl substrate bearing a long alkyl chain and a paracyclophanoxime (*2a* or *2b*) would be surrounded by highly structured water molecules already in the ground state of the reaction, further development of water structure should not be required to any significant extent in the dipolar transition state of acyl transfer. In other words, the stabilization of the dipolar transition state is more readily achieved in a water cage with a more developed structure for which reorganization of the water molecules is least needed in the transition state. Consequently, the enhanced reactivity of the hydroxyimino groups of *2a* and *2b* seems to be partly due to an entropy effect.

3.3 Electrostatic—Hydrophobic Double-Field Catalysis [38]

The hydrolysis of PNPP is accelerated by *20c* relative to the spontaneous hydrolysis under the identical kinetic conditions: initial PNPP concentration of 1.0×10^{-5} mol dm^{-3}, μ 0.2 with NaCl, in methanol-dioxane-water (1:1:98 v/v), at 40.0 °C. The observed rates are 1.3×10^{-4} and 0.14×10^{-4} s^{-1} for catalyzed and spontaneous reactions at pH 9.7, respectively. The increase in rate is significant in the presence of a small amount of *20c* (0.88×10^{-5} mol dm^{-3}). The catalytic effect of *20c* must

be developed by the quaternary ammonium group since *20a*, which lacks a positive charge, shows no acceleration effect in the PNPP hydrolysis.

The presence of either ethanolamine or glycine in the *20c*-catalyzed deacylation of PNPP results in a further increase in rate. This increase is brought about by aminolysis of PNPP with the amines as confirmed by product analysis. At constant pH (9.70), the rate constant of *20c*-catalyzed deacylation (k_{obsd}) is correlated linearly with the amine concentration; $k_{obsd} = k_{OH} + k_{amine}$[Amine] where k_{OH} is the rate factor of hydrolysis as a function of pH and k_{amine} the rate constant for aminolysis with either glycine or ethanolamine. The k_{amine} value for glycine is 5 times as large as that for ethanolamine. A novel reaction must take place in the deacylation of PNPP effected by glycine due to the following facts.

i) The basicities of glycine and ethanolamine are comparable; the pK_a(amine) values determined potentiometrically under the kinetic conditions are 9.4 and 9.3 for glycine and ethanolamine, respectively. The rate—basicity correlation has been established for amine bases in the deacylation of *p*-nitrophenyl acetate [39]. In the light of such a correlation, the nucleophilic reactivity of glycine is greater only by 1.2 fold than that of ethanolamine in the deacylation of a *p*-nitrophenyl ester.

ii) A hydrophobic environment provided by the inclusion complex of *20c* and PNPP favors the attack of neutral ethanolamine rather than that of charged glycine unless some other effect comes into play. In fact, the deacylation of PNPP in the absence of *20c* is moderately accelerated by ethanolamine but hardly affected by glycine. Furthermore, the uncharged paracyclophane (*20a*) causes an increase in the rate of aminolysis of PNPP but not in the rate of hydrolysis, ethanolamine being more effective than glycine in such aminolysis.

iii) The steric interaction between an amine nucleophile and the inclusion complex formed between *20c* and PNPP may possibly be an important factor governing the reactivity. However, the bulkiness of ethanolamine is comparable to that of glycine. On the basis of these considerations, the enhanced reactivity of glycine may be attributed to the favorable electrostatic interaction between the negative carboxylate group of glycine and the positive ammonium group of *20c*.

Since the macrocyclic skeleton of *20c* incorporates the substrate (PNPP) through hydrophobic interactions, the hydrophobic field provided by the macrocyclic skeleton and the electrostatic field formed by the ammonium group act to bring PNPP and glycine, respectively, close to each other so that a pseudo-intramolecular reaction (proximity effect) becomes possible (*22*).

3.4 Metal-Coordinating—Nucleophilic Bifunctional Catalysis [40]

In the absence of Cu^{2+} ions, both *2d* and *20d* (5.0×10^{-6} mol dm^{-3}) effectively deacylate PNPP (initial concentration, 1.0×10^{-5} mol dm^{-3}); the imidazolyl group acts as a nucleophile and the reaction ceases after complete acylation of the group. The initial rate constants for the reactions with *2d* and *20d* are comparable with each other in ethanol-dioxane-water (10.9:1:88.1 v/v) at pH 8.12, μ 0.10 (KCl), and 40 °C: 337 s^{-1} mol^{-1} dm^3 for *2d* and 357 s^{-1} mol^{-1} dm^3 for *20d*. A small amount of $Cu(NO_3)_2$ drastically reduces the rate of the *20d*-catalyzed reaction (Fig. 11), suggesting that Cu^{2+} undergoes coordination with the imidazolyl group

and hence its nucleophilicity is masked nearly completely. The $2d$-catalyzed reaction shows a similar kinetic behavior upon addition of Cu^{2+} ions. The rate constant decreases as the Cu^{2+} concentration increases until it reaches ca. 1.0×10^{-5} mol dm^{-3}; a further increase has no effect on the rate. The rate constant of the $2d$-catalyzed reaction at the saturation level with respect to Cu^{2+} concentration is, however, significantly larger (ca. 15 fold) than that of the $20d$-catalyzed one. This result clearly suggests that the imidazolyl group of $2d$ is coordinated to Cu^{2+} and the nucleophilic attack of the hydroxyimino group on the ester carbonyl is responsible for the ready deacylation of PNPP; acylation of the hydroxyimino group was confirmed by product analysis. The reactivity of the hydroxyimino group in $2d$-Cu^{II} is surprisingly high for its unionized form and may be assisted by Cu^{2+}. To make this point clear, the pseudo-first-order rate constants of the deacylation of PNPP (1.0×10^{-6} mol dm^{-3}) were determined in the presence of various amounts of $2d$-Cu^{II} at pH 8.12 together with the corresponding rate constants in the presence of $2a$ at pH 11.6 (the hydroxyimino group is deprotonated at this pH). Both systems exhibit saturation-type kinetics which is consistent with a mechanism involving preequilibrium complexation followed by pseudo-intramolecular acyl transfer from the bound substrate to the unionized hydroxyimino group of $2d$-Cu^{II} or to the ionized hydroxyimino group of $2a$ (Scheme 4, where C refers to $2d$-Cu^{II} or $2a$): for the $2d$-Cu^{II} system: $K_b = 0.91 \times 10^5$ mol^{-1} dm^3 and $k = 8.7 \times 10^{-3}$ s^{-1}; for the $2a$ system: $K_b = 2.1 \times 10^5$ mol^{-1} dm^3 nad $k = 3.8 \times 10^{-3}$ s^{-1}. Both systems were studied under comparable conditions (see Fig. 11). The Cu^{2+}-assisted nucleophilic reaction of the unionized hydroxyimino group in $2d$-Cu^{II} with the bound PNPP proceeds at a rate comparable to or even larger than that for the ionized hydroxyimino group.

Scheme 4:

$$S + C \xrightleftharpoons{K_b} (SC) \xrightarrow{k} P'$$
$$\downarrow k_0$$
$$P$$
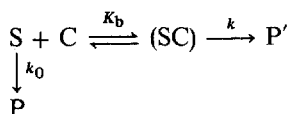
k_0: rate of spontaneous hydrolysis
P: hydrolysis products
P': acylated cyclophane and phenol

The following novel catalysis may be demonstrated using the $2d$-Cu^{II} complex.

i) The substrate ester is brought into the proximity of the catalytic center due to noncovalent hydrophobic interactions, Cu^{2+} playing no significant role in the substrate-binding process since $2d$-Cu^{II} and $2a$ have comparable binding constants.

ii) The reactivity of the poor nucleophile (unionized hydroxyimino group) is enhanced most plausibly by marked activation of the carbonyl group of the substrate through coordination with Cu^{2+} ion in the transition state as shown in 23.

3.5 Bifunctional Catalysis of Ester Hydrolysis with Turnover [41]

The catalytic behavior of a [10.10]paracyclophane, bearing two imidazolyl groups (24 in Fig. 12), in the presence of Cu^{2+} ions was investigated in ethanol-dioxane-water
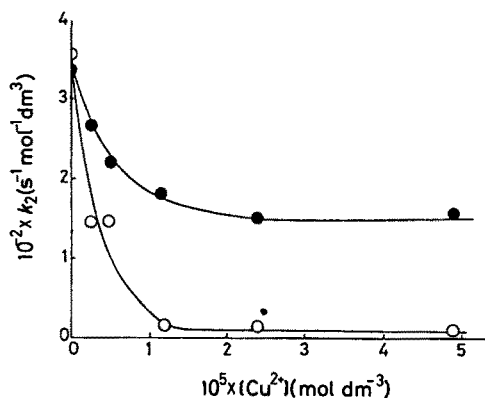
Fig. 11. Kinetic effect of Cu^{2+} ions in the deacylation of p-nitrophenyl hexadecanoate (1.0×10^{-5} mol dm^{-3}) catalyzed by *2d* (●, 5.0×10^{-6} mol dm^{-3}) and *20d* (○, 5.0×10^{-6} mol dm^{-3}) in ethanol-dioxane-water ($10.9:1:88.1$ v/v) at pH 8.12, μ 0.10 (KCl), and 40.0 °C: $k_2 = v_i/$ ([C] [PNPP]), where v_i is the observed initial rate and C either *2d* or *20d* (taken from Ref. [40])

($20.5:1:78.5$ v/v) at 40.0 °C, pH 8.12, and μ 0.10 (KCl); the initial substrate concentration was 1.0×10^{-6} mol dm^{-3} and the initial cyclophane concentration 1.0×10^{-6} mol dm^{-3}. The initial substrate and cyclophane concentrations and the composition of the reaction medium were chosen such that both substrate and cyclophane are in their monomeric states. A correlation between the rate constant of catalysis and the concentration of *24* indicates that no aggregation takes place in the concentration range investigated (Fig. 13). The apparent second-order rate constant for the reaction of *24* with PNPL at 1:1 stoichiometry sharply increases with increasing Cu^{2+} concentration until it reaches a maximum at a slight excess of Cu^{2+} over *24*. A further increase in the Cu^{2+} concentration shows practically no effect on the rate. This observation indicates that the copper complex of *24* (*24*-Cu^{II}) exhibits a higher reactivity than *24* and the complex persists even with a 46-fold excess of Cu^{2+} ions; the stability constant of the copper complex must be very high since this complex is almost completely formed at a 1:1 molar ratio of Cu^{2+} to *24*. Both systems shown in Fig. 13 exhibit a kinetic feature consistent with a mechanism which involves preequilibrium complexation of the cyclophane with the substrate (binding constant, K_b) followed by pseudo-intramolecular acyl transfer (rate constant, k): for *24*-Cu^{II}: $K_b = 0.6 \times 10^5$ mol^{-1} dm^3 and $k = 2 \times 10^{-2}$ s^{-1}; for *24*: $K_b = 3 \times 10^5$ mol^{-1} dm^3 and $k = 1.5 \times 10^{-3}$ s^{-1}. Consequently, the Cu^{2+} ion apparently plays a dual role: enhancement of intra-complex acyl transfer on the one hand and reduction in the substrate-binding ability on the other as compared with the metal-free catalyst.

The kinetic effect of Cu^{2+} ions on the catalysis of *24* was found to be different from that on the *20d*-catalyzed reaction in the presence of excess substrate. PNPP (1.0×10^{-5} mol dm^{-3}) was chosen as a substrate for experiments performed in ethanol-dioxane-water ($10.9:1:88.1$ v/v) so that the contribution of its spontaneous hydrolysis to the overall reaction is minimized. The reaction of *20d* with excess PNPP or PNPL in the absence of Cu^{2+} ions is stoichiometric rather than catalytic,
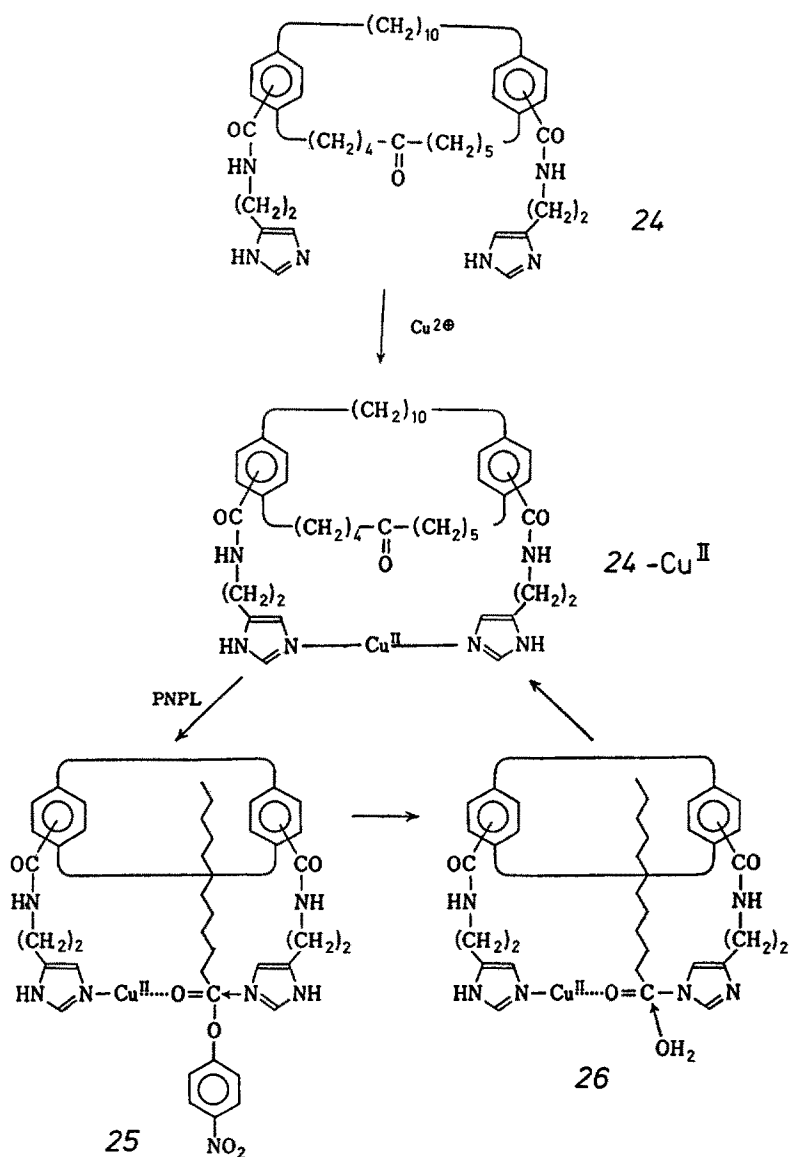
133

Fig. 12. Acylation-deacylation cycle for the hydrolysis of a *p*-nitrophenyl carboxylate of hydrophobic nature with *24*-Cu[II]

and the amount of released *p*-nitrophenol corresponds exactly to the initial amount of *20d*. Fig. 14 shows correlations between the amount of *p*-nitrophenol released from excess PNPP and the reaction time as catalyzed by *24* and *20d* in the presence of Cu²⁺ ions. Both reactions proceed beyond a stoichiometric range of conversion.

The kinetic behavior of the *24*-Cu[II] system differs from that of *20d*-Cu[II] in two aspects. First, the *24*-Cu[II] complex exhibits a reactivity which is significantly higher
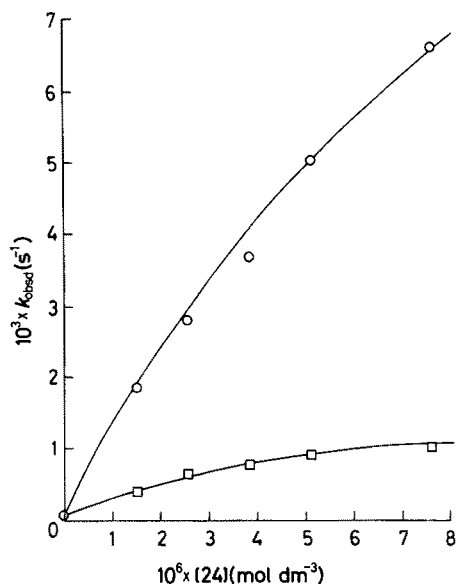
Fig. 13. Dependence of the pseudo-first-order rate constant (k_{obsd}) on the concentration of *24* for the release of *p*-nitrophenol from *p*-nitrophenyl dodecanoate (1.0×10^{-6} mol dm^{-3}) in ethanol-dioxane-water (20.5:1:78.5 v/v) at pH 8.12, μ 0.10 (KCl), and 40.0 °C in the presence (4.6×10^{-5} mol dm^{-3}) (○) and in the absence (□) of Cu(NO$_3$)$_2$ (taken from Ref. [41])

than that of the metal-free species. Secondly, the correlation between the amount of *p*-nitrophenol released from excess substrate and the reaction time for the *24*-Cu^{II}-catalyzed reaction is consistent with a double reaction step (biphasic kinetics) as shown in Fig. 14; the initial rapid (burst) reaction step is followed by the slower one. The extent of the initial burst reaction indicates that only one imidazolyl group is reactive at this stage. These observations are consistent with a two-step reaction involving rapid acylation of one of the imidazolyl groups with the ester substrate, corresponding to the initial burst stage (*25*), and deacylation of the resulting mono-
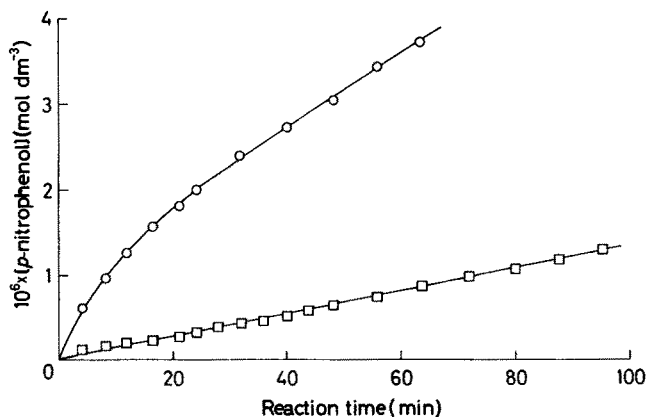
Fig. 14. Release of *p*-nitrophenol from *p*-nitrophenyl hexadecanoate (1.0×10^{-5} mol dm^{-3}) as a function of time, as catalyzed by *24* (1.2×10^{-6} mol dm^{-3}) (○) and *20d* (0.98×10^{-6} mol dm^{-3}) (□) in the presence of Cu(NO$_3$)$_2$ (4.9×10^{-5} mol dm^{-3}) in ethanol-dioxane-water (10.9:1:88.1 v/v) at pH 8.12, μ 0.10 (KCl), and 40.0 °C (taken from Ref. [41])

135

acylcyclophane intermediate (26) giving rise to regeneration of the original catalyst (Fig. 12). The acylation and deacylation processes are balanced to give a steady-state concentration of the catalyst (24-Cu^{II}) after the burst step. If all molecules of 24-Cu^{II} are occupied by the substrate through hydrophobic interactions in the presence of an excess amount of the latter, the initial rate (V_0) of the release of p-nitrophenol is given by Eq. (5), where 24-Cu^{II} is represented as PCP, PCP $\cdot$ S is its association complex with the substrate, P p-nitrophenol, and k_a the first-order rate constant for the acylation of one of the imidazolyl groups. The rate observed after the stationary state is attained is given by Eq. (6),

$$V_0 = dP/dt = k_a[PCP \cdot S]_0 = k_a[PCP]_0 \tag{5}$$

$$V_s = dP/dt = k_a[PCP \cdot S]_s = k_a[PCP]_s \tag{6}$$

where the suffix (s) denotes the stationary-state conditions. The stationary state expression with respect to the acylated species of 24-Cu^{II} (PCP $\cdot$ Ac) is given by Eq. (7), where [PCP]$_0$ is the total concentration of the cyclophane species and k_d the first-order rate constant of the deacylation of the acylcyclophane intermediate.

$$d[PCP \cdot Ac]/dt = k_a[PCP \cdot S]_s - k_d[PCP \cdot Ac]_s$$
$$= k_a[PCP]_s - k_d([PCP]_0 - [PCP]_s) \tag{7}$$

The biphasic kinetics, as represented by the correlation between the amount of released p-nitrophenol and the reaction time (Fig. 14), is analyzed on the basis of Eqs. (5)–(7): k_a (obtained from the initial burst step by Eq. (5)) is 2.1×10^{-3} s^{-1}; [PCP]$_s$ (obtained from the linear portion of the correlation by Eq. (6) which is referred to the second slow step) 3.4×10^{-7} mol dm^{-3}; k_d (obtained by Eq. (7)) 1.1×10^{-3} s^{-1}.

It must be pointed out here that the biphasic kinetic behavior is not sufficient evidence of the deacylation of the acylcyclophane intermediate. Another possibility is that the linear portion of the curve (Fig. 14) simply corresponds to the catalytic action of the copper site of the acylated species of 24-Cu^{II}, the mechanism involved being similar to that of the $20d$-Cu^{II} catalysis. In the latter catalysis, the nucleophilic reactivity of the imidazolyl group of $20d$ is masked through complex formation and the N^{Im}-bound Cu^{2+} ion in turn provides a catalytic site. A coordination interaction of the Cu^{2+} ion and the carbonyl group of the ester substrate may facilitate polarization of the latter in the transition state. Consequently, the attack of external nucleophiles (H$_2$O and OH$^-$) on the substrate is presumably considerably enhanced. To deal with this problem, it is necessary to advance an alternative kinetic criterion. The extent of deacylation of the acyl intermediate in a given period can be evaluated by kinetic titration of the regenerated catalyst using the same substrate. PNPL (1.0×10^{-6} mol dm^{-3}) was reacted with an equimolar amount of 24-Cu^{II} in ethanol-dioxane-water (20.5:1:78.5 v/v), the initial second-order rate constant being 1.3×10^3 s^{-1} mol^{-1} dm^3. The reaction (release of p-nitrophenol) was completed in 20 min. Then, the same amount of PNPL was added; p-nitrophenol was released at the same rate (1.2×10^3 s^{-1} mol^{-1} dm^3). This finding indicates that the acyl intermediate had been completely deacylated before the second addition of the substrate was

performed, the lower limit for the deacylation rate constant (k_d) being ca. 1×10^{-3} s^{-1} if 10 min (half the time required for completion of the first reaction) is taken as the upper limit of the half-life of deacylation. Although 24-Cu^{II} must be completely saturated with the substrate in the presence of an excess amount of the substrate (biphasic kinetic conditions shown in Fig. 14) and the deacylation of the acylcyclophane intermediate becomes the rate-determining step, only part of the cyclophane is occupied by the substrate under the conditions employed for the kinetic titration, and the whole reaction turns out to be controlled by the acylation step.

The rate constants of the hydrolysis of PNPL are summarized in Table 9. The striking differences in the catalytic action between 24 and $20d$ systems are as follows: (i) in contrast to the system of $20d$-Cu^{II} which lacks nucleophilic reactivity,

Table 9. Rate constants of the hydrolysis of p-nitrophenyl dodecanoate[a]

Catalyst species	Rate constant[b]	Medium[c]
$20d$	k_a, 1.8×10^2 s^{-1} mol^{-1} dm^3	A
	k_a, 8.8×10^2 s^{-1} mol^{-1} dm^3	B
	k_d, $\lesssim 1 \times 10^{-5}$ s^{-1}	B
$20d$-Cu^{II}	k_h, 1.8×10^2 s^{-1} mol^{-1} dm^3	A
	k_h, 2.4×10^2 s^{-1} mol^{-1} dm^3	B
	k_d, $\lesssim 1 \times 10^{-5}$ s^{-1}	B
24	k_a, 2.3×10^2 s^{-1} mol^{-1} dm^3	A
24-Cu^{II}	k_a, 1.3×10^3 s^{-1} mol^{-1} dm^3	A
	k_d, $\gtrsim 1 \times 10^{-3}$ s^{-1}	A

[a] At 40.0 °C, pH 8.12, and $\mu = 0.10$ (KCl).

[b] k_a: rate constant for the acylation of the imidazolyl group; k_d: rate constant for the deacylation of the acylated imidazolyl intermediate; k_h: rate constant for the direct hydrolysis of the substrate.

[c] A: ethanol-dioxane-water (20.5:1:78.5 v/v); B: ethanol-dioxane-water (10.9:1:88.1 v/v).
(Cited from Ref. [41])

one imidazolyl group of 24-Cu^{II} acts as a nucleophile (the latter catalyst is even more reactive than 24 itself by a factor of 5–6 without correction for a statistical factor); (ii) the monoacylated species of 24-Cu^{II} is readily deacylated at a rate which is at least by a factor of 10^2 higher than that of the deacylation of the acylated species of $20d$ observed both in the presence and in the absence of Cu^{2+} ions. Thus, the catalytic efficiency of 24-Cu^{II}, which can be assumed to be a good model for carboxypeptidase A, is without doubt ascribed to the cooperation of the imidazole function and the imidazole-bound copper ion.

3.6 General Acid Catalysis by an Ammonium Group [18]

As mentioned in Section 2.1.2, 3 deacylates carboxylic esters of hydrophobic nature in two different ways as shown in Scheme 2. In a higher pH region, the free amino group of 3 attacks by its nucleophilic reactivity on the carbonyl carbon of the substrates; pK_a values of the amino group of 3 being 8.1–8.3 when 3 forms complexes with PNPL and PNPP.

Paracyclophane *3* appreciably catalyzes the deacylation of PNPL and PNPP in a pH region where the amino group is protonated (abbreviated as *3*$^+$) and spontaneous hydrolysis of the substrates proceeds to a negligible extent. In the alkaline region where *3* with the free amino group is the dominant species, the rate plots deviate downwards from the linear first-order correlation lines, because the amino group of *3* is consumed progressively in the course of the reaction. On the other hand, the rate plots deviate upwards from the first-order correlation lines in the neutral pH region in a manner observed in the spontaneous hydrolysis of *p*-nitrophenyl carboxylates of hydrophobic nature (the initial concentration being 1.0×10^{-5} mol dm^{-3} or higher) over the whole pH range. In the case of hydrophobic substrates such as PNPL and PNPP, the substrates become progressively free from intermolecular aggregation as their deacylation or hydrolysis reactions proceed even in the absence of any host molecule. The above kinetic behavior observed in the neutral pH region suggests that the deaggregated substrate is more readily incorporated into the paracyclophane cavity. In addition, it is clear that the protonated amino group catalyzing deacylation is not consumed during the course of reaction in the neutral pH region. The protonated amino group must play a catalytic function by either of the following two mechanisms. The first involves electrostatic catalysis effected by the positively charged ammonium group which stabilizes the anionic tetrahedral intermediate formed by the attack of hydroxide ion and/or water molecule on the ester carbonyl. The deacylation of PNPL and PNPP in alkaline aqueous media is enhanced by *2c* due to the electrostatic effect of the positively charged ammonium group (see Sect. 3.1). In order to examine the possible electrostatic catalysis by the protonated amino group of *3*$^+$, the kinetic effect of *20c* in the hydrolysis of PNPL was investigated in ethanol-water (20.8:79.2 v/v) at pH 7.28, μ 0.10 (KCl), and 40.0 °C; initial concentration of PNPL being 1.0×10^{-5} mol dm^{-3}. The observed first-order rate constants (2.33×10^{-5} s^{-1} with 0.88×10^{-5} mol dm^{-3} of *20c*, and 2.92×10^{-5} s^{-1} with 1.53×10^{-5} mol dm^{-3} of *20c*) are much smaller than those observed in the presence of *3* (8.25×10^{-4} s^{-1} at pH 7.16 in the presence of *3* with its initial concentration of 1.0×10^{-5} mol dm^{-3}), even though the former rate constants are still larger than that of the spontaneous hydrolysis (ca. 1.3×10^{-5} s^{-1}) under the same conditions. Apparent first-order rate constants for the reactions of PNPL with *3*$^+$ and *3* are $(1.4 \pm 0.5) \times 10^{-4}$ s^{-1} and $(6.65 \pm 0.10) \times 10^{-3}$ s^{-1}, respectively, under the following experimental conditions: medium, ethanol-water (20.8:79.2 v/v) at 40.0 °C and μ 0.10 (KCl); initial concentrations of PNPL and *3*, 1.0×10^{-5} mol dm^{-3}; kinetic pK_a for the amino group of *3*, 8.07. Thus, the contribution of the electrostatic effect may be ruled out even if the structural difference between *3*$^+$ and *20c* has to be taken into consideration. In addition, the solvent deuterium isotope effect ($k_{H_2O}/k_{D_2O} = 0.67$) seems to support this view, since no isotope effect would be expected for the electrostatic catalysis which involves no proton transfer process. An alternative mechanism is the general acid catalysis in which the ammonium group of *3*$^+$ attacks the ester carbonyl as the general acid. Even though the solvent deuterium isotope effect is usually greater than unity for this mechanism, there are other examples in which the isotope effect is smaller than unity: the dehydration step of oxime formation, 0.30 [42]; the acid-catalyzed addition of thiol to aldehyde, 0.59 [43]. Although the kinetic efficiency of the general acid catalysis by the protonated amino group of *3*$^+$ is not so high as that of the nucleo-

philic deacylation by the free amino group of 3, a characteristic turnover behavior with respect to the catalyst species was observed by the former mechanism. A similar general acid catalysis has been postulated for the deacylation of PNPP by 27 [44]

3.7 Micellar Catalysis [24]

The kinetic effect of a [20]paracyclophane bearing an imidazolyl moiety ($20d$) on the deacylation of various p-nitrophenyl carboxylates was investigated in ethanol-dioxane-water (10.9:1:88.1 v/v) at μ 0.10 (KCl) and 40.0 °C. Since p-nitrophenyl carboxylates bearing a long alkyl chain tend to aggregate above the critical concentrations (e.g. 2.0×10^{-6} mol dm^{-3} for p-nitrophenyl decanoate in dioxane-water (1:99 v/v) at 40 °C) [17], the initial substrate concentrations were adjusted to 7.0×10^{-7} mol dm^{-3} for most kinetic runs. The p-nitrophenyl esters used are classified into four categories on the basis of the data on the acceleration of deacylation rates listed in Table 10:

i) those having a long alkyl chain ($28c$–e) undergoing a more than 240-fold acceleration;

ii) those having a cyclodecyl moiety or a cyclohexyl one with an additional methyl group or methyl groups ($28h$–j) undergoing a 20 to 170-fold acceleration;

iii) those with a less hydrophobic acyl moiety ($28b$, f, g, and l) undergoing a 4 to 8-fold acceleration;

iv) those with a much less hydrophobic acyl portion ($28a$ and k), for which an acceleration is barely detected.

Thus, the hydrophobic interaction of $20d$ with the acyl portion of each substrate seems to be responsible for the catalytic efficiency. This is evidenced by the effect of

Table 10. Pseudo-first-order rate constants for the deacylation of p-nitrophenyl carboxylates in the absence (k_{hyd}) and in the presence (k_{obsd}) of $20d$[a]

Substrate (28)	$k_{hyd} \times 10^5$ [s^{-1}]	$k_{obsd} \times 10^5$ [s^{-1}]	k_{obsd}/k_{hyd}
a	7.8	8.2	1.0
b	3.2	20	6.2
c	2.0	480	240
d	1.4	590	420
e	0.73	680	930
f	1.5	8.3	5.5
g	2.1	9.7	4.6
h	0.18[b]	3.7	20
i	2.0	69	35
j	1.0	170	170
k	17.3	24	1.4
l	1.0	7.9	7.9

[a] At 40.0 °C, pH 8.33, and μ 0.10 (KCl) in ethanol-dioxane-water (10.9:1:88.1 v/v); initial substrate concentration: 7.0×10^{-7} mol dm^{-3} unless stated otherwise; initial concentration of $20d$: 5.0×10^{-6} mol dm^{-3}.

[b] Initial concentration of $28h$: 1.0×10^{-5} mol dm^{-3}.

(Cited from Ref. [24])

ethanol content on the catalytic activity of *20d*. As the ethanol content is raised the hydrophobic interaction between *20d* and the substrate is progressively reduced; consequently, the catalytic efficiency is lowered as exemplified by the deacylation of *p*-nitrophenyl decanoate $(7.0 \times 10^{-7} \text{ mol dm}^{-3})$ with *20d* $(5.0 \times 10^{-6} \text{ mol dm}^{-3})$: the apparent second-order rate constants are 970 in 10% (v/v), 123 in 15% (v/v), 20 in 20% (v/v), and 11 $\text{s}^{-1} \text{ mol}^{-1} \text{ dm}^3$ in 30% (v/v) aqueous ethanol.

The kinetic pK_a value, evaluated from the pH—rate profile for the deacylation of *p*-nitrophenyl decanoate in the presence of *20d*, is 6.8; it is related to the acid dissociation of the imidazolyl group of the catalyst. The facile reaction of *20d* with a hydrophobic ester results in the accumulation of the N^{im}-acyl derivative of *20d* as the reaction proceeds. The rate of regeneration of *20d* (turnover) upon deacylation of such an acylated cyclophane is negligibly small under the kinetic conditions compared with the corresponding acylation rate. With excess substrate, the amount of *p*-nitrophenol liberated in the course of reaction reaches a maximum value which exactly corresponds to the amount of *20d* used.

The pseudo-first-order rate constants at pH 8.33 for the deacylation of active esters are plotted for selected cases in Figs. 15 and 16 as a function of the initial concentration of *20d*. In all cases, the overall feature is similar to those observed for micelle-catalyzed reactions [27]. The linear portion in each correlation below the breaking point corresponds to the reaction of the monomeric species of *20d* with the corresponding active ester, and a sharp increase above the breaking point may be due to aggregation or micelle formation of *20d*. In marked contrast to the kinetic behavior of other [20]paracyclophanes and [10.10]paracyclophane derivatives cited in this review, which is referred to as normal saturation-type kinetics without any breaking point under comparable conditions, the kinetic feature displayed by *20d* is rather surprising.
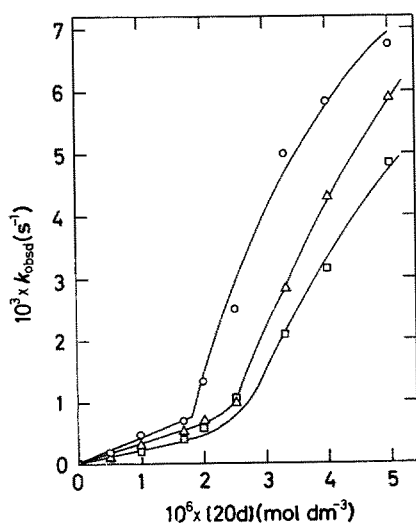
Fig. 15. Dependence of k_{obsd} on the initial concentration of *20d* for the deacylation of *28c* (□), *28d* (△), and *28e* (○) at pH 8.33, μ 0.10 (KCl), and 40.0 °C in ethanol-dioxane-water (10.9:1:88.1 v/v); initial substrate concentration, $7.0 \times 10^{-7} \text{ mol dm}^{-3}$ (taken from Ref. [24])
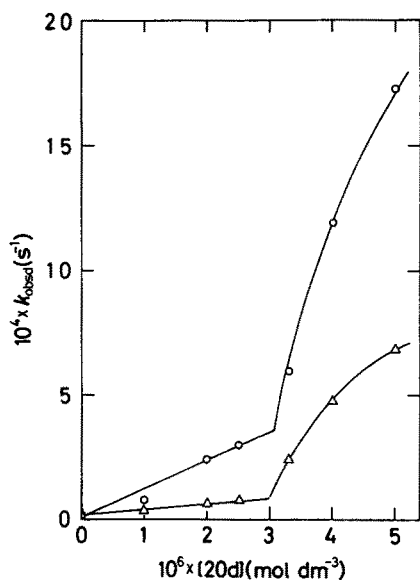
Fig. 16. Dependence of k_{obsd} on the initial concentration of *20d* for the deacylation of *28i* ($\triangle$) and *28j* ($\bigcirc$) at pH 8.33, μ 0.10 (KCl), and 40.0 °C in ethanol-dioxane-water (10.9:1:88.1 v/v); initial substrate concentration, 7.0×10^{-7} mol dm^{-3} (taken from Ref. [24])

The overall feature of deacylation reactions of *p*-nitrophenyl carboxylates in the presence of *20d* is consistent with the reaction pathway shown in Scheme 5. The

Scheme 5:

$$\text{S + micelle} \underset{}{\overset{K_b}{\rightleftharpoons}} \text{S-micelle complex}$$

$$\text{S + monomer} \qquad \downarrow k_m$$

$$\underbrace{\qquad\qquad\qquad}\qquad \text{products}$$

$$\downarrow k_{hyd} + k_2[PCP]_{CMC}$$

products
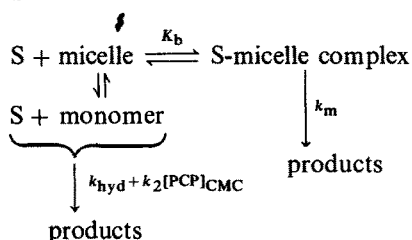
PCP: paracyclophane (*20d*)

kinetic parameters are determined on the basis of Eq. (8), where k_{hyd} is the rate constant for spontaneous hydrolysis, k_2 the second-order rate constant for the reaction of an ester with the monomeric form of *20d*, k_m the first-order rate

$$\frac{1}{k_{obsd} - (k_{hyd} + k_2[20d]_{CMC})} = \frac{1}{k_m - (k_{hyd} + k_2[20d]_{CMC})}$$

$$\times \left\{ 1 + \frac{N}{K_b([20d] - [20d]_{CMC})} \right\} \qquad (8)$$

141

constant for the reaction of an ester in the micellar phase, k_{obsd} the observed pseudo-first-order rate constant, K_b the association constant for the formation of the ester—micelle complex, N the aggregation number of the micelle; the suffix CMC indicates the critical micelle concentration of $20d$ which depends on the nature of a particular substrate used. For systems which do not allow k_m and K_b/N to be evaluated due to kinetic reasons, the apparent second-order rate constants defined by $k_2(app) = (k_{obsd} - k_{hyd})/[20d]$ are given for the purpose of comparison. All the kinetic parameters are summarized in Table 11 along with the second-order rate constants for reactions of the esters with imidazole (k_{Im}).

All the esters except p-nitrophenyl acetate are subjected to intensive catalysis by $20d$. The second-order rate constants (k_2) of the reactions of the monomeric species of $20d$ with relatively hydrophobic esters are considerably larger than the corresponding second-order rate constants for the imidazole-catalyzed reactions. This suggests the significant hydrophobic interaction between $20d$ and each hydrophobic ester; k_2/k_{Im} may be used as a measure of the extent of hydrophobic interaction. Care should be taken of long-chain esters. Hydrophobic coiling of the alkyl chain, which results in protection of the ester carbonyl against the attack of the nucleophile, seems to be responsible for the decrease in k_{Im} in going from p-nitrophenyl decanoate to hexadecanoate. If intramolecular coiling were retained in the transition state of acyl transfer from the ester to $20d$, the ratio k_2/k_{Im} would allow a comparison of the relative catalytic efficiencies. However, the esters most plausibly undergo decoiling or elongation before the transition state is reached. The k_{Im} value for p-nitrophenyl acetate, which is not influenced by the coiling effect, may be used as the plausible reference for the evaluation of the catalytic efficiency of the monomeric $20d$ (Table 11). As expected from the hydrophobic affinity, k_2/k_{Im} increases with increasing length of the alkyl chain of the ester ($28b < c < d < e$). This value also increases in the order $28h < i < j$. Thus, the hydrophobic interaction between the monomeric species of $20d$ and an ester having an aliphatic ring moiety in its acyl portion may be primarily governed by the surface area [45] or more directly by the number of carbon atoms in the acyl moiety of the ester concerned.

The binding constants for micellar complex formation of $20d$ with $28c–e$, i, and j are greater than 10^5 mol^{-1} dm^3. The decrease in K_b/N in going from $28i$ to j may be surprising since $28j$ is expected to be more hydrophobic than $28i$ as judged from the k_2/k_{Im} ratios for the two esters. This may be an example of the substrate selectivity for the binding process. However, we are not certain whether or not the micelle of $20d$ has the same aggregation number (N) for different substrates. It may be assumed that N is relatively small for hydrophobic macrocycles in a similar manner as observed for cholic acid derivatives ($N = 5$–22) [46]. Under such circumstances, the aggregation number as well as CMC may significantly depend on the nature of a particular substrate employed.

The product of the rate constant of the micellar reaction and the corresponding binding constant ($k_m K_b$) is referred to as the second-order rate constant of the reaction of a substrate and a micelle; consequently, $k_m K_b/N$ corresponds to the second-order rate constant for the same reaction as evaluated per mole of $20d$ forming micelles. There is indeed a wide range of variation in $k_m K_b/N$ as can be seen from Table 11, and the long-chain carboxylates ($28c–e$) show the highest values in the range 2000–3000 s^{-1} mol^{-1} dm^3. These values are the largest ever obtained

Table 11. Kinetic parameters for the deacylation of p-nitrophenyl carboxylates catalyzed by $20d$ and imidazole[a]

Substrate (28)	k_2 [s^{-1} mol^{-1} dm^3]	k_{Im} [s^{-1} mol^{-1} dm^3]	k_2/k_{Im} [b]	CMC[c] [mol dm^{-3}]	k_m [s^{-1}]	K_b/N [mol^{-1} dm^3]	$k_m K_b/N$ [s^{-1} mol^{-1} dm^3]	k_a(app)[d] [s^{-1} mol^{-1} dm^3]
a		0.79						0.8
b	10	0.57	18 (13)	3.1×10^{-6}			70	33
c	210	0.44	480 (270)	2.4×10^{-6}	ca. 0.02	1×10^5	2000	970
d	310	0.21	1500 (390)	2.3×10^{-6}	ca. 0.02	1.3×10^5	2600	1200
e	420	0.004	11000 (530)	1.8×10^{-6}	ca. 0.02	1.5×10^5	3000	1400
f		0.44						14
g		0.13						15
h	2.3	0.014	160	3.3×10^{-6}			30	7.0
i	22	0.093	240	3.0×10^{-6}	0.001	5×10^5	500	130
j	110	0.075	1500	3.0×10^{-6}	0.005	2×10^5	1000	340
k		1.6						14
l	7.5	0.033	230	3.3×10^{-6}			40	14

[a] At 40.0 °C, pH 8.33, and μ 0.10 (KCl) in ethanol-dioxane-water (10.9:1:88.1 v/v); initial substrate concentration: 7.0×10^{-7} mol dm^{-3}.
[b] Values in parentheses: k_{Im} for acetate (28a) was taken as the reference value.
[c] Critical micelle concentration of $20d$.
[d] k_2(app) = (k_{obsd} − k_{hyd})/[$20d$], [$20d$] = 5.0×10^{-6} mol dm^{-3}.
(Cited from Ref. [24])

143

for reactions of synthetic 4-substituted imidazoles with *p*-nitrophenyl esters [47–50]. They are comparable to or greater than the second-order rate constant of the acylation of chymotrypsin with *p*-nitrophenyl acetate (410 s^{-1} mol^{-1} dm^3 at 25 °C and pH 7.75) [51]

3.8 Induced-Fit Catalysis [22]

As mentioned in Section 2.3, azaparacyclophanes bearing long alkyl branches (octopus cyclophanes) incorporate hydrophobic substrates of various bulkiness by an induced-fit mechanism. Azaparacyclophane *11* catalyzes the hydrolysis of PNPL to a detectable extent only in a pH range greater than 8 in ethanol-methanol-dioxane-water (5:1:1:95 v/v) at μ 0.10 (KCl) and 30.0 °C; the initial concentrations of *11* and PNPL are 5.55×10^{-5} and 4.90×10^{-6} mol dm^{-3}, respectively. However, since the hydrolysis of PNPL proceeds too fast above pH 9.5, reliable determination of the rate constants by the usual methods is not possible. In the pH region 8–9.5, a breaking point in the correlation between log k_{obsd} and pH appears at pH 9.2. A potentiometric titration of *11* indicated the presence of two functional groups with the pK_a values of 3.6 and 9.1 in the pH range 1.5–11.5. The pK_a value of 9.2 obtained from the kinetic correlation may be due to acid dissociation of the tertiary amino group of *11*. More convincing evidence of the presence of such a kinetic breaking point has been provided by fluorescence spectroscopy (see Sect. 2.3). This is further confirmed by the pH-rate profile for the hydrolysis of PNPD in the presence of *10*; no breaking point is detected in the pH range 8.3–10.5 [in ethanol-methanol-dioxane-water (5:1:1:95 v/v) at μ 0.10 (KCl) and 30.0 °C; the initial concentrations of *10* and PNPD are 2.66×10^{-4} and 4.83×10^{-6} mol dm^{-3}, respectively], and the potentiometric titration of *10* shows only one pK_a value (3.5) for the imidazolyl group. The (first) pK_a value of the imidazolyl group of *10* is comparable to that of dimethyl(imidazolylmethyl)hexadecylammonium chloride in its micellar state [52]. This indicates that the microenvironment of the reaction site (i.e. location of the imidazolyl groups) provided by the octopus cyclophanes is quite similar to that provided by functionalized micelles.

The slopes of the log k_{obsd}-pH correlation for the *11*-PNPL system are 3.6 and 1.8 below and above pH 9.2, respectively. On the other hand, only a single slope is obtained for the corresponding correlation of the *10*-PNPD system, namely 1.2 over the whole pH region used for the kinetic runs (8.3–10.5). Over such a pH region, the reactive functional group is the anionic imidazolyl group as inferred from the following experimental findings.

i) The catalytic activities of *10* and *11* increase considerably above pH 8.5.

ii) Azaparacyclophane *8* does not catalyze the hydrolysis of *p*-nitrophenyl carboxylates under comparable kinetic conditions owing to the lack of an imidazolyl group.

iii) The microenvironment of the reaction site provided by the octopus cyclophanes is similar to that provided by functionalized micelles as mentioned above. In a microenvironment such as that provided by cationic micelles, the reactivity of an anionic imidazolyl group is considerably higher than that of a neutral one, namely by a factor of 10^6–10^7 [53,54]. The second pK_a of the imidazolyl group

is presumably not determined by the usual kinetic method owing to the extremely rapid reaction in such a high pH region. The second pK_a values of the imidazolyl groups of 10 and 11 are between 11.5 and 13.0, as judged from the reported values for cationic micelles and a macrocyclic compound [52, 55, 56] [triethyl(imidazolylmethyl)ammonium chloride: $pK_{a1} = 4.3 \pm 0.1$; $pK_{a2} = 11.2 \pm 0.3$. S,S'-bis(cycloglycyl-L-hemicystylglycyl-L-histidyl-6-aminohexanoyl-ω-aminoundecanoyl): $pK_{a2} = 12.3$].

iv) The pH-rate correlations for the azaparacyclophane-catalyzed hydrolysis of p-nitrophenyl esters seems to be related to the pH dependence of the substrate-binding ability of the cyclophanes; i.e. the apparent rate acceleration with increasing pH may be attributed to the enhancement in the binding ability of 11 (slope of 3.6 of the linear relation obtained from a plot of $\log k_{obsd}$ vs. pH below pH 9.2) caused by an increase in the proportion of unprotonated tertiary amino groups along with conformational changes as illustrated in Fig. 8. To prove this, the constants for binding interaction of 11 with PNPL were evaluated by kinetic methods on the basis of the Michaelis-Menten treatment (Scheme 6):

Scheme 6:

$$E + S \underset{}{\overset{K_b}{\rightleftharpoons}} (ES) \overset{k_m}{\longrightarrow} \text{products}$$
$$\downarrow k_{hyd}$$
$$\text{products}$$
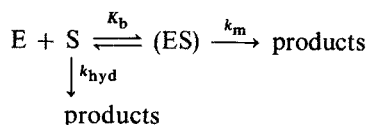
E: catalyst
S: substrate
(ES): inclusion complex

$K_b = 470 \pm 40$ mol^{-1} dm^3, $k_m = (3.9 \pm 2.2) \times 10^{-2}$ s^{-1} at pH 8.34; $K_b = 1710 \pm 380$ mol^{-1} dm^3, $k_m = (3.7 \pm 0.8) \times 10^{-2}$ s^{-1} at pH 8.50. The kinetic parameters (K_b and k_m) were not reasonably evaluated below and above these pH's due to the limitation of the kinetic conditions. The difficulty in determining the binding constants is apparently due to the large pH-dependence of the catalytic activity. Complete dissociation of the protons from the tertiary amino groups of 11 may cause loss of two positive charges; consequently, the electrostatic repulsion between the long alkyl chains of 11 may be weakened.

The sole reaction mechanism for the hydrolysis of PNPL catalyzed by 11 must therefore involve initial attack of the anionic imidazolyl group on the ester carbonyl. The unprotonated tertiary amino group may assist the removal of the imidazolyl NH-proton and enhance the binding of the substrate during the acylation process. The acylated imidazolyl moiety is not accumulated since the acylimidazolyl residue (λ_{max} 245 nm) is not detected spectrophotometrically in any of the kinetic experiments, but subsequently cleaved to afford a carboxylic acid and the regenerated catalyst. Such regeneration of the catalyst (turnover behavior) is confirmed by the kinetic experiment in the presence of an excess amount of the substrate. In fact, p-nitrophenol is released continuously from excess PNPL beyond the equimolar conversion range with respect to the active imidazolyl group. It should be noted that the induced-fit catalysis by octopus cyclophanes also gives rise to substrate selectivity as described in Section 2.3 (Fig. 6).

145

4 Rate Acceleration through Intramolecular Interaction in Nonaqueous Media

4.1 Structural Properties of Bis(1,4-dihydronicotinamide)s [57)]

Recently, the redox reactivity of various 1,4-dihydronicotinamides has been investigated extensively in connection with the chemistry of coenzyme NAD(P). Coenzyme NAD(P)H reduces various substrates while it is converted to the corresponding dehydrogenated species, $NAD(P)^+$ (Scheme 7). In order to manipulate the reactivity of 1,4-dihydronicotinamide by giving the molecule a multi-center character, which can be achieved by an intramolecular assembly of several dihydronicotinamide moieties, we prepared a series of closely related bis(1,4-dihydronicotinamide)s and investigated their reactivities in the reduction of a carbonyl substrate.

Scheme 7:
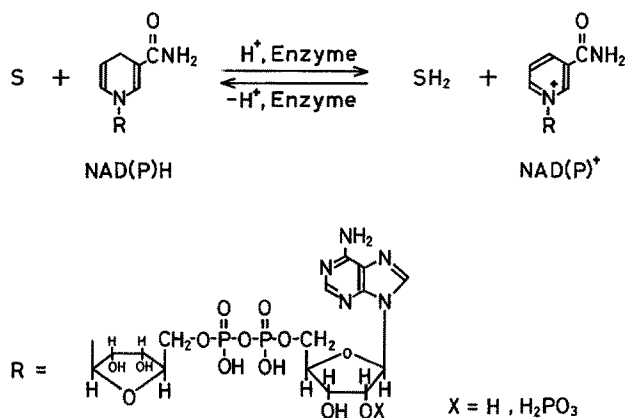
The ^{1}H-NMR chemical shifts of the dihydronicotinamide ring protons are sensitive to conformational changes of the rings (Table 12). The space-filling CPK molecular models for cBisNAH(C_4, o-Xyl) and its dehydrogenated species indicate that the two rings assume a close face-to-face conformation (Fig. 17a) with a perpendicular orientation of the benzene ring relative to the nicotinamide moieties so that the 2-H protons of the nicotinamide groups are placed right on the benzene ring (Fig. 17b), i.e. into the shielding zone. In agreement with this view, the resonance signals of the 2-H protons of cBisNAH(C_4,o-Xyl) and its dehydrogenated species [cBisNA$^+$(C_4,o-Xyl)] are shifted upfield by 0.3 and 0.5 ppm relative to those of (N-Et)BNAH and (N-Et)BNA$^+$, respectively. The ring current effects, which are specifically acting on the 2-H protons in the conformationally fixed state, are better understood when one compares the NMR spectrum of cBisNAH(C_4,o-Xyl) with that of its open-chain analog [BisNAH(Et,o-Xyl)], a large difference in the chemical

shift being observed only for the 2-H protons. BisNAH(Et,o-Xyl) exhibits a normal resonance of its 2-H protons. The CPK molecular models of the *p*-xylylene-bridged cyclic derivatives, cBisNAH(C_n,p-Xyl), and their dehydrogenated species [cBisNA$^+$-(C_n,p-Xyl)] indicate that the two nicotinamide planes are tilted relative to each other (Fig. 18). In the tilted orientation, the nicotinamide 2-H protons are placed inside the benzene ring while the 6-H protons are displaced outside this ring. This geometry is reflected in the NMR spectra of cBisNAH(C_n,p-Xyl) and cBisNA$^+$(C_n,p-Xyl) in which ring-current effects provided by the benzene ring are reasonably site-sensitive and also manipulated by the chain length (n); thus, upfield shifts of 2-H protons and downfield shifts of 6-H protons relative to the chemical shifts of those protons of (N-Et)BNAH and (N-Et)BNA$^+$ are observed. On the other hand, flexible noncyclic bis(1,4-dihydronicotinamide)s, BisNAH(C_n,Bzl), BisNAH(Et,p-Xyl), and BisNAH-(Et,m-Xyl), and their dehydrogenated counterparts show normal NMR spectra due to their extended structures, the chemical shifts of the respective protons being almost identical with those of the corresponding protons of (N-Et)BNAH and (N-Et)BNA$^+$.

1,4-Dihydronicotinamides generally show a characteristic absorption at around 350 nm. The absorption maxima for the bisdihydronicotinamides are listed in Table 12. Most of the bisdihydronicotinamides exhibit their absorption maxima in the same region as that observed for (N-Et)BNAH, with the exception of cBisNAH-(C_4,o-Xyl). The apparent blue shift observed for cBisNAH(C_4,o-Xyl) is an evidence of the electronic interaction occurring between two dihydronicotinamide moieties which are in enforced proximity.

(N-Et)BNAH

BisNAH(C_n,Bzl)
n = 4,6,8,10

BisNAH(Et,x-Xyl)
x = o,m,p

cBisNAH(C_n,p-Xyl)
n = 4,6

cBisNAH(C_4,o-Xyl)
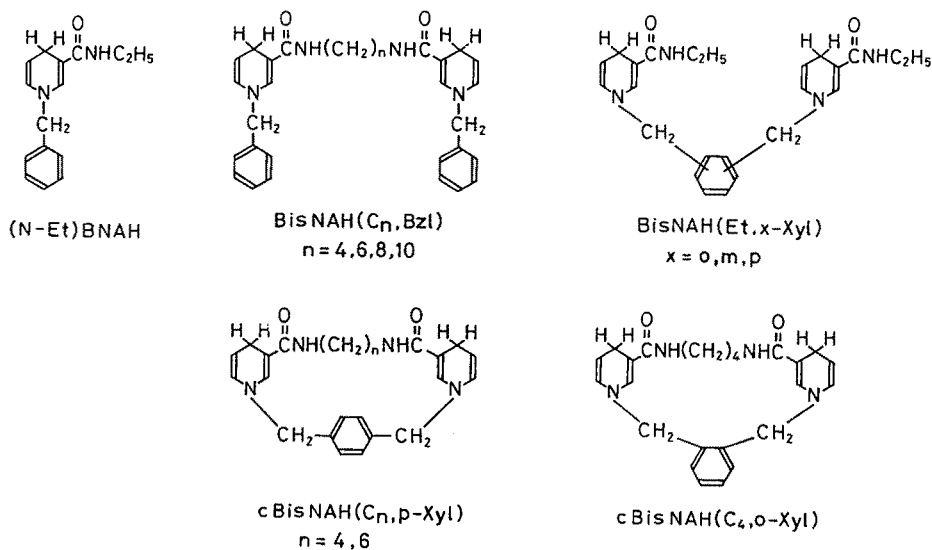
Chart. 1. Structural formulae of dihydronicotinamides

Table 12. Electronic absorption maxima[a] and ^{1}H-NMR chemical shifts[b] of dihydronicotinamides

Dihydro-nicotinamide	λ_max [nm]	[1]H Chemical shifts, δ									
		2-H[c]	4-H[c]	5-H[c]	6-H[c]	phenyl protons	CONH	NCH_2	CONHCH_2	CH_2[d]	CH_3
BisNAH(C_4, Bzl)	350	7.03	3.10	4.63	5.65	7.19	5.65	4.20	3.28	1.55	
BisNAH(C_6, Bzl)	350	7.06	3.12	4.66	5.70	7.21	5.40	4.22	3.24	1.37	
BisNAH(C_8, Bzl)	350	7.03	3.10	4.65	5.68	7.19	5.40	4.20	3.22	1.30	
BisNAH(C_10, Bzl)	350	7.04	3.10	4.65	5.68	7.19	5.30	4.22	3.22	1.29	
BisNAH(Et, p-Xyl)	348	7.00	3.08	4.63	5.65	7.11	5.40	4.19	3.22		1.11
BisNAH(Et, m-Xyl)	348	7.08	3.13	4.70	5.72	7.20	5.16	4.25	3.34		1.14
BisNAH(Et, o-Xyl)	348	7.11	3.20	4.79	5.73	7.35	5.42	4.32	3.43		1.17
cBisNAH(C_4, p-Xyl)	345	6.38	3.08	4.70	5.93	7.24	5.20	4.20	3.25	1.35	
cBisNAH(C_6, p-Xyl)	348	6.70	3.11	4.71	5.92	7.20	5.35	4.16	3.18	1.30	
cBisNAH(C_4, o-Xyl)	343	6.72	3.13	4.73	5.75	7.20	6.20	4.27	3.30	1.55	
(N-Et)BNAH	348	7.02	3.10	4.62	5.65	7.17	5.65	4.18	3.30		1.10

[a] Measured in CH_2Cl_2.
[b] Measured in CDCl_3. Chemical shifts are given in ppm downfield from Me_4Si. Multiplicities: 2-H, s; 4-H, m; 5-H, m; 6-H, d; phenyl protons, s [m for BisNAH(Et, m-Xyl)]; CONH, broad; NCH_2, s; CONHCH_2, q; other methylene protons, m; CH_3, t.
[c] Pyridine-ring protons.
[d] Other methylene protons.
(Cited from Ref. [57])
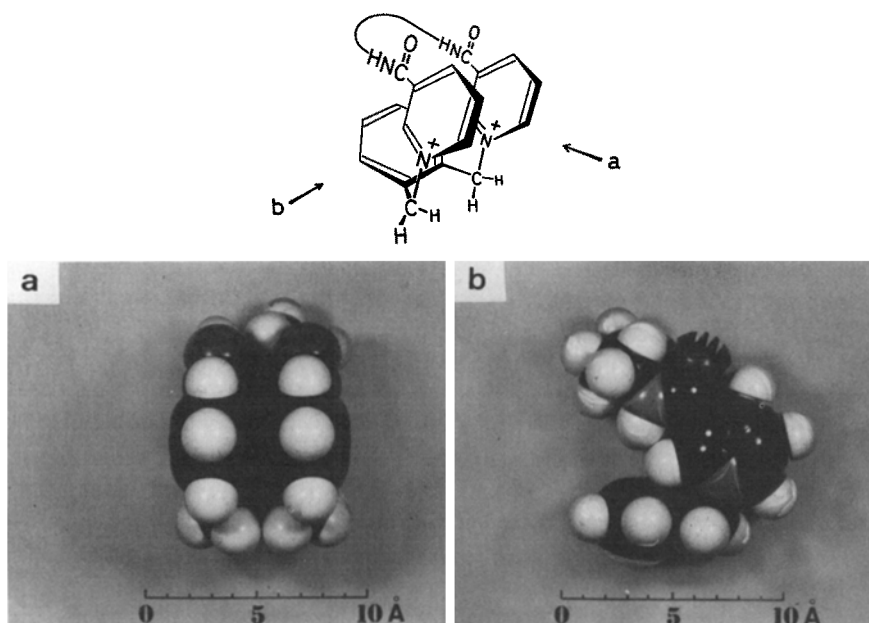
Fig. 17a and b. CPK molecular model of cBisNA$^+$(C$_4$, o-Xyl): **a**, view from a direction parallel to the nicotinamide rings; **b**, view from a direction perpendicular to the nicotinamide rings (taken from Ref. [57])
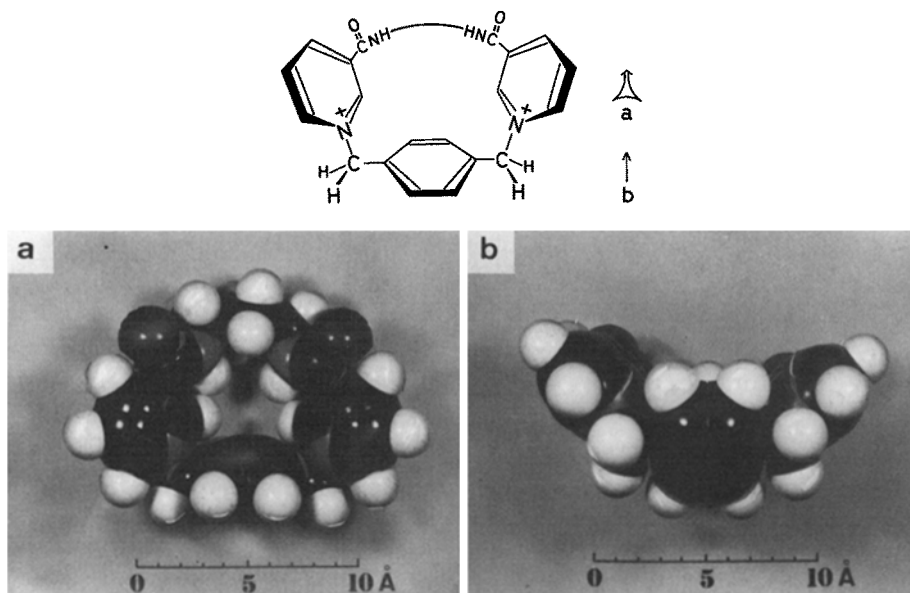
Fig. 18a and b. CPK molecular model of cBisNA$^+$(C$_4$, p-Xyl): **a**, top view of the macrocyclic ring; **b**, side view of the macrocyclic ring (taken from Ref. [57])

4.2 Reactivities of Bis(1,4-dihydronicotinamide)s: Geometrical Requirements for Electronic Interactions [57]

Hexachloroacetone is reduced with bisdihydronicotinamides in both acetonitrile and dichloromethane to give the corresponding bisnicotinamides and 1,1,1,3,3,3-hexachloro-2-propanol as confirmed by product analysis. The reactivities of bis-(1,4-dihydronicotinamide)s are summarized in Table 13. The reactivity is given in terms of pseudo-first-order rate constant evaluated from the rate of disappearance of the bis(1,4-dihydronicotinamide) at the initial stage of the reaction in the presence of excess substrate under aerobic conditions. Whenever the bis(1,4-dihydronicotinamide)s shown here exhibit a reactivity which is significantly higher than that of (N-Et)BNAH in dichloromethane under aerobic conditions, the reaction pathway is consistent with the one shown in Fig. 19, regardless of cyclic or noncyclic structures. The initial reaction (rate constant k_1) involves reduction of the substrate without participation of molecular oxygen, and the resulting intermediate (NAH-NA$^+$) readily undergoes oxidation with molecular oxygen (rate constant k_2). The last (k_2) step seems to be reasonable since the protonated pyridyl radical (NAH$\cdot^+$), produced electrochemically by one-electron oxidation of dihydronicotinamides, readily undergoes oxidation with molecular oxygen to afford NA$^+$ species [58]. The significant acceleration of the k_1 process, the facile oxidation of NAH-NA$^+$, and also the specific solvent effect thereupon (see below) can be well understood by postulating an intramolecular electronic interaction of charge-transfer character occurring in NAH-NA$^+$ and in the transition state of its formation. The rate constant

Table 13. Reactivities[a] of dihydronicotinamides in the reduction of hexachloroacetone[b] at 25.0 °C

Dihydronicotinamide	$k \times 10^3$ [s^{-1}]		k_{rel}[c]
	in CH$_3$CN	in CH$_2$Cl$_2$	
BisNAH(C$_4$, Bzl)	5.7	11	17
BisNAH(C$_6$, Bzl)	5.9	11	17
BisNAH(C$_8$, Bzl)	6.2	4.8	7.3
BisNAH(C$_{10}$, Bzl)		3.1	4.7
BisNAH(Et, p-Xyl)	5.9	0.69	1.0
BisNAH(Et, m-Xyl)		4.6	7.0
BisNAH(Et, o-Xyl)		8.6	13
cBisNAH(C$_4$, p-Xyl)	6.1	4.9	7.4
cBisNAH(C$_6$, p-Xyl)		3.3	5.0
cBisNAH(C$_4$, o-Xyl)	5.9	15	23
(N-Et)BNAH	5.7	0.66	1.0

[a] Given in pseudo-first-order rate constants at the initial stage of reaction as evaluated from absorbance change at 350 nm due to disappearance of the dihydronicotinamide.

[b] Concentrations: NAH unit: 1.0×10^{-4} mol dm^{-3}; (Cl$_3$C)$_2$CO: 1.0×10^{-2} mol dm^{-3}.

[c] Relative rate with respect to a selected reference, (N-Et)BNAH, in CH$_2$Cl$_2$. (Cited from Ref. [57])

k given in Table 13 refers to the k_1 step in Fig. 19, since $k_2 \gg k_1$ was confirmed for experiments performed in dichloromethane under aerobic conditions.

The reactivities of some reductants [BisNAH(C_n,Bzl) with n = 4, 6, and 8; BisNAH(Et,p-Xyl), cBisNAH(C_4,p-Xyl), and cBisNAH(C_4,o-Xyl)] are in a range of $(5.7\text{–}6.2) \times 10^{-3}\ \text{s}^{-1}$ in acetonitrile and comparable to that of (N-Et)BNAH. This implies that the intramolecular electronic interaction between the two nicotinamide moieties cannot be kinetically effective in such a polar solvent (solvent polarity parameter $E_T(30)$, 46.0) [59] which stabilizes a state with an isolated charge more strongly than one with a delocalized charge (Fig. 19). On the other hand, a wide range of reactivities is observed in dichloromethane ($E_T(30)$, 41.1) [59]. Among the bisdihydronicotinamides regarded as dimers of (N-Et)BNAH, cBisNAH(C_4,-o-Xyl) is the most reactive one. This is consistent with the assumption that a close face-to-face arrangement of the two nicotinamide rings is the primary requirement for an electronic interaction of kinetic significance (Fig. 17). The p-xylylene-bridged cyclic species, cBisNAH(C_n,p-Xyl) with n = 4 and 6, are 3.1 and 4.6 times less reactive than cBisNAH(C_4,o-Xyl), respectively. This unfavorable reactivity is attributed to some deviation of geometry from an ideal, close face-to-face arrangement of two dihydronicotinamide moieties; an intramolecular distance between the two nicotinamide planes is somewhat increased and these planes are tilted relative to each other (Fig. 18).

As regards noncyclic bisdihydronicotinamides, a variation of the reactivity associated with o-, m-, and p-xylylene linkage isomers [BisNAH(Et,x-Xyl), x = o, m, and p, respectively] clearly indicates that the intramolecular separation and relative orientation of two nicotinamide moieties are the factors governing an effective electronic interaction. BisNAH(Et,p-Xyl) is simply a functionally identical analog of (N-Et)BNAH on the basis of the reactivity criterion and the kinetic solvent and oxygen effects. In addition to the fact that the two nicotinamide moieties in BisNAH-(Et,p-Xyl) are separated by a p-xylylene bridge, they may assume various orientations
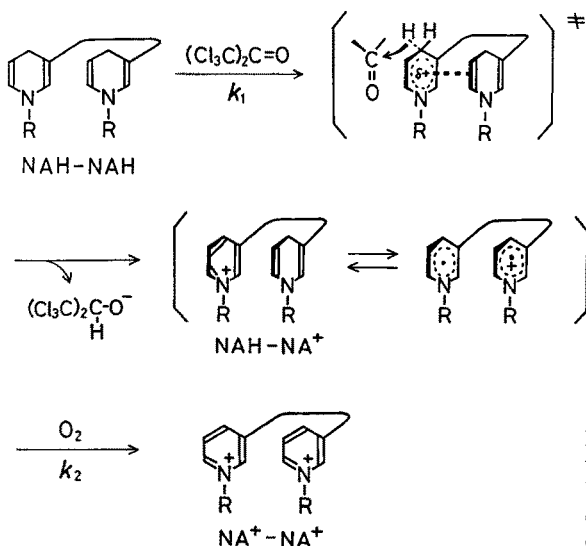
Fig. 19. Mechanism of the reduction of hexachloroacetone with bis(1,4-dihydronicotinamide) in dichloromethane under aerobic conditions (taken from Ref. [57])

relative to each other, due to rotation about C(aromatic)—CH$_2$ and CH$_2$—N bonds; thus, they become electronically independent of each other. Another class of noncyclic bisdihydronicotinamides [BisNAH(C$_n$, Bzl)] shows an interesting reactivity pattern. In contrast to the rigid p-xylylene bridge, the flexible polymethylene chain in BisNAH(C$_n$,Bzl) may allow the two nicotinamide moieties to assume a close face-to-face conformation in the transition state of reduction if n = 4 or 6. The extent of electronic interaction between the nicotinamide moieties is also markedly affected by the chain length (n); an increment by only two CH$_2$ groups results in a considerable reduction in reactivity (n = 6 and 8).

A comparison of the reactivities of noncyclic and cyclic bisdihydronicotinamides further allows the intrinsic electronic interaction to be characterized. The p-xylylene-bridged cyclic bisdihydronicotinamides [cBisNAH(C$_n$,p-Xyl)] are several times more reactive than the corresponding noncyclic counterpart [BisNAH(Et,p-Xyl)]. This reflects the electronic effect arising from the fixation of the relative orientation of the two nicotinamide moieties. Meanwhile, cBisNAH(C$_n$,p-Xyl) shows a reduced reactivity as compared with another noncyclic family [BisNAH(C$_n$,Bzl)]. The overall reactivity order is as follows: BisNAH(C$_n$,Bzl) (n = 4, 6) > cBisNAH(C$_n$,p-Xyl) (n = 4, 6) > BisNAH(Et,p-Xyl) = (N-Et)BNAH. On the basis of this correlation, cBisNAH(C$_n$,p-Xyl) is considered to be conformationally fixed but rather in a wrong way with respect to both the distance and the angle between the nicotinamide rings. On the other hand, the two nicotinamide moieties in BisNAH(C$_n$,Bzl) (particularly with n = 4 and 6) may assume a close face-to-face geometry without inducing significant strain in the molecules in the transition state, even though these molecules may adopt an extended geometry in the ground state with minimum electronic interaction between the nicotinamide moieties as judged from their ^{1}H-NMR, electronic, and fluorescence spectra. In summary, effective charge-transfer interactions, which result in acceleration of the reaction rate, are due to the favorable face-to-face arrangement of the two dihydronicotinamide moieties in the transition state. The nature of the bridging components, which link the two nicotinamide moieties, certainly controls the intramolecular arrangement of such moieties. As regards the nature of these components, a flexible single bridge [BisNAH(C$_n$,Bzl)] can give rise to a better kinetic effect than a double bridge unfavorably fixing the nicotinamide moieties [cBisNAH(C$_n$,p-Xyl)] which, in turn, is better than a less flexible single bridge [BisNAH(Et,p-Xyl)]. The conformational fixation in fact results in an increase in reactivity in the case of an o-xylylene bridge, even if it is adopted as a single bridge component. A double bridge favorably fixing the nicotinamide moieties [cBisNAH(C$_4$,o-Xyl)] is more effective than both of the single bridge types.

The extensive intramolecular electronic interactions between the two nicotinamide moieties give rise to large kinetic effects in the reduction of hexachloroacetone. These interactions must become effective in the transition state rather than in the ground state; they are of charge-transfer character between the two dihydronicotinamide moieties placed in a close face-to-face conformation. This face-to-face geometry must be attained without the development of internal steric strain regardless of the nature of the bridging components which link the two dihydronicotinamide moieties. However, when the dihydronicotinamide groups are rigidly fixed in such a favorable geometry already in the ground state, the kinetic effect becomes most pronounced

due to the entropy effect. In the reaction described above, one of the dihydronicotin-amide groups serves as an electron pool which does not attack a carbonyl substrate directly. Consequently, such an electron pool can be replaced by other electron-donating moieties. A guideline has been given here for designing 1-alkyl-1,4-dihydro-nicotinamides which undergo self-activation via charge-transfer interaction in the transition state of reduction.

5 Concluding Remarks

Not only [20]- and [10.10]paracyclophanes dealt with in this article but also other paracyclophanes may provide effective binding sites for a variety of hydrophobic substrates in aqueous media. These paracyclophanes may bind the substrates in either penetration-type or face-to-face mode, depending on the shape and bulkiness of the latter as compared with the spatial dimension of the macrocyclic cavities of the former (see Sects. 2.1 and 2.2). Since the paracyclophane skeleton itself constitutes a rather rigid macrocyclic framework, interactions between the host and guest molecules are compared to the lock-and-key mode which is often encountered in enzymatic processes. It is rather difficult to prepare intricate paracyclophanes which provide sufficiently deep cavities and polyfunctional catalytic sites. Therefore, octopus cyclophanes are more suitable for the construction ·of deeper hydrophobic cavities than ordinary paracyclophanes. Since such octopus cyclophanes bear flexible alkyl branches, the induced-fit mechanism is operative in the substrate-binding process so that a relatively wide range of substrate selectivity can be anticipated (see Sect. 2.3). On the other hand, the substrate-binding capability of paracyclophanes with elaborated structures would be more sensitive to the molecular shape of the substrate due to the rigid framework of their hydrophobic cavities. In any event, functionalized [20]- and [10.10]paracyclophanes accelerate the deacylation of carboxylic esters of reasonable hydrophobicity according to the Michaelis-Menten type mechanism. The paracyclophanes, which are modified by an appropriate intramolecular assembly of functional groups, may demonstrate various features of polyfunctional catalysis (see Sect. 3). This polyfunctional character is readily achieved by introducing one functional group into each alkyl branch of octopus cyclophanes (see Sect. 3.8). In conclusion, there is a wide range of possibilities in designing such macrocycles to develop novel catalytic functions for the reactions with various hydrophobic substrates. Such elaborated macrocycles are expected to simulate closely enzymatic processes in aqueous media and to be utilized as effective organic catalysts at ordinary temperatures.

Another valuable feature of the macrocyclic skeleton lies in its ability to fix functional groups intramolecularly in a favorable orientation for the cooperative catalysis as demonstrated by bis(1,4-dihydronicotinamide)s (see Sect. 4). An enforced intramolecular interaction between such functional groups reflects the polyfunctional and cooperative feature effective at the active sites of enzymes. We have prepared a [20]paracyclophane bearing a 1,4-dihydronicotinamide residue on the benzene ring and a pyridine-2-carboxylic acid moiety as a metal-binding ligand at C-10 of the macrocycle as a model for the NAD-dependent alcohol dehydrogenase. The coordi-nation behavior of this [20]paracyclophane with zinc ions [60] and the kinetic

activity of the resulting zinc complex in the reduction of carbonyl compounds in nonaqueous media were investigated [61]. In addition, a macrocycle which bears a vitamin B_6-like moiety has been prepared in our laboratory [62] as a model for evaluating the hypothesis of Dunathan [63].

6 Acknowledgements

7 References

1. Murakami, Y. et al.: Bull. Chem. Soc. Jpn. *47*, 1238 (1974)
2. Murakami, Y. et al.: Bull. Chem. Soc. Jpn. *48*, 1537 (1975)
3. Murakami, Y. et al.: J. Chem. Soc., Perkin Trans. 2 *1977*, 24
4. VanEtten, R. L. et al.: J. Am. Chem. Soc. *89*, 3242 (1967)
5. VanEtten, R. L. et al.: J. Am. Chem. Soc. *89*, 3253 (1967)
6. VanderJagt, D. L. et al.: J. Am. Chem. Soc. *92*, 1016 (1970)
7. Cramer, F. et al.: J. Am. Chem. Soc. *89*, 14 (1967)
8. Jencks, W. P.: Catalysis in Chemistry and Enzymology, New York, McGraw-Hill 1969
9. Danklicker, W. B., de Saussure, V. A.: Stabilization of Macromolecules by Hydrophobic Bonding. Role of Water Structure and of Chaotropic Ions, in: The Chemistry of Biosurfaces, Vol. 1 (ed.) Hair, M. L., New York, Marcel Dekker 1971
10. Rabinowitch, E. et al.: J. Am. Chem. Soc. *63*, 69 (1941)
11. Tanizaki, Y. et al.: Bull. Chem. Soc. Jpn. *38*, 264 (1965)
12. Munck, A. et al.: Biochim. Biophys. Acta *26*, 397 (1957)
13. Stoesser, P. R. et al.: J. Phys. Chem. *71*, 564 (1967)
14. Gill, S. J. et al.: Biochemistry *6*, 272 (1967)
15. Maugh II, T. et al.: J. Am. Chem. Soc. *93*, 6584 (1971)
16. Blyth, C. A. et al.: J. Am. Chem. Soc. *93*, 3021 (1971)
17. Murakami, Y. et al.: J. Chem. Soc., Perkin Trans. 2 *1977*, 1947
18. Murakami, Y. et al.: Bull. Chem. Soc. Jpn. *50*, 2420 (1977)
19. Hirs, C. H. W. et al.: Arch. Biochem. Biophys. *111*, 209 (1965)
20. Murakami, Y. et al.: J. Chem. Soc., Perkin Trans. 1 *1979*, 1560
21. Murakami, Y. et al.: J. Chem. Soc., Perkin Trans. 1 *1979*, 1669
22. Murakami, Y. et al.: J. Chem. Soc., Perkin Trans. 1 *1981*, 2800
23. Benesi, H. A. et al.: J. Am. Chem. Soc. *71*, 2703 (1949)
24. Murakami, Y. et al.: Bull. Chem. Soc. Jpn. *50*, 3365 (1977)
25. Koshland, D. E.: J. Theoret. Biol. *2*, 75 (1962)
26. Westheimer, F. H.: Adv. Enzymol. *24*, 441 (1962)
27. Fendler, J. H., Fendler, E. J.: Catalysis in Micellar and Macromolecular Systems, New York, Academic Press 1975
28. Kirby, A. J. et al.: J. Chem. Soc., Perkin Trans. 2 *1972*, 1206
29. Storm, D. R. et al.: J. Am. Chem. Soc. *94*, 5805, 5815 (1972)

30. Murakami, Y. et al.: J. Chem. Soc., Perkin Trans. 2 *1977*, 32
31. Frank, H. S. et al.: Discuss. Faraday Soc. *24*, 133 (1957)
32. Hankins, D. et al.: J. Chem. Phys. *53*, 4544 (1970)
33. Gordon, J. E.: J. Am. Chem. Soc. *94*, 650 (1972)
34. Hibbert, F. et al.: J. Am. Chem. Soc. *94*, 7637 (1972)
35. Butler, A. R. et al.: J. Chem. Soc. *1961*, 2305
36. Engbersen, J. F. J. et al.: J. Am. Chem. Soc. *97*, 1563 (1975)
37. Fife, T. H. et al.: J. Am. Chem. Soc. *91*, 7481 (1969)
38. Murakami, Y. et al.: Bull. Chem. Soc. Jpn. *49*, 3633 (1976)
39. Jencks, W. P. et al.: J. Am. Chem. Soc. *82*, 1778 (1960)
40. Murakami, Y. et al.: J. Chem. Soc., Chem. Commun. *1978*, 494
41. Murakami, Y. et al.: J. Chem. Soc., Perkin Trans. 2 *1980*, 1665
42. Williams, A. et al.: J. Am. Chem. Soc. *88*, 2508 (1966)
43. Lienhard, G. E. et al.: J. Am. Chem. Soc. *88*, 3982 (1966)
44. Sunamoto, J. et al.: Tetrahedron Lett. *1977*, 1329
45. Reynolds, J. A. et al.: Proc. Nat. Acad. Sci. US *71*, 2925 (1974)
46. Menger, F. M. et al.: J. Am. Chem. Soc. *96*, 121 (1974)
47. Gitler, C. et al.: J. Am. Chem. Soc. *90*, 5004 (1968)
48. Tagaki, W. et al.: J. Chem. Soc., Chem. Commun. *1972*, 219
49. Moss, R. A. et al.: J. Am. Chem. Soc. *99*, 627 (1977)
50. Tagaki, W. et al.: J. Chem. Soc., Chem. Commun. *1977*, 29
51. Gutereund, H. et al.: Biochem. J. *63*, 656 (1956)
52. Tonellato, U.: J. Chem. Soc., Perkin Trans. 2 *1976*, 771
53. Martinek, K. et al.: Tetrahedron Lett. *1975*, 1279
54. Martinek, K. et al.: Tetrahedron *31*, 709 (1975)
55. Tagaki, W. et al.: J. Org. Chem. *44*, 555 (1979)
56. Murakami, Y. et al.: Bull. Chem. Soc. Jpn. *51*, 2690 (1978)
57. Murakami, Y. et al.: J. Am. Chem. Soc. *104*, 5189 (1982)
58. Blaedel, W. J. et al.: Anal. Chem. *42*, 918 (1970)
59. Reichardt, C.: Solvent Effects in Organic Chemistry, Weinheim, Verlag Chemie 1979
60. Murakami, Y. et al.: J. Chem. Soc., Perkin Trans. 1 *1981*, 2809
61. Murakami, Y. et al.: Bull. Chem. Soc. Jpn. *55*, 2898 (1982)
62. Murakami, Y., Kikuchi, J., Deguchi, S., unpublished results
63. Dunathan, H. C.: Adv. Enzymol. *35*, 79 (1971)

Concluding Remarks

This volume presented a selection of research work in the field of (cyclo-)phane chemistry. The reader may have realized the continuous extension of this topic and its increasing influence on neighbouring disciplines.

In future, synthetic chemistry will increase the amount and value of such phane molecules, the size of which ranges between low molecular and macromolecular compounds. They may be called *"mediomolecules"* with molecular masses between approx. 1000 and 20000 and contain acyclic as well as cyclic exponents — the medio- and macrocyclic compounds. Not only primary structures but also *secondary and tertiary structures* are included into the synthetic strategy directed to such molecules stimulated by further developments of synthetic procedures and of spectroscopic methods. It will be important to find means to handle molecules of this size in solution and to investigate their static and dynamic structures, their intermolecular host/ guest interactions and reactions.

Apart from the impetus of phane chemistry to other fields of chemical research work attention should be drawn to desirable molecules, which are pure cyclophane hydrocarbons, however, might effect the design of further, less puristic extraordinary molecular structures. Such target molecules apart from leading to new findings may also simply appear as nice symmetric structures and therefore delight the eye of the "molecular designer" at the end of this volume:

After [2₆]cyclophane, postulated in 1972, .designated as "superphane" (*1*) has been synthesized, its hexaene *2* remains to be done and the preparation of the extended [2₆]hexaphenylbenzenophane *3* also can be attacked.

1   *2*   *3*

4

6

5

7
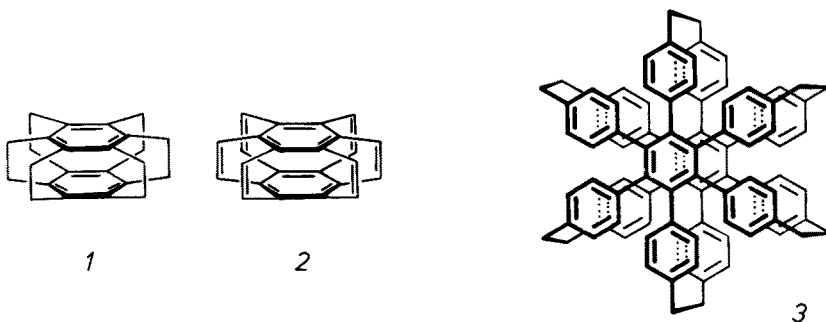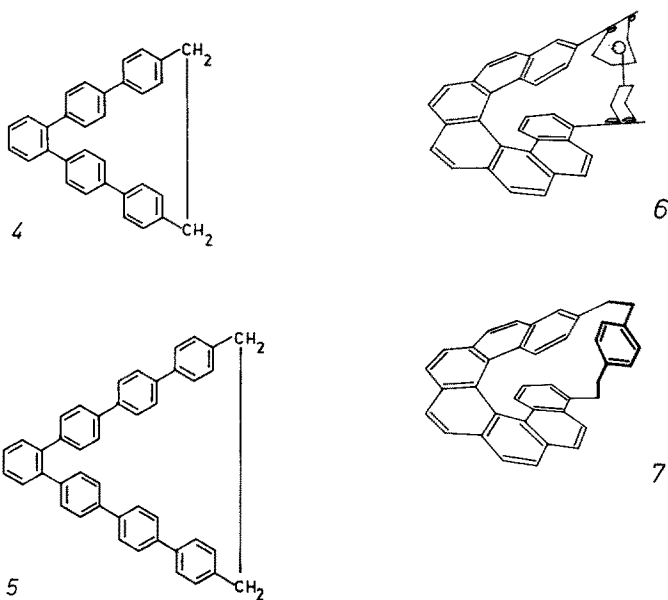
Molecules with only clamped aromatic assemblies like *4*, *5*, in which benzene rings are forced into boat conformations, and also spacered (cf. *6*) helices like *7* will be synthesizable, as well as annulenophanes such as *8* and the phane molecule *9*, which is interpreted with a sensitive artistic understanding to a gyro-wheel. Structure *9* opens the field of tube-shaped aromatic molecules: Will it be possible to succeed in the condensation and aromatisation of the skeleton to end up with a cyclic pyreno/peryleno oligomer?

8

9
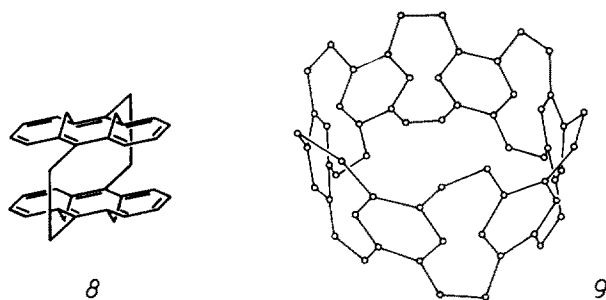
The $[0_{10}]$paracyclophane *10* and similar oligo-paraphenylenes hopefully will be synthesized; they are of interest not only in account of the increasing large ring strain with decreasing ring width.

Tube-shaped molecules looking like bracelettes, for example *11*, fully aromatic or partly aliphatic, belong to the stars under the phanes-to-be. The aromatic representative of *11* might be designated as a "super-acen" in analogy to super-
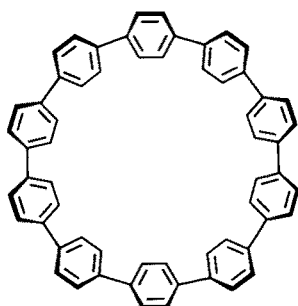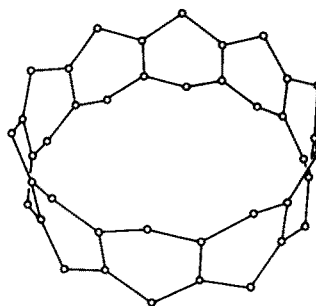
10   11

phane. Apart from questions regarding aromaticity a second point of interest here is coming from the reducibility of the ring width. This aspect reminds of the classic question of the smallest cyclic alkene or alkyne.

By insertion of heteroatoms or affixing of substituents into known compounds, analogues with improved properties of solubility will be available. Obviously, challenges calling for innovations are waiting for generations of chemists. Research connected with structures like and beyond the few ones shown above — and those in the contribution collected in this (and the coming) volume — will impart new conclusions and set up new ideas for future trends based on stronger fundaments.

Cyclophane chemistry as a "bridge builder in the molecular architecture" already led to a directive bridging between research fields and departments, which is also evident in the studies presented.

F. Vögtle

Author Index Volumes 101–115

Reetz, M. T.: Organotitanium Reagents in Organic Synthesis. A Simple Means to Adjust Reactivity and Selectivity of Carbanions. *106*, 1–53 (1982).
Rolla, R., see Montanari, F.: *101*, 111–145 (1982).
Rossa, L., Vögtle, F.: Synthesis of Medio- and Macrocyclic Compounds by High Dilution Principle Techniques, *113*, 1–86 (1983).
Rzaev, Z. M. O.: Coordination Effects in Formation and Cross-Linking Reactions of Organotin Macromolecules. *104*, 107–136 (1982).

Saenger, W., see Hilgenfeld, R.: *101*, 3–82 (1982).
Schmeer, G., see Barthel, J.: *111*, 33–144 (1983).
Schöllkopf, U.: Enantioselective Synthesis of Nonproteinogenic Amino Acids. *109*, 65–84 (1983).
Shibata, M.: Modern Syntheses of Cobalt(III) Complexes. *110*, 1–120 (1983).
Siegel, H.: Lithium Halocarbenoids Carbanions of High Synthetic Versatility. *106*, 55–78 (1982).
Steudel, R.: Homocyclic Sulfur Molecules. *102*, 149–176 (1982).
Steudel, R., and Laitinen, R.: Cyclic Selenium Sulfides. *102*, 177–197 (1982).
Suzuki, A.: Some Aspects of Organic Synthesis Using Organoboranes. *112*, 67–115 (1983).
Szele, J., Zollinger, H.: Azo Coupling Reactions Structures and Mechanisms. *112*, 1–66 (1983).

Tabushi, I., Yamamura, K.: Water Soluble Cyclophanes as Hosts and Catalysts, *113*, 145–182 (1983).
Thieme, P. C., see Pommer, H.: *109*, 165–188 (1983).
Tollin, G., see Edmondson, D. E.: *108*, 109–138 (1983).

Veith, M., and Recktenwald, O.: Structure and Reactivity of Monomeric, Molecular Tin(II) Compounds. *104*, 1–55 (1982).
Venugopalan, M., and Veprek, S.: Kinetics and Catalysis in Plasma Chemistry. *107*, 1–58 (1982).
Veprek, S., see Venugopalan, M.: *107*, 1–58 (1983).
Vögtle, F., see Rossa, L.: *113*, 1–86 (1983).
Vögtle, F.: Concluding Remarks. *115*, 153–155 (1983).
Vostrowsky, O., see Bestmann, H. J.: *109*, 85–163 (1983).
Voronkov. M. G., and Lavrent'yev, V. I.: Polyhedral Oligosilsequioxanes and Their Homo Derivatives. *102*, 199–236 (1982).

Wachter, R., see Barthel, J.: *111*, 33–144 (1983).
Wilke, J., see Krebs, S.: *109*, 189–233 (1983).

Yamamura, K., see Tabushi, I.: *113*, 145–182 (1983).
Yang, Z., see Heilbronner, E.: *115*, 1–55 (1983).

Zollinger, H., see Szele, I.: *112*, 1–66 (1983).